NANOTECHNOLOGY FOR EFFICIENT DELIVERY OF SHORT THERAPEUTIC OLIGONUCLEOTIDES (ANTISENSE ODN AND SIRNA) AND CODELIVERY WITH CHEMICAL ANTICANCER DRUGS FOR EFFECTIVE CANCER THERAPY

by

MINHUA CHEN

A Dissertation submitted to the

Graduate School – Newark

Rutgers, the State University of New Jersey

in partial fulfillment of requirements

for the degree of

Doctor of Philosophy

Graduate Program in Chemistry

written under the direction of

Professor Huixin He

and Professor Tamara Minko

and approved by

_____

_____

_____

_____

Newark, New Jersey

May, 2009

ABSTRACT OF THE DISSERTATION

Nanotechnology for Efficient Delivery of Short Therapeutic Oligonucleotides (Antisense ODN and siRNA) and Codelivery with Chemical Anticancer Drugs for Effective Cancer Therapy

By MINHUA CHEN

Dissertation Directors: Dr. Huixin He and Dr. Tamara Minko

Despite great progress in recent years, efficient delivery of gene therapy or chemotherapy drugs into their target sites with minimal side effects remains one of the biggest challenges for effective cancer therapy. Co-delivery of siRNA targeted for proteins responsible for drug resistance and chemical anticancer drugs represents a promising new approach to overcome drug resistance and to make cancer therapy more effective. However, efficient co-delivery systems that can deliver siRNA and anti-cancer drugs simultaneously into cancer cells have rarely been developed.

This thesis is aimed at developing novel non-viral nanocarriers for efficient delivery of antisense ODN and siRNA and codelivery with chemical anticancer drugs for effective cancer therapy. We began by performing a systematic investigation on the efficacy of five generations of polypropyleneimine (PPI) dendrimers to provoke nanoparticle formation from antisense ODNs and then deliver the ODN nanoparticles into cancer cells (**Chapter 2**). We then developed a novel approach to efficiently package and deliver siRNAs into cancer cells with low generation non-toxic PPI dendrimers by using gold nanoparticles as a "labile catalytic" packaging agent (**Chapter 3**). Relying on the fundamental understanding gained from Chapters 2 and 3, we then continued the

utilization of dendrimers and developed polyamidoamine (PAMAM) dendrimer-modified mesoporous silica nanoparticles (MSNs) as a stimuli-responsive controlled-release delivery system for a chemotherapy drug (**Chapter 4**). By using a non-gatekeeping approach, we demonstrated nearly zero release of doxorubicin in H_2O and complete release once delivered into cancer cells. In **Chapter 5**, we further utilized MSNs as a codelivery system to simultaneously deliver Doxorubicin and a Bcl-2-targeted siRNA into A2780/AD human ovarian cancer cells for enhanced chemotherapy efficacy. We then investigated the effect of each component in the PAMAM-dendrimer modified MSN-based codelivery system on the cell uptake efficiency of siRNA and its intracellular release and localization (**Chapter 6**). We further studied the effect of temperature and different inhibitors on the cell uptake efficiency of MSN-Dox-G2 and found that MSN-Dox-G2 might internalize into cells through a non-endocytic process (**Chapter 7**). Finally, we demonstrated a specific cancer cell-targeted delivery by PEGylating the MSN-Dox-G2/siRNA complex and tagging it with a specific cancer-targeting group (**Chapter 8**).

Dedicated to

My wife Suling Zhang

My father Linxi Chen and my mother Fengxian Chen

ACKNOWLEDGMENTS

It finally comes to the moment when I am practically allowed to write the acknowledgements. This moment only comes after I achieved the goals of my Ph.D. research and I am materially ready and permitted, which would not be possible without the help of all the people I am going to acknowledge. Therefore, I can't stop being emotional as I am writing this.

I can not wait for another word to express my deepest gratitude to my wife Suling Zhang. There were too many nights and weekends when I was away for experiments. No matter how late I came home, she was always there waiting for me, with hot meals, love and care. Thank you, Suling! My next gratitude goes to my father Linxi Chen and my mother Fengxian Chen. It was them who always sacrificed themselves to create the best opportunities possible for my education. It was them who taught me to be honest, responsible and always persistent to achieve my goal.

Words cannot express my appreciation for my advisors Dr. Huixin He and Dr. Tamara Minko. The trust and support they have given to me was beyond what I hoped for. It is their continuous inspiration, encouragement and guidance that have kept me moving forward. If I could claim I became more mature on scientific research after five years' Ph.D. study, it is mainly their credit.

My cordial appreciation also goes to Dr. T.J. Thomas and Dr. Thresia Thomas. It was the coordination with them that led me into the exciting field of gene delivery. My thanks also go to Dr. Latha Santhakumaran and Dr. Sandhya Nair for their coordination and help.

I would also like to thank my thesis committee members Dr. Phillip Huskey and Dr. Richard Mendelsohn for their valuable time and suggestions.

My deep appreciation also goes to Dr. Dongguang Wei. It was him who drove more than 200 miles from Boston to NYC to help me set up and perform the TEM experiments on the weekend. His enthusiasm and persistence for research have deeply inspired me, not to mention his always pleasant sense of humor.

My thanks must also go to Dr. Oleh Taratula, who was my lab mate working on the same field of drug delivery. There were so many valuable discussions between us that kept me learning. He always shared his experience and expertise without any reservation. I would also greatly thank Ms. Min Zhang for her generous help. She trained me on all cell-related experiments and helped me to be up to speed within a short period of time. We always had great discussions and her serious attitude for research has been very impressive.

My thanks must also go to Dr. Dirk Stueber for his help on solid state NMR experiment, Dr. Qiang Tu for his help on ICP-AES experiment and Mr. Henryk Mach for his help on Zeta potential measurement. Their expertises are much appreciated.

My thanks also go to my good friend Dr. Jinlou Gu, who is an expert in the field of mesoporous silica nanoparticles. It was a midnight conversation with him that inspired me to start the research on mesoporous silica nanoparticles.

I would also like to thank Mr. Todd Stamatakos, Mr. Ipsit Pandya and Ms. Jowairia Chaudhry for their direct help on my projects. My appreciation also extends to other colleagues in Dr. He's and Dr. Minko's group for their assistance and friendship, particularly Dr. Yufeng Ma, Mr. William Cheung, Mr. Pui Lam Chiu, Mr. Rishi Parajuli,

TABLE OF CONTENTS

Chapter 2. Oligodeoxynucleotide Nanostructure Formation in the Presence of Polypropyleneimine Dendrimers and Their Uptake in Breast Cancer Cells

Chapter 3. Labile Catalytic Packaging and Delivering of siRNA/DNA to Cancer Cells: Control of Gold Nanoparticles "out" of siRNA/DNA Complexes

Chapter 5. Co-delivery of Doxorubicin and Bcl-2 siRNA by Mesoporous Silica Nanoparticles Enhances the Efficacy of Chemotherapy in Multidrug Resistant Cancer Cells

Chapter 7. Probing the Internalization Mechanism of a Mesoporous Silica Nanoparticle-based Drug Delivery System: a Possible Non-endocytic Internalization Process

Chapter 8. Toward In-vivo Targeting Codelivery of Doxorubicin and siRNA for Effective Cancer Therapy

Curriculum Vitae

LIST OF TABLES

LIST OF FIGURES

List of Abbreviations

AFM	Atomic Force Microscopy
Å	Angstrom
a.u.	Arbitrary units
AACR	American Association for Cancer Research
ATP	Adenosine triphosphate
Au	Gold
Au NPs	Gold Nanoparticles
BCA	Bicinchoninic acid
bp	Base pairs
BPEI	Branched PEI
DIC	Differential interference contrast
DLS	Dynamic Light Scattering
DMSO	Dimethyl Sulfoxide
DNA	Deoxyribonucleic acid
DOPC	1,2-dioleoyl-*sn*-glycero-3-phosphatidylcholine
Dox	Doxorubicin
DPBS	Dulbecco's phosphate buffered saline
DTBP	Dimethyl-3-3'-Dithiobispropionimidate-HCl
EDTA	Ethylenediaminetetraacetic acid
EM	Electron Spectroscopy
EPR	Enhanced permeability and retention
FITC	Fluorescein isothiocyanate
G1	Generation 1
G2	Generation 2
G3	Generation 3
G4	Generation 4
G5	Generation 5
G2.5	Generation 2.5
G4.5	Generation 4.5
GNPs	Gold Nanoparticles
GRAS	Generally recognized as safe
H	Hour or Hours
H2O	Water
HEPES	(4-(2-hydroxyethyl)-1-piperazineethanesulfonic acid)
HPMA	N-(2-Hydroxypropyl)methacrylamide
i.p.	intraperitoneal
kDa	Kilodaltons
Kg	Kilogram

LHRH	Luteinizing hormone-releasing hormone
LPEI	Linear PEI
MAL	Maleimide group
MDR	Multidrug Resistant
MEM	Minimum Essential Medium
Min	Minutes
mL	Microliter
mL	Milliliter
Mμ	Micromole per liter
MRI	Magnetic resonance imaging
mRNA	Messenger ribonucleic acid
MRP	Multidrug Resistant Protein
MSNs	Mesoporous Silica Nanoparticles
MTT	(3-(4,5-dimethylthiazol-2-yl)-2,5-diphenyltetrazolium bromide)
MWCO	Molecular weight cutoff
MWNTs	Multiwalled carbon nanotubes
ng	Nanogramm
NHS	N-hydroxysulfosuccinimide
NIR	Near-infrared
nm	Nanometer
NP	Nanoparticle
NPs	Nanoparticles
nt	Nucelotide
ºC	Celsius degree
ODN	Oligodeoxynucleotide
ORMOSIL	Organically-modified silica nanoparticles
PAMAM	Polyamidoamine dendrimer
PBS	Phosphate buffered saline
PDDA	Poly(diallyldimethylammonium chloride)
pDNA	Plasmid DNA
PEG	Poly(ethylene glycol)
PEI	Polyethylenimine
PGA	Polyglutamate
PLL	Poly-L-lysine
PMAA	Poly(methacrylic acid)
PMAO	Poly(maleic anhydride alt-1- octadecene
PPI	Polypropylenimine
QD	Quantum dots

RES	Reticulo-endothelial system
RISC	RNA silencing complex
RNA	Ribonucleic acid
RNAi	RNA interference
RT	Room Temperature
RT-PCR	Reverse transcriptase-polymerase chain reaction
siRNA	Short interfering RNA or small interfering RNA
SLN	Solid lipid nanoparticle
SPIONs	Superparamagnetic iron oxide nanoparticles
SWNTs	Single-walled carbon nanotubes
TEM	Transmission Electro Microscopy
TERT	Telomerase reverse transcriptase
TNBS	2,4,6-trinitrobenzenesulphonic acid
TNF	Tumor necrosis factor
TRAIL	Tumor necrosis factor–related apoptosis-inducing ligand
UV-Vis	Ultraviolet-Visible

Chapter 1

Introduction

1.1. Cancer Therapy

Cancer is one of the most fatal diseases and causes about 13% of all deaths worldwide each year. According to the American Cancer Society, 7.6 million people died from cancer during 2007. The common types of cancer therapies include surgery, chemotherapy, radiation therapy and gene therapy. Among all, chemotherapy represents one of the most extensively studied conventional therapies while gene therapy represents the most attractive and promising new therapy.

1.1.1. Chemotherapy

The development of cancer chemotherapy started in the 1940s with the first use of nitrogen mustards, a chemical warfare agent, as an effective treatment for cancer.(*1*) Since then, hundreds of anti-cancer chemical drugs have been developed and used to treat various types of cancers. Most of these drugs are designed to kill or stop the growth of cancer cells. Based on their specific mechanisms, the cancer chemotherapy drugs can be divided into several groups including alkylating agents, antimetabolites, anti-tumor antibiotics, topoisomerase inhibitors, mitotic inhibitors, etc.(*2*) However, despite decades of research, progress in cancer chemotherapy is relatively slow, in part due to the lack of appropriate delivery systems to deliver anti-cancer drugs selectively to tumors. Severe toxicity to normal body tissues remains a critical obstacle in systemic delivery of anti-

cancer drugs for cancer therapy. In efforts to reduce the side effects and to improve the therapeutic efficacy of anti-cancer drugs, many drug delivery systems have been developed, including liposomes, micelles, polymeric conjugates, and solid-lipid nanoparticles.(*3-23*) However, their application is still largely limited by several drawbacks including low loading capacity, premature leakage of anti-cancer drugs before reaching the target site, and lack of efficient and controlled release in the target site. Furthermore, the development of drug resistance in cancer cells is another major limiting factor for effective cancer chemotherapy. In most cases, drug resistance is still the main cause for failure of cancer chemotherapy. Therefore, therapeutic strategies to overcome drug resistance should have a great impact on the treatment of cancer.

1.1.2. Gene Therapy

Sequencing of the human genome and functional genomics offers unprecedented opportunities to combat a large number of diseases including cancers by disrupting the expression of disease-related genes with short synthetic nucleic acid sequences.(*24*) Antigene and antisense ODNs, aptamers, ribozymes (catalytic RNAs) and siRNAs are among the nucleic acid based drugs under development. Due to the high degree of specificity, gene therapy by antisense and siRNA drugs have received particularly tremendous attention.

1.1.2.1. Antisense/ODN Therapy

In the antisense strategy, the antisense single-stranded ODN molecule is delivered inside a cell where it binds complementarily with its targeted mRNA, producing a partially

double-stranded ODN/mRNA complex. Translation of this modified mRNA into protein is blocked either by a non-RNA cleaving mechanism of action or by antisense-mediated cleavage of RNA.(*25, 26*) One typical approach of a non-mRNA cleaving mechanism is to hybridize an ODN to specific RNA sequences to prevent the binding of important regulatory proteins, while the antisense-mediated cleavage of RNA usually involves the recruitment and utilization of endogenous enzymes such as RNase H, RNase P, RNase L, or by inducing structural changes in RNA that result in its degradation. Antisense drugs are being developed to treat various types of cancers including lung cancer, colorectal carcinoma, pancreatic carcinoma, malignant glioma and malignant melanoma as well as other diseases. Due to extensive work in this field, there is already one antisense drug, fomivirsen (marketed as Vitravene), approved for the local treatment of a non-cancer disease cytomegalovirus retinitis, with nearly twenty others in late-stage clinical trials.(*27*) However, the success of antisense therapy is still largely limited by the lack of efficient delivery systems to deliver ODN into cells and subsequently release them to their intracellular targets.

1.1.2.2. RNA Interference by siRNA

In contrast to antisense ODN which has been studied for many years, gene therapy by small interfering RNA (siRNA) is a relatively new approach. RNA interference (RNAi) by siRNA was first discovered in 2001 and has since received emerging interests in recent years. In this process, double-stranded siRNA with complementary nucleotide sequences to the targeted RNA strand guides the specific RNAi pathway proteins to the targeted mRNA, where they "cleave" the target, breaking it down into small portions that

can no longer be translated into protein. The research on RNAi was first reported in 1998 by Andrew Fire and his coworkers who demonstrated that double-stranded RNA injected into worms could turn off genes.(*28*) Following the discovery of RNAi, just three years later, in 2001, Thomas Tuschl and his colleagues reported their discovery that small interfering RNA (siRNA) could silence genes containing complementary sequences in human cells.(*29*) It was this study that raised the possibility for the first time that RNAi could be used as a drug. Since then, the interest in exploring RNAi for biomedical research and drug development has surged. The main advantage of RNAi compared to other gene therapeutic strategies, including antisense strategy, lies in its high specificity and potency of gene silencing, coupled with the facts that it can target every gene, and every cell, which has the necessary machinery. Also importantly, the effect of siRNA lasts longer than that of antisense ODN. Promising results have been attained for siRNAs, however, many challenges remain to be overcome for any practical therapeutic applications. Similar to antisense ODN, inefficient transport of siRNA across cell membrane and delivery to the target sites remain the main obstacle to the success of siRNA therapy. As far as siRNA is concerned, a delivery system must be able to not only efficiently deliver the siRNA into cells but also effectively release it into the cytoplasm where siRNA can enter the RNAi pathway and guide the sequence-specific mRNA degradation. However, delivery systems of these types are still largely lacking.

1.1.2.3. Gene Therapy for Cancer Treatment

Gene therapy is being explored in different ways for cancer treatment.(*30*) One common approach has been to replace missing or altered genes with healthy genes. Because some

missing or altered genes (e.g., p53) may cause cancer, substituting "working" copies of these genes may be used to treat cancer.(*31*) Researchers are also studying ways to improve a patient's immune response to cancer. In this approach, gene therapy is used to stimulate the body's natural ability to attack cancer cells.(*32*) Another approach that has been under extensive investigation is to use antisense or siRNA to overcome the drug resistance, to make the cancer cells more sensitive to chemotherapy drugs. For example, special sequences of antisense ODNs or siRNAs targeted against mRNA encoding major proteins responsible for pump and nonpump cellular defense have been developed and showed a substantial efficacy *in vitro*.(*33*) Other researchers are also focused on the use of gene therapy to prevent cancer cells from developing new blood vessels (angiogenesis). As gene therapy further advances, we can expect many other different approaches to be explored for cancer treatment. Nevertheless, the major challenges facing gene therapy for cancer treatment will most likely remain similar as those facing gene therapy for other diseases.

1.1.2.4. Major Challenges

As briefly mentioned above, one of the major challenges for both antisense ODN and siRNA therapy is their inefficient transport across cell membranes. In general, a gene cannot be directly internalized into a cell. It must be delivered to the cell using a carrier, or "vector." Viral vectors, or viruses, are efficient of accomplishing this due to their unique ability to recognize certain cells. Many clinical trials of gene therapy rely on retroviruses to deliver the desired genes. Other viruses used as vectors include adenoviruses, adeno-associated viruses, lentiviruses, poxviruses, and herpes viruses.

These viruses differ in how well they transfer genes to the cells they recognize and are able to infect. Thus, researchers may use different vectors, depending on the specific characteristics and requirements of the study. However, the immune response elicited by viral proteins has posed a major challenge to this approach.(*34*) For example, in 1999, a severe immune response to the adenovirus carrier of a gene therapy triggered multiple organ failures and caused the death of a patient after he participated in a gene therapy trial for 4 days.(*35*) Other drawbacks of the viral delivery system include toxicity, the difficulties of repeated administration and limited control over transduced cell type. Hence, there is an urgent need in developing nonviral gene delivery vectors.

1.1.3. Combination of Chemotherapy and Gene Therapy

A combination of chemotherapy and gene therapy for cancer treatment has received increased interest among researchers due to its superior efficacy compared to chemotherapy or gene therapy alone. A common strategy has been to use gene therapy to increase the sensitivity of cancer cells to apoptosis induction and then to use chemotherapy to induce apoptosis and to kill cancer cells. One such effort was reported by Lin et al. (*36*). They investigated the combined effect of TRAIL gene therapy and chemotherapeutic agents, including doxorubicin, paclitaxel, vinorelbine, gemcitabine, irinotecan, and floxuridine, in different breast cancer cell lines. They found that in all the cell lines tested, including a breast cancer cell line that is resistant to chemotherapy, the combination of TRAIL gene therapy and cytotoxic agents had either a synergistic or an additive effect. A different strategy was employed by Park et al.(*37*) They combined chemotherapy with a gene therapy designed to disrupt the growth of blood vessels to a

tumor, and found that the combination was far more effective than chemotherapy or gene therapy alone. Specifically, in their study, they used a modified cold virus to insert the gene for tumor necrosis factor (TNF) into tumor cells. TNF is a potent biological substance that can kill cancer cells directly and disrupt their blood supply, but it can be very toxic when given systemically. To avoid this toxicity, the researchers have used Ad.Egr.TNF.11D, a replication-deficient adenoviral vector containing CArG elements cloned upstream of the cDNA for human recombinant TNF-α, to treat tumor cells. They demonstrated the TNF-α production could only be induced in tumor cells with the combination of Ad.Egr.TNF.11D and cisplatin, a common anti-cancer chemotherapy drug. Their studies further demonstrated an enhanced antitumor response without an increase in toxicity following treatment with Ad.Egr.TNF.11D and cisplatin, compared with either agent alone. This was a great example how a chemo-inducible cancer gene therapy can provide a means to control transgene expression while enhancing the effectiveness of commonly used chemotherapeutic agents.

In both examples above, a viral vector was employed to transfect the cells with designed genes inserted into plasmid DNA. In both cases, the gene therapy and chemotherapy drugs were not required to be simultaneously delivered into the cancer cells or tumors in order to achieve the synergistic or combined effects. However, for *in vivo* application, it would be more advantageous to deliver the gene therapy and chemotherapy drugs in the same carrier so that both gene therapy and chemotherapy drug could be delivered to the same cells with similar ratio for combined actions and synergistic effects. Until now, most ongoing clinical trials that combine gene therapy and chemotherapy have used viral vectors as delivery vectors for gene therapy drug. The

development of non-viral vectors as co-delivery system, although more desirable, is still in its infancy and requires much more investigation before any can be widely implemented in clinical trials. The ideal non-viral co-delivery system should not only simultaneously deliver chemotherapy drugs and gene therapy drugs into cells but also release both drugs efficiently into their respective targets to exert its respective effect. Compared to the delivery of gene therapy or chemotherapy drug alone, the problems facing the co-delivery are thus much more challenging.

1.2. Nanotechnology in Drug Delivery for Cancer Therapy

Nanotechnology can be defined as the design and manipulation of materials at the atomic and molecular scale. Nanotechnology is, essentially, the use of atomic and molecular structures as core building blocks to create new products and devices. The first hint of nanotechnology can be traced back to a talk entitled "There's Plenty of Room at the Bottom", given by physicist Richard Feynman in 1959.(*38*) The term 'Nanotechnology' was then coined and popularized in 1980s by K. Eric Drexler.(*39*) Nanotechnology typically uses particles in 10nm-1μm range. Some have mentioned that this technology uses particles in the range of 1nm-100 nm. The American Association for Cancer Research (AACR) website mentions that the component size for nanotechnology ranges from 5 to 500 nanometers.(*40*) Although there is still no strict definition of the size range for nanoparticles, particles with size from a few nanometers to a few hundred nanometers have been commonly considered as nanoparticles.

Nanotechnology has offered us tremendous opportunities to understand and conquer the various problems faced in many different areas such as medicine, electronics,

energy production, cosmetics, etc. Drug delivery is one of the most promising fields of utility for nanotechnology. Particularly, in the field of drug delivery for cancer therapy, with the aid of nanotechnology, researchers are resolving the numerous challenges facing the efficient delivery of chemotherapy drugs and gene therapy drugs or co-delivery of both for effective cancer therapy at an unprecedented speed.

1.2.1. Nanotechnology-enabled Delivery Systems for Chemotherapy

Nanotechnology enabled researchers to develop many nanoparticle-based drug delivery systems for chemotherapy. These delivery systems include polymeric conjugates, micelles, liposomes, solid-lipid nanoparticles, and hollow nanoparticles.(*3-15*) Most of these drug delivery systems displayed the great advantages of protecting anti-cancer drugs from degradation during delivery, increasing their accumulation in tumor tissues, and enhancing the efficacy while at the same time reducing adverse side effects to normal tissues. The sub-micron size featured by most of these drug delivery systems enables the anti-cancer drug-loaded delivery carriers to preferentially extravasate into the leaky tumor sites and be retained there. This is known as the enhanced permeability and retention (EPR) effect.(*41*) Moreover, due to the versatile structures of these drug delivery systems, they can further be modified with cancer-targeting moieties, enabling targeted delivery of anti-cancer drugs to cancer cells.

1.2.1.1. Liposomes

Liposomes, which are the small vesicles of spherical shape that can be produced from natural phospholipids and cholesterol, are by far the most extensively studied nanoparticles used to deliver chemotherapy drugs.(*16-23, 42-46*) They were first discovered in 1961 by Alec D. Bangham, who found that phospholipids combined with water immediately form a bi-layered sphere. This is due to the fact that one end of each molecule is water soluble while the opposite end is water insoluble.(*47*) Based on their structure, liposomes can be broadly classified as multilamellar liposomes and unilamellar liposomes.(*19*) The size, lamellarity (unilamellar or multilamellar) and lipid composition of the bilayers influence many of the important properties like the fluidity, permeability, stability and structure. These properties can be controlled and customized to serve specific needs. The properties are also influenced by external parameters like temperature, ionic strength and the presence of certain close approaching molecules. Liposomes are biodegradable, usually non-toxic and they can be used to encapsulate both hydrophilic and hydrophobic materials. When lipids self assemble to liposomes, water-soluble drugs will be trapped inside the liposomal cavity; while fat-soluble drugs are incorporated within the phospholipid bilayer. The lipid bilayer of some liposomes can also fuse with bilayers of cell membrane, thus providing a special mechanism for the delivery of the liposome contents into cells. A typical design of liposome-based drug delivery is illustrated in Figure 1.1.

Liposome for Drug Delivery
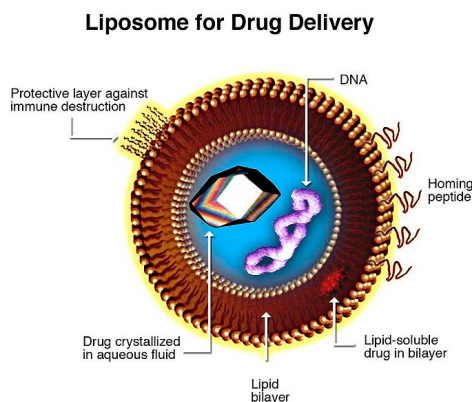
Figure 1.1. Design of liposome-based drug delivery.

To date, many liposomal formulations, including Doxil, DaunoXome, Ambisome, Amphotec, Abelect, have been FDA approved, with many more under clinical trials. Doxil, a PEGylated liposomal formulation for doxorubicin, is the first liposomal formulation approved by FDA to treat patients with ovarian cancer whose disease has progressed or recurred after platinum-based chemotherapy. Theses PEGylated liposomes are labeled "stealth" liposomes with a size of <200nm which are long circulating with hydrophilic PEG surface. This liposomal delivery of doxorubicin improves drug penetration into tumors due to the EPR effect and decreases drug clearance, thereby increasing the duration of therapeutic drug effects. This liposomal formulation of doxorubicin also modulates toxicity, specifically the cardiac effects commonly seen with anthracycline antitumor drugs.

In addition to the conventional liposomal formulation of chemotherapy drugs without active targeting, tumor cell-targeted liposomal delivery has the potential to further enhance the therapeutic efficacy and reduce the toxicity of anti-cancer agents, and therefore has also been under extensive development.(*17, 44, 48-53*) Typically, the targeting was enabled by modifying liposomes with cancer-targeting antibodies, peptides

(e.g., LHRH) or other ligands (e.g., folate, transferrin). An example of antibody-based targeting was demonstrated by Lukyanov et al.(*52*). They modified the commercially available doxorubicin-loaded long-circulating liposomes (Doxil) with the monoclonal nucleosome (NS)-specific 2C5 antibody (mAb 2C5) that recognizes a broad variety of tumors via the tumor cell surface-bound NSs. They demonstrated that the 2C5-targeted Doxil liposomes acquired the ability to recognize NSs and specifically bind to various tumor cells. It was further realized that the Dox-loaded, long-circulating liposomes modified with the mAb 2C5 kill various tumor cells *in vitro* with efficiency higher than non-targeted doxorubicin-loaded liposomes.

Furthermore, pH-sensitive liposomes have also emerged in recent years as an alternative to conventional liposomes in effectively targeting and accumulating anti-cancer drugs in tumors.(*45, 54*) The use of pH-sensitive liposomes allows more complete release of anti-cancer drugs upon the internalization of liposomes into cancer cells.

1.2.1.2. Micelles

Micelles represent another type of self-assembled nanosized aggregates that have been used to encapsulate and deliver anti-cancer drugs.(*11, 55-61*) Different from liposomes that can encapsulate both hydrophilic and hydrophobic drugs, micelles have been mainly used to encapsulate hydrophobic drugs. This is due to the unique core-shell structure of normal phase micelles, which are typically formed by amphiphilic copolymers in aqueous solutions with hydrophobic cores and hydrophilic shells. However, despite being much less common, the use of micelles for encapsulation of hydrophilic anti-cancer drugs has

also been demonstrated in various research, such as through utilization of electrostatic interaction.(*56*)

To date, several formulations of Dox comprising drug-loaded micelles of either mixtures of Pluronic® PEO-b-PPO-b-PEO copolymers (SP1049C) or PEG-b-poly(aspartic acid) (NK911) as well as formulations of paclitaxel based on PEG-b-poly(D,L-lactide) (Genexol-PM) or PEG-b-poly(aspartic acid) with some carboxyl residues esterified into 4-phenyl-1-butanolate (NK105) have advanced into clinical trials.(*59*) Many tumor-targeting polymeric micellar formulations are currently in the preclinical development.(*60, 61*)

1.2.1.3. Polymeric Conjugates

Polymeric conjugate-based chemotherapy drug delivery represents another strategy to favorably alter the pharmacokinetics and biodistribution of derivatized drugs and to reduce their severe toxicity to normal body tissues.(*62*) A comprehensive review on the development of polymeric-anti-cancer drug conjugates can be found in Reference(*63*). In all cases, the clinical aims of polymer-drug conjugation are to achieve improved drug targeting to the tumour, to reduce drug toxicity and to overcome the mechanisms of drug resistance. Conjugation to hydrophilic polymeric carriers can also improve the water solubility of hydrophobic drugs such as paclitaxel and Dox, enabling easier formulation and patient administration. Clinical trials of many polymer-anti-cancer drug conjugates are ongoing.(*63*) The polymers used in these conjugates include polyglutamate (PGA), N-(2-hydroxypropyl)methacrylamide (HPMA) copolymer, Dextran, PEG, etc. Among these, a HPMA copolymer-doxorubicin conjugate represents the first synthetic polymer-

anti-cancer conjugate that has entered clinical trials. To date, HPMA copolymer-conjugates have been most extensively studied. Another exciting clinical trial involves a PGA-paclitaxel conjugate. In contrast to HPMA copolymer-drug conjugate, where typically ~10% drug loading is used, this conjugate contains a high drug loading (~37%). In addition, unlike HPMA copolymer, the PGA polymer chain is biodegradable, making it especially attractive.

Almost all the polymeric-drug conjugates in clinical trials displayed increased tumor vascular permeability due to the EPR effect. Tumor-specific targeting of polymeric conjugates has also been rigorously developed. To date, one such targeted conjugate, HPMA copolymer-doxorubicin-galactosamine, has been studied clinically. Many other polymers have also been studied to conjugate with anti-cancer drugs but have not been in clinical trials. Many problems, including inherent polymer-related toxicity, polymer-related immunogenicity, inadequate drug loading, and the use of unsuitable polymer-drug linkers, have limited their further development and remain to be overcome.

1.2.1.4. Solid-lipid Nanoparticles

Solid lipid nanoparticles (SLN) emerged as another type of promising novel nanocarrier to deliver chemotherapy drugs.(*3, 64*) SLNs, with mean diameter typically ranging from 50 to 1000 nm, consist of biodegradable physiological lipids or lipidic substances and stabilizers which are generally recognized as safe (GRAS) or have a regulatory accepted status. They remain in the solid state at both room and body temperature. Compared to other nanosized delivery systems such as liposomes, micelles and polymeric conjugates, SLNs possess various advantages, including easy preparation, long time physical stability

and the possibility of protection of labile drugs from degradation. Furthermore, the cost for large scale production of SLNs is significantly lower than those for liposomal formulations. Additionally, they have fewer storage and drug leakage problems compared to liposomes. Furthermore, it was found that even non-stealth SLNs were able to prolong drug circulation and thus alter the pharmacokinetics of cytotoxic drugs delivered. When it was further coated with PEG, the ability to evade the RES clearance can be further improved. However, unfortunately, there is currently limited data concerning whether drugs delivered by SLN can preferentially accumulate into tumors via the EPR effect.

Compared to other delivery systems, the history of SLN is relatively short. Although many SLNs have been tested in preclinical studies, none have yet to enter clinical trial.(*3*) One of the major challenges facing SLNs has been the low drug loading of hydrophilic, water-soluble anti-cancer drugs. During the SLN preparation process, the lipid is melted and dispersed into lipid droplets of submicron size in aqueous medium to form nanoparticles. The drugs to be encapsulated must be adequately partitioned into these melted lipid droplets to achieve good drug loading. Lipophilic anti-cancer drugs can be efficiently encapsulated into SLNs due to their good partitioning into lipids, however, the loading of a number of hydrophilic or ionic anti-cancer drugs is difficult. This problem can be partially overcome by developing variations of SLN (e.g. polymer-lipid hybrid nanoparticles or lipid-drug conjugate nanoparticles), but will continue to be a major obstacle for the wide application of SLN for anti-cancer drugs.

1.2.1.5. Hollow Nanoparticles

Hollow nanoparticles are a relative new type of nanoparticle that has also been developed as delivery carrier for chemotherapy drugs. In a recent report by Yang et al.(*15*), novel hollow silica nanoparticles (HSNPs), with diameter < 100nm, were synthesized using silica-coated magnetic assemblies, which are composed of a number of Fe_3O_4 nanocrystals, as templates. The core cavity was obtained by removal of the Fe_3O_4 phase with hydrochloric acid and subsequent calcination at high temperature. They demonstrated that ~ 20 wt% Dox can be efficiently loaded into the cavity of the HSNPs. Furthermore, they demonstrated that by modifying the HSNPs with positively-charged amine groups and further PEGylating with PEG, the solubility of HSNPs in aqueous medium was increased and a notable sustained release of Dox from HSNPs was achieved.

In addition to HSNPs, hollow nanoparticles synthesized from other materials such as organic polymer, carbon, and phosphates have also been reported.(*15*) However, their application as delivery carriers for chemotherapy drugs has rarely been reported. We speculate that the inherent hollow structures make it extremely difficult to avoid the premature release of the cytotoxic anti-cancer drugs. Furthermore, it is also very challenging to develop a controlled mechanism for drug release.

1.2.2. Nanotechnology-enabled Delivery Systems for Gene Therapy

Studies of non-viral gene therapy based on plasmid DNA and antisense ODNs have been ongoing for years and research will continue toward improving systemic delivery and transfection efficiencies to the levels required for *in vivo* clinical trials. In contrast, studies on siRNA delivery are still relatively new. With advancements of nanotechnology,

however, researchers are developing various non-viral nanocarriers for efficient delivery and effective release of siRNA at an unprecedented pace.

A comprehensive review on nonviral delivery systems for plasmid DNA and ODN delivery can be found in references.(*65-69*) The most promising nanocarriers that have been developed for siRNA delivery are summarized in these reviews. In general, an ideal non-viral siRNA delivery system needs to meet several criteria: (1) It should protect the siRNA against degradation by nuclease in intracellular matrices; (2) It should deliver the siRNA across cell membrane and efficiently release siRNA into cytoplasm for RNAi. (3) It should have minimal toxicity.

1.2.2.1. Liposomes

Similar to delivery of chemotherapy drugs, liposomes are ideal delivery systems for siRNA. Both neutral liposomes and cationic liposomes have been used for siRNA delivery *in vitro* and *in vivo*.

An early example of using neutral liposomes for *in vivo* delivery of siRNA was demonstrated by Landen et al.(*70*) They used siRNA incorporated into the neutral liposome 1,2-dioleoyl-*sn*-glycero-3-phosphatidylcholine (DOPC) for efficient *in vivo* siRNA delivery into nude mice bearing i.p. ovarian tumors. They found that DOPC-encapsulated siRNA targeting the oncoprotein EphA2 was highly effective in reducing *in vivo* EphA2 expression 48 hours after a single dose. Furthermore, they found that after three weeks of treatment with EphA2-targeting siRNA-DOPC (150 µg/kg twice weekly), tumor growth was reduced when compared with a nonsilencing siRNA. Using the same neutral liposome DOPC, this group further demonstrated(*71*) that a single dose of FAK

siRNA-DOPC was also highly effective in reducing *in vivo* FAK expression for up to 4 days. Treatment with FAK siRNA-DOPC (150 μg/kg twice weekly) reduced mean tumor weight by 44% to 72% in the three cell lines ((HeyA8, A2780-CP20, and SKOV3ip1) compared with the control group.

Compared to neutral liposomes, cationic liposomes have been more widely used to deliver siRNA, similar as the case for delivery of other nucleic acids. Cationic lipids play two roles in liposomal nucleic acid formulations.(*72*) First, they enhance the interaction between the cationic lipid bilayer and the negatively charged nucleic acids, allowing for higher encapsulation efficiency than that which would be achieved using passive loading in neutral liposomes. Cationic lipids also function by providing the liposome with a net positive charge, which in turn enables binding of the nucleic acid complex to negatively charged surface of cell membrane. However, the role of cationic lipids in liposomal uptake presents a dilemma(*72*): highly charged systems are rapidly cleared from the blood, thereby limiting accumulation in target tissues. Neutral liposomes, in contrast, display good biodistribution profiles, but are less efficiently internalized by cells. To avoid these problems, efforts were made to further PEGylate the cationic liposomes, enhancing their stability and circulation in systemic delivery and thus enhancing the accumulation in target sites.

By using such PEGylated cationic liposomes as delivery vehicle for siRNA, a significant breakthrough in RNAi-mediated gene silencing was reported in 2006 by scientists from Alnylam Pharmaceuticals.(*73*) They showed for the first time, that siRNAs, when delivered systemically in a liposomal formulation, can silence the disease target apolipoprotein B (ApoB) in non-human primates. ApoB-specific siRNAs were

encapsulated in stable nucleic acid lipid particles (SNALP), with size of ~80 nm and administered by intravenous injection to cynomolgus monkeys at doses of 1 or 2.5 mg/kg. A single siRNA injection resulted in dose-dependent silencing of ApoB messenger RNA expression in the liver 48 h after administration, with maximal silencing of >90%. Furthermore, significant reductions in ApoB protein, serum cholesterol and low-density lipoprotein levels were observed as early as 24 h after treatment and lasted for 11 days at the highest siRNA dose, thus demonstrating an immediate, potent and lasting biological effect of siRNA treatment. It was noted in their study that the silencing effect of SNALP-formulated siRNA represents more than a 100-fold improvement in potency compared with systemic administration of cholesterol-conjugated siApoB-1 (chol–siApoB-1). It was further worth noting that in their studies, a scalable, extrusion-free method for efficient liposomal encapsulation of siRNA(*74*) was adapted to allow for a high encapsulation efficiency of ~ 92-97%. Using this novel cationic liposomal formulation, Alnylam further obtained promising preclinical data in a rodent model in 2007. These data showed successful silencing of both VEGF and KSP expression in the liver and stopping of cancer cell proliferation by targeting KSP using siRNA therapeutics. Alnylam expects to submit an investigational new drug (IND) application for this program in 2008. Another novel liposomal siRNA formulation based on cationic lipids (siRNA-lipoplex/AtuPLEX), containing neutral fusogenic and PEG-modified lipid components, has been developed by scientists from Silence Therapeutics AG (*75, 76*), and has shown promising preclinical data for the treatment of advanced solid cancer.

1.2.2.2. Cationic Polymers

Synthetic and naturally occurring cationic polymers constitute another type of nanocarriers for efficient delivery of nucleic acids, including siRNA. Due to their positive charges, cationic polymers can rapidly interact with negatively charged siRNA through electrostatic interaction and condense siRNA into nanoparticles. Using an appropriate ratio of siRNA to the cationic polymers, the thus-formed siRNA nanoparticles can be positively charged and thus easily adsorb to negatively charged cell membrane surface and internalize into cells through endocytosis. Many cationic polymers, such as polyethylenimine or imidazole-containing polymers, have protonatable groups between pH 5 and 7, which allow them to escape from endosomes and deliver siRNA into the cytoplasm through the so-called "proton sponge" effect. During the intracellular trafficking, the polycationic nature of these polymers is thought to buffer low endosomal pH through enhanced influx of protons and water, thus maximizing in endosomes rupture.

Many cationic polymers, which had been utilized for delivery of plasmid DNA and antisense ODN, have also been developed as delivery vectors for siRNA. These cationic polymers include polyethylenimine (PEI), poly-L-lysine (PLL), polyallylamine, cationic dextran, chitosan and etc. Among all, PEI has been most widely studied. PEI polymers with different molecular weights, different degrees of branching and different modification have been evaluated for their efficiency in delivering siRNA into cells *in vitro* and *in vivo*.(*77-80*) For example, in one study reported by Urban-Klein et al.,(*77*) it was shown that noncovalent complexation of synthetic siRNAs with low molecular weight polyethylenimine (PEI) efficiently stabilizes siRNAs and delivers siRNAs into cells where they display full bioactivity at completely nontoxic concentrations. More

importantly, in a subcutaneous mouse tumor model, the systemic (intraperitoneal, i.p.) administration of complexed, but not of naked siRNAs, leads to the delivery of the intact siRNAs into the tumors. The i.p. injection of PEI-complexed, but not of naked siRNAs targeting the c-erbB2/neu (HER-2) receptor results in a marked reduction of tumor growth through siRNA-mediated HER-2 downregulation. In a recent communication by Creusat et al.(*80*), it was found that modifying branched PEI with amino acids led to efficient siRNA delivery into mammalian cell lines, even in the presence of serum, and at dose as low as 1 nM.

However, the use of PEI as a gene delivery vector suffers from one major drawback, the toxicity due to its nonbiodegradable nature.(*81, 82*) It is known that the toxicity and gene transfection efficiency of PEI is molecular weight–dependent. The most active commercial PEI is 25K branched PEI (BPEI) and 22K linear PEI (LPEI). PEI with a molecular weight larger than 25K is also active but exhibits greater toxicity. BPEI of 5-10 K appears to be more efficient in gene transfection and less toxic when compared with 25K BPEI.(*83*) PEI of 2K or smaller is relatively nontoxic but not efficient in transfection. In efforts to make low-molecular weight PEI efficient in gene delivery, different approaches have been employed. One approach has been treatment of low–molecular weight PEI with several bifunctional cross-linking reagents, thus generating PEI oligomers that are efficient in transfection. Cross-linking of small PEI with a biodegradable bond such as a disulfide or ester bond resulted in oligomers that were as active as 25K BPEI but significantly less toxic to cells.(*84, 85*) Another novel approach was to covalently coat the surface of non-charged nanoparticles such as gold nanoparticles,(*86*) polymethylacrylate nanogels,(*87*) and silica gels(*88*) with low-

molecular weight PEI and thus increase the transfection efficiency. However, in this approach, due to the non-covalent linking, the toxicity of PEI was also likely to increase.

1.2.2.3. Dendrimers

Dendrimers are a special class of tree-like polymers, with unique molecular structures, with defined molecular weight, surface charge and surface functionality.(*89*) These properties of dendrimers make them ideal delivery carriers for a systematic study, with less complication from the heterogeneity and variable chemistry, commonly seen in other nonviral delivery agents, such as cationic lipids and polyethylenimine (PEI). Of all dendrimers, polycationic dendrimers, such as polypropylenimine (PPI) dendrimers (Figure 1.2) and polyamidoamine (PAMAM) dendrimer (Figure 1.3), can interact with negatively charged nucleic acids directly through electrostatic interaction and are most promising dendrimers for delivery of nucleic acids, including siRNA. In recent years, several reports on using these polycationic dendrimers for efficient siRNA delivery have emerged. In one report by Zhou et al.(*90*), it was found that genuine, nondegraded generation-7 (G-7) PAMAM dendrimers can complex siRNA into nanoparticles that are efficient in internalizing into cancer cells and inducing potent endogenous gene silencing. In another recent report by Patil et al.(*91*), a novel internally quarternized and surface-acetylated poly(amidoamine) generation-4 (G-4) dendrimer (QPAMAM-NHAc) was synthesized and evaluated for intracellular delivery of siRNA. Their data showed that the proposed dendrimer as a nanocarrier possesses several advantages including, low cytotoxicity due to the modified neutral surface, high transfection efficiency, and possible protection of siRNA from degradation due to the compact nanostructures. The application
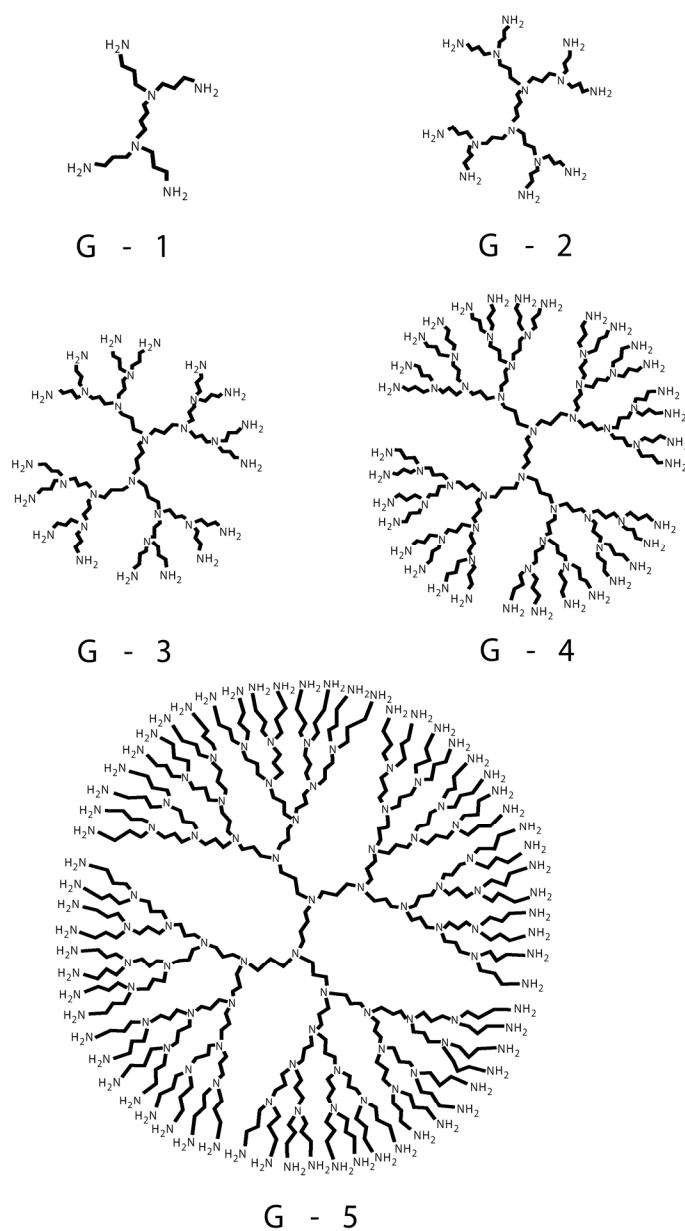
Figure 1.2. Chemical structures of five generations of polypropylenimine dendrimers. The designations are: G-1, generation-1 dendrimer; G-2, generation-2 dendrimer; G-3, generation-3 dendrimer; G-4, generation-4 dendrimer and G-5, generation-5 dendrimer.
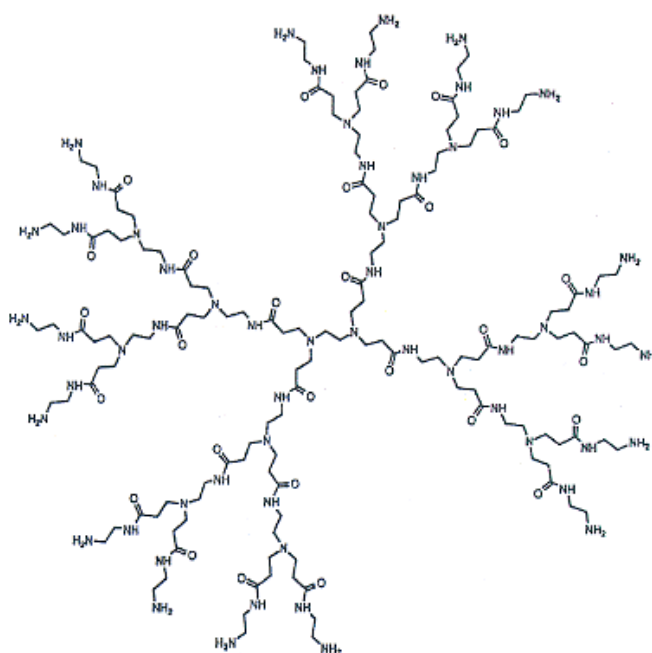
Figure 1.3. Chemical structure of generation-2 polyamidoamine dendrimer.

of PPI dendrimers for siRNA delivery was recently studied by our group.(*92*) It was found that while G3, G4 G5 PPI dendrimers are all able to complex siRNA into nanostructures and deliver into cancer cells, the transfection efficiency of PPI dendrimers is the highest for G4 PPI dendrimer, followed by G5 PPI and G3 PPI. Overall, the application of dendrimers for siRNA delivery is still in its early stage and more systematic studies should be performed to further explore the unique properties of this special class of polymers for siRNA delivery.

1.2.2.4. Inorganic Nanoparticles

In addition to organic nanoparticles including liposomes, cationic polymers and dendrimers, inorganic nanoparticles are another category of nanocarriers that have been actively explored for gene transfection as well as the tracking and imaging of gene transfection process. Unlike liposomes or polymers, the size and shape of engineered

inorganic nanoparticles can be controlled precisely, thus conferring them with more flexibility for gene transfection optimization. Furthermore, inorganic nanoparticles often posses unique optical, magnetic, or electrical properties that can be used for imaging and thus make them ideal multifunctional platforms, combining therapeutic and imaging functions together. Up to date, inorganic nanoparticles have been engineered from a variety of materials, and among those most widely studied for gene transfection are carbon nanotubes, quantum dots, paramagnetic iron oxide nanoparticles, gold nanoparticles, silica nanoparticles as well mesoporous silica nanoparticles.
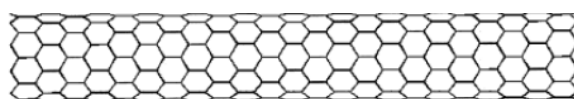
Figure 1.4. A schematic drawing of a SWNT

Carbon nanotubes have recently emerged as a new family of inorganic nanoparticles for nuclei acid delivery. While both single-walled carbon nanotubes (SWNTs) and multiwalled carbon nanotubes (MWNTs) have been employed for this purpose, SWNTs are most widely studied. SWNTs have a diameter of close to 1 nanometer, with a tube length that can be hundreds or thousands of nm (Figure 1.4). It has been found that the toxicity of SWNTs is mainly dependent on their functionalization (*93-95*) and SWNTs with suitable functionalization have been shown to deliver siRNAs across the cell membrane without toxicity either *in vitro* or *in vivo*. For example, Xu *et al.* have used ammonium-functionalized SWNTs to deliver siRNA targeted to cyclin A2 in chronic myelogenous leukemia K562 cells, resulting in suppression of cyclin A2 expression.(*96*) The ammonium-functionalized SWNTs was also employed to mediate

the delivery of telomerase reverse transcriptase (TERT) siRNA into tumor cells,(*97*) wherein the siRNAs successfully silenced the targeted TERT gene, which is critical for the development and growth of tumors. Injection of this complex in mice bearing Lewis lung carcinoma tumor was further shown to inhibit tumor growth and reduce the average tumor weight when compared to that of the untreated animals. The remarkable efficiency of SWNTs to deliver siRNA into human T cells and primary cells was recently demonstrated by Dai and his colleagues.(*98*) They showed that by conjugating siRNA onto PEGylated SWNTs via a cleavable disulfide bond, superior silencing effect over conventional liposome-based nonviral agents was achieved.

Quantum dots, highly luminescent semiconducting nanoparticles, are another type of inorganic nanoparticles that have been explored for siRNA delivery as well as for imaging.(*99, 100*) Using a PEGylated quantum dot (QD) core as a scaffold and conjugating siRNA and tumor-homing peptides (F3) onto the surface, Derfus et al. have demonstrated targeted delivery of siRNA into tumor cells and efficient silencing of the target genes.(*99*) Recently, Yezhelyev et al. (*100*) have used QDs to achieve 10−20-fold improvement in siRNA gene silencing efficiency and 5−6-fold reduction in cellular toxicity. In this approach, they formed a proton-sponge layer on the QD surface by covalent grafting of tertiary amine groups to ensure efficient siRNA release from intracellular vesicles. They have also shown that the QD-siRNA nanoparticles are dual-modality optical and electron microscopy (EM) probes, allowing for real-time tracking and ultrastructural localization of QDs during delivery and transfection. However, despite their attractive properties, QDs are composed of cytotoxic cadmium selenide and are

often difficult to shield from the cellular medium and present a significant toxicity issue for in-vivo application. Up to date, QDs have not been approved for human use.

Superparamagnetic iron oxide nanoparticles (SPIONs) have attracted much attention as an alternative to QDs due to its low toxicity. SPIONs have been approved by FDA for human use as an MRI contrast agent. Development of SPIONs for tumor imaging or DNA delivery have been a while, however, development of SPIONs as dual-purpose probes for *in vivo* transfer of siRNA and the simultaneous imaging of its accumulation in tumors is still very new. This dual-purpose probe was recently developed by Medarova et al.(*101*) In their design, they labeled the SPIONs with a near-infrared probe and covalently linked with siRNA molecules specific for model or therapeutic targets. Additionally, they modified the nanoparticles with a membrane translocation peptide for intracellular delivery. They showed the feasibility of *in vivo* tracking of tumor uptake of these probes by MRI and optical imaging in two separate tumor models.

Gold nanoparticles (GNPs) have been used as an attractive nanocarrier for delivery of various payloads, including small molecules or large molecules, like proteins, DNA or RNA. Many properties make GNPs particularly attractive and these properties include ease of synthesis, low toxicity, ready functionalization as well as their unique photo-physical properties due to the surface plasmon resonance. For this reason, GNPs have recently also emerged as an efficient siRNA delivery vehicles.(*102-104*) One such effort was reported by Baea et al.(*103*). They have developed gold nanoparticles chemically modified with primary amine groups as intracellular delivery vehicles for therapeutic siRNA. They found that the positively charged gold nanoparticles could form stable polyelectrolyte complexes with negatively charged siRNA–polyethylene glycol

(PEG) conjugates having a cleavable disulfide linkage under reductive cytosol condition. The resultant core/shell type siRNA-containing nanoparticles were efficiently internalized in human prostate carcinoma cells, and significantly silenced the target genes without showing severe cytotoxicity. Smart PEGylated gold nanoparticles were also developed for cytoplasmic delivery of siRNA to induce enhanced gene silencing in HuH-7 cells.(*102*) In this approach, siRNA were modified with thiols and then grafted onto gold nanoparticles, taking advantage of the unique properties of gold nanoparticles to react with thiol group.

Promising data on using silica nanoparticles for gene delivery have been obtained in recent years. For example, silica nanoparticles modified with aminosilanes were reported to condense and deliver DNA into cells.(*105, 106*) Bharali et al. recently reported another success in using organically-modified silica nanoparticles (namely ORMOSIL) for *in vivo* gene delivery in brain.(*107*) The ORMOSIL's transfection efficiency was equal to or even better than Herpes Simplex Virus-1 (HSV-1). Moreover, the ORMOSIL-mediated delivery does not cause the tissue damage or immunological side effects that have been commonly observed with viral-mediated gene delivery. Mesoporous silica nanoparticles (MSNs), a special type of silica nanoparticles with uniform pore structures, has also been developed as efficient delivery vehicle for plasmid DNA.(*108*) In this design, low-generation PAMAM dendrimers were covalently modified on the surface of MSNs, thus making it an efficient transfection agent. However, to date, development of silica nanoparticles for siRNA delivery has been rarely reported. We envision that the good biocompatibility and superior tunability of silica nanoparticles, including MSNs, would make it also an ideal nanocarrier for siRNA delivery, and

exploring silica nanoparticles for siRNA delivery is not only interesting but also important.

1.2.3. Nanotechnology-enabled Co-delivery Systems for Simultaneous Delivery of Chemotherapy and Gene Therapy

While a significant progress has been made in combining the chemotherapy and gene therapy together for a synergistic anti-cancer efficacy, most efforts have focused on delivering chemotherapy and gene therapy through different routes. However, for *in vivo* application, it would be more advantageous to deliver the gene therapy and chemotherapy drugs in the same vehicle so that both drugs could be delivered to the same cells with similar ratio for combined actions and synergistic effects. While viral vectors are not feasible in achieving this, non-viral vectors, including liposomes and other nanoparticles, should have great potential as co-delivery systems due to their versatile structures. However, up until now, the development of co-delivery systems that can simultaneously deliver chemotherapy drug and gene therapy drug in a single vehicle is still in a very early stage, with only a few efforts reported.

One of such efforts was reported by Wang et al.(*109*) In their report, cationic core-shell nanoparticles (or micelles), that were self-assembled from a biodegradable amphiphilic copolymer, were used to successfully co-deliver a chemotherapy drug, paclitaxel, with an interleukin-12-encoded plasmid into cancer cells. They found that the co-delivery of drugs and DNA suppressed cancer growth more efficiently than the delivery of either paclitaxel or the plasmid alone in a 4T1 mouse breast cancer model. Moreover, they demonstrated the co-delivery of paclitaxel with Bcl-2-targeted small

interfering RNA (siRNA) increased cytotoxicity in MDA-MB-231 human breast cancer cells.

In another series of experiments investigated by Tamara Minko's group,(*110*) liposomes were used to codeliver antisense ODN and chemotherapy drugs into cancer cells. In their studies, antisense ODNs targeted against mRNAs encoding several multidrug resistance proteins (Bcl-2, MDR-1 or MRP-1) were chosen. They found that co-delivery of doxorubicin (Dox) and antisense ODN by liposomes substantially increased their specific activity. Furthermore, their data showed that simultaneous suppression of pump and nonpump resistance dramatically enhanced the ability of Dox for inducing apoptosis leading to higher *in vitro* cytotoxicity and *in vivo* antitumor activity.

Recent studies have shown that mesoporous silica nanoparticles (MSNs) with various functionalizations can efficiently internalize into mammalian cells via an endocytosis pathway.(*111, 112*) Its large pore volumes and surface areas make it an ideal platform to load a large amount of chemical drugs inside the pores (*113, 114*) and genes on the surface and then simultaneously deliver into cells.(*115*) Lin and co-workers (*108, 115*) reported that by encapsulating a fluorescent dye inside the pores and complexing with plasmid DNA on the surface, MSNs can efficiently deliver the plasmid DNA into cancer cells using the fluorescent dye to visualize the interaction of MSNs and cells.(*108*) In another recent report by them,(*116, 117*) it was further demonstrated that MSNs can simultaneously deliver DNA and chemicals into plants. However, this ideal feature of MSNs has yet to be utilized to codeliver a chemotherapy drug together with a gene therapy drug for a synergistic anti-cancer efficacy.

1.3. Obstacles for *in vivo* Systemic Delivery of Chemotherapy and Gene Therapy for Cancer Treatment

A good fundamental understanding of any delivery systems *in vitro* is the foundation for their further application *in vivo*. However, one must be aware that a perfect *in vitro* performance does not necessarily guarantee a success *in vivo*.

The challenges facing the *in vivo* systemic delivery of drugs are very different from those facing the *in vitro* delivery.(*118, 119*) When nanoparticles are administered intravenously, they become recognizable by the non-specific immune system of the body, the reticulo-endothelial system (RES), and are subsequently cleared from the circulation by phagocytosis, through a process called opsonization.(*120, 121*) An opsonin is a proteinaceous molecule that acts as a binding enhancer for the process of phagocytosis. Phagocytic cells express receptors that bind opsonin molecules. As a result, the chances of nanoparticles reaching the targeting tissues are greatly diminished. Therefore the first challenge for systemic delivery of drugs by nanoparticles is to increase the circulation time of the delivery system in the blood. It has been reported that by modifying nanoparticles with hydrophilic PEG polymer on the surface, longer blood circulation time and retention in the body can be achieved and the removal of nanoparticles due to the immune response can be overcome.(*121*) It was suggested that the adsorption of opsonins and other serum proteins can be reduced by the PEG molecules on the surface of nanoparticles through a mechanism known as the steric repulsion effect.(*122*) Due to the chain flexibility and electrical neutrality of the PEG backbone, it has been hypothesized that PEG molecules on the surface of a nanoparticle will form a dynamic molecular "cloud" over the particle surface.(*123*) This cloud of mobile and flexible PEG molecules

imparts a repulsive effect which makes it energetically unfavorable for proteins to adsorb to PEG molecules. Up to now, PEGylation is still the most common approach to increase the circulation of nanoparticles in blood.

The second major challenge of systemic delivery of drugs, especially the toxic chemotherapy drugs for cancer therapy, is their adsorption to normal body tissues. This challenge can be partially overcome by using the nanoparticles as delivery systems.(*3-15*) The sub-micron size featured by most nanoparticles enabled them to preferentially extravasate into the tumor and be retained there, known as enhanced permeability and retention (EPR) effect, due to the abnormal tumor vasculature with increased vessel permeability and poor lymphatic drainage. This phenomenon is constantly called passive targeting.(*124*) However, this passive targeting is not clinically satisfactory. The treatment of cancers by chemotherapy drugs delivered by nanoparticles has still been largely hampered by their toxic side effects to normal body tissues. Furthermore, for most chemotherapy drugs such as Dox, the toxicity to normal body tissues can also be accumulated and thus limit the total dose that may be administered to each patient.(*119*) Therefore, it is of urgent need to develop delivery systems that can deliver chemotherapy drugs to tumor tissues with greater target specificity (i.e. active targeting).(*125*) Thanks to the versatile structures and relatively large surface area of nanoparticles, one common approach has been to tag the nanoparticle surfaces with cancer-targeting ligands, which can specifically interact with receptors that are only rich in cancer cells.(*125*) This active tumor-targeting has been implemented in many delivery systems that are under preclinical or clinical trials and will continue to be a preferred approach for delivery of cancer therapy.

In addition to the above two challenges, for systemic delivery of gene therapy drugs, including siRNA delivery, there exists another major obstacle, which is the stability in the extracellular environment before reaching the target sites.(*126*) It was reported that siRNA can be rapidly degraded by the nucleolytic enzymes present in the extracellular environment and therefore necessary protection should be made before subjecting siRNA to systemic delivery.(*127*) It was found that by complexing the siRNA with cationic polymers, or loading into liposomes and other nanoparticles, the extracellular stability of siRNA can be greatly improved; however, further protection by PEGylation is often needed to ensure satisfactory protection from the aggressive extracellular environment and to achieve a sufficient stability for systemic delivery.

In summary, there has been great progress on utilizing nanotechnology-enabled non-viral delivery systems to resolve the numerous challenges facing effective cancer therapy. However, the lack of non-viral delivery systems that can efficiently deliver the gene therapy drug or chemotherapy drug into their target sites with minimal side effects remains one of the biggest challenges. In addition, the development of multidrug resistance in cancer cells is another major hurdle for effective cancer chemotherapy. Therefore, therapeutic strategies to overcome drug resistance should have a great impact on the treatment of cancer. To effectively suppress the overall cancer resistance to chemotherapy, it is essential to simultaneously inhibit both pump and nonpump mechanisms of cellular resistance. Special sequences of siRNAs targeted against mRNA encoding major proteins responsible for pump and nonpump cellular defense have been developed and showed a substantial efficacy in vitro. Co-delivery of such types of siRNA with a traditional anti-cancer drug to cancer cells is therefore very promising for

overcoming the resistance and enhancing the anti-cancer efficacy, however, efficient co-delivery methods/systems that can codeliver siRNA and anti-cancer drugs into cancer cells have rarely been reported or developed.

1.4. Specific Aims

This thesis is focused on utilizing nanotechnology to develop novel non-viral nanocarriers for efficient delivery of gene therapy, chemotherapy and co-delivery of both into cancer cells for effective cancer therapy.

There has been considerable literature on the condensation of plasmid and long linear DNA to nanoparticles. However, investigations into the condensation of short ODNs or siRNAs to nanoparticles are scant, even though their transfection has been widely studied. The unique molecular structures of PPI dendrimers made them ideal platforms for a systematic study, with less complication from heterogeneity and variable chemistry. Furthermore, polypropylenimine (PPI) dendrimers are members of a class of amine-terminated polymers, demonstrated to be efficient gene delivery vectors in a wide range of mammalian cell lines. Thus, studies on structure-activity relationships of PPI dendrimers are expected to have important therapeutic applications. For this reason, in **Chapter 2**, using atomic force microscopy, combined with other traditional techniques, we have systematically studied the efficacy of five generations (G-1 to G-5) of PPI dendrimers to provoke nanoparticle formation from a 21-nucleotide (nt) antisense ODN. For the first time, we revealed the mechanism of how short 21-nucleotide (nt) antisense ODNs can be packaged into nanometer-scale nanoparticles. We demonstrated ODN nanoparticles formed with G-4 and G-5 dendrimers could undergo facile transport in a

breast cancer cell line, MDA-MB-231. Our results showed that the structure and charge density of the dendrimers are important in ODN nanoparticle formation and cellular transport and that G-4 and G-5 dendrimers are useful in cellular delivery of antisense ODN.

While higher generation dendrimers show higher cytotoxicity(*128-130*) and their synthesis and purification are usually tedious with low yield, low generation dendrimers are nontoxic and easy to synthesize.(*131-133*) However, as found in Chapter II as well as in other literatures,(*134*) the limited surface charge of low generation dendrimers makes them inefficient in complexing with nucleic acids and delivering into cells. To conquer this limitation, in **Chapter 3**, we advanced our study of PPI dendrimers and developed a novel approach to efficiently package and deliver siRNAs with low generation PPI dendrimers by using Au nanoparticles (NPs) as a "labile catalytic" packaging agent. The Au NPs helped low generation dendrimers to package nucleic acids but are not included in the final siRNA complexes. Compared to the siRNA particles fabricated by low generation dendrimers alone (G3 PPI), the siRNA nanoparticles packaged through this novel approach (by Au nanoparticles modified with G3 PPI) can efficiently internalize into cancer cells and the internalized siRNAs can efficiently silence their target mRNA. The efficiency is even superior to higher generation dendrimers (G5 PPI). More importantly, this approach provides a possibility to remove the gold nanoparticles before the nucleic acid nanoparticles are delivered, therefore the possible long-term toxic problem accompanied with the Au nanoparticles can be solved. This is a new concept in using inorganic engineered nanoparticles in nucleic acid packaging and delivery applications.

Mesoporous silica nanoparticles (MSNs), with tunable diameters of 50-300 nm and pore size of 2-10 nm, has recently emerged as a novel intracellular drug delivery system due to its uniform pore structures, high surface area and pore volumes, high chemical and physical stability as well as its easy functionalization.(*135-139*) MSNs with different functionalization were found to efficiently internalize into different cells without cytotoxic effects and with good biocompatibility. Furthermore, the large pore volumes and surface areas of MSNs make it an ideal platform to load a large amount of chemical drugs inside the pores (*113, 114*) and genes on the surface and then simultaneously deliver into cells.(*115*) However, to date, MSNs have rarely been used as a delivery carrier for chemotherapy drugs. Its utilization as a delivery carrier for siRNA or as a co-delivery carrier for simultaneous delivery of an anti-cancer drug together with siRNAs for a synergistic cancer therapy effect has yet to be reported.

Relying on the fundamental understanding gained from Chapters II and III, we were determined to continue the utilization of dendrimers and developed PAMAM dendrimer-modified mesoporous silica nanoparticles (MSNs) as a stimuli-responsive controlled-release delivery system for chemotherapy drug, and as an efficient co-delivery system for simultaneous delivery of chemotherapy drug and siRNA drug into cancer cells for effective cancer therapy (**Chapters 4-8**).

In **Chapter 4**, we developed PAMAM dendrimer-modified MSNs as an intracellular controlled release delivery system to load a representative anti-cancer drug, doxorubicin, at a very high loading capacity (up to 220 wt%) into the MSN pores and then efficiently deliver into human ovarian cancer cells. We have successfully used a non-gatekeeping approach in achieving nearly zero release of Dox in H_2O while stimuli-

responsive controlled and complete release once delivered into the cancer cells. In order to achieve the high loading capacity, we have employed a design that allows multiple interactions between Dox and pore surfaces, including hydrophobic interaction, electrostatic interaction, hydrogen bonding as well as possible chemical conjugation. We further demonstrated that the Dox delivered by our system are highly toxic and very effective in killing cancer cells.

Development of multidrug resistance in cancer cells and adverse side effects are the major obstacles for effective cancer chemotherapy. Therapeutic strategies to overcome drug resistance and specific tumor targeting with minimal premature drug release should have a great impact on the treatment of cancer. In **Chapter 5**, we made the first effort of utilizing MSNs as a co-delivery system to simultaneously deliver Doxorubicin (Dox) (as a model hydrophobic apoptosis-inducing anti-cancer drug), and a Bcl-2-targeted siRNA (as a suppressor of cellular antiapoptotic defense) into A2780/AD human ovarian cancer cells for enhanced chemotherapy efficacy. Our results showed that by delivering Dox and Bcl-2 siRNA simultaneously into cancer cells, the Bcl-2 siRNA can effectively silence the Bcl-2 mRNA and significantly suppress the antiapoptotic cellular defense of Bcl-2 protein, thus conquering the non-pump resistance and substantially enhancing the anti-cancer action of Dox. Furthermore, the Dox was primarily localized in perinuclear region after internalization, possibly bypassing the efflux pump induced by membrane-associated P-gp and further enhancing the cytotoxicity. We envisioned that this co-delivery system can be generalized to other anti-cancer drugs and other cancer cell lines for a synergistic cancer therapy effect.

In **Chapter 6**, we took further efforts to systematically investigate the effect of each component in our PAMAM-dendrimer modified MSN-based co-delivery system on the siRNA uptake efficiency and its intracellular release and localization. Our result suggested it is highly likely that the same component may play different roles when used in different multi-component delivery system and this needs to be seriously taken into account in designing multi-component delivery system. Furthermore, our data suggested that the Dox in our co-delivery system of MSN-Dox-G2-siRNA is very critical for homogeneous distribution of siRNA inside cells and in ensuring the effective gene knockdown of siRNA. Without Dox, although the delivery system of MSN-G2 was still able to efficiently deliver siRNA into cells, the delivered siRNA was distributed in discrete large aggregates inside cells and was not able to silence the targeted mRNA.

In **Chapter 7**, in an attempt to understand the internalization mechanism of the delivery system of MSN-Dox-G2, we have studied the effect of temperature and different inhibitors on the cell uptake efficiency by use of flow cytometry. The cells were treated with different temperatures or without/with different endocytosis inhibitors at 37 °C. Our data showed that none of the endocytosis inhibitors under study inhibited the cell uptake of our delivery system MSN-Dox-G2. Furthermore, we have found that while internalization of free Dox was almost completely inhibited at 4 °C, the internalization of MSN-Dox-G2 was not inhibited at 4 °C at all, with intracellular concentration of Dox in cells even slightly higher than those cells incubated at 37 °C. Our results together suggest that MSN-Dox-G2 possibly internalize into cells through a non-endocytic, energy and temperature-independent process.

To make our co-delivery system applicable in vivo and to achieve tumor cell targeted delivery, in **Chapter 8**, we further PEGylated the MSN-Dox-G2/siRNA complex and then tagged it with a specific cancer-targeting group, Luteinizing hormone-releasing hormone (LHRH) peptide, which can be targeted for tumor cells in which LHRH receptors are over-expressed, including breast, lung, ovarian and prostate cancer cells. Our data demonstrated that the complex thus packaged enhanced the serum stability for up to 48 h and the complex conjugated with tumor cell targeting moiety can be efficiently internalized into LHRH-receptor positive cancer cells such as A549 lung cancer cells and A2780/AD cancer cells while showed minimal internalization into LHRH-receptor negative cancer cells such as SKOV-3 cancer cells.

1.5. References

1. Goodman, L. S., Wintrobe, M. M., Dameshek, W., Goodman, M. J., Gilman, A., and McLennan, M. T. (1946) Nitrogen mustard therapy, *JAMA 132*, 26-32.

2. (2008) What Are the Different Types of Chemotherapy Drugs?, American Cancer Society.

3. Wong, H. L., Bendayan, R., Rauth, A. M., Li, Y., and Wu, X. Y. (2007) Chemotherapy with anti-cancer drugs encapsulated in solid lipid nanoparticles, *Advanced Drug Delivery Reviews 59*, 491-504.

4. Minko, T., Kopeckova, P., and Kopecek, J. (2000) Efficacy of the chemotherapeutic action of HPMA copolymer-bound doxorubicin in a solid tumor model of ovarian carcinoma, *Int. J. Cancer. 86*, 108-117.

5.   Lam, W., Leung, C.-H., Chan, H.-L., and Fong, W.-F. (2000) Toxicity and DNA binding of dextran-doxorubicin conjugates in multidrug-resistant KB-V1 cells: optimization of dextran size, *Anti-cancer Drugs 11*, 377-384.

6.   Dubowchik, G. M., Firestone, R. A., Padilla, L., Willner, D., Hofstead, S. J., Mosure, K., Knipe, J. O., Lasch, S. J., and Trail, P. A. (2002) Cathepsin B-Labile Dipeptide Linkers for Lysosomal Release of Doxorubicin from Internalizing Immunoconjugates: Model Studies of Enzymatic Drug Release and Antigen-Specific In Vitro Anti-cancer Activity, *Bioconjugate Chemistry 13*, 855-869.

7.   Gillies, E. R., and Frechet, J. M. J. (2005) pH-Responsive Copolymer Assemblies for Controlled Release of Doxorubicin, *Bioconjugate Chemistry 16*, 361-368.

8.   Nystrom, A. M., Xu, Z., Xu, J., Taylor, S., Nittis, T., Stewart, S. A., Leonard, J., and Wooley, K. L. (2008) SCKs as Nanoparticle Carriers of Doxorubicin: Investigation of Core Composition on the Loading, Release and Cytotoxicity Profiles, *Chem. Commun.*, 3579-3581.

9.   Goren, D., Horowitz, A. T., Tzemach, D., Tarshish, M., Zalipsky, S., and Gabizon, A. (2000) Nuclear delivery of doxorubicin via folate-targeted liposomes with bypass of multidrug-resistance efflux pump, *Clinical Cancer Research 6*, 1949-1957.

10.   Missirlis, D., Kawamura, R., Tirelli, N., and Hubbell, J. A. (2006) Doxorubicin Encapsulation and Diffusional Release from Stable, Polymeric, Hydrogel Nanoparticles, *European Journal of Pharmaceutical Sciences 29*, 120-129.

11. Lee, E. S., Na, K., and Bae, Y. H. (2005) Doxorubicin loaded pH-sensitive polymeric micelles for reversal of resistant MCF-7 tumor, *Journal of controlled release 103*, 405-418.

12. Wong, H. L., Bendayan, R., Rauth, A. M., Xue, H. Y., Babakhanian, K., and Wu, X. Y. (2006) A mechanistic study of enhanced doxorubicin uptake and retention in multidrug resistant breast cancer cells using a polymer-lipid hybrid nanoparticle system, *J. Pharm. Exper. Ther. 317*, 1372-1381.

13. Choucair, A., Soo, P. L., and Eisenberg, A. (2005) Active Loading and Tunable Release of Doxorubicin from Block Copolymer Vesicles, *Langmuir 21*, 9308-9313.

14. Jayant, S., Khandare, J. J., Wang, Y., Singh, A. P., Vorsa, N., and Minko, T. (2007) Targeted Sialic Acid–Doxorubicin Prodrugs for Intracellular Delivery and Cancer Treatment, *Pharmaceutical Research 24*, 2120-2130.

15. Yang, J., Lee, J., Kang, J., Lee, K., Suh, J.-S., Yoon, H.-G., Huh, Y.-M., and Haam, S. (2008) Hollow Silica Nanocontainers as Drug Delivery Vehicles, *Langmuir 24*, 3417-3421.

16. Kozubek, A., Gubernator, J., Przeworska, E., and Stasiuk, M. (2000) Liposomal drug delivery, a novel approach: PLARosomes, *Acta Biochimica Polonica 47*, 639-649.

17. Ishidaa, T., Kirchmeiera, M. J., Moasea, E. H., Zalipskyb, S., and Allen, T. M. (2001) Targeted delivery and triggered release of liposomal doxorubicin enhances cytotoxicity against human B lymphoma cells, *Biochimica et Biophysica Acta (BBA) - Biomembranes 1515*, 144-158.

18. Wollina, U., Dummer, R., Brockmeyer, N. H., Konrad, H., Busch, J.-O., Kaatz, M., Knopf, B., Koch, H.-J., and Hauschild, A. (2003) Multicenter Study of Pegylated Liposomal Doxorubicin in Patients with Cutaneous T-Cell Lymphoma, *Cancer 98*, 993-1001.

19. Samad, A., Sultana, Y., and Aqil, M. (2007) Liposomal Drug Delivery Systems: An Update Review, *Current Drug Delivery 4*, 297-305.

20. Muggia, F. M. (2001) Liposomal encapsulated anthracyclines: new therapeutic horizons, *Current oncology reports 3*, 156-162.

21. Martino, R., Perea, G., Caballero, M. D., Mateos, M. V., Ribera, J. M., Oteyza, J. P. D., Arranz, R., Terol, M. J., Sierra, J., and Miguel, J. F. S. (2002) Cyclophosphamide, pegylated liposomal doxorubicin (Caelyx), vincristine and prednisone (CCOP) in elderly patients with diffuse large B-cell lymphoma: results from a prospective phase II study, *Haematologica 87*, 822-827.

22. Wollina, U., Graefe, T., and Karte, K. (2000) Treatment of relapsing or recalcitrant cutaneous T-cell lymphoma with pegylated liposomal doxorubicin, *Journal of the American Academy of Dermatology 42*, 40-46.

23. Avilés, A., Neri, N., Castañeda, C., Talavera, A., Huerta-Guzmán, J., and González, M. (2002) Pegylated liposomal doxorubicin in combination chemotherapy in the treatment of previously untreated aggressive diffuse large-B-cell lymphoma, *Medical Oncology 19*, 55-58.

24. Kalota, A., Shetzline, S. E., and Gewirtz, A. M. (2004) Progress in the development of nucleic acid therapeutics for cancer, *Cancer Biology and Therapy 3*, 4-12.

25.   Baker, B. F., and Monia, B. P. (1999) Novel Mechanisms for Antisense-Mediated Regulation of Gene Expression, *Biochimica et Biophysica Acta 1489*, 3-18.

26.   Crooke, S. T. (1999) Molecular Mechanisms of Action of Antisense Drugs., *Biochimica et Biophysica Acta 1489*, 31-44.

27.   Patil, S. D., Rhodes, D. G., and Burgess, D. J. (2005) DNA-Based Therapeutics and DNA Delivery Systems: A Comprehensive Review, *The AAPS Journal 7*, 61-77.

28.   Fire, A., Xu, S., Montgomery, M. K., Kostas, S. A., Driver, S. E., and Mello, C. C. (1998) Potent and specific genetic interference by double-stranded RNA in Caenorhabditis elegans, *Nature 391*, 806-811.

29.   Elbashir, S. M., Harborth, J., Lendeckel, W., Yalcin, A., Weber, K., and Tuschl, T. (2001) Duplexes of 21-nucleotide RNAs mediate RNA interference in cultured mammalian cells, *Nature 411*, 494-498.

30.   (2006) Gene Therapy for Cancer: Questions and Answers, National Cancer Institute.

31.   Nemunaitis, J., Landers, S. A., Mccarty, T. M., and Kuhn, J. A. (1999) Cancer treatment involving the p53 gene, *BUMC Proceedings 12*, 93-96.

32.   Fukuda, T., Chen, L., Endo, T., Tang, L., Lu, D., Castro, J. E., Widhopf, G. F., Rassenti, L. Z., Cantwell, M. J., Prussak, C. E., Carson, D. A., and Kipps, T. J. (2008) Antisera induced by infusions of autologous Ad-CD154-leukemia B cells identify ROR1 as an oncofetal antigen and receptor for Wnt5a, *PNAS 105*, 3047-3052.

33. Pakunlu, R. I., Wang, Y., Tsao, W., Pozharov, V., Cook, T. J., and Minko, T. (2004) Enhancement of the efficacy of chemotherapy for lung cancer by simultaneous suppression of multidrug resistance and antiapoptotic cellular defense: novel multicomponent delivery system, *Cancer Research 64*, 6214-6224.

34. Manoharan, M. (2004) RNA interference and chemically modified small interfering RNAs, *Current Opinion in Chemical Biology 8*, 570-579.

35. Marshall, E. (1999) Gene Therapy Death Prompts Review of Adenovirus Vector, *Science 286*, 2244-2245.

36. Lin, T., Zhang, L., Davis, J., Gu, J., Nishizaki, M., Ji, L., Roth, J. A., Xiong, M., and Fang, B. (2003) Combination of TRAIL Gene Therapy and Chemotherapy Enhances Antitumor and Antimetastasis Effects in Chemosensitive and Chemoresistant Breast Cancers, *Molecular Therapy 8*, 441-448.

37. Park, J. O., Lopez, C. A., Gupta, V. K., Brown, C. K., Mauceri, H. J., Darga, T. E., Manan, A., Hellman, S., Posner, M. C., Kufe, D. W., and Weichselbaum, R. R. (2002) Transcriptional control of viral gene therapy by cisplatin, *The Journal of Clinical Investigation 110*, 403-410.

38. Feynman, R. P. (1960) There's Plenty of Room at the Bottom, *Engineering and Science magazine XXIII*.

39. Drexler, K. E. (1986) *Engines of Creation: The Coming Era of Nanotechnology*, Doubleday.

40. Ahmad, S. (2007) Nanotechnology in Drug Delivery: Introduction and Recent Developments, *The Internet Journal of Nanotechnology 2*.

41.   Matsumura, Y., and Maeda, H. (1986) A New Concept for Macromolecular Therapeutics in Cancer Chemotherapy:Mechanism of Tumoritropic Accumulation of Proteins and the Antitumor Agent Smancs, *Cancer Research 46*, 6387-6392.

42.   Gabizon, A. A. (1995) Liposome circulation time and tumor targeting: implications for cancer chemotherapy, *Advanced Drug Delivery Reviews 16*, 285-294.

43.   Bella, N. J. D., Khan, M. M., Dakhil, S. R., Logie, K. W., Marsland, T. A., Weinstein, R. E., Mirabel, M. Y., and Asmar, L. (2003) Pegylated liposomal doxorubicin as single-agent treatment of low-grade non-Hodgkin's lymphoma: a phase II multicenter study, *Clinical lymphoma 3*, 235-240.

44.   Yoshida, o., Oide, N., Sakamoto, T., Yotsumoto, S., Negishi, Y., Tsuchiya, S., and Aramaki, Y. (2006) Induction of cancer cell-specific apoptosis by folate-labeled cationic liposomes, *Journal of controlled release 111*, 325-332.

45.   Huth, U. S., Schubert, R., and Peschka-Süss, R. (2006) Investigating the uptake and intracellular fate of pH-sensitive liposomes by flow cytometry and spectral bio-imaging, *Journal of controlled release 110*, 490-504.

46.   Saitoa, R., Krauzea, M. T., Bringasa, J. R., Nobleb, C., McKnightc, T. R., Jacksonc, P., Wendlandc, M. F., Mamotb, C., Drummondd, D. C., Kirpotind, D. B., Hongd, K., Bergera, M. S., Parkb, J. W., and Bankiewicz, K. S. (2005) Gadolinium-loaded liposomes allow for real-time magnetic resonance imaging of convection-enhanced delivery in the primate brain, *Experimental Neurology 196*, 381-389.

47.   Bangham, A. D. (1980) *Liposomes in biological systems*, John Wiley and Sons: Chichester.

48.   Noble, C. O., Kirpotin, D. B., Hayes, M. E., Mamot, C., Hong, K., Park, J. W., Benz, C. C., Marks, J. D., and Drummond, D. C. (2004) Development of ligand-targeted liposomes for cancer therapy, *Expert Opinion on Therapeutic Targets 8*, 335-353.

49.   Tseng, Y.-L., Liu, J.-J., and Hong, R.-L. (2002) Translocation of Liposomes into Cancer Cells by Cell-Penetrating Peptides Penetratin and Tat: A Kinetic and Efficacy Study, *Molecular Pharmacology 62*, 864-872.

50.   Sapra, P., Tyagi, P., and Allen, T. M. (2005) Ligand-targeted liposomes for cancer treatment, *Current Drug Delivery 2*, 369-381.

51.   Pan, X., and Lee, R. J. (2008) Tumour-selective drug delivery via folate receptor-targeted liposomes, *Expert Opinion on Drug Delivery 1*, 7-17.

52.   Lukyanov, A. N., Elbayoumi, T. A., Chakilam, A. R., and Torchilin, V. P. (2004) Tumor-targeted liposomes: doxorubicin-loaded long-circulating liposomes modified with anti-cancer antibody, *Journal of controlled release 100*, 135-144.

53.   Park, J. W. (2002) Liposome-based drug delivery in breast cancer treatment, *Breast Cancer Research 4*, 95-99.

54.   Karanth, H., and Murthy, R. S. R. (2007) pH-Sensitive liposomes—principle and application in cancer therapy, *Journal of Pharmacy and Pharmacology 59*, 469-483.

55. Liua, P., Wang, B., Li, J., and Qiao, W. (2008) Multi-anti-cancer drugs encapsulated in the micelle: A novel chemotherapy to cancer, *Medical Hypotheses 71*, 379-381.

56. Bromberg, L. (2008) Polymeric micelles in oral chemotherapy, *Journal of controlled release 128*, 99-112.

57. Torchilin, V. P. (2005) Fluorescence microscopy to follow the targeting of liposomes and micelles to cells and their intracellular fate, *Advanced Drug Delivery Reviews 57*, 95-109.

58. Soo, P. L., and Luo, L. B. (2002) Incorporation and Release of Hydrophobic Probes in Biocompatible Polycaprolactone-block-poly(ethylene oxide) Micelle: Implications for Drug, *Langmuir 18*, 9996-10004.

59. Lee, H., Soo, P. L., Liu, J., Butler, M., and Allen, C. (2007) Polymeric micelles for formulation of anti-cancer drugs, in *Nanotechnology for Cancer Therapy* (Amiji, M. M., Ed.), pp 317-355, CRC Press, Boca Raton.

60. Xiong, X.-B., Aliabadi, H. M., and Lavasanifar, A. (2007) PEO-modified poly(L-amino acid) micelles for drug delivery, in *Nanotechnology for Cancer Therapy* (Amiji, M. M., Ed.), pp 357-383, CRC Press, Boca Raton.

61. Torchilin, V. P. (2007) Tumor-targeted delivery of sparingly-soluble anti-cancer drugs with polymeric lipid-core immunomicelles,, in *Nanotechnology for Cancer Therapy* (Amiji, M. M., Ed.), pp 409-420, CRC Press, Boca Raton.

62. Vasey, P. A., Kaye, S. B., Morrison, R., Twelves, C., Wilson, P., Duncan, R., Thomson, A. H., Murray, L. S., Hilditch, T. E., Murray, T., Burtles, S., Fraier, D., Frigerio, E., and Cassidy, J. (1999) Phase I Clinical and Pharmacokinetic Study of

PK1 [N-(2-Hydroxypropyl)methacrylamide Copolymer Doxorubicin]: First Member of a New Class of Chemotherapeutic Agents—Drug-Polymer Conjugates, *Clinical Cancer Research 5*, 83-94.

63. Duncan, R. (2006) Polymer conjugates as anti-cancer nanomedicines, *Nature Reviews 6*, 688-701.

64. Mu¨hlen, A. z., Schwarz, C., and Mehnert, W. (1998) Solid lipid nanoparticles (SLN) for controlled drug delivery-Drug release and release mechanism, *European Journal of Pharmaceutics and Biopharmaceutics 45*, 149-155.

65. (2004) *Gene delivery to mammalian cells*, Humana Press.

66. Pack, D. W., Hoffman, A. S., Pun, S., and Stayton, P. S. (2005) Design and development of polymers for gene delivery, *Nature Reviews Drug Discovery 4*, 581-593.

67. Akhtar, S., Hughes, M. D., Khan, A., Bibby, M., Hussain, M., Nawaz, Q., Double, J., and Sayyed, P. (2000) The delivery of antisense therapeutics, *Advanced Drug Delivery Reviews 44*, 3-21.

68. Israel, Z. H., and Domb, A. J. (1998) Polymers in gene therapy: antisense delivery systems, *Polymers for Advanced Technologies 9*, 799-805.

69. Elias, F., Patrick, C., and Catherine, D. (2004) "Smart" delivery of antisense oligonucleotides by anionic pH-sensitive liposomes, *Advanced Drug Delivery Reviews 56*, 931-946.

70. Landen, C. N., Chavez-Reyes, A., Bucana, C., Rosemarie Schmandt, Deavers, M. T., Lopez-Berestein, G., and Sood, A. K. (2005) Therapeutic EphA2 Gene

Targeting In vivo Using Neutral Liposomal Small Interfering RNA Delivery, *Cancer Research 65*, 6910-6918.

71. Halder, J., Kamat, A. A., Landen, C. N., Han, L., Lutgendorf, S. K., Lin, Y. G., WilliamM.Merritt, Jennings, N. B., Chavez-Reyes, A., Coleman, R. L., Gershenson, D., Schmandt, R., Cole, S., Lopez-Berestein, G., and Sood, A. K. (2006) Focal Adhesion KinaseTargeting Using In vivo Short Interfering RNA Delivery in Neutral Liposomes for Ovarian CarcinomaTherapy, *Clinical Cancer Research 12*, 4916-4924.

72. MacLachlan, I. Liposomal formulations for nucleic acid delivery, in *Antisense Drug Technology:Principles, Strategies, and Applications* (Crooke, S. T., Ed.), CRC Press.

73. Zimmermann, T. S., Lee, A. C. H., Akinc, A., Bramlage, B., Bumcrot, D., Fedoruk, M. N., Harborth, J., Heyes, J. A., Jeffs, L. B., John, M., Judge, A. D., Lam, K., McClintock, K., Nechev, L. V., Palmer, L. R., Racie, T., Ro¨hl, I., Seiffert, S., Shanmugam, S., Sood, V., Soutschek, J. r., Toudjarska, I., Wheat, A. J., Yaworski, E., Zedalis, W., Koteliansky, V., Manoharan, M., Vornlocher, H.-P., and MacLachlan, I. (2006) RNAi-mediated gene silencing in non-human primates, *Nature 441*, 111-114.

74. Jeffs, L. B., Palmer, L. R., Ambegia, E. G., Giesbrecht, C., Ewanick, S., and MacLachlan, I. (2005) A Scalable, Extrusion-Free Method for Efficient Liposomal Encapsulation of Plasmid DNA, *Pharmaceutical Research 22*, 362-372.

75. Santel, A., Aleku, M., Keil, O., Endruschat, J., Esche, V., Fisch, G., Dames, S., Löffler, K., Fechtner, M., Arnold, W., Giese, K., Klippel, A., and Kaufmann, J. (2006) A novel siRNA-lipoplex technology for RNA interference in the mouse vascular endothelium, *Gene Therapy 13*, 1222-1234.

76. Aleku, M., Schulz, P., Keil, O., Santel, A., Schaeper, U., Dieckhoff, B., Janke, O., Endruschat, J., Durieux, B., Ro¨der, N., Lo¨ffler, K., Lange, C., Fechtner, M., Mo¨pert, K., Fisch, G., Dames, S., Arnold, W., Jochims, K., Giese, K., Wiedenmann, B., Scholz, A., and Kaufmann, J. r. (2008) Atu027, a Liposomal Small Interfering RNA Formulation Targeting Protein Kinase N3, Inhibits Cancer Progression, *Cancer Research 68*, 9788-9798.

77. Urban-Klein, B., Werth, S., Abuharbeid, S., Czubayko, F., and Aigner, A. (2005) RNAi-mediated gene-targeting through systemic application of polyethylenimine (PEI)-complexed siRNA in vivo, *Gene Therapy 12*, 461-466.

78. Read, M. L., Singh, S., Ahmed, Z., Stevenson, M., Briggs, S. S., Oupicky, D., Barrett, L. B., Spice, R., Kendall, M., Berry, M., Preece, J. A., Logan, A., and Seymour, L. W. (2005) A versatile reducible polycation-based system for efficient delivery of a broad range of nucleic acids, *Nucleic Acids Research 33*, e86.

79. Thomas, M., Lu, J. J., Ge, Q., Zhang, C., Chen, J., and Klibanov, A. M. (2005) Full deacylation of polyethylenimine dramatically boosts its gene delivery efficiency and specificity to mouse lung, *PNAS 102*, 5679-5684.

80. Creusat, G., and Zuber, G. (2008) Tyrosine-modified PEI: A novel and highly efficient vector for siRNA delivery in mammalian cells, *Nucleic Acids Symposium Series 52*, 91-92.

81. Gao, X., Kim, K.-S., and Liu, D. (2007) Nonviral Gene Delivery: What We Know and What Is Next, *The AAPS Journal 9*, E92-E104.

82. Fischer, D., Li, Y., Ahlemeyer, B., Krieglstein, J., and Kissel, T. (2003) In vitro cytotoxicity testing of polycations: influence of polymer structure on cell viability and hemolysis, *Biomaterials 24*, 1121-1131.

83. Fischer, D., Bieber, T., Li, Y., Elsasser, H. P., and Kissel, T. (1999) A novel non-viral vector for DNA delivery based on low molecular weight, branched polyethylenimine: effect of molecular weight on transfection efficiency and cytotoxicity, *Pharmaceutical Research 16*, 1273-1279.

84. Gosselin, M. A., Guo, W., and Lee, R. J. (2001) Efficient gene transfer using reversibly cross-linked low molecular weight polyethylenimine, *Bioconjugate Chemistry 12*, 989-994.

85. Forrest, M. L., Koerber, J. T., and Pack, D. W. (2003) A degradable polyethylenimine derivative with low toxicity for highly effi cient gene delivery, *Bioconjugate Chemistry 14*, 934-940.

86. Thomas, M., and Klibanov, A. M. (2003) Conjugation to gold nanoparticles enhances polyethylenimine's transfer of plasmid DNA into mammalian cells, *Proc. Natl. Acad. Sci. 100*, 9138-9143.

87.   Zhu, J., Tang, A., Law, L. P., Feng, M., Ho, K. M., Lee, D. K. L., Harris, F. W., and Li, P. (2005) Amphiphilic core-shell nanoparticles with poly(ethylenimine) shells as potential gene delivery carriers, *Bioconjugate Chemistry 16*, 139-146.

88.   Manuel, W. S., Zheng, J. I., and Hornsby, P. J. (2001) Transfection by polyethylenimine-coated microspheres, *Journal of Drug Targeting 9*, 15-22.

89.   Newkome, G. R., Moorefield, C. N., and Vögtle, F. (2001) Dendrimers and Dendrons: Concepts, Synthesis, Applications, Wiley-VCH, New York.

90.   Zhou, J., Wu, J., Hafdi, N., Behr, J.-P., Erbacher, P., and Peng, L. (2006) PAMAM dendrimers for efficient siRNA delivery and potent gene silencing, *Chem. Commun.*, 2362-2364.

91.   Patil, M., Zhang, M., Betigeri, S., Taratula, O., He, H., and Minko, T. (2008) Surface-modified and Internally Cationic Polyamindoamine Dendrimers for Efficient siRNA Delivery, *Bioconjugate Chemistry 19*, 1396-1403.

92.   Taratula, O. (2008) PPI Dendrimers as Potential siRNA Delivery Agents for Cancer Therapy, in *Chemistry Department*, p 25, Rutgers University, Newark.

93.   Kang, S., Herzberg, M., Rodrigues, D. F., and Elimelech, M. (2008) Antibacterial effects of carbon nanotubes: size does matter!, *Langmuir 24*, 6409-6413.

94.   Leeuw, T. K., Retin, R. M., Simonette, R. A., Harden, M. E., Cherukuri, P., Tsyboulski, D. A., Beckingham, K. M., and Weisman, R. B. (2007) Single-walled carbon nanotubes in the intact organism: near-IR imaging and biocomaptibility studies in drosophila, *Nano Letters*, 2650-2654.

95.   Prato, M., Kostarelos, K., and Bianco, A. (2008) Functionalized carbon nanotubes in drug design and discovery, *Accounts of Chemical Research 41*, 60-68.

96. Wang, X., Ren, J., and Qu, X. (2008) Targeted RNA Interference of Cyclin A2 Mediated by Functionalized Single-Walled Carbon Nanotubes Induces Proliferation Arrest and Apoptosis in Chronic Myelogenous Leukemia K562 Cells, *ChemMedChem 3*, 940-945.

97. Zhang, Z., Yang, X., Zhang, Y., Zeng, B., Wang, S., Zhu, T., Roden, R. B. S., Chen, Y., and Yang, R. (2006) Delivery of Telomerase Reverse Transcriptase Small Interfering RNA in Complex with Positively Charged Single-Walled Carbon Nanotubes Suppresses Tumor Growth, *Clinical Cancer Research 12*, 4933-4939.

98. Liu, Z., Winters, M., Holodniy, M., and Dai, H. (2007) siRNA Delivery into Human T Cells and Primary Cells with Carbon Nanotube Transporters, *Angew. Chem. Int. Ed. 46*, 2023-2027.

99. Derfus, A. M., Chen, A. A., Min, D.-H., Ruoslahti, E., and Bhatia, S. N. (2007) Targeted Quantum Dot Conjugates for siRNA Delivery, *Bioconjugate Chemistry 18*, 1391-1396.

100. Yezhelyev, M. V., Qi, L., O'Regan, R. M., Nie, S., and Gao, X. (2008) Proton-Sponge Coated Quantum Dots for siRNA Delivery and Intracellular Imaging, *J. Am. Chem. Soc. 130*, 9006-9012.

101. Medarova, Z., Pham, W., Farrar, C., Petkova, V., and Moore, A. (2007) In vivo imaging of siRNA delivery and silencing in tumors, *Nature Medicine 13*, 372-377.

102. Oishi, M., Nakaogami, J., Ishii, T., and Nagasaki, Y. (2006) Smart PEGylated Gold Nanoparticles for the Cytoplasmic Delivery of siRNA to Induce Enhanced Gene Silencing, *Chemistry Letters 35*, 1046.

103. Leea, S. H., Baea, K. H., Kima, S. H., Leea, K. R., and Park, T. G. (2008) Amine-functionalized gold nanoparticles as non-cytotoxic and efficient intracellular siRNA delivery carriers, *International Journal of Pharmaceutics 364*, 94-101.

104. Ghosha, P., Hana, G., Dea, M., Kima, C. K., and Rotello, V. M. (2008) Gold nanoparticles in delivery applications, *Advanced Drug Delivery Reviews 60*, 1307-1315.

105. Luo, D., and Saltzman, W. M. (2006) Thinking of silica, *Gene Therapy 13*, 585-586.

106. Kneuer, C., Sameti, M., Bakowsky, U., Schiestel, T., Schirra, H., Schmidt, H., and Lehr, C.-M. (2000) A Nonviral DNA Delivery System Based on Surface Modified Silica-Nanoparticles Can Efficiently Transfect Cells in Vitro, *Bioconjugate Chemistry 11*, 926-932.

107. Bharali, D. J., Klejbor, I., Stachowiak, E. K., Dutta, P., Roy, I., Kaur, N., Bergey, E. J., Prasad, P. N., and Stachowiak, M. K. (2005) Organically modified silica nanoparticles: A nonviral vector for in vivo gene delivery and expression in the brain, *PNAS 102*, 11539-11544.

108. Radu, D. R., Lai, C.-Y., Jeftinija, K., Rowe, E. W., Jeftinija, S., and Lin, V. S.-Y. (2004) A polyamidoamine dendrimer-capped mesoporous silica nanosphere-based gene transfection reagent, *J. Am. Chem. Soc. 126*, 13216-13217.

109. Wang, Y., Gao, S., Ye, W.-H., Yoon, H. S., and Yang, Y.-Y. (2006) Co-delivery of drugs and DNA from cationic core-shell nanoparticles self-assembeled from a biodegradable copolymer, *Nature Materials 5*, 791-796.

110. Pakunlu, R. I., Wang, Y., Saad, M., Khandare, J. J., Starovoytov, V., and Minko, T. (2006) In vitro and in vivo intracellular liposomal delivery of antisense oligonucleotides and anti-cancer drug, *J. Controlled Release 114*, 153-162.

111. Slowing, I., Trewyn, B. G., and Lin, C. S.-Y. (2006) Effect of Surface Functionalization of MCM-41 Type Mesoporous Silica Nanoparticles on the Endocytosis by Human Cancer Cells, *J. Am. Chem. Soc. 128*, 14792-14793.

112. Slowing, I., Vivero-Escoto, J. L., Wu, C.-W., and Lin, V. S.-Y. (2008) Mesoporous Silica Nanoparparticles as Controlled Release Drug Delivery and Gene Transfection Carriers, *Adv. Drug Deliv. Rev. 60*, 1278-1288.

113. Vallet-Regi, M., Balas, F., and Aros, D. (2007) Mesoporous Materials for Drug Delivery, *Angew. Chem. Int. Ed. 46*, 7548-7558.

114. Lu, J., Liong, M., Zink, J. I., and Tamanoi, F. (2007) Mesoporous Silica Nanoparticles as a Delivery System for Hydrophobic Anti-cancer Drugs, *Small 3*, 1341-1346.

115. Radu, D. R., Lai, C.-Y., Jeftinija, K., Rowe, E. W., Jeftinija, S., and Lin, C. S.-Y. (2004) A Polyamidoamine Dendrimer-Capped Mesoporous Silica Nanosphere-Based Gene Transfection Reagent, *J. Am. Chem. Soc. 126*, 13216-13217.

116. Torney, F., Trewyn, B. G., Lin, V. S. Y., and Wang, K. (2007) Mesoporous Silica Nanoparticles Deliver DNA and Chemicals into Plants, *Nature Nanotech. 2*, 295-300.

117. Torney, F., Trewyn, B. G., Lin, V. S.-Y., and Wang, K. (2007) Mesoporous silica nanoparticles deliver DNA and chemicals into plants, *Nature Nanotechnology 2*, 295-300.

118. Liu, F., and Huang, L. (2002) Development of non-viral vectors for systemic gene delivery, *Journal of controlled release 78*, 259-266.

119. Ranson, M. R., Cheeseman, S., White, S., and Margison, J. (2001) Caelyx (stealth liposomal doxorubicin) in the treatment of advanced breast cancer, *Critical Reviews in Oncology:Hematology 37*, 115-120.

120. Ma, L. L., Jie, P., and Venkatraman, S. S. (2008) Block copolymer 'stealth' nanoparticles for chemotherapy: interactions with blood cells in vitro, *Advanced Functional Materials 18*, 716-725.

121. Zahr, A. S., Davis, C. A., and Pishko, M. V. (2006) Macrophage Uptake of Core-Shell Nanoparticles Surface Modified with Poly(ethylene glycol), *Langmuir 22*, 8178-8185.

122. Mosqueira, V. C. F., Legrand, P., Gref, R., Heurtault, B., Appel, M., and Barratt, G. (1999) Interactions between a Macrophage Cell Line (J774A1) and Surface-modified Poly(D,L-lactide) Nanocapsules Bearing Poly(ethylene glycol), *Journal of Drug Targeting 7*, 65-78.

123. Gref, R., Domb, A., Quellec, P., Blunk, T., Müller, R. H., Verbavatz, J. M., and Langer, R. (1995) The controlled intravenous delivery of drugs using PEG-coated sterically stabilized nanospheres, *Advanced Drug Delivery Reviews 16*, 215-233.

124. Seymour, L. (1992) Passive tumor targeting of soluble macromolecules and drug conjugates, *Critical reviews in therapeutic drug carrier systems 9*, 135-187.

125. Petrak, K. (2005) Essential properties of drug-targeting delivery systems, *Drug Discover Today 10*, 1667-1673.

126. Nielsen, P. E. (2005) Systemic delivery: The last hurdle?, *Gene Therapy 12*, 956-957.

127. Bartlett, D. W., and Davis, M. E. (2006) Effect of siRNA nuclease stability on the in vitro and in vivo kinetics of siRNA-mediated gene silencing, *Biotechnology and Bioengineering 97*, 909-921.

128. Malik, N., Wiwattanapatapee, R., Klopsch, R., Lorenz, K., Frey, H., Weener, J. W., Meijer, E. W., Paulus, W., and Duncan, R. (2000) Relationship between Structure and Biocompatibility in vitro, and Preliminary Studies on the Biodistribution of 125I-labelled Polyamidoamine Dendrimers in vivo, *Journal of Controlled Release 65*, 133-148.

129. Zhang, Z. Y., and Smith, B. D. (2000) High-Generation Polycationic Dendrimers Are Unusually Effective at Disruptig Anioinic Vesicles: Membrane Bending Model, *Bioconjugate Chem. 11*, 805-814.

130. Hong, S., Bielinska, A. U., Mecke, A., Keszler, B., Beals, J. L., Shi, X., Balogh, L., Orr, B. G., Baker, J. R. J., and Banaszak Hall, M. M. (2004) Interaction of Poly(amidoamine) Dendrimers with Supported Lipid Bilayers and Cells: Hole Formation and the Relation to Transport, *Bioconjugate Chem. 2004*, 774-782.

131. (2001) *Dendrimers and Dendrons: Concepts, Synthesis, Applications*, Wiley-VCH, New York, NY.

132. Tomalia, D. A., Baker, H., Dewald, J., Hall, M., Kallos, G., Martin, S., Roeck, J., Ryder, J., and Smith, P. (1985) A New Class of Polymers: Starbust-Dendritic Macromolecules, *Polym. J.(Tokyo) 17*, 117-132.

133. De Brabander-van den Berg, E. M. M., and Meijer, E. M. (1993) Poly(propylene imine) Dendrimers: Large-scale Synthesis via Heterogeneously Catalyzed Hydrogenation, *Angew. Chem. 105*, 1370-1373.

134. Dennig, J., and Duncan, E. (2002) Gene Transfer into Eukaryotic Cells using Activated Polyamidoamine Dendrimers, *Rev. Mol. Biotechnol. 90*, 339-347.

135. Han, Y., and Ying, J. Y. (2005) Generalized Fluorocarbon-surfactant-mediated Synthesis of Nanoparticles with Various Mesoporous Structures, *Angew. Chem. Int. Ed. 44*, 288-292.

136. Huh, S., Wiench, J. W., Yoo, J.-C., Pruski, M., and Lin, V. S. Y. (2003) Organic Functionalization and Morphology Control of Mesoporous Silicas via A Co-condensation Synthesis Method, *Chem. Mater. 15*, 4247-4256.

137. Moeller, K., Kobler, J., and Bein, T. (2007) Colloidal Suspensions of Nanometer-sized Mesoporous Silica, *Adv. Funct. Mater. 17*, 605-612.

138. Slowing, I. I., Trewyn, B. G., and Lin, V. S.-Y. (2007) Mesoporous silica nanoparticles for intracellular delivery of membrane-impermeable proteins, *J. Am. Chem. Soc. 129*, 8845-8849.

139. Gu, J., Fan, W., Shimojima, A., and Okubo, T. (2007) Organic-inorganic mesoporous nanocarriers integrated with biogenic ligands, *Small 3*, 1740-1744.

Chapter 2

Oligodeoxynucleotide Nanostructure Formation in the Presence of Polypropyleneimine Dendrimers and Their Uptake in Breast Cancer Cells

2.1. Introduction

Sequencing of the human genome and functional genomics offer unprecedented opportunities to disrupt the expression of disease-related genes by short synthetic nucleic acid sequences. Anti-gene and antisense oligodeoxynucleotides (ODNs), aptamers, ribozymes (catalytic RNAs) and siRNAs are among the nucleic acid based drugs under development.(*1, 2*) Because of the high affinity of these ODNs to their targeted sites, they exert a high degree of specificity. However, the success of oligonucleotide-based therapeutics is dependent on the ability of these nucleic acids to reach gene targets in cells. A pre-requisite for cellular transport of the therapeutic ODNs through the cell membrane is their compaction to nanoparticles.(*3-5*)

There has been considerable literature on the condensation of plasmid and long linear DNA to nanoparticles.(*3-7*) However, investigations into the condensation of ODNs to nanoparticles are scant,(*8, 9*) even though their transfection has been widely studied.(*10-15*) Both long DNA and short ODNs have anionic phosphodiester backbones and therefore should interact electrostatically with cationic delivery agents to form nanoparticles that undergo facile transport through the cell membrane. However, ODNs

are different from plasmids and long linear DNAs in molecular weight and molecular topography, with potentially important consequences. For example, it was previously assumed that a DNA with a minimum of 400 base pairs could be condensed to nanoparticles by mechanisms involving either the spooling of DNA or the formation of a constant loop, followed by wrapping of the DNA around this loop.(*4, 16-18*) Recent studies show that nanoparticles with a size of ~100 nm can be formed from single stranded ODNs,(*8, 9*) although the mechanism(s) involved in their assembly is not clear.

It is likely that ODNs follow a pathway different from that of high molecular weight DNAs to form nanoparticles. Studies on structure-activity relationships of condensing agents in nanoparticle formation of short ODNs have not been reported. We studied the efficacy and mechanism of 5 generations (G-1 to G-5) of PPI dendrimers to provoke nanoparticle formation from a 21-nucelotide (nt) antisense ODN, targeted to inhibit the translation of c-*myc* mRNA by hybridization to the AUG translational initiation region.

We chose PPI dendrimers as condensing agents in this study due to their unique molecular structures, with defined molecular weight, surface charge and surface functionality.(*19, 20*) These properties of dendrimers provide a platform for a systematic study, with less complication from heterogeneity and variable chemistry, commonly seen in other nonviral delivery agents, such as cationic lipids and polyethylenimine (PEI).(*3*) Furthermore, PPI dendrimers are members of a class of amine-terminated polymers, demonstrated to be efficient gene delivery vectors with low cytotoxicity in a wide range of mammalian cell lines.(*19, 21-24*) The multiple functional groups on dendrimers also allow the design of multifunctional delivery agents. Thus, studies on structure-activity relationships of PPI dendrimers are expected to have important therapeutic applications.

We demonstrate the formation of ODN nanoparticles using light scattering, atomic force microscopy (AFM) and electron microscopy (EM). Nanoparticles formed with G-4 and G-5 dendrimers could undergo facile transport in a breast cancer cell line, MDA-MB-231. Using AFM to monitor the condensation process, we found that extended nanofibers were formed in the initial states of ODN condensation in the presence of G-1 to G-5 dendrimers. With higher generations, more aggregates of the nanofibers were found. With longer periods of condensation, they became more tightly compacted nanoparticles. Based on these results, we propose that ODN molecules undergo a zipping condensation pathway in the presence of PPI dendrimers. The zipping condensation pathway is that the PPI dendrimers first "zip" the ODN molecules by electrostatic interactions to form extended nanofibers, followed by secondary folding and compaction into nanoparticles often seen with high molecular weight linear and plasmid DNAs. Understanding the unique condensation pathways will be useful to the rational design of more effective vectors specifically for short therapeutic ODNs.

2.2. Results

2.2.1. ODN Condensation

Figure 2.1 shows representative plots of total scattered light intensity against the concentrations of different generations of dendrimers. The intensity of scattered light was similar to that of the buffer at low concentrations of dendrimers, showing that ODN in solution has a low surface area to scatter light. However, a sharp increase in intensity of scattered light occurred at a critical concentration of each dendrimer, and then leveled off

at higher concentrations. This increase in scattered light intensity identifies the presence of nanoparticles.(*25*)
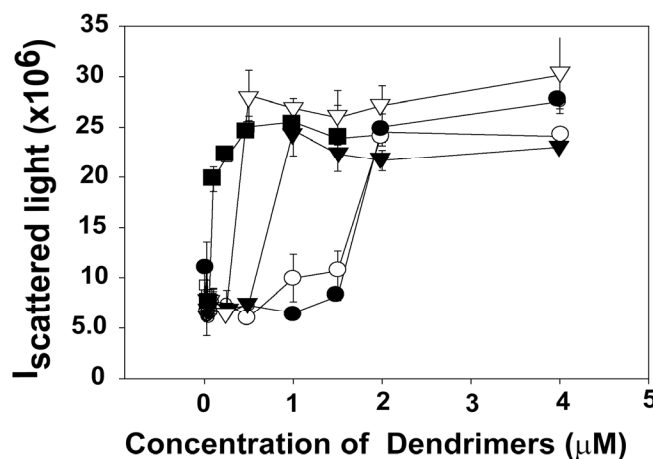
Figure 2.1. Typical plots of the intensity of scattered light at 90° plotted against the concentrations of dendrimers. Symbols are G-1 (●), G-2 (O), G-3 (▼), G-4 (▽), G-5 (■); ODN concentration was 0.2 µM in 10 mM Na cacodylate buffer, pH 7.4.

The efficacy of each dendrimer to condense the ODN was quantified by calculating the concentration of dendrimer at the midpoint (50%) of ODN condensation (EC$_{50}$) (Table 2.1). There was a molecular weight dependent decrease in EC$_{50}$ values, from 1.7 µM in the case of G-1 dendrimer to 0.1 µM in the case of G-5 dendrimer. The decrease in EC$_{50}$ value with the increase of dendrimer generation number might be a result of the increase in the number of primary amino groups in higher generation dendrimers, with consequent increase in the number of positive charges per molecule. ODN condensation was also studied in 10 mM Na cacodylate buffer containing the approximate physiological concentration of cations. Condensation was found to occur at lower concentrations of dendrimer than that in 10 mM Na cacodylate buffer. The EC$_{50}$ values were 0.42, 0.15, 0.095, 0.045 and 0.035 µM, respectively, for G-1, G-2, G-3, G-4

and G-5 dendrimers (Table 2.1). This result suggests that cations and dendrimers had additive/synergistic effect on condensing the ODN.

We also determined hydrodynamic radii of ODN nanoparticles formed in the presence of dendrimers using the DLS equipment (Table 2.1). The ODN concentration was 0.2 µM and dendrimer concentrations were 5-fold of their EC_{50} values. Higher dendrimer concentration was used to ensure that ODN molecules were fully condensed. We found that G-1 dendrimer produced the largest particles and G-4 dendrimer produced the smallest particles.

Table 2.1. Effective Concentration of PPI Dendrimers for ODN Condensation.

Dendrimer and Molecular Weight	Number of Terminal Amino Groups	EC_{50} (µM)[a]		Hydrodynamic Radius (R_h, nm)	
		10 mM Na$^+$	Physiol.[b]	(Physiol.)[c]	N/P[d]
G-1 (316)	4	1.7 ± 0.2	0.42 ± 0.05	109 ± 9	2
G-2 (773)	8	1.7 ± 0.1	0.15 ± 0.02	87 ± 1	4.1
G-3 (1686)	16	0.95 ± 0.15	0.095 ± 0.010	103 ± 6	4.4
G-4 (3514)	32	0.45 ± 0.07	0.045 ± 0.005	44 ± 1	4.2
G-5 (7168)	64	0.1 ± 0.02	0.035 ± 0.002	80 ± 3	1.8

[a]EC_{50} values are the mean of 3 separate experiments, ± S.D. [b]10 mM Na cacodylate buffer containing the approximate physiological concentration of cations (120 mM NaCl, 10 mM NaCl, 2 mM $MgCl_2$, 0.1 mM $CaCl_2$) (Physiol.). [c]R_h values were determined using a DLS equipment at dendrimer concentrations 5-fold of the EC_{50} values, under physiological salt concentrations. R_h values are mean ± S.D from 3-5 separate experiments. [d]N/P value is the ratio of peripheral nitrogen of dendrimer to phosphorus of ODN. For N/P values in the text, we used the physiological EC_{50} value.

We next studied the stability of ODN nanoparticles as a function of time. ODN nanoparticles were prepared with 0.2 µM ODN and 2.0 µM concentration of each of the

dendrimer in 10 mM Na cacodylate buffer. The scattered light intensity was measured at several time points up to 24 hours (Figure 2.2). There was no significant difference in scattered light intensity during this period, suggesting that the nanoparticles did not undergo aggregation or decondensation.
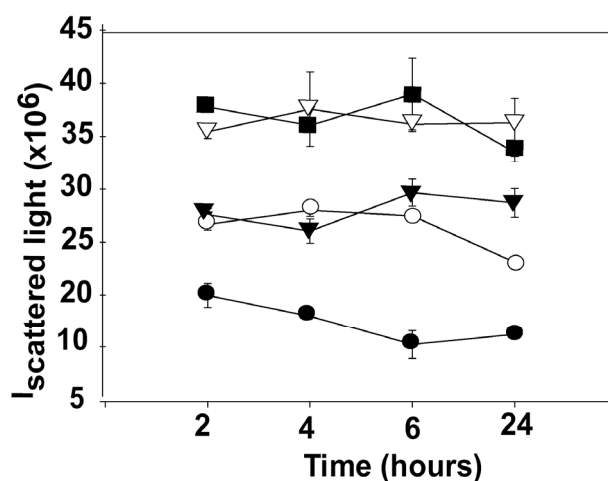
Figure 2.2. Stability of nanoparticles by total light scattering. ODN nanoparticles were prepared by mixing ODN and dendrimers to obtain final concentrations of 0.2 μM ODN and 2.0 μM dendrimers in 10 mM Na cacodylate buffer, pH 7.4. Scattered light intensity was monitored as a function of time up to 24 hours. Symbols are G-1 (●), G-2 (O), G-3 (▼), G-4 (▽), G-5 (■).

2.2.2. Atomic Force Microscopy (AFM)

AFM has been used to complement light scattering studies to visualize different nanostructures of DNA in solution. Here we used AFM to monitor the ODN condensation process in the presence of different generation PPI dendrimers. As shown in Figure 2.3, extended nanofiber-shaped structures as well as aggregates of nanowires were formed in the presence of G-1 to G-5 dendrimers after 10 minutes of condensation. With lower generations, we found more isolated wires as shown in Panel A. The height of the

isolated wires was ~0.5 nm and the length varied from 200 to 600 nm. Occasionally, these isolated fiber-shaped structures were also found in higher generations, but the height of the wires was slightly higher than those found in G-1 and G-2. Panel F shows several isolated nanofibers formed from G-5, with an average height of 0.7-0.8 nm. Nanofibers could then interact with each other in parallel to form ribbon- and rod-like structures. In Panel F and the inset of Panel C, we could clearly see that nanofibers lie in parallel. The isolated nanofibers, and the ribbon- and rod-like structures interconnected to each other in a "head to tail" style to form extended fibers, which then formed curved and looped structures (Panel B). They could also aggregate to form
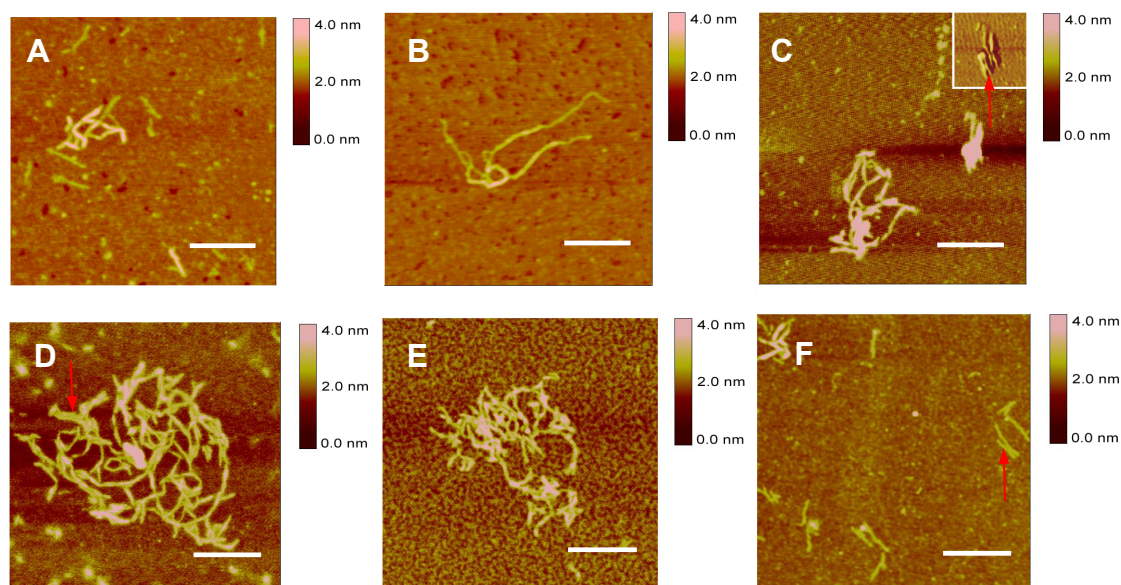
Figure 2.3. AFM images of condensates formed by the 21-nt ODN in the presence of PPI dendrimers after 10-minute condensation. ODN had a concentration of 0.4 µM and dendrimer was 2.5 µM in a solution containing the approximate physiological concentration of salts. Panels are (A) G-1, (B) G-2, (C) G-3, (inset) Phase image with the same scale of the main image indicated by a red arrow. (D) G-4, (E) G-5, and (F) G-5. Bar represents 250 nm in all panels.
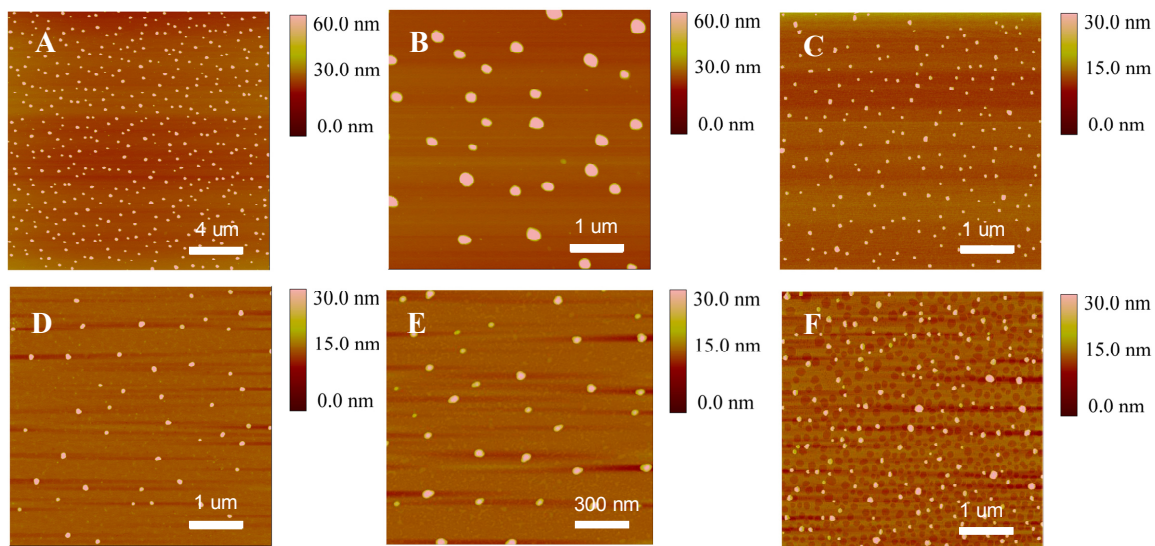
Figure 2.4. AFM images of condensates formed by the 21-nt ODN in the presence of PPI dendrimers after 1 hour of condensation (panels A, B, C, D, E and F). ODN had a concentration of 0.4 µM and dendrimer was 2.5 µM in a solution containing the approximate physiological concentration of salts. (A) G-1, (B) G-1 (zoom image of one part of panel (A)), (C) G-2, (D) G-3, (E) G-4, (F) G-5. Bar represents 4 µm in panel (A), 1 µm in panels (B, C, D, F) and 300 nm in panel (E).

complex structures (Panel C, D and E). It was noticed that with higher generations, more aggregated complex structures were formed. In controlled AFM experiments, we found that dendrimers alone or ODN alone could not form these fiber-shaped structures.

After 1 hour of condensation, spheroidal nanoparticles were predominant for ODN condensates formed with all five generations of dendrimers (Figure 2.4). Table 2.2 presents the mean diameter and height of these particles. ODN nanoparticles formed in the presence of G-1 dendrimer were significantly larger (210 ± 40 nm) than those formed with other 4 generations of dendrimers. The height of these particles was also 2- to 3-fold higher than that of other particles. The diameter and height of the nanoparticles formed

with G-2, G-3, G-4 and G-5 dendrimers were comparable, although nanoparticles formed

in the presence of G-4 dendrimer had the smallest size (diameter = 54 ± 18 nm; height =

9 ± 5 nm). Given that free dendrimers or ODNs may exist in the solution and these

dendrimers or ODN molecules may form aggregates in solution or upon solution

evaporation during sample preparation, controlled AFM experiments were performed

with dendrimers alone and ODN alone. We found that monolayer and multilayer of

dendrimers with occasionally aggregates were formed on mica surface. The aggregates

had an average diameter of 33-132 nm and an average height of 1.3-3.5 nm. Complicated

aggregated structures with different shapes and size were observed on the samples

prepared from free ODN molecules. The height of these aggregates was all less than 1

nm from AFM measurement. These results suggested that dendrimers or ODN

Table 2.2. Particle Size Analysis of ODN Nanoparticles Formed with PPI Dendrimers by AFM[a].

Generation of dendrimer	Diameter (nm)	Height (nm)	Count
G-1	210 ± 40	54 ± 11	476
G-2	74 ± 18	17 ±5	955
G-3	98 ± 20	21 ± 4	183
G-4	54 ± 18	9 ± 5	247
G-5	71 ± 21	20 ± 6	846

[a]Particle size analysis was performed on the AFM images of condensates formed by the 21-nt ODN in the presence of PPI dendrimers after 1 hour of condensation by using software Nanoscope 5.12b. ODN had a concentration of 0.4 µM and dendrimer was 2.5 µM in a solution containing the approximate physiological concentration of salts.

themselves could form some aggregates in solution or form aggregates during the sample preparation. However, the height of all aggregates was much lower than the height of ODN condensates shown in the AFM images.

2.2.3. Electron Microscopy (EM)

EM experiments were further performed to confirm the formation of nanoparticles. Figure 2.5 shows representative electron micrographs of ODN nanoparticles formed in the presence of different generations of dendrimers. The nanoparticles were predominantly clusters of spheroids and toroids when G-1 (Panel A), G-2 (Panel B) and G-3 (Panel C) dendrimers were used as condensing agents. Uncondensed and interconnected chains were also seen with G-1, G-2 and G-3 dendrimers. We found
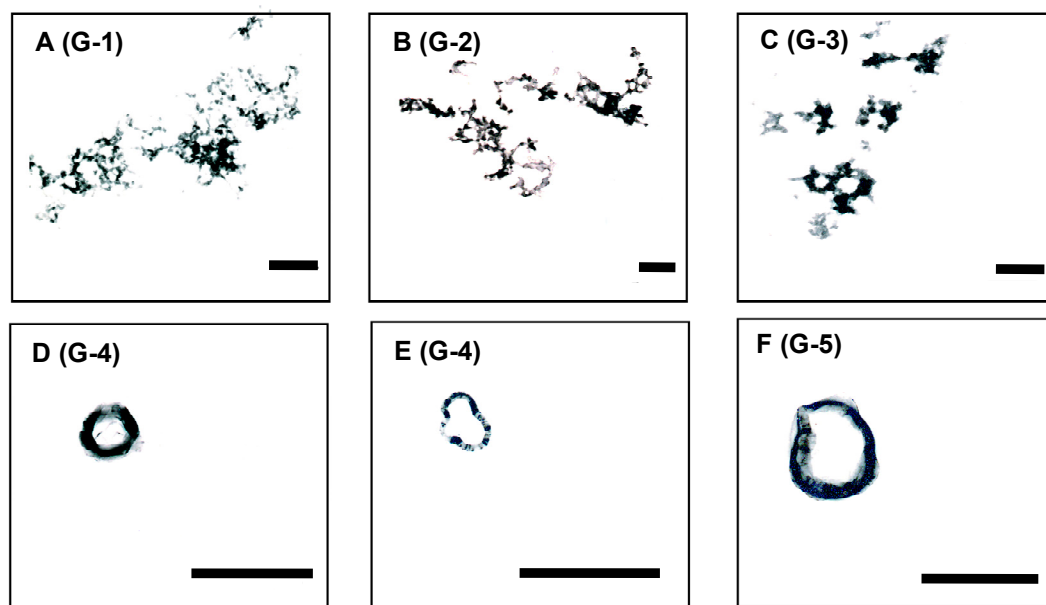
Figure 2.5. Typical electron microscopic images of 0.4 μM ODN complexed with 2.5 μM concentration of each dendrimer. Panels are (A) G-1, (B) G-2, (C) G-3, (D) G-4, (E) G-4, and (F) G-5. Bar represents 100 nm.

occasional toroids (Panel D) or imperfect circular structures (Panels E and F) when the ODN condensation was performed with higher generation (G-4 and G-5) dendrimers. We also found aggregates of spheroidal condensates with higher generation of dendrimers.

2.2.4. Particle Surface Charge

ζ-Potential measurements were conducted to evaluate the surface charge of particles formed with different generations of dendrimers. Our results show that all generations were capable of producing nanoparticles with positive surface charge (Table 2.3). However, particles produced with G-1, G-2 and G-3 dendrimers had significantly lower ζ-potential (5.2-6.5 mV) compared to those produced with G-4 and G-5 (12-18 mV) dendrimers.

Table 2.3. ζ-Potential of ODN Nanoparticles Formed with PPI Dendrimers[a].

Generation of dendrimer	ζ-Potential (mV)
G-1	5.6 ± 0.5
G-2	5.2 ± 0.7
G-3	6.5 ± 0.4
G-4	12.1 ± 2.1
G-5	17.7 ± 3.5

[a]A solution containing 0.2 μM ODN and 2.5 μM dendrimer was prepared in 10 mM Na cacodylate buffer containing the approximate physiological concentration of cations and incubated for 1 hour at room temperature and then injected for ζ-Potential measurement.

2.2.5. Confocal Microscopy

We next examined the cellular uptake of the 21-nt antisense ODN (fluorescein-tagged) by MDA-MB-231 cells. Figure 2.6 shows representative confocal images of cells treated with ODN alone or in the presence of G-4 dendrimer. In these experiments, we incubated the ODN/dendrimer mixture for 10 minutes before adding to the cell culture media. In previous experiments, we used 10 minute and 1 hour incubation periods, as well as 10 minute incubation followed by storage of the mixture at -70 °C overnight before adding the ODN to cell culture media.(*26, 27*) Cellular uptake of ODN was quantified by scintillation counting of the [^{32}P]-labeled ODN. We found a comparable level of ODN uptake, irrespective of the time of incubation. Therefore, we used the 10 minute incubation period for the present series of confocal microscopic experiments.

Control consisted of cells that were treated with fluorescein-tagged ODN alone. In the absence of dendrimer (control), there was no green fluorescence in cells, indicating the lack of ODN uptake in cells. With G-4 dendrimer, the presence of ODN was evident in both cytoplasm and nuclei of cells, as indicated by the green fluorescence. In separate experiments, we found that G-1 or G-2 dendrimer did not support the transport of ODN to the cytoplasm or nucleus of MDA-MB-231 cell. However, there was a high level of ODN uptake in the presence of G-5 dendrimer (Figure 2.7). However, in this case, nuclear and cytoplasmic staining was not clearly discernible. Nevertheless, we found that the structure of the dendrimers influenced the ODN uptake in MDA-MB-231 breast cancer cells. It is interesting to note that G-4 and G-5 dendrimers produced nanostructures with maximal surface charge, which might have assisted cellular uptake.

It is important to note here that the observed cellular uptake is for nanostructures formed after 10-minute incubation of the dendrimer and fluorescently tagged ODN. Since

we found different structures after 10-minute and 1-hour incubation periods, the cellular uptake might be different for structures formed after 1-hour of incubation.
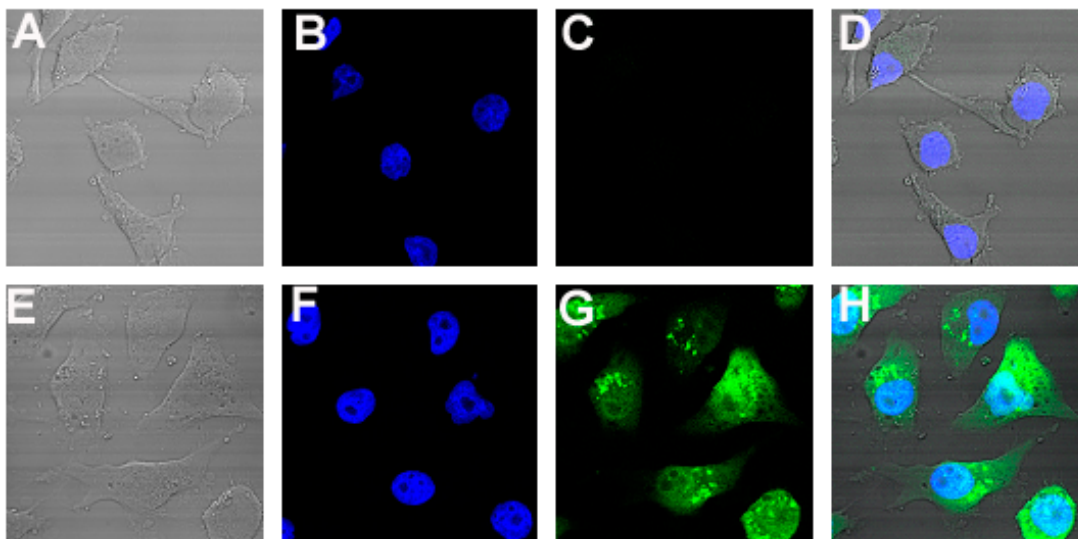
Figure 2.6. Representative images of cellular uptake of fluorescein-labeled 21-nt ODN by MDA-MB-231 cell by confocal microscopy. ODN uptake in the absence (A, B, C, D) or the presence (E, F, G, H) of G-4 dendrimer is shown. Differential interference contrast (DIC) images of cells are shown in panels A and E. Nuclei stained with DAPI (B and F), detection of fluorescein-labeled oligonucleotide (C and G) and overlay of images (D and H) are shown. Final concentration of ODN and G-4 dendrimer in the cell culture medium were 0.2 μM each.
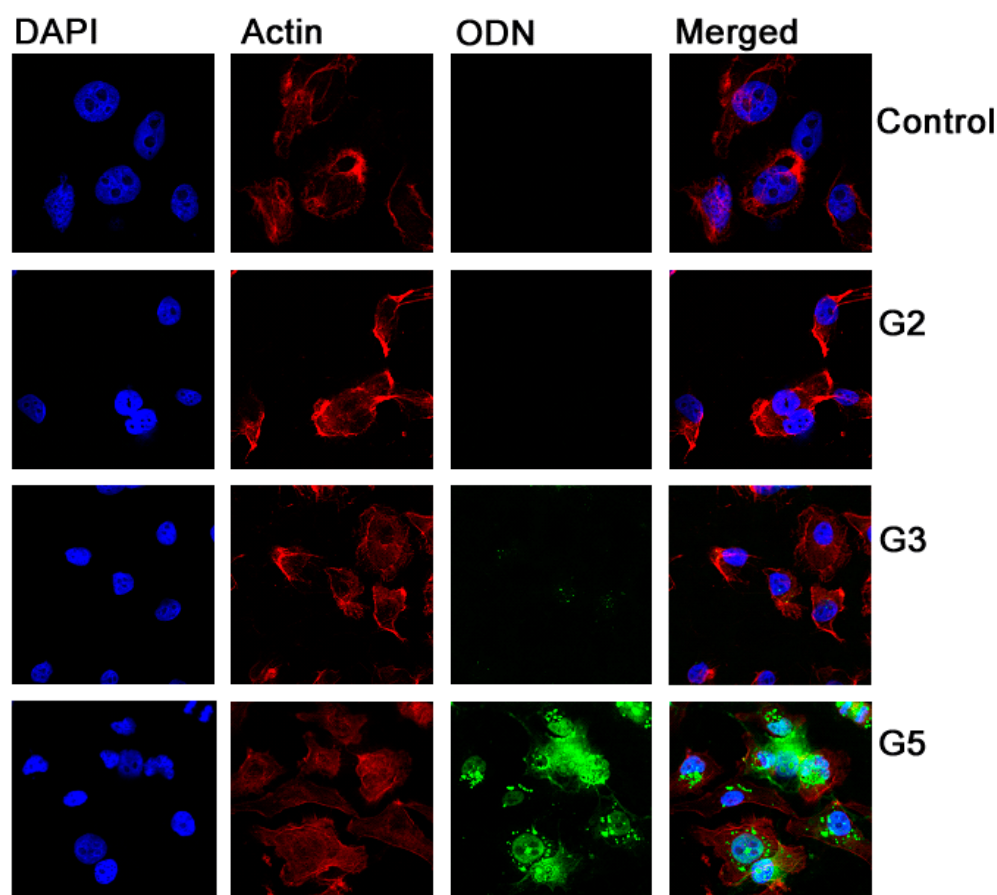
Figure 2.7. Representative images of cellular uptake of fluorescein-labeled 21-nt ODN by MDA-MB-231 cell by confocal microscopy. MDA-MB-231 cells were plated (25,000/well) and treated with a fluorescein-labeled 21-mer antisense ODN/dendrimer mixture for 24 hours. G-1, G-2, G-3 and G-5 and c-myc antisense ODN were mixed and incubated for 10 minutes at 22 °C prior to cell treatment. Final concentrations of dendrimers and ODN in the cell culture medium were as follows: G-1, 2 µM; G-2, 0.75 µM; G-3, 0.5 µM; G-5, 0.2 µM; and ODN, 0.2 µM. After 24 hours, cells were fixed with 1% paraformaldehyde in phosphate buffered saline. Nuclei were stained using 4',6-diamidino-2-phenylindole (DAPI). Actin was stained with Alexa Fluor 546-phalloidin. Cells were mounted with aqueous mounting medium containing antifading agents for analysis by confocal microscopy. G-1 and G-2 dendrimers showed similar results and hence images with G-1 are not shown here. Left to Right; Nuclei stained with DAPI, Actin stained with phalloidin, fluorescein-labeled ODN and overlay (merged) images.

2.2.6. Analysis of [^{32}P]-labeled ODN by Polyacrylamide Gel Electrophoresis

A major problem associated with ODNs for therapeutic use is their degradation by serum-derived endonuclease. We previously found that G-4 dendrimer could protect a 31-nt triplex forming ODN from degradation by cellular enzymes.(*26*) In order to test whether complexing of the 21-nt ODN with the dendrimer could protect it from degradation within the cell, we next conducted polyacrylamide gel electrophoresis of the [^{32}P]-labeled ODN extracted from MDA-MB-231 cells at different time periods after treatment (Figure 2.8). Lane 1 (C) shows a control sample of [^{32}P]-labeled ODN, while
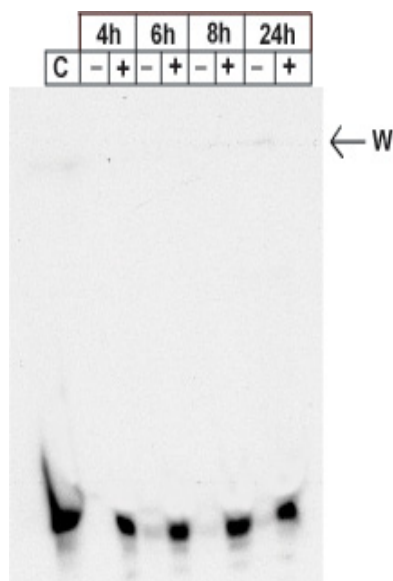
Figure 2.8. Stability of [^{32}P]-labeled ODN in MDA-MB-231 cells. Cells were treated with [^{32}P]-labeled ODN alone or [^{32}P]-labeled ODN/G-4 dendrimer complex for the indicated time periods. [^{32}P]-Labeled ODN was extracted from cells, and characterized by 20% polyacrylamide gel electrophoresis. Lanes 2, 4, 6, and 8 show [^{32}P]-labeled ODN extracted from cells treated with [^{32}P]-labeled ODN alone. Lanes 3, 5, 7, and 9 show [^{32}P]-labeled ODN extracted from cells treated with [^{32}P]-labeled ODN/G-4 complex. Lane 1-C is [^{32}P]-labeled ODN in sterile water, used as a marker for the intact [^{32}P]-labeled ODN migration in the gel. W indicates the gel well.

lanes 2, 4, 6 and 8 (all marked (-) on top) show samples extracted from cells treated with [^{32}P]-labeled ODN alone for 4, 6, 8 and 24 h, respectively. Lanes 3, 5, 7 and 9 (all marked (+) on top) show samples extracted from cells treated with [^{32}P]-labeled ODN/G-4 dendrimer complex. About 10- to 25-fold increase in intensity was observed after treatment with dendrimer complex of [^{32}P]-labeled ODN compared to that in cells treated with [^{32}P]-labeled ODN alone. It is to be noted that high level of intact ODN was observed in [^{32}P]-labeled ODN/G-4 dendrimer treated cells even after DNAse I washing of the cells. Although this does not guarantee lack of externally adsorbed ODN, these results are indicative of increased cellular uptake and retention in the presence of the dendrimer.

2.3. Discussion

The condensation of high molecular weight DNA has been extensively studied. (*3-7*) It is believed that the major factor governing the compaction of DNA is charge neutralization by electrostatic interaction between negatively charged phosphate groups of DNA and positively charged groups of the condensing agent. Charge neutralization increases the flexibility of the DNA chain, which bends spontaneously leading to the formation of rods, toroids and spheroids. Early physical and biochemical studies supported a mechanism of condensation by circumferential winding of DNA, often denoted as the spool model.(*28-30*) Hud *et al.*(*17*) proposed an alternate model in which DNA in the nanoparticles is organized within a series of equally sized contiguous loops around the toroid axis. It was also suggested that formation of toroids is a coil-globule transition.(*4, 31-35*)

Antisense, anti-gene and siRNA oligonucleotides are being developed for inhibition of target gene expression. Although efforts have been made to improve delivery of these short therapeutic genes with various transfection agents, including dendrimers,(*10-15*) detailed studies of the mechanism of condensation of short ODNs is scant.(*8*) Previous theories (*4, 17, 18, 29*) assumed that short DNA (<400 bp) could not form into discrete nanoparticles: their length was insufficient for condensation mechanisms described above. However, recent studies show that nanoparticles of ~100 nm diameter can be formed from individual short single stranded ODNs.(*8, 9*) Hud *et al*.(*36*) also reported that individual short ODNs could be condensed into well-defined nanoparticles by using a different formulation from that for condensing plasmid DNA. To improve the condensation and packaging of ODNs into nanoparticles, they designed ODNs with half-sliding complementary sequences with flexible sites at regular points along the double helix, in the form of single-stranded nicks and single-stranded gaps. The long nicked- and gapped-DNA duplexes were more easily condensed into smaller and more homogenous particles than the continuous duplex DNA of comparable length due to the increased local flexibility by the nicks and gaps, which provide both kinetic and thermodynamic advantages to DNA condensation.

Our study demonstrates the formation of nanoparticles from a short single-stranded ODN in the presence of PPI dendrimers. All five generations of PPI dendrimers used in our study were capable of provoking ODN condensation, as monitored by total intensity light scattering, electron microscope and atomic force microscope. However, the efficacy of the dendrimer increased with increase in the generation number of the dendrimer, as reflected in the EC_{50} values (Table 2.1). Since higher generations are formed by sequential addition of monomer units, increase in the generation number has a

multiplying effect on the number of surface primary amino groups that are positively charged under the conditions of our experiment. Molecular modeling studies on the interaction of dendrimers with plasmid DNA indicated an increase in dendrimer-DNA binding site per molecule with increase in dendrimer generation.(*37*) The final ODN condensates were predominantly spheroids, although toroids were also found occasionally (Figure 2.5). The size of the spheroidal and toroidal condensates is similar to the size of the plasmid DNA condensates formed in the presence of pentamine and hexamine analogues of the natural polyamine, spermine in our recent findings.(*38*)

It should be noted here that the size of the nanoparticles measured by AFM is significantly lower than that obtained from DLS measurement. In AFM, we measured the size of particles on freshly cleaved mica surface, after drying the sample in air, whereas we measured the size of hydrated nanoparticles using the light scattering technique. Comparable size differences in measurements by these two techniques were reported by Choi et al.(*39*) In general the size of DNA nanoparticles measured by AFM and EM is much lower than that measured by DLS.(*3*)

In order to understand the condensation mechanism of the ODNs with the PPI dendrimers, we studied the morphology of the condensates at the early stages of condensation. We detected isolated nanofiber-shaped structures with lower generation dendrimers, and more ribbon-like, looped, and spaghetti-like structures with higher generation dendrimers. It was previously reported that amine-terminated PPI dendrimers form interpolyelectrolyte complex with DNA over a wide range of pH below 10.(*40*) Chen *et al*.(*41*) proposed a binding model for dendrimer/DNA complex, involving one dendrimer molecule binding to each of the successive units of the DNA helix or to two or more independent DNA chains. Based on the observed intermediate structures, we

propose that dendrimers can play an active role in linking ODN molecules to form high molecular weight polymer chains. The chain extension of a short ODN in the presence of coralyne has recently been reported by Hud and colleagues.(*42*) They found fibrous
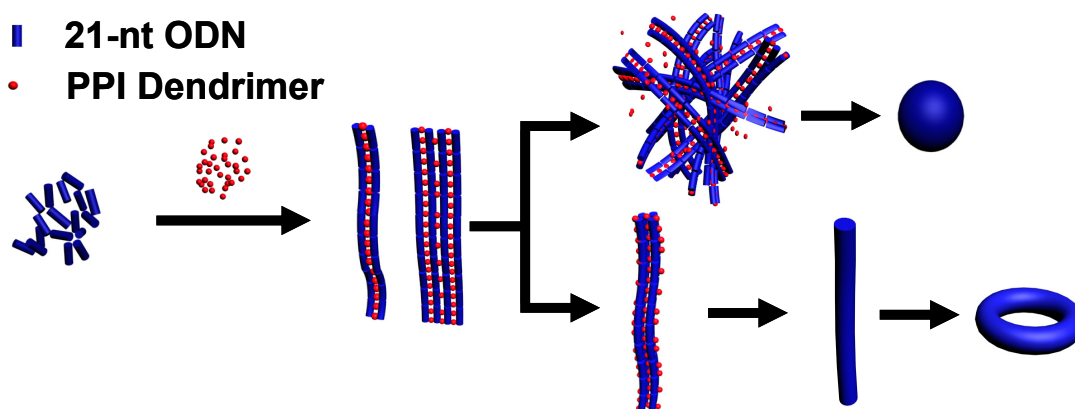
Figure 2.9. Schematic representation of the proposed zipping mechanism for the condensation of the 21-nt ODN by PPI dendrimers. PPI dendrimers first "zip" the ODN molecules by electrostatic interactions to form extended chains. The extended chains could wrap around to form aggregated complex structures, which then further condense into spheroidal structures. The extended chains could also interact with each other in parallel to form ribbon- and rod-like structures and then wrap around to form toroidal structures.

structures after the complexation of oligomers, $(dA)_8$, $(dA)_{16}$ and $(dA)_{32}$ with coralyne. They believe that the coralyne molecules intercalate into the duplex in which two ODN strands are assembled in an anti-parallel orientation. In our case, dendrimer is believed to act as a "zipper", electrostatically interacting with phosphate groups from different ODN chains. Initial end-to-end arrangements of ODN many be formed along the amino groups of dendrimers yielding nanofibers. Extended fibers are produced from multiple ODNs

through dendrimer junctions, as shown in the schematic drawing (Figure 2.9). These nanofibers may interact to produce spherical particles by multi-moleuclar associations of dendrimer/ODN macromolecules.

The height of the isolated extended fibers formed from dendrimer G-1 and G-2 was ~0.5 nm and those formed with G-5 dendrimer had a height of ~0.7-0.8 nm. The highest fibers in the AFM images from all 5 generations had a height of 1.6 ± 0.5 nm. Considering that the diameter is 1.9-2.8 nm for PPI G-2 to G-4 dendrimers,(*43*) the measured values are much lower than the expected values. In fact, AFM height value of single-stranded DNA is almost always lower than the theoretical diameter of 2 nm. A measured value from 0.3 nm to 1.5 nm is often seen in related DNA research,(*6, 44, 45*) including ours.(*38, 46, 47*) The cause of this discrepancy is discussed in a recent publication(*38*) and review(*48*). Briefly, the presence of a salt layer around the extended ODN-dendrimer fibers may contribute to this discrepancy. In addition, elastic deformation induced by tip-sample interaction and the compression of the molecule caused by the attractive forces between the fiber and the substrate may contribute to the reduction in measured height. Therefore, the low height fibers in the AFM images may be the single extended chains of ODN-dendrimer, and the higher ones may account for multiple rods connected in z direction. At this point, it is not clear if the fibers extend in x-y plain, because the convolution effect of the AFM tip prevents us from measuring the diameter accurately. However, we do find that some nanofibers interact with each other in parallel, as indicated in the inset of Panel C and Panel F of Figure 2.3.

Tightly or loosely interacting nanofiber may be another intermediate state in the formation of final products of spheroids and toroids. Using electron microscope, Böttcher et al.(*28*) showed the presence of a series of intermediate multimolecular condensates

with parallel bundles of DNA in the presence of spermidine. The model proposed by Ha and Liu(*49*) postulates an indefinite number of rods that bundle together to a condensate due to the counterion correlation across the bundle. AFM images also revealed early precollapse intermediates with interesting morphologies, such as flower and disk-like structures formed by the crossing over of multiple loops on the DNA strand at the same point.(*50-53*) Looped and spaghetti-like intermediates by AFM and EM were also reported during condensation of high molecular weight DNA.(*37, 52, 53*) In our AFM and EM images, the presence of loops, branched structures and toroids (Figure 2.3 Panels B, C, D and E and Figure 2.5) in the presence of the dendrimers, indicate that a secondary folding of the extended ODN fibers occurs. Taken together, our data suggest that the initial steps in the compaction of ODN to nanoparticles occur by a mechanism different from those observed during the condensation of a long DNA polymer. It is possible that PPI dendrimers first "zip" the ODN molecules by electrostatic interactions to form extended chains. During the formation of nanofibers, the dendrimers may form a "zipper" as well as counter-ions for charge neutralization. AFM data (Figure 2.3B) suggest that DNA nanofibers wrap around a central loop or aggregate to a central core (Figure 2.3D). In previous studies, we and others have found similar folding pathways in the condensation of high molecular weight linear DNA and plasmid DNA (in the presence of polyamines or other cations).(*17, 38*) It should be noted that in AFM measurement is that the DNA nanoparticles in solution must be transferred and immobilized onto a solid substrate (usually mica surface). This process may introduce artifacts in the size and shape of the particles observed. EM also shares some of these drawbacks. However, EM measurement avoids some of the problems associated with AFM measurement, such as tip convolution effects and buffer residues on the substrate surface; therefore it can

achieve more precise measurements. The use of AFM, EM, and light scattering as complementary techniques can lead to better understanding of different DNA structures in solution.

The compacted nanostructures formed from ODNs and dendrimers are expected to pass through the cell membrane more efficiently as compared to the naked ODN. Accordingly, confocal microscopic study demonstrated that only G-4 and G-5 dendrimers were highly efficient in transporting the ODN to the cells. Even though dendrimer concentrations used for confocal microscopy were higher than the EC_{50} values required for DNA condensation, G-1 and G-2 dendrimers were completely inefficient in facilitating cellular uptake of ODN. This result is comparable to our recent studies using PPI dendrimers in delivering triplex forming ODNs in different cancer cell lines.(*26*) The difference in efficacy of dendrimers could be partially attributed to the smaller size of the ODN nanoparticles formed with higher generations of dendrimers. However, the G-2 condensed ODN nanoparticles (diameter, 74 ± 18 nm and height, 17 ± 5) have approximately the same size as G-5 condensed DNA nanoparticles (diameter 71 ± 21 nm and height of 20 ± 6 nm), but G-2 was unable to transport the ODN to cells. Our data on ζ potential provide clues to another essential requirement for cellular uptake. The nanoparticles produced with G-1, G-2 and G-3 dendrimers had significantly lower ζ-potential (5.2-6.5 mV) compared to those produced with G-4 and G-5 (12-18 mV) dendrimers. Nanoparticles formed with G-2 dendrimer had the least ζ potential (5.2 mV). It was suggested that a net positive charge is necessary for cellular uptake of ODN nanoparticles.(*8*) Our results indicate that both the size and surface charge of nanoparticles are important in their cellular uptake.

Studies of Zinselmeyer et al.(*37*) showed that PPI dendrimers could be used for the delivery of plasmid DNA in cells. However, their report indicated a maximal uptake with G-2 dendrimer. Compared to the short ODNs used in this study, it is possible that the greater conformational mobility and the length of the plasmid DNA molecule could achieve sufficient binding sites with lower generation dendrimers, which could provoke nanoparticle formation and facilitate cellular uptake. Thus, conditions for transfection of plasmid DNA could be different from conditions for transfection of short ODNs. This is consistent with reports showing that short DNAs were more difficult to condense into well-defined nanoparticles.(*17, 37, 42, 54*)

2.4. Conclusions

In summary, this study demonstrates that amine-terminated PPI dendrimers are capable of inducing nanostructure formation from a 21-nt single-stranded ODN. Nanoparticles were predominantly spheroids, with occasional toroids, as visualized by AFM and EM. We propose a zipping condensation mechanism. The zipping mechanism involves "zipping" of ODN molecules by PPI dendrimers by electrostatic interactions to form extended nanofibers, followed by sequential folding and compaction into nanoparticles. Although all five generations of PPI dendrimers provoked ODN nanoparticle formation, only the ODN nanoparticles formed from G-4 and G-5 could undergo facile cellular uptake in MDA-MB-231 cells. These results demonstrate that both the size and the surface charge properties of the ODN nanoparticles are important in cellular transport. In contrast to studies on the delivery of plasmid DNA by PPI dendrimers,(*37*) ODN nanoparticles formed with G-1 to G-2 dendrimers were not taken up by MDA-MB-231

cells. ODN nanoparticles formed with G-3 dendrimers were only slightly taken up by cancer cells, indicating that formulations for high molecular weight DNA delivery might not be directly applied to deliver ODNs to intracellular compartments. Specific formulation parameters are necessary for enabling the delivery of short ODNs as therapeutic entities into cancer cells.

2.5. Experimental Section

2.5.1. Oligodeoxynucleotide

The 21-nt ODN used in this study was purchased from Oligos, Etc. (Wilsonville, OR). The sequence of the ODN was as follows: 5'-GAAGTTCACGTTGAGGGGCAT-3'. The molar concentration of the ODN was calculated using an extinction coefficient of 241.6 mM^{-1} cm^{-1} at 260 nm. All experiments were conducted either in 10 mM Na cacodylate buffer (10 mM Na cacodylate, pH 7.4, 0.5 mM EDTA)(*26*) or in 10 mM Na cacodylate buffer containing the approximate physiological concentration of cations (120 mM KCl, 10 mM NaCl, 2 mM MgCl$_2$, and 0.1 mM CaCl$_2$), as indicated in Figure/Table legends. Buffers were filtered through 0.25 μm GS Millipore filters to remove insoluble particles.

2.5.2. Cell Culture

Breast cancer cell line, MDA-MB-231, was obtained from ATCC (Manassas, VA). MDA-MB-231 cells were maintained in MEM medium, supplemented with 10% fetal bovine serum, 100 units/mL penicillin, 100 μg/mL streptomycin, 40 μg/mL gentamycin, 0.4 mM Na pyruvate and 2 mM L-glutamine.(*26*)

2.5.3. Dendrimers and Chemicals

Dendrimers, polypropyleneimine tetraamine (DAB Am-4, generation-1 (G-1)), polypropyleneimine octaamine (DAB-Am-8, generation-2 (G-2)), polypropyleneimine hexadecaamine (DAB Am-16, generation-3 (G-3)), polypropyleneimine dotriacontaamine (DAB Am-32, generation-4 (G-4)), and polypropyleneimine tetrahexacontaamine (DAB-Am-64, generation-5 (G-5)) were purchased from Aldrich (Milwaukee, WI), and used without further purification. According to the manufacturer, generations 1-4 showed a single spot in gel electrophoresis, while G-5 showed a second minor spot, indicating the presence of a small amount of impurity. Other chemicals used in this study were purchased from Sigma-Aldrich (St. Louis, MO), and used without further purification.

2.5.4. Total Intensity Light Scattering

Total intensity light scattering experiment was conducted using a Fluoromax-2 spectrofluorometer (Jobin Yvon-Spex Instruments, S. A., Edison, NJ).(*38*) Light from a 150 W Xenon lamp was filtered through double monochromators. The scattered light intensity was measured at an angle of 90° to the incident beam. The excitation and emission wavelengths were set at 305 nm, with 5 nm band-pass. The integration time was set at 5 s. The ODN solution was taken in a disposable borosilicate glass tube. Dendrimer was added to this solution, vortexed, and kept undisturbed for 30 minutes at 22 ^{o}C to attain equilibrium. The solution was then centrifuged at 500 x g for 10 minutes using a Beckman GS 6KR centrifuge to remove any aggregates or dust particles in the solution. Our previous study demonstrated that centrifugation at 500 x g did not result in phase

separation or a reduction in DNA concentration in solution.(*38*) Dendrimers were used at 0.025 to 4 µM concentrations for the study.

2.5.5. Dynamic Light Scattering

Dynamic light scattering experiments were performed using a DynaPro model MSX equipment (Protein Solutions, Inc., Charlottesville, VA).(*38*) Dendrimer solution was added to ODN solution (0.2 µM) to achieve the desired condensing agent concentration. The dendrimer concentrations used in DLS experiments were 5-fold of the EC_{50} values under the buffer conditions in order to ensure complete condensation of the oligonucleotides. The samples were mixed and allowed to attain equilibrium for 30 minutes at 22 °C, and centrifuged for 10 minutes at 500 x g. Scattered light was measured from a 45 µL of sample in a standard quartz cuvette. All measurements were performed in the same cuvette. A laser beam from a 2W laser (800 nm wavelength) was passed through a quartz cell with the sample (dendrimer/ODN mixture), and the scattered light was detected at a 90° angle with respect to the incident beam. The scattered light was analyzed with an autocorrelator to generate the first-order autocorrelation function. The following equation describes the autocorrelation function, $g^{(1)}$ (τ), for monodisperse particles that are much smaller than the incident beam:

$g^{(1)}(\tau) = \exp[-Dq^2(\tau)]$

In this equation τ is the decay time, q ($= 4\pi n/[\lambda \sin(\theta/2)]$) is the scattering vector which is a function of the incident beam wavelength λ, the scattering angle θ, the refractive index of the solvent n, and the diffusion coefficient D. The hydrodynamic radius (R_h) is calculated from the diffusion coefficient using the Stokes-Einstein equation:

$R_h = kT/6\pi\eta D$,

where T is the absolute temperature, η is solvent viscosity, and k is the Boltzmann constant. Data were analyzed by a Dynamics Version 6 software package (Protein Solutions, Inc., Lakewood, NJ).

2.5.6. Atomic Force Microscopy

AFM images were obtained using a Nanoscope IIIA equipment (Digital Instruments, Santa Barbara, CA) in tapping mode, operating in ambient air. A 125 μm long rectangular silicon cantilever/tip assembly was used with a spring constant of 40 N/m, resonance frequency of 315-352 kHz, and tip radius of 5-10 nm. The applied frequency was set on the lower side of the resonance frequency. The image was generated by the change in amplitude of the free oscillation of the cantilever as it interacted with the sample. The height differences on the surface are indicated by the color code, lighter regions indicating increase in height of the nanoparticles. In order to image ODN nanoparticles, 5 μL of ODN/dendrimer solutions were deposited on a freshly cleaved mica surface. After 3-6 minutes of incubation, the surface was rinsed with 2-3 drops of nanopure water (Barnstead), and dried under a flow of dry nitrogen. Height and outer diameter of nanoparticles were measured using the Nanoscope software. Data are given as mean ± standard error of the mean.

2.5.7. Electron Microscopy

EM of condensed ODN nanoparticles was performed using a JEOL 1200 VX electron microscope. ODN solution was mixed with dendrimer solution and incubated for 1 hour. One drop of this solution was deposited on a carbon coated 200 mesh copper grid that

was glow discharged for 1 minute. The ODN solution on the grid was stained with 1% uranyl acetate solution for 30 seconds. Excess liquid was removed using a filter paper with an average of pore size of 11 μm (Whatman) and the sample viewed on the electron microscope and photographed with an attached camera.

2.5.8. Zeta Potential Measurements

ζ-Potential measurements were carried out using a Zetasizer 3000 HS (Malvern Instruments Ltd, UK) at 25 °C. Samples were injected in an M3 quartz capillary cell and analyzed under a constant voltage after focusing with a nominal 5 mW Helium Neon continuous power model having a wavelength output of the laser of 633 nm. The ζ-potential, in mV, was automatically calculated from the electrophoretic mobility based on the Smolukowski formula. Average ζ–potential values were calculated from the data of 7-9 runs. The instrument was calibrated with a DTS1050 Malvern ζ–potential transfer standard (-50 mV±5 mV). A solution containing 0.2 μM ODN and 2.5 μM dendrimer was prepared and incubated for 1 hour at room temperature and then injected for ζ-potential measurement.

2.5.9. Confocal Microscopy

The confocal microscopic imaging of the cellular uptake of the 21-nt fluorescein-tagged ODN by MDA-MB 231 cells was performed as follows. MDA-MB 231 cells (2.5 x 10^3 cells/well) were seeded in a chamber slide system (Nalgene Nunc). After 24 hours, cells were treated with fluorescein-tagged ODN-dendrimer mixture. Final concentrations of dendrimers in the cell culture medium were as follows: G-1, 2 μM; G-2, 0.75 μM; G-3, 0.5 μM; G-4, 0.2 μM; and G-5, 0.2 μM. The dendrimer and ODN were mixed and

incubated for 10 minutes at 22 °C prior to cell treatment. After 24 hours, cells were fixed with 1% paraformaldehyde in phosphate buffered saline (PBS). Nuclei were stained using 4',6-diamidino-2-phenylindole (DAPI). Cellular margins were marked by Alexa fluor-546 tagged phalloidin, which reacted with actin. Cells were mounted with aqueous mounting medium containing antifading agents (Gel mount, Sigma) for analysis by confocal microscopy using a Zeiss LSM-510 laser scanning microscope (Carl Zeiss, Thornwood, NY, U.S.A.).

2.5.10. Polyacrylamide Gel Electrophoresis of [^{32}P]-labeled ODN

MDA-MB-231 cells were incubated with [^{32}P]-labeled ODN or [^{32}P]-labeled ODN/G-4 dendrimer complexes at 37 °C for 48 h. Cells were harvested at 4, 6, 8, and 24 h after treatment. Cells were first washed three times with PBS and then incubated for 2 minutes with 300 units/ml of DNAse I in 50 mM Tris.HCl (pH, 7.6) containing 10 mM MgCl$_2$. Cells were then washed with PBS, trypsinized, collected in 1 mL PBS, centrifuged at 1,000 x g for 5 minutes, and the supernatant was removed. The cell pellet was lysed with 500 µL of 1% SDS lysis buffer (10 mM Tris.HCl pH 7.4, 150 mM NaCl and 1% sodium dodecyl sulfate). The lysate was centrifuged at 3,000 x g for 15 minutes and supernatant collected in microcentrifuge tubes. ODN was precipitated by adding 50 µL of 5 M NaCl and 1 mL of cold 100% ethanol. After 1 hour at −70°C, the solution was centrifuged at 12,000 x g for 15 minutes. The supernatant was removed and the precipitate dried in air. Samples were dissolved in 50 µL of a solution containing 10 mM Tris.HCl and 50 mM NaCl, and analyzed by gel electrophoresis using 20 % polyacrylamide gel at 250 V for 3 h. The gel was dried, and exposed to X-ray film.

2.6. References

1. Ito, M., Kawano, K., Miyagishi, M., and Taira, K. (2005) Genome-wide application of RNAi to the discovery of potential drug targets, *FEBS Letters 579*, 5988-5995.

2. Aboul-Fadl, T. (2005) Antisense oligonucleotides: the state of the art, *Current Medicinal Chemistry 12*, 2193-2214.

3. Vijayanathan, V., Thomas, T., and Thomas, T. J. (2002) DNA Nanoparticles and Development of DNA Delivery Vehicles for Gene Therapy, *Biochemistry 41*, 14085-14094.

4. Bloomfield, V. A. (1996) DNA condensation, *Current Opinion in Structural Biology 6*, 334-341.

5. Seeman, N. C. (2003) At the Crossroads of Chemistry, Biology, and Materials: Structural DNA Nanotechnology, *Chemistry & Biology 10*, 1151-1159.

6. Wang, H., Yang, Y., Schofield, M. J., Du, C., Fridman, Y., Lee, S. D., Larson, E. D., Drummond, J. T., Alani, E., Hsieh, P., and Erie, D. A. (2003) DNA bending and unbending by MutS govern mismatch recognition and specificity, *PNAS 100*, 14822-14827.

7. Koltover, I., Wagner, K., and Safinya, C. R. (2000) DNA condensation in two dimensions, *Proc. Natl. Acad. Sci. 97*, 14046-14051.

8. Junghans, M., Kreuter, J., and Zimmer, A. (2001) Phosphodiester and phosphorothioate oligonucleotide condensation and preparation of antisense nanoparticles, *Biochimica et Biophysica Acta (BBA) - Protein Structure and Molecular Enzymology 1544*, 177-188.

9.   Dauty, E., Behr, J.-P., and Remy, J.-S. (2002) Development of plasmid and oligonucleotide nanometric particles, *Gene Therapy 9*, 743-748.

10.   Bielinska, A., Kukowska-Latallo, J. F., Johnson, J., Tomalia, D. A., and J R Baker, J. (1996) Regulation of in vitro gene expression using antisense oligonucleotides or antisense expression plasmids transfected using starburst PAMAM dendrimers, *Nucleic Acids Research 24*, 2176-2182.

11.   Delong, R., Stephenson, K., Loftus, T., Fisher, M., Alahari, S., Nolting, A., and Juliano, R. L. (2000) Characterization of complexes of oligonucleotides with polyamidoamine starburst dendrimers and effects on intracellular delivery, *Journal of Pharmaceutical Sciences 86*, 762-764.

12.   Jaukb, D. L. E., and Zimmer, A. (2004) Drug delivery of oligonucleotides by peptides, *European Journal of Pharmaceutics and Biopharmaceutics 58*, 237-251.

13.   Hussain, M., Shchepinov, M., Sohail, M., Benter, I. F., Hollins, A. J., Southern, E. M., and Akhtar, S. (2004) A novel anionic dendrimer for improved cellular delivery of antisense oligonucleotides, *Journal of controlled release 99*, 139-155.

14.   Zhao, X. B., and Lee, R. J. (2004) Tumor-selective targeted delivery of genes and antisense oligodeoxyribonucleotides via the folate receptor, *Advanced Drug Delivery Reviews 56*, 1193-1204.

15.   Yang, L., Li, J., Zhou, W., Yuan, X., and Li, S. (2004) Targeted delivery of antisense oligodeoxynucleotides to folate receptor-overexpressing tumor cells, *Journal of controlled release 95*, 321-331.

16.   Bloomfield, V. A. (1998) DNA condensation by multivalent cations, *Biopolymers 44*, 269-282.

17. Hud, N. V., Downing, K. H., and Balhorn, R. (1995) A constant radius of curvature model for the organization of DNA in toroidal condensates, *Proc. Natl. Acad. Sci. 92*, 3581-3585.

18. Widom, J., and Baldwin, R. L. (1980) Cation-induced toroidal condensation of DNA: Studies with Co3+(NH3)6, *Journal of Molecular Biology 144*, 431-453.

19. Newkome, G. R., Moorefield, C. N., and Vögtle, F. (2001) Dendrimers and Dendrons: Concepts, Synthesis, Applications, Wiley-VCH, New York.

20. Tomalia, D. A., Baker, H., Dewald, J., Hall, M., Kallos, G., Martin, S., Roeck, J., Ryder, J., and Smith, P. (1985) A New Class of Polymers: Starburst-Dendritic Macromolecules, *Polymer Journal 17*, 117-132.

21. Liu, M., and Fréchet, J. M. J. (1999) Designing dendrimers for drug delivery, *Pharmaceutical Science & Technology Today 2*, 393-401.

22. Tang, M. X., Redemann, C. T., and Francis C. Szoka, J. (1996) In Vitro Gene Delivery by Degraded Polyamidoamine Dendrimers, *Bioconjugate Chemistry 7*, 703-714.

23. Choi, Y., Thomas, T., Kotlyar, A., Islam, M. T., and James R. Baker, J. (2005) Synthesis and Functional Evaluation of DNA-Assembled Polyamidoamine Dendrimer Clusters for Cancer Cell-Specific Targeting, *Chemistry & Biology 12*, 35-43.

24. Malik, N., Wiwattanapatapee, R., Klopsch, R., Lorenz, K., Frey, H., Weener, J. W., Meijer, E. W., Paulus, W., and Duncan, R. (2000) Dendrimers:: Relationship between structure and biocompatibility in vitro, and preliminary studies on the biodistribution of 125I-labelled polyamidoamine dendrimers in vivo, *Journal of controlled release 65*, 133-148.

25. Wilson, R. W., and Bloomfield, V. A. (1979) Counterion-induced condensation of deoxyribonucleic acid. A light-scattering study, *Biochemistry 18*, 2192-2196.

26. Santhakumaran, L. M., Thomas, T., and Thomas, T. J. (2004) Enhanced cellular uptake of a triplex-forming oligonucleotide by nanoparticle formation in the presence of polypropylenimine dendrimers, *Nucleic Acids Research 32*, 2102-2112.

27. Thomas, R. M., Thomas, T., Wada, M., Sigal, L. H., Shirahata, A., and Thomas, T. J. (1999) Facilitation of the Cellular Uptake of a Triplex-Forming Oligonucleotide by Novel Polyamine Analogues: Structure-Activity Relationships, *Biochemistry 38*, 13328-13337.

28. Böttcher, C., Endisch, C., Fuhrhop, J.-H., Catterall, C., and Eaton, M. (1998) High-Yield Preparation of Oligomeric C-Type DNA Toroids and Their Characterization by Cryoelectron Microscopy, *J. Am. Chem. Soc. 120*, 12-17.

29. Marx, K. A., and Reynolds, T. C. (1982) Spermidine-condensed phi X174 DNA cleavage by micrococcal nuclease: torus cleavage model and evidence for unidirectional circumferential DNA wrapping, *PNAS 79*, 6484-6488.

30. Kornyshev, A. A., and Leikin, S. (1998) Symmetry laws for interaction between helical macromolecules, *Biophys. J. 75*, 2513-2519.

31. Livolant, F., and Leforestier, A. (1996) Condensed phases of DNA: Structures and phase transitions, *Progress in Polymer Science 21*, 1115-1164.

32. Saminathan, M., Antony, T., Shirahata, A., Sigal, L. H., Thomas, T., and Thomas, T. J. (1999) Ionic and Structural Specificity Effects of Natural and Synthetic Polyamines on the Aggregation and Resolubilization of Single-, Double-, and Triple-Stranded DNA, *Biochemistry 38*, 3821–3830.

33. Mel'nikov, S. M., Sergeyev, V. G., and Yoshikawa, K. (1995) Discrete Coil-Globule Transition of Large DNA Induced by Cationic Surfactant, *J. Am. Chem. Soc. 117*, 2401-2408.

34. Zinchenko, A. A., Sergeyev, V. G., Murata, S., and Yoshikawa, K. (2003) Controlling the Intrachain Segregation on a Single DNA Molecule, *J. Am. Chem. Soc. 125*, 4414-4415.

35. Chen, N., Zinchenko, A. A., Murata, S., and Yoshikawa, K. (2005) Specific Formation of Beads-on-a-Chain Structures on Giant DNA Using a Designed Polyamine Derivative, *J. Am. Chem. Soc. 127*, 10910-10916.

36. Sarkar, T., Conwell, C. C., Harvey, L. C., Santai, C. T., and Hud, N. V. (2005) Condensation of oligonucleotides assembled into nicked and gapped duplexes: potential structures for oligonucleotide delivery, *Nuclei Acids Research 33*, 143-151.

37. Zinselmeyer, B. H., Mackay, S. P., Schatzlein, A. G., and Uchegbu, I. F. (2002) The Lower-Generation Polypropylenimine Dendrimers Are Effective Gene-Transfer Agents, *Pharmaceutical Research 19*, 960-967.

38. Vijayanathan, V., Thomas, T., Antony, T., Shirahata, A., and Thomas, T. J. (2004) Formation of DNA nanoparticles in the presence of novel polyamine analogues: a laser light scattering and atomic force microscopic study, *Nuclei Acids Research 32*, 127-134.

39. Choi, Y., Mecke, A., Orr, B. G., Holl, M. M. B., and James R. Baker, J. (2004) DNA-Directed Synthesis of Generation 7 and 5 PAMAM Dendrimer Nanoclusters, *Nano Letters 4*, 391-397.

40. Kabanov, V. A., Sergeyev, V. G., Pyshkina, O. A., Zinchenko, A. A., Zezin, A. B., Joosten, J. G. H., Brackman, J., and Yoshikawa, K. (2000) Interpolyelectrolyte Complexes Formed by DNA and Astramol Poly(propylene imine) Dendrimers, *Macromolecules 33*, 9587-9593.

41. Chen, W., Turro, N. J., and Tomalia, D. A. (2000) Using Ethidium Bromide To Probe the Interactions between DNA and Dendrimers, *Langmuir 16*, 15-19.

42. Persil, Ö., Santai, C. T., Jain, S. S., and Hud, N. V. (2004) Assembly of an Antiparallel Homo-Adenine DNA Duplex by Small-Molecule Binding, *J. Am. Chem. Soc. 126*, 8644-8645.

43. Crooks, R. M., Chechik, V., Lemon, B. L., Sun, L., Yeung, L. K., and Zhao, M. (2002) Metal Nanoparticles, Synthesis, Characterization, and Applications, (Feldheim, D. L., Ed.).

44. Deng, Z., and Mao, C. (2003) DNA-Templated Fabrication of 1D Parallel and 2D Crossed Metallic Nanowire Arrays, *Nano Letters 3*, 1545-1548.

45. Nakao, H., Gad, M., Sugiyama, S., Otobe, K., and Ohtani, T. (2003) Transfer-Printing of Highly Aligned DNA Nanowires, *J. Am. Chem. Soc. 125*, 7162-7163.

46. Zhang, J., Ma, Y., Stachura, S., and He, H. (2005) Assembly of Highly Aligned DNA Strands onto Si Chips, *Langmuir 21*, 4180-4184.

47. Ma, Y., Zhang, J., Zhang, G., and He, H. (2004) Polyaniline Nanowires on Si Surfaces Fabricated with DNA Templates, *J. Am. Chem. Soc. 126*, 7097-7101.

48. Moreno-Herrero, F., Colchero, J., and Baró, A. M. (2003) DNA height in scanning force microscopy, *Ultramicroscopy 96*, 167-174.

49. Ha, B.-Y., and Liu, A. J. (1998) Effect of Non-Pairwise-Additive Interactions on Bundles of Rodlike Polyelectrolytes, *Physical Reivew Letters 81*, 1011-1014.

50. Fang, Y., and Hoh, J. H. (1999) Cationic silanes stabilize intermediates in DNA condensation, *FEBS Letters 459*, 173-176.

51. Dunlap, D. D., Maggi, A., Soria, M. R., and Monaco, L. (1997) Nanoscopic structure of DNA condensed for gene delivery, *Nuclei Acids Research 25*, 3095-3101.

52. Golan, R., Pietrasanta, L. I., Hsieh, W., and Hansma, H. G. (1999) DNA Toroids: Stages in Condensation, *Biochemistry 38*, 14069-14076.

53. Fang, Y., and Hoh, J. H. (1998) Early Intermediates in Spermidine-Induced DNA Condensation on the Surface of Mica, *J. Am. Chem. Soc. 120*, 8903-8909.

54. Bloomfield, V. A. (1997) DNA condensation by multivalent cations, *Biopolymers 44*, 269-282.

Chapter 3

Labile Catalytic Packaging and Delivering of siRNA/DNA to Cancer Cells: Control of Gold Nanoparticles "out" of siRNA/DNA Complexes

3.1. Introduction

The inefficient transport of nucleic acids through the cell membrane is a major limiting factor in clinical application of therapeutic nucleic acids, including antisense, anti-gene, and short interference RNA (siRNA) strategies. It has been recognized that a prerequisite for the facile transport of DNA/RNA through the cell membrane is packaging of the nucleic acid to nanoparticles of ~100 nm size.(*1, 2*) Viral vectors are efficient of accomplishing this. However, the immune response elicited by viral proteins has posed a major challenge to this approach.(*3*) Hence, there is much interest in developing nonviral gene delivery vehicles.

Dendrimers are highly branched three-dimensional polymers with a large number of controllable peripheral functionalities, useful as gene delivery agents, drug delivery vehicles, and magnetic resonance imaging agents.(*4-8*) Protonated amino groups of dendrimers appear to buffer acidic endosomal compartment and release DNA to the cytoplasm.(*6, 9, 10*) While higher generation dendrimers show higher cytotoxicity(*8, 11, 12*) and their synthesis and purification are usually tedious with low yield, low generation

dendrimers are nontoxic and easy to synthesize.(*4, 13, 14*) However, the limited surface charges of low generation dendrimers lead to their inefficient complexation with DNA and low cellular uptake efficacy.(*15*) In our recent studies we found that only higher generations of polypropylenimine (PPI) dendrimers could enhance oligodeoxynucleotide (ODN) uptake to breast cancer cells as demonstrated by confocal microscopy.(*16*)

There is a surge of interest in using inorganic engineered nanoparticles for medical and biological applications. They are expected to solve some difficult human health problems due to their unique properties and their remarkably large surface area. Studies using inorganic engineered nanoparticles modified with cationic molecules, including dendrimers have demonstrated enhancement in DNA condensation, delivery and transfection in mammalian cells.(*17-28*) Luo et al. also reported that DNA transfection by cationic transfection reagents can be dramatically enhanced by unmodified silica nanoparticles via a unique "concentration" mechanism (*29*).

However, the inorganic nanoparticles were encapsulated inside the resulting DNA nanoparticles. Toxicity of the inorganic nanoparticles in human body is a major concern. Currently the toxicology of most inorganic engineered nanomaterials is not available and is in the process of assessment. A new field of nanotoxicology was just born to study the effects of engineered nanodevices and nanostructures in living organisms. Conflicting data have emerged and long-term fate of the nanomaterials in human body is not known yet.

In this work, we report a new usage of gold nanoparticles (Au NPs) to help low generation dendrimers to effectively package and deliver nucleic acids (both long plasmid DNA and siRNA) but the Au NPs are not included in the final nucleic acid

nanoparticles. Therefore the potential long-term toxic problem accompanied with the Au NPs can be solved by selectively removing the Au NPs before the nucleic acid nanoparticles are delivered. More importantly, the siRNA nanoparticles packaged by this novel approach can efficiently internalize into cancer cells and effectively silence their target mRNA. The efficiency is even superior to higher generation dendrimers.

3.2. Results and Discussion

Our approach relies on the competing affinities of Au and nucleic acids for the amine sites of low generation polypropyleneimine (PPI) dendrimers. In neutral pH solutions, the primary amines of the dendrimers are protonated (pKa~9.8),(*30-34*) while most of their tertiary amines (pKa~5.9-7.0)(*30, 34*) are not, which provide strong Au/amine interactions, so that each Au NP anchors several low generation dendrimers through multiple Au/amine interactions. The largely increased positive charges on each of the delivery vehicles (here Au NPs modified with low-generation dendrimers) resemble higher generation dendrimers (Figure 3.1) and enable effective packaging of nucleic acids (both long plasmid DNA and siRNA) into nanostructures. However, when multiple nucleic acids interact with the delivery vehicle, the local pH effects caused by the presence of nucleic acids increase the local acidity of the dendrimers. (*33*) As a result, the number of unprotonated tertiary amine sites on dendrimer is decreased due to protonation, which in turn decreases the affinity of dendrimer to Au(*35*) while increasing the affinity to nucleic acids. The large local pH effect has been used to extend the conductivity of polyaniline to neutral or slightly basic solutions,(*36, 37*) including our previous work.(*38*)

To examine the feasibility of this hypothesis, we prepared Au NPs modified with generation 3 (G3) PPI dendrimer according to a protocol described by Wang and his colleagues.(*39*) Briefly, 32.8 mg of G3 dendrimer was mixed with 8.8 ml of 2.45 mM HAuCl$_4$ solution at a molar ratio of 0.9:1 and then heated at 80° C for 1 h with continuous stirring. As a result, a clear and reddish Au NP solution was obtained with each Au NP physically anchoring 6-8 G3 dendrimers.(*39-43*) The largely increased positive charges on each of the condensing agents (here Au NPs modified with G3 dendrimers) enabled the low generation dendrimers to effectively condense DNA as higher generation dendrimers do.(*17, 18, 23-25, 44-48*) To remove the un-reacted HAuCl$_4$, the solution thus obtained was cooled to 22 °C and dialyzed (3.5k-Da cutoff) against 200 ml of double-distilled water twice before it was used to condense nucleic acids. UV-visible spectroscopy was used to characterize the formed nanoparticle solution. A strong absorption was observed at ~523 nm, which was due to the surface plasmon resonance of the Au NPs. The mean hydrodynamic radius of Au NPs was 8.6 ± 1.7 nm as determined by dynamic light scattering (DLS).

3.2.1. Condensation of PGL3 Plasmid DNA

We first tested the ability of the Au NPs to condense DNA. We used PGL3 plasmid DNA for our initial experiments. The condensates of DNA were prepared by mixing the dialyzed and appropriately diluted G3 dendrimer-modified Au NP solution and DNA solution. The condensates were imaged using atomic force microscope (AFM, Nanoscope III A). Figure 3.2.a and 3.2.b show the height and phase image of the condensates. Flower
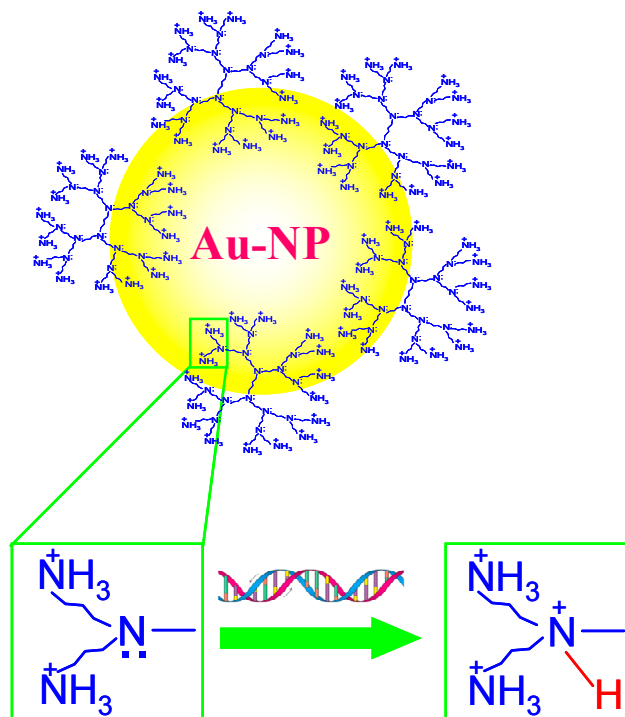
Figure 3.1. An Au NP anchored with several low generation dendrimers through Au-amine bonds. Addition of DNA/siRNA leads to an increase of local acidity, which protonates the tertiary amines, weakening the Au-amine interactions. As a result, the Au NPs are released from the dendrimers and are not included in the final DNA/siRNA nanoparticles.

shaped structures that might be intermediates of compaction as well as highly compacted DNA nanoparticles, with an average height of 3.9 ± 0.7 nm and diameter of 81 ± 36 nm were observed. In addition, smaller nanoparticles close to the size of Au NPs in transmission electron microscopy (TEM) measurement were seen in the AFM image. We assigned this set of nanoparticles as the Au NPs, which left the dendrimers upon DNA condensation. The arrow in Figure 3.2.b indicates an Au NP leaving a condensate. The phase image in Figure 3.2.b shows that the two sets of nanoparticles have different phase shifts. The phase of the small nanoparticles shifted 6.1 ± 1.1 degree (appearing brighter)

and that of the larger ones only shifted 0.8-1.7 degree, suggesting differences in their composition.
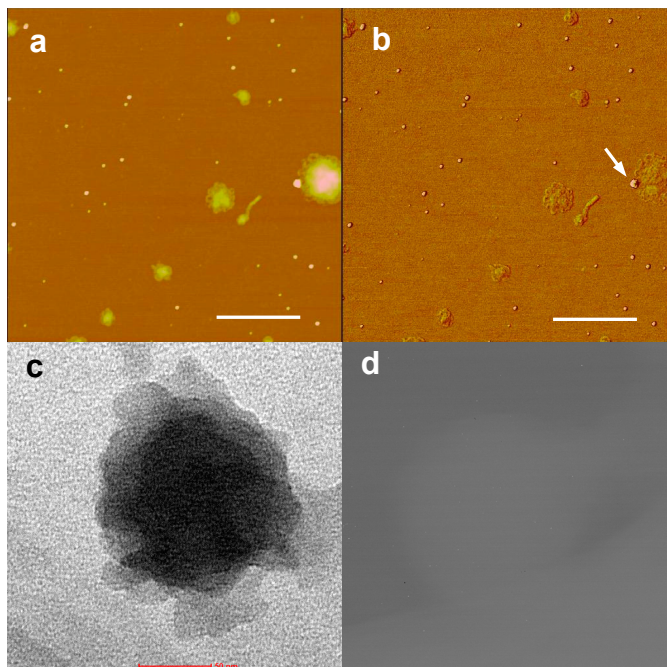
Figure 3.2. AFM images (panels a and b) and TEM images (panels c and d) of condensates formed by plasmid DNA in the presence of G3 PPI dendrimer modified Au NPs (1-h condensation). (a) Height image, z range = 18.0 nm; (b) phase image, z range=10 degree. The bar represents 500 nm in panels a and b. It showed that the Au NPs were isolated from the condensed nanoparticles. (c) One DNA nanoparticle imaged by TEM. (d) The same DNA nanoparticle imaged by TEM in the electron filtering mode, the energy slit was set to the energy edge of Au element, 2386 eV. It showed that no Au NPs were present in the condensate of plasmid DNA. Scale bar represents 50 nm in panels c and d.

To further confirm that the Au NPs left the dendrimers upon DNA condensation, the same solution sample was imaged using a TEM (Libra 120 Energy Filtering, Zeiss). If Au NPs were included in the condensates, as found in previous reports,(*18, 19, 26-28, 49, 50*) we should be able to see them due to the native high contrast of Au in TEM. Figure 3.2.c shows a typical TEM image of a DNA condensate. The diameter of the condensates

is 100 nm ± 30 nm. The size and shape of the condensates was similar to that of the bigger flower-shaped nanoparticles in the AFM images. By imaging the same condensates in the energy filtering TEM mode,(*51, 52*) setting the energy slit to 2386 eV, which is the energy edge of Au element, we performed Au elemental analysis of the condensates. As shown in Figure 3.2.d, the image was blank, as there was no Au signal from the DNA condensate, indicating that the Au NPs left the products upon condensation. The result found here is very different from previous reported DNA condensation by using Au NPs and other nanoparticles as condensing agents, which were encapsulated in the final DNA nanoparticles.(*17-19, 23-28, 44-47, 50, 53, 54*)

3.2.2. Packaging of 21-bp siRNAs to Nanoparticles

There is an increasing enthusiasm for developing therapies based on RNA interference (RNAi), a post-transcriptional gene silencing method, mediated by small duplex RNAs of 19-23 base pairs.(*55-58*) The advantage of RNAi compared to other gene therapeutic strategies lies in its high specificity and potency of gene silencing, coupled with the facts that it can target every gene, and every cell, which has the necessary machinery.(*57, 58*) However, just like other gene therapeutic strategies, the main obstacle to the success of siRNA therapies is in delivering it across the cell membrane to the cytoplasm where it can enter the RNAi pathway and guide the sequence-specific mRNA degradation.(*55, 58-60*) It is reported that the short oligonucleotides are more difficult to package into well-defined particles than the long plasmid DNA.(*16, 61, 62*) In our recent studies,(*63*) we found that in contrast to long plasmid DNA, siRNA required higher generation dendrimers to reach the maximum transfection efficiency (G4 PPI for siRNA vs. G2 PPI for plasmid DNA), possibly due to the less negative charge per molecule and the more
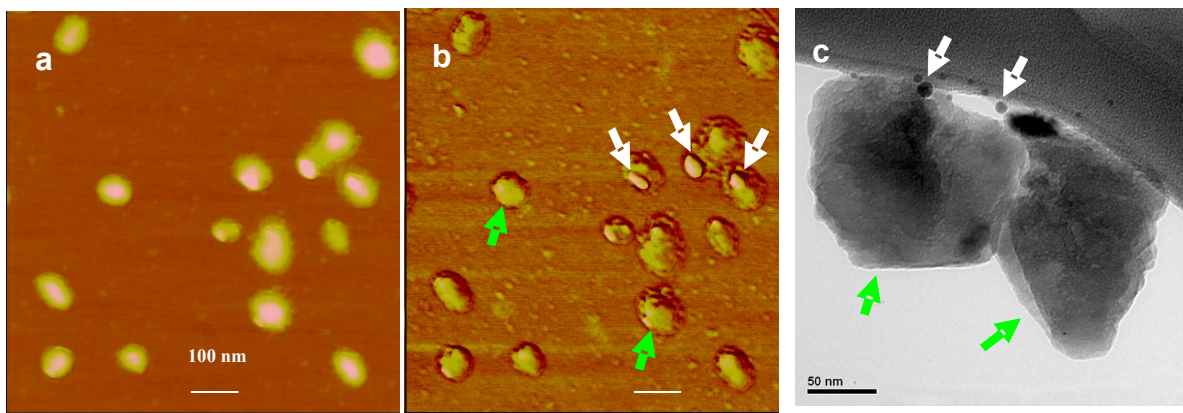
Figure 3.3. AFM images (panels a and b) and TEM image (panel c) of siRNA nanoparticles formed from 0.4 µM 21 bp siRNA in the presence of Au NPs modified with G3 PPI dendrimer (2.5 µM). (a) AFM image, z range= 20.0 nm; (b) phase image, z range=40 degree. The bar represents 100 nm in panels a and b. (c) TEM image of NPs. The bar represents 50 nm in panel c. AFM phase image and TEM image clearly show the Au NPs (indicated by white arrows) were not included in the siRNA nanoparticles.

rigid structure of siRNA. Recently, Huang *et al* (*64, 65*) reported that by adding high molecular weight calf thymus DNA into the siRNA formulation, the size of the formed nanoparticles decreased by 10-30% and the delivery efficiency increased by 20-80%.(*66, 67*)

To demonstrate the wide application of this new packaging approach in gene therapy, we next tested whether the Au NPs modified with G3 PPI dendrimer could catalytically provoke siRNA nanoparticles formation. The complex formation is driven mainly by electrostatic interaction between negatively charged siRNA and positively charged dendrimers on the Au NPs. Such binding leads to the formation of positively

charged complexes that can be retarded in gel electrophoresis when compared with free siRNA which can not. Therefore the sufficient amount of G3 PPI dendrimers needed for the complex formation can be determined from an agarose gel electrophoresis experiment. It was found that when the N/P (nitrogen/phosphate) ratios, which refer to the ratios of the positively charged primary amine groups of the G3 dendrimer on the Au-NPs to negatively charged phosphate groups from siRNAs, were equal to or higher than 1.2, the siRNA was completely retained in the sample wells with negligible electrophoretic shift corresponding to free siRNA. This indicated that all siRNAs formed stable complex with Au-G3 at N/P ratios equal to or higher than 1.2. Based on this, we prepared siRNA nanoparticles by mixing the G3 PPI dendrimer-modified Au NPs solution and siRNA solution in physiological buffer at an N/P ratio of 2.4 and then incubating for 30 min at room temperature. We then visualized the nanoparticles using AFM and TEM as mentioned above. Figure 3.3a shows that siRNA nanoparticles with an average height of 10 ± 3 nm and diameter of 70 ± 10 nm were formed after 30 min of condensation. siRNA nanoparticles were also observed in TEM images (Figure 3.3.c), indicated by green arrows. Remarkably, both AFM and TEM images clearly show that the Au NPs were not included inside the siRNA nanostructures.

3.2.3. Cellular Uptake by Regular Fluorescence and Flow Cytometry

We next studied the ability of the siRNA nanoparticles to undergo facile cellular uptake in A549 human lung cancer cell line. Au NPs modified with G3 PPI dendrimers (Au-G3) and G3 PPI dendrimer were respectively complexed with siGLO green siRNA transfection indicator (FAM-labeled) and then added to A549 lung cancer cells and
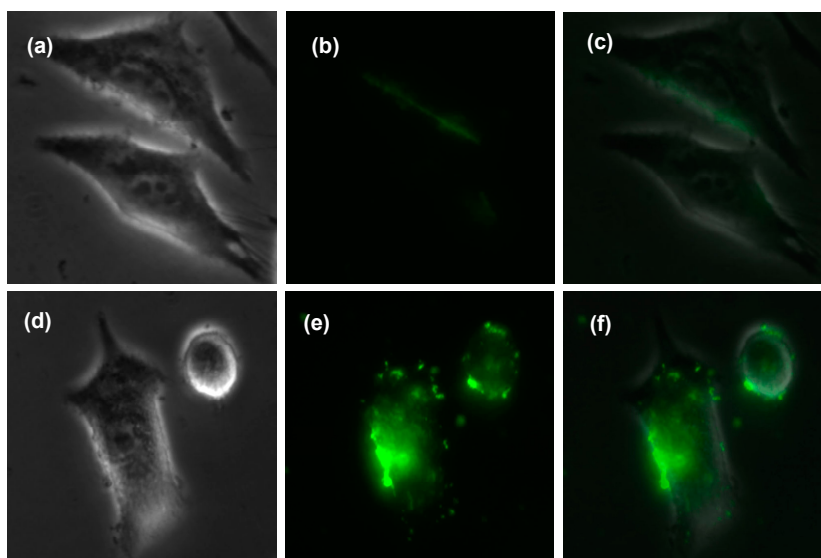
Figure 3.4. Representative fluorescence microscopic images of cellular uptake of FAM-labeled siRNA complexed with G3 PPI dendrimers (a, b, c) or Au NPs modified with G3 PPI dendrimers (d, e, f). An N/P ratio of 2.4 was used and the final siRNA concentration was 0.25 µM. Incubation was 24 h at 37 °C. Light images of cells are shown in panels a and d. Detection of FAM-labeled siRNA (b and e) and overlay of images (c and f) are shown.

incubated for 24 h. The cells were then washed with PBS buffer and then fresh medium was added for fluorescence imaging. As shown in Figure 3.4, cells dosed with siRNA nanoparticles fabricated by G3 PPI alone showed very mild green fluorescence on the surface and inside of the cells (Figure 3.4.b, c), indicating a low level of siRNA uptake. Similar result was obtained when G3 PPI dendrimer was used to deliver antisense oligodeoxynucleic acids in our previous study.(*16*) In contrast, the siRNA nanoparticles fabricated by Au-G3 was highly effective in transporting siRNA to the cell, as shown by the green fluorescence in the cells (Figure 3.4.e, f). This result clearly demonstrated that the Au NPs can help the low generation dendrimers effectively deliver siRNA into cancer cells. The reason why siRNA nanoparticles can be internalized is still under investigation.

We hypothesize that the siRNA nanoparticles fabricated by Au NPs modified with G3 PPI dendrimers may include more G3 dendrimers, which results in larger positive surface charges, which are essential for nonspecific delivery.

To gain more quantitative information on the cell uptake of siRNA delivered by Au-G3 vs. G3 PPI dendrimers, the cell uptake of siRNA was further studied by flow cytometry. A549 cells were placed in 6-well plates at a density of 500K cells/well and cultured for 24 h. The cells were then treated with siRNA (Fam-labeled siGLO green siRNA transfection indicator) nanoparticles fabricated by Au-G3 and G3 PPI dendrimers respectively for 24 h. After that, the cells were trypsinized and collected for flow cytometry analysis. As shown in Figure 3.5, when an N/P ratio of 0.6 was used, only 20% of cells treated with Au-G3/siRNA were transfected and none of the cells treated with G3/siRNA were transfected. When N/P ratio was increased to 1.2, siRNA internalized into ~80% of cells in the case of treatment with Au-G3/siRNA, while only ~10% of cells treated with G3/siRNA was transfected with siRNA. As N/P ratio further increased to 2.4, the cell uptake reached maximum in the case of treatment with Au-G3/siRNA, with 90% cells transfected and the mean green fluorescence intensity of each cell reaching 1.82. Similarly, the transfection of cells treated with G3/siRNA also significantly increased when N/P ratio increased to 2.4, with ~60% cells transfected and the mean fluorescence intensity of each cell reaching 1.15. When N/P ratio further increased to 4.8, the percentage of cells transfected were respectively 78% and 71% for cells treated with Au-G3/siRNA and G3/siRNA and the mean fluorescence intensity were respectively 1.2 and 1.4. This data clearly indicated that the siRNA nanoparticles fabricated by Au-G3 are more easily to internalize into cells. To achieve same percentage of cell transfection, a
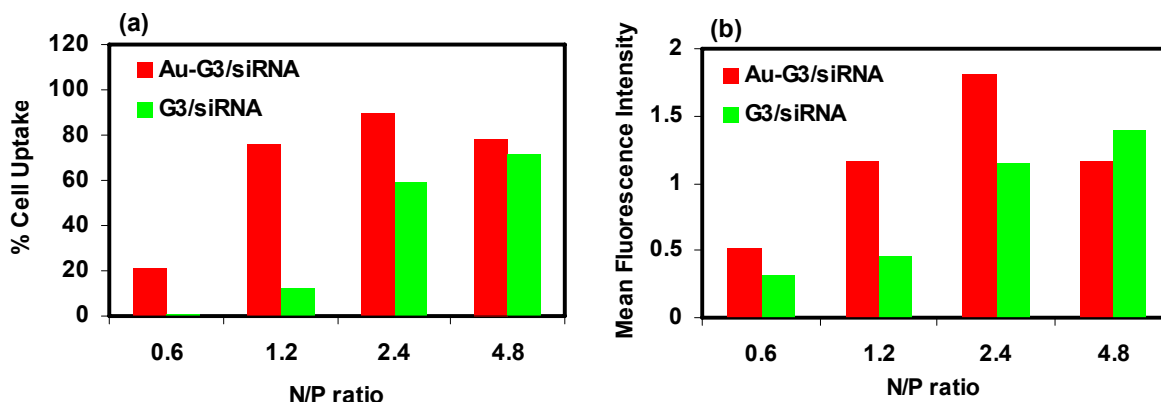
Figure 3.5. Cell uptake of siRNA nanoparticles fabricated by Au-G3 vs. G3 PPI dendrimers at different N/P ratios by flow cytometry. (a). Percentage of cell uptake as a function of N/P ratio. (b). Mean green fluorescence intensity of each individual cell as a function of N/P ratio. A549 cells were incubated by Au-G3/siRNA and G3/siRNA respectively at 37 °C for 24 h at N/P ratios of 0.6, 1.2, 2.4, and 4.8.

much lower N/P ratio was required in the case of Au-G3/siRNA due to the higher efficiency of Au-G3 to complex with siRNA and compact siRNA into nanoparticles. Particularly at N/P ratio of 2.4, not only were more cells transfected in the case of Au-G3/siRNA than the case of G3/siRNA (90% vs. 60%), the mean green fluorescence intensity of each cell is ~ 60% higher in the case of Au-G3/siRNA than the case of G3/siRNA. This result quantitatively confirms that the Au-G3 is significantly more efficient in delivering siRNA into cancer cells.

3.2.4. Gene Knockdown

The ability of the siRNA nanoparticles fabricated by Au-G3 to silence the target mRNA expression were studied with quantitative reverse transcriptase-polymerase chain reaction

(RT-PCR). 21-bp siRNA designed to silence BCL2 mRNA to suppress non-pump drug resistance was used.(*68, 69*) For comparison, we also performed the same experiment on the siRNA nanoparticles fabricated by G3 PPI dendrimers as well as higher generation G5 PPI dendrimers. G5 PPI dendrimers have been demonstrated much more efficient in packaging and delivering antisense ODNs into breast cancer cells compared to G3 PPI dendrimers.(*16*) A549 cancer cells were incubated for 24 h with siRNA nanoparticles fabricated by G3 PPI, G5 PPI and Au-G3 respectively. Gene expression was calculated as a ratio of band intensity of BCL2 mRNA to that of internal standard, β2-m and then the ratio of each sample was normalized to that of sample without treatment. As shown in Figure 3.6, Au-G3, G3 PPI, G5 PPI alone without siRNA showed similar level of BCL2 mRNA (lanes 2, 3, 4) as that of control cells without treatment (lane 1). This indicated minimal influence of Au-G3, G3 PPI or G5 PPI on the expression of BCL2 gene. In contrast, after incubation with G3/BCL2 siRNA and G5/BCL2 siRNA, the BCL2 mRNA level was suppressed to ~ 80% (Figure 3.6, lane 6) and 52% (Figure 3.6, lane 7) respectively. However, the BCL2 siRNA nanoparticles fabricated by Au-G3 are even more efficient than those fabricated by G5 PPI in inhibiting the BCL2 mRNA expression. The BCL2 mRNA level was significantly suppressed to ~28% after incubated with Au-G3/BCL2 siRNA nanoparticles. These results are striking, which soundly demonstrated that the Au NPs can help the low generation dendrimers effectively deliver siRNAs into cancer cells and efficiently inhibit their target mRNA expression.(*30*)

To further study the gene knockdown specificity of the BCL2 siRNA delivered by Au-G3, Au-G3 was complexed with a scrambled siRNA and the BCL2 mRNA level of the cell was analyzed after incubated with Au-G3/scramble siRNA for 24 h. As shown in
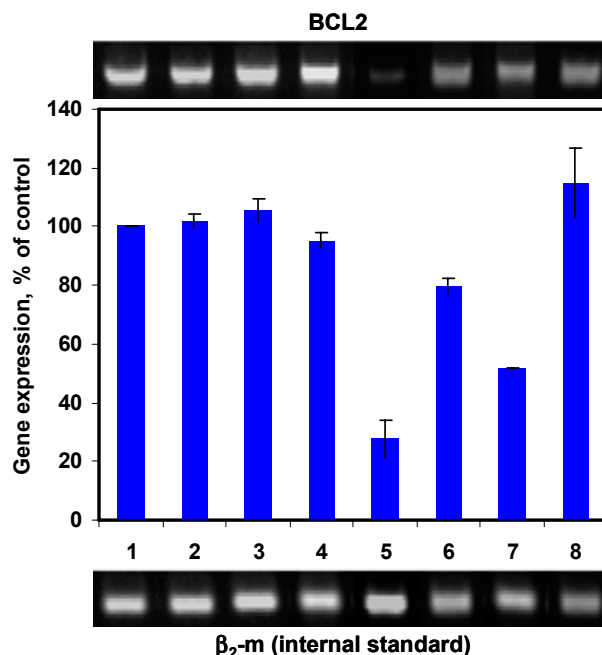
Figure 3.6. Effect of different formulations on the expression of BCL2 mRNA in A549 lung cancer cells.   (1) No treatment; (2) Au-G3; (3) G3; (4). G5; (5) Au-G3/BCL2 siRNA; (6) G3/BCL2-siRNA; (7) G5/BCL2-siRNA; (8) Au/G3-scrambled siRNA. Gene expression was calculated as a ratio of band intensity of BCL2 gene to that of internal standard, β2-m and then the ratio of each sample was normalized to that of sample without treatment. In samples (5-8), an N/P ratio of 2.4 was used and final concentration of siRNA in cell medium was 0.25 μM. The concentration of primary amine in all samples (2-8) was 25 μM.

Figure 3.6 (lane 8), there was no inhibition on BCL2 gene expression after the treatment of A549 cells with control scrambled siRNA complexed with Au-G3, confirming the specificity of BCL2 siRNA delivered by Au-G3 to knockdown its target mRNA.

3.2.5. In vitro cytotoxicity of G3 PPI vs. Au-G3

In order to examine whether Au-G3 influenced the cell viability of A549 cancer cells, the cytotoxicity of Au-G3 was determined by MTT assay and compared with that of G3 PPI dendrimers alone. As shown in Figure 3.7, it showed at a concentration of G3 PPI

dendrimers up to 4 µM, both G3 PPI dendrimers and Au NPs modified by G3 PPI dendrimers are non toxic. In all our experiments, a concentration of G3 PPI dendrimer up to 1.57 µM has been used.

3.2.6. Preliminary Study on Separation of Au Nanoparticles from the siRNA Complexes: Effect of Ionic Strength and pH on Stability of Au-G3/siRNA Complexes

To study the effect of ionic strength and pH on the stability of Au-G3/siRNA complexes, Au-G3 NPs were first complexed with siRNA at an N/P ratio of 1.2 to prepare the Au-
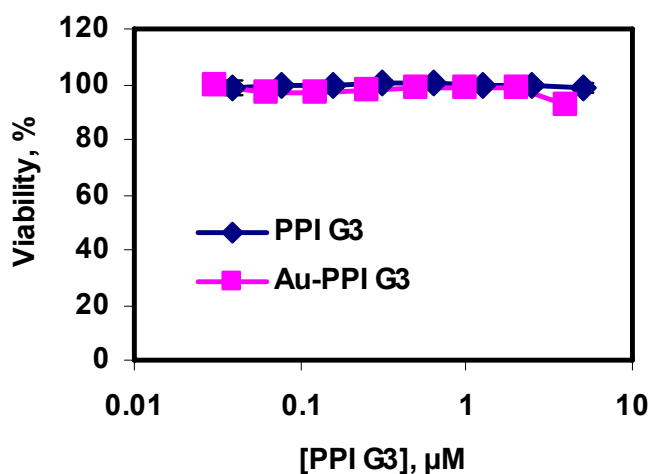
Figure 3.7. Viability of A549 cells after incubated for 24 h at 37 °C with G3 PPI dendrimers or Au NPs modified with G3 PPI dendrimers. It showed that at a concentration of G3 PPI dendrimer up to 4 µM (which is relevant to our cell uptake study), both G3 PPI dendrimer and Au NPs modified by G3 PPI dendrimers are non-toxic.

G3/siRNA complex. Then the obtained complex solution was diluted 12 times into H2O, 100 mM pH=7.4, 6.0 and 4.5 phosphate buffers respectively. After storing at RT for 1 h

and then at 4 °C for 21 h, supernatants from each sample were collected and analyzed by UV-Vis directly. The UV-Vis spectra of all four supernatants are shown in Figure 3.8.a. It showed that under all three 100 mM phosphate buffers with different pH, significant amount of Au NPs precipitated, as indicated by the decreased absorbance of supernatant at ~523 nm, the characteristic absorption of Au NPs in solution. It further showed that the amount of Au precipitation is inversely proportional to the pH, with more precipitation at lower pH. We wondered whether the siRNA complexes also experienced aggregation and then precipitated out of the solution with the Au nanoparticles. We overlaid the UV-Vis spectra of supernatants collected from suspensions of Au-G3/siRNA in H2O and from suspensions of same concentration of Au NPs in H2O after stored at RT for 1 h and at 4 °C for 21 h (Figure 3.8.a inset). It showed that the difference of absorbance spectra of Au-G3/siRNA complex as compared to that of Au-G3 is mainly in the region of 200-310 nm, where the siRNA has absorbance. To relatively compare the amount of siRNA remaining in each supernatant, the absorbance at 260 nm was subtracted by the absorbance at 320 nm (where the siRNA has no absorbance). After correction, the absorbance at 260 nm of each supernatant was normalized to that of the supernatant colleted from suspensions of Au-G3/siRNA in H2O and then plotted in Figure 3.8.b (green bars). Similarly, the absorbance at 523 nm of each supernatant is also normalized to that of the supernatant collected from suspensions of Au-G3/siRNA in H2O at 523 nm. It showed that the absorbance at 260 nm of supernatant from suspension of complex in three different pH buffers was only slightly reduced when compared to that in H2O (Figure 3.8.b green bars). This was in sharp contrast to the absorbance at 523 nm (Figure 3.8.b pink bars),
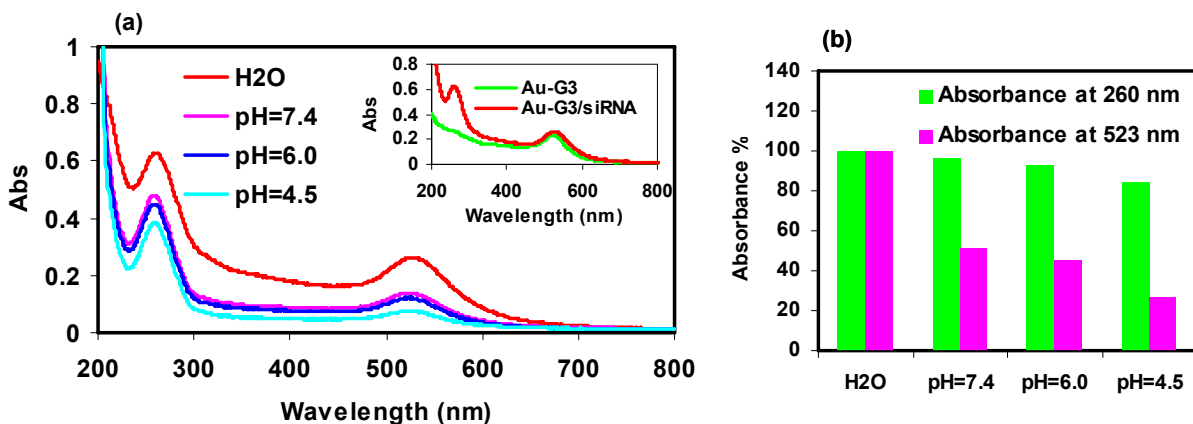
Figure 3.8. (a). UV-Vis spectra of supernatants collected from suspensions of complex of Au NPs with siRNA in H$_2$O, 100 mM pH=7.4, 6.0, and 4.5 buffer respectively after stored at RT for 1 h and at 4 °C for 21 h. **Inset.** UV-Vis spectra of supernatants collected from suspensions of complex of Au NPs with siRNA in H$_2$O vs. from suspensions of same concentration of Au NPs in H$_2$O after stored at RT for 1 h and at 4 °C for 21 h. (b). Absorbance at 260 nm and at 523 nm of supernatants collected from suspensions of Au-G3/siRNA complex in H$_2$O, 100 mM pH=7.4, 6.0, and 4.5 buffer respectively after stored at RT for 1 h and at 4 °C for 21 h. The absorbance at 260 nm was reported after subtracting the absorbance at 320 nm. After correction, the reported absorbance at 260 nm can be approximately correlated to the amount of siRNA in each supernatant.

which was significantly decreased for supernatants from suspensions of complex in three different pH buffers when compared to that in H2O. This data indicated that different amounts of Au NPs can be successfully separately from each complex in 100 mM

phosphate buffers with different pH. Furthermore, upon separation of Au NPs, majority of siRNAs remained dispersed in supernatant without precipitation.

3.3. Conclusions

In conclusion, we report a novel approach to efficiently package and deliver nucleic acids with low generation dendrimers by using Au NPs as a "labile catalytic" packaging agent. The Au NPs helped low generation dendrimers to package nucleic acids but are not included in the final DNA/siRNA complexes. Compared to the siRNA particles fabricated by low generation dendrimer alone (G3 PPI), the siRNA nanoparticles packaged through this novel approach (by Au NPs modified with G3 PPI) can be internalized by cancer cells and the internalized siRNAs can efficiently silence their target mRNA. The efficiency is even superior to higher generation dendrimers (G5 PPI). More importantly, this approach provides a possibility to remove the Au NPs before the nucleic acid NPs are delivered, therefore the possible long-term toxic problem accompanied with the Au NPs can be solved. This is a new concept in using inorganic engineered NPs in nucleic acid packaging and delivery applications. Additionally, we confirmed that the Au NPs modified by G3 PPI dendrimers are not toxic at a concentration of G3 PPI dendrimer up to 4 µM. This confirmed that under the concentration studied, Au-G3 PPI dendrimers can deliver siRNA into cancer cells and knockdown target genes more efficiently than G3 and G5 PPI dendrimers without increasing any toxicity. Furthermore, the preliminary study demonstrated that the Au NPs can be separated from the siRNA complex solution. Currently, detailed studies on removing the Au NPs completely from the nucleic acid complex solution, and the cell

uptake and gene knockdown efficiency, and the toxicity of the nucleic acid complex after the removal of Au NPs are under investigation.

3.4. Experimental Section

3.4.1. Materials

The PGL-3 luciferase control vector (5256 bp), which contains the SV40 promoter and enhancer sequences, was purchased from Promega (Madison, WI). Polypropyleneimine hexadecaamine dendrimer (PPI dendrimer) generation-3 (G3) and generation-5 (G5) and other chemicals used in this study were purchased from Aldrich (Milwaukee, WI), and used without further purification. siRNA that are sequence specific for human BCL2 mRNA was custom synthesized by Ambion (Austin, TX). The sequence of the siRNA used as follows: sense strand, 5'-GUGAAGUCAACAUGCCUGC-dTdT-3'; antisense strand, 5'-GCAGGCAUGUUGACUUCAC-dTdT-3'.

3.4.2. Fabrication of Au NPs Modified with G3 PPI Dendrimers

32.8 mg of G3 PPI dendrimer was mixed with 8.8 ml of 2.45 mM $HAuCl_4$ solution with a molar ratio of 0.90:1 and then heated at 80° C for 1 h with continuous stirring. The clear solution thus obtained was cooled to RT and dialyzed (3.5k Da cutoff regenerated cellulose tubular membrane) against 200 ml of double-distilled water twice for a total of 4 h. The dialyzate thus obtained was used as stock solution.

3.4.3. Determination of PPI G-3 Dendrimer Concentration in the Au NPs Modified with PPI G-3 Dendrimers

To determine the PPI G-3 dendrimer concentration in the Au NP modified with PPI G-3 dendrimer stock solution, an improved 2, 4, 6-Trinitrobenzenesulfonic acid method was used. Briefly, 75 µl of aqueous 0.03 M TNBS is added to 4.0 ml of 0.042 M sodium tetraborate buffer containing different amount of samples. Thus-obtained solution was shaken in a shaking block for 1 h and then ~ 3 ml of the solution was transferred into a quartz cuvette for UV-Vis analysis. 75 µl of aqueous 0.03 M TNBS in 4 ml of 0.042 M sodium tetraborate buffer was used as blank solution. The absorbance at 420 nm was used to obtain the calibration curve and determine the dendrimer concentration in the Au stock solution.

3.4.4. Plasmid DNA Condensation by the Au NPs modified with G3 PPI dendrimers

Condensation experiments were conducted in DI water by adding a suitable amount of stock solution of Au NPs A and B respectively added to a diluted plasmid DNA solution in water. The resultant mixture was mixed by a vertex machine for several seconds. The final DNA phosphate concentration is 2.0 µM and the ratio of peripheral nitrogen of PPI G-3 dendrimer to the phosphorus of plasmid DNA (N/P value) is 6:1 for both samples.

3.4.5. Packaging siRNA with G5 PPI dendrimers and with Au NPs modified with G3 PPI dendrimers for cell uptake experiment

The condensed siRNA complexes were prepared at N/P ratio of 2.4 either in DI water or 10 mM Hepes buffer (pH 7.2) by adding a stock solution of PPI G5 dendrimer or a stock solution of Au-G3 into prepared siRNA solution. The samples were vortexed briefly, and the solutions were then incubated at room temperature for 30 min before being dosed.

3.4.6. Cell Lines

Human lung carcinoma cell line A549 was obtained from the ATTC (Manassas, VA, USA). Cells were cultured in RPMI 1640 medium (Sigma Chemical Co., Louis, MO) supplemented with 10% fetal bovine serum (Fisher Chemicals, Fairlawn, NJ). Cells were grown at 37ºC in a humidified atmosphere of 5% CO_2 (v/v) in air. All of the experiments were performed on the cells in exponential growth phase.

3.4.7. Cytotoxicity

The cellular cytotoxicity of G3 PPI dendrimers and Au-G3 was assessed using a modified MTT (3-(4,5-dimethylthiazol-2-yl)-2,5-diphenyltetrazolium bromide) assay. Cells were seeded into 96-well microtiter plates at the density of 10,000 cells per well. After incubation for 24 h, medium were aspirated and various concentrations of G3 or Au-G3 in fresh cell growth medium (200 µl/well) were added. Control cells were added with equivalent volume of fresh media. Cells were cultured for 24 h before the cell viability assay was performed. The old medium was removed and 100 µl of fresh medium and 25 µl of a 5 mg/ml MTT (Fluka) solution in DPBS was added to each well. Plates were then incubated under cell culture conditions for 3 h. Every well was then added with 100 µl of 50% (v/v) dimethylformamide in water containing 20% (w/v) sodium doecyl sulfate (with pH adjusted to 4.7 by acetic acid) and incubated overnight to dissolve the formazan crystals. The absorbance of each sample was measured at 570 nm with a background correction at 630 nm. Based on these measurements, IC50 doses of G3 PPI dendrimers and Au-G3 (the concentrations of G3 necessary to inhibit the cell growth by 50%) were calculated.

3.4.8. Cellular Internalization

Cellular internalization of FITC-labeled siRNA nanoparticles packaged with Au NPs modified with G3 PPI and G3 PPI alone were analyzed by fluorescence microscope (Olympus America Inc., Melville, NY). Prior the visualization A549 cells were plated (20,000 cells/well) in 6-well tissue culture plate. The cells were treated with siRNA nanoparticles packaged with Au NPs modified with G3 PPI and G3 PPI alone for 24 h. The concentration of G3 PPI dendrimer for both cases was 1.57 μM and the concentration of siRNA was 0.25 μM. After 24 h of treatment, cells were washed three times with phosphate buffered saline (PBS) and 1 mL of media was added to each well.

3.4.9. Gene Knockdown

The ability of the siRNA delivered by Au NPs modified with G3 PPI, G3 PPI dendrimers and G5 PPI dendrimers to silence the target mRNA expression were studied with quantitative reverse transcriptase-polymerase chain reaction (RT-PCR). A549 cells were placed in small flasks at a density of 750,000 cells/flask and cultured for 24 h. Then the cells were treated with different siRNA nanoparticles. Cells were also treated with Au-G3 complex with scrambled siRNA, Au-G3, G3 PPI, and G5 PPI respectively as control. After 24hrs of incubation of A-549 lung cancer cells with different formulations, the total cellular RNA was isolated using an RNeasy kit (Qiagen, Valencia, CA). First strand cDNA was synthesized by Ready-To-GO You-Prime First-Strand Beads (Amersham Biosciences, Piscataway, NJ) with 4mg of total cellular RNA and 100 ng of random hexadeoxynucleotide primer (Amersham Bioscience). After synthesis, the reaction mixture was immediately subjected to polymerase chain reaction, which was carried out using GenAmp PCR System 2400. The pairs of BCL2 and 2-m primers used to amplify each type of cDNA. PCR products were seperated in 4% NuSieve 3:1 Reliant agarose

gels in **1**×TBE buffer (0.089 M Tris/Borate, 0.002 M EDTA, pH 8.3; Research Organic Inc., Cleveland OH) by submarine electrophoresis. The gels were stained with ethidium bromide, digitally photographed and scanned using Gel Documentation System 920 (NucleoTech, San Mateo, CA). Gene expression was calculated as the ratio of mean band density of analyzed RT-PCR product to that of the internal standard (β2-m). In preparing all siRNA complex, an N/P ratio of 2.4 was used and final concentration of siRNA in cell medium was 0.25 µM. The concentration of primary amine of PPI dendrimers in all samples was 25 µM.

3.4.10. Atomic Force Microscopy

AFM images were obtained using Nanoscope IIIA equipment (Digital Instruments, Santa Barbara, CA) in tapping mode, operating in ambient air. A 125 µm long rectangular silicon cantilever/tip assembly was used with a spring constant of 40 N/m, resonance frequency of 315-352 kHz, and tip radius of 5-10 nm. The applied frequency was set on the lower side of the resonance frequency. The image was generated by the change in amplitude of the free oscillation of the cantilever as it interacted with the sample. The height differences on the surface are indicated by the color code, lighter regions indicating increase in height of the NPs. In order to image DNA or siRNA nanoparticles, 5 µL of the prepared complex solutions were deposited on a freshly cleaved mica surface. After 3-6 minutes of incubation, the surface was rinsed with 2-3 drops of nanopure water (Barnstead), and dried under a flow of dry nitrogen. Height and outer diameter of nanoparticles were measured using the Nanoscope software. Data are given as mean ± standard error of the mean.

3.4.11. UV-Vis Absorbance

An appropriately diluted solution of Au NPs was transferred to a UV-Vis cuvette for analysis by Cary 300 UV-Vis Spectrophotometer (Varian Inc., CA). The sample was scanned from 800 nm to 200 nm.

3.4.12. Transmission Electron Microscopy (TEM)

TEM analyses of siRNA/DNA condensates were performed using Libra 120 Energy Filtering TEM (Carl Zeiss). 5 μl of the siRNA/DNA condensate solution was deposited on a carbon coated 200 mesh copper grid that was glow discharged for 1 minute. After 3 minutes, the sample was drained off with a filter paper and further dried with a flow of N_2 gas. Then the sample was viewed on the electron microscope and photographs were taken using a camera attached to the microscope. Some of the solution were also imaged in the energy filtering TEM mode(*70*) and analyzed by Au elemental analysis by setting the energy slit to 2386 eV, which is the energy edge of Au element.

3.4.13. Flow cytometry

Flow cytometry analyses were performed on a Cytomics FC500 cytometer (Beckman-Coulter). A 488 nm air-cooled argon laser was used to excite the siGLO green siRNA transfection indicator (FAM-labeled), and the emitted light was filtered by a 525 nm band-pass filter. The cells were gated by forward and side-scatter parameters, and data were collected from a population of 10000 gated cells. The data were analyzed using the Cytomics FC500 RXP software.

3.5. References

1.   Vijayanathan, V., Thomas, T., and Thomas, T. J. (2002) DNA Nanoparticles and Development of DNA Delivery Vehicles for Gene Therapy, *Biochemistry 41*, 14085-14094.

2.   Blessing, T., Remy, J. S., and Behr, J. P. (1998) Monomolecular Collapse of Plasmid DNA into Stable Virus-like Particles, *Proc. Natl. Acad. Sci, USA 95*, 1427-1431.

3.   Bessis, N., GarciaCozar, F. J., and Boissier, M. C. (2004) Immune Responses to Gene Therapy Vectors: Influence on Vector Function and Effector mechanisms, *Gene Ther. 11*, S10-17.

4.   (2001) *Dendrimers and Dendrons: Concepts, Synthesis, Applications*, Wiley-VCH, New York, NY.

5.   Liu, M., and Frechet, J. M. (1999) Designing Dendrimers for Drug Delivery, *Pharm. Res. Tech. Today 2*, 393-401.

6.   Tang, M. X., Redemann, C. T., and Szoka Jr, F. C. (1996) In vitro Gene Delivery by Degraded Polyamidoamine Dendrimers, *Bioconjugate Chem. 7*, 703-714.

7.   Choi, Y., Thomas, T., Kotlyar, A., Islam, M. T., and Baker, J. R. J. (2005) Synthesis and Functional Evaluation of DNA-Assembled Polyamidoamine Dendrimer Clusters For Cancer Cell-Specific Targeting, *Chem. & Biol. 12*, 35-43.

8.   Malik, N., Wiwattanapatapee, R., Klopsch, R., Lorenz, K., Frey, H., Weener, J. W., Meijer, E. W., Paulus, W., and Duncan, R. (2000) Relationship between Structure and Biocompatibility in vitro, and Preliminary Studies on the

Biodistribution of 125I-labelled Polyamidoamine Dendrimers in vivo, *Journal of Controlled Release 65*, 133-148.

9.   Kukowska-Latallo, J. F., Bielinska, A. U., Johnson, J., Spindler, R., Tomalia, D. A., and Baker, J. R., Jr. (1996) Efficient Transfer of Genetic Material into Mammalian Cells Using Starburst Polyamidoamine Dendrimers, *Proc. Natl. Acad. Sci, USA 93*, 4897-4902.

10.   Dennig, J. (2003) Gene Transfer in Eukaryotic Cells Using Activated Dendrimers, *Top. Curr. Chem. 2003*, 227-236.

11.   Zhang, Z. Y., and Smith, B. D. (2000) High-Generation Polycationic Dendrimers Are Unusually Effective at Disruptig Anioinic Vesicles: Membrane Bending Model, *Bioconjugate Chem. 11*, 805-814.

12.   Hong, S., Bielinska, A. U., Mecke, A., Keszler, B., Beals, J. L., Shi, X., Balogh, L., Orr, B. G., Baker, J. R. J., and Banaszak Hall, M. M. (2004) Interaction of Poly(amidoamine) Dendrimers with Supported Lipid Bilayers and Cells: Hole Formation and the Relation to Transport, *Bioconjugate Chem. 2004*, 774-782.

13.   Tomalia, D. A., Baker, H., Dewald, J., Hall, M., Kallos, G., Martin, S., Roeck, J., Ryder, J., and Smith, P. (1985) A New Class of Polymers: Starbust-Dendritic Macromolecules, *Polym. J.(Tokyo) 17*, 117-132.

14.   De Brabander-van den Berg, E. M. M., and Meijer, E. M. (1993) Poly(propylene imine) Dendrimers: Large-scale Synthesis via Heterogeneously Catalyzed Hydrogenation, *Angew. Chem. 105*, 1370-1373.

15.   Dennig, J., and Duncan, E. (2002) Gene Transfer into Eukaryotic Cells using Activated Polyamidoamine Dendrimers, *Rev. Mol. Biotechnol. 90*, 339-347.

16.   Chen, A., Santhakumaran, L. M., Nair, S. K., Amenta, P. S., Thomas, T., He, H. X., and Thomas, T. J. (2006) Oligodeoxynucleotide Nanostructure Formation in the Presence of Polypropyleneimine Dendrimers and Their Uptake in Breast Cancer Cells, *Nanotechnology 17*, 5449-5460.

17.   Radu, D. R., Lai, C.-Y., Jeftinija, K., Rowe, E. W., Jeftinija, S., and Lin, C. S.-Y. (2004) A Polyamidoamine Dendrimer-Capped Mesoporous Silica Nanosphere-Based Gene Transfection Reagent, *J. Am. Chem. Soc. 126*, 13216-13217.

18.   Thomas, M., and Klibanov, A. M. (2003) Conjugation to Gold Nanoparticles Enhances Polyethylenimine's Transfer of Plasmid DNA in Mammalian Cells, *Proc. Natl. Acad. Sci, USA 100*, 9138-9143.

19.   Jen, C.-P., Chen, Y.-H., Fan, C.-S., Yeh, C.-S., Lin, Y.-C., Shieh, D.-B., Wu, C.-L., Chen, D.-H., and Chou, C.-H. (2004) A Nonviral Transfection Approach in Vitro: The Design of a Gold Nanoparticle Vector Joint with Microelectrochemical Systems, *Langmuir 20*, 1369-1374.

20.   Hazarika, P., Giorgi, T., Reibner, M., Ceyhan, B., and Niemeyer, C. M. (2004) Synthesis and Characterization of Deoxyribonucleic Acid-Conjugated Gold Nanoparticles, *Methods Mol. Biol. 283*, 295-304.

21.   Rosi, N. L., Thaxton, C. S., and Mirkin, C. A. (2004) Control of Nanoparticle Assembly by Using DNA-Modified Diatom Templates, *Angew. Chem. Int. Ed. 43*, 5500-5503.

22.   Grohn, F. G., Bauer, B. J., Akpalu, Y. A., Jackson, C. L., and Amis, E. J. (2000) Dendrimer Templates for the Formation of Gold Nanoclusters, *Macromolecules 33*, 6042-6050.

23. Lou, D., Han, E., Belcheva, N., and Saltzman, W. M. (2004) A Self-assembled, Modular DNA Delivery System Mediated by Silica Nanoparticles, *J. Controlled Release 95*, 333-341.

24. Bianco, A., Hoebeke, J., Godefroy, S., Chaloin, O., Pantarotto, D., Briand, J.-P., Muller, S., Prato, M., and Partidos, C. D. (2005) Cationic Carbon Nanotubes Bind to CpG Oligodeoxynucleotides and Enhance Their Immunostimulatory Properties, *J. Am. Chem. Soc. 127*, 58-59.

25. Pantarotto, D., Singh, R., McCarthy, D., Erhardt, M., Briand, J.-P., Prato, M., Kostarelos, K., and Bianco, A. (2004) Functionalized Carbon Nanotubes for Plasmid DNA Gene Delivery, *Angew. Chem. 116*, 5354-5358.

26. McIntosh, C. M., Esposito, E. A., Boal, A. K., Simard, J. M., Martin, C. T., and Rotello, V. M. (2001) Inhibition of DNA Transcription Using Cationic Mixed Monolayer Protected Gold Clusters, *J. Am. Chem. Soc. 123*, 7626-7629.

27. Sandhu, K. K., McIntosh, C. M., Simard, J. M., and Rotello, V. M. (2002) Gold Nanoparticle-Mediated Transfection of Mammalian Cells, *Bioconjugate Chem. 13*, 3-6.

28. Bhattacharya, R., Mukherjee, P., Xiong, Z., Atala, A., Soker, S., and Mukhopadhyay, D. (2004) Gold Nanoparticles Inhibit VEGF165-Induced Proliferation of HUVEC Cells, *Nano Lett. 4*, 2479-2481.

29. Luo, D., and Saltzman, W. M. (2000) Enhancement of transfection by physical concentration of DNA at the cell surface, *Nature Biotechnology 18*, 893-895.

30. Pack, D. W., Hoffman, A. S., Pun, S., and Stayton, P. S. (2005) Design and Development of Polymers for Gene Delivery, *Nat. Rev. Drug Discovery 4*, 581-593.

31.   Schatzleina, A. G., Zinselmeyera, B. H., Elouzib, A., Dufes, C., Chimc, Y. T. A., Robertsc, C. J., Daviesc, M. C., Munrob, A., Grayb, A. I., and Uchegbu, I. F. Preferential Liver Gene Expression with Polypropylenimine Dendrimers, *J. Controlled Release 101*, 247-258.

32.   Koper, G. J. M., van Genderen, M. H. P., Elissen-Roman, C., Baars, M. W. P. L., Meijer, E. W., and Bordovec, M. (1997) Protonation Mechanism of Poly(propylene imine) Dendrimers and Some Associated Oligo Amines, *J. Am. Chem. Soc. 119*, 6512-6521.

33.   Sideratou, Z., Tsiourvas, D., and Paleos, C. M. (2000) Quaternized Poly(propylene imine) Dendrimers as Novel pH-Sensitive Controlled-Release Systems, *Langmuir 16*, 1766-1769.

34.   Sun, J., Paik, H.-Y., and Hwang, B. Y. (1994) Ionization of Poly(ethylenimine) and Poly(allylamine) at Various pH's, *Bioorg. Chem. 22*, 318-327.

35.   Tokuhisa, H., Zhao, M., Baker, L. A., Phan, V. T., Dermody, D. L., Garcia, M. E., Peez, R. F., Crooks, R. M., and Mayer, T. M. (1998) Preparation and Characterizatoin of Dendrimer Monolayers and Dendrimer-Alkanethiol Mixed Monolayers Adsorbed to Gold, *J. Am. Chem. Soc. 120*, 4492-4501.

36.   Nagarajan, R., Roy, S., Kumar, J., Tripathy, S. K., Dolukhanyan, T., Sung, C., Bruno, F., and Samuelson, L. A. (2001) Enzymatic Synthesis of Molecular Complexes of Polyaniline with DNA and Synthetic Oligonucleotides: Thermal and Morphological Characterization, *J. Mocromo. Sci---Pure. Appl. Chem. A38*, 1519-1537.

37.	Liu, W., Cholli, A. L., Nagarajan, R., Kumar, J., Tripathy, S., Bruno, F. F., and Samuelson, L. (1999) The Role of Template in Enzymatic Synthesis of Conducting Polyaniline, *J. Am. Chem. Soc. 121*, 11345.

38.	Ma, Y. F., Zhang, J. M., Zhang, G. J., and He, H. X. (2004) Polyaniline Nanowires on Si surfaces Fabricated with DNA Templates, *J. Am. Chem. Soc. 126*, 7097-7101.

39.	Sun, X., Dong, S., and Wang, E. K. (2004) One-Step Preparation and Characterization of Poly(propyleneimine) Dendrimer-Protected Silver Nanoclusters, *Macromolecules 37*, 7105-7108.

40.	Esumi, K., Isono, R., and Yoshimura, T. (2004) Preparation of PAMAM - and PPI - Metal (Silver, Platinum, and Palladium) Nanocomposites and Their Catalytic Activities for Reduction of 4-Nitrophenol, *Langmuir 20*, 237-243.

41.	Esumi, K., Suzuki, A., Aihara, N., Usui, K., and Torigoe, K. (1998) Preparation of Gold Colloids with UV Irradiation Using Dendrimers as Stabilier, *Langmuir 14*, 3157-3159.

42.	Hayakawa, K., Yoshimura, T., and Esumi, K. (2003) Preparation of Gold-Dendrimer Nanocomposites by Laser Irradiation and Their Catalytic Reduction of 4-Nitrophenol, *Langmuir 19*, 5517-5521.

43.	Garcia, M. E., Baker, L. A., and Crooks, R. M. (1999) Preparation and Characterization of Dendrimer-Gold Colloid Nanocomposites, *Anal. Chem. 71*, 256-258.

44.	Kneuer, C., Sameti, M., Bakowsky, U., Schiestel, T., Schirra, H., Schmidt, H., and Lehr, C.-M. (2000) A Nonviral DNA Delivery System Based on Surface

Modified Silica-Nanoparticles Can Efficiently Transfect Cells in Vitro, *Bioconjugate Chem. 11*, 926-932.

45.   Bharali, D. J., Klejbor, I., Stachowiak, E. K., Dutta, P., Roy, I., Kaur, N., Bergey, E. J., Prasad, P. N., and Stachowiak, M. K. (2005) Organically Modified Silica Nanoparticles: A Nonviral Vector for in vivo Gene Delivery and Exprssion in the Brain, *Proc. Natl. Acad. Sci, USA 102*, 11539-11544.

46.   Liu, Y., Wu, C.-L., Zhang, W.-D., Jiang, X., He, C.-B., Chung, T. S., Goh, S. H., and Leong, K. W. (2005) Polyethylenimine-Grafted Multiwalled Carbon Nanotubes for Secure Noncovalent Immobilization and Efficient Delivery of DNA, *Angew. Chem. Int. Ed. 44*, 4782-4785.

47.   Roy, I., Ohulchanskyy, T. Y., Bharali, D. J., Pudavar, H. E., Mistretta, R. A., Kaur, N., and Prasad, P. N. (2005) Optical Tracking of Oranically Modified Silica Nanoparticles as DNA Carriers: A Nonviral Nanomedicine Approach for Gene Delivery, *Proc. Natl. Acad. Sci, USA 102*, 279-284.

48.   Golan, R., Pietrasanta, L. I., Hsieh, W., and Hansma, H. G. (1999) DNA Toroids: Stages in Condensation, *Biochemistry 38*, 14069-14076.

49.   Goodman, C. M., McCusker, C. D., Yilmaz, T., and Rotello, V. M. (2004) Toxicity of Gold Nanoparticles Functionalized with Cationic and Anionic Side Chains, *Bioconjugate Chem. 15*, 897-900.

50.   Bielinska, A., Eichman, J. D., Lee, I., Baker, J. R., Jr., and Balogh, L. (2002) Imaging {Au0-PAMAM} Gold-dendrimer Nanocomposites in Cells, *J. Nanoparticle Res. 4*, 395-403.

51.   Park, C., Crooks, R. E., Siochi, E., Harrison, J. S., Evans, N., and Kenik, E. (2003) Adhesion Study of Polyimide to Single Wall Carbon Nanotube Bundles by

Energy-Filtered Transmission Electron Microscopy, *Nanotechnology 14*, L11-L14.

52.   Bleher, R., Meyer, D. A., and Albrecht, R. M. (2005) *High Resolution Multiple Labeling for Immuno-EM applying Metal Colloids and Energy Filtering Transmission Electron Microscopy (EFTEM).* Vol. 11, Cambridge University Press.

53.   He, H. X., Zhang, H., Li, Q. G., Zhu, T., Li, S. F. Y., and Liu, Z. F. (2000) Fabrication of Designed Architectures of Au Nanoparticles on Solid Substrate with Printed Self-Assembled Monolayers as Templates, *Langmuir 16*, 3846-3851.

54.   Tan, W. B., Jiang, S., and Zhang, Y. (2007) Quantum-dot Based Nanoparticles for Targeted Silencing of HER 2/neu Gene Via RNA Interference, *Biomaterials 28*, 1565-1571.

55.   de Fougerolles, A., Vornlocher, H.-P., Maraganore, J., and Lieberman, J. (2007) Interfering with Disease: A Progress Report on siRNA-based Therapeutics, *Nat. Rev. Drug Discovery 6*, 443-453.

56.   Elbashir, S. M., Harborth, J., Lendeckel, W., Yalcin, A., Weber, K., and Tuschl, T. (2001) Duplexes of 21-nucleotide RNAs Mediate RNA Interference in Cultured Mammalian Cells, *Nature 411*, 494-498.

57.   Dykxhoorn, D. M., and Lieberman, J. (2005) The Silent Revolution: RNA Interference as Basic Biology, Research Tool and Therapeutic, *Annu. Rev. Med. 56*, 401-423.

58.   Uprichard, S. L. (2005) The Therapeutic Potential of RNA Interference, *FEBS Lett. 579*, 5996-6007.

59.   Song, E., Zhu, P. C., Lee, S.-K., Chowdhury, D., Kussman, S., Dykxhoorn, D. M., Feng, Y., Palliser, D., Weiner, D. B., Shankar, P., Marasco, W. A., and Lieberman, J. (2005) Antibody Mediated in vivo Delivery of Small Interfering RNAs via Cell-Surface Receptors, *Nature Biotech. 23*, 709-717.

60.   Chiu, Y.-L., Ali, A., Chu, C.-Y., Cao, H., and Rana, T. M. (2004) Visualizing a Correlation Between siRNA Localization, Cellular Uptake, and RNAi in Living Cells, *Chem. & Biol. 11*, 1165-1175.

61.   Sarkar, T., Conwell, C. C., Harvey, L. C., Santai, C. T., and Hud, N. V. (2005) Condensation of Oligonucleotides Assembled into Nicked and Gapped Duplexes: Potential Structures for Oligonucleotide Delivery, *Nucleic Acids Res. 33*, 143-151.

62.   Gary, D. J., Puri, N., and Won, Y.-Y. (2007) Polymer-based siRNA Delivery: Perspectives on the Fundamental and Phenomenological Distinctions from Polymer-based DNA Delivery, *J. Controlled Release 121*, 64-73.

63.   Taratula, O., Savla, R., Pandya, I., Kirkpatrick, P., Minko, T., and He, H. (2009) PPI Dendrimers as Potential siRNA Delivery Vehicles for Efficient Cancer Therapy: Structure-Function Relationship, *Submitted*.

64.   Li, S.-D., and Huang, L. (2006) Targeted Delivery of Antisense Oligodeoxynucleotide and Small Interference RNA into Lung Cancer Cells, *Mol. Pharm. 3*, 579-588.

65.   LI, S.-D., Chen, Y.-C., Hackett, M. J., and Huang, L. (2008) Tumor-targeted Delivery of siRNA by Self-assembled Nanoparticles, *Molecular Ther. 16*, 163-169.

66.   Li, S.-D., Chen, Y.-C., Hackett, M. J., and Huang, L. (2007) Tumor-targeted Delivery of siRNA by Self-assembled Nanoparticles, *Molecular Therapy 16*, 163-169.

67.   Li, S.-D., and Huang, L. (2006) Targeted Delivery of Antisense Oligodeoxynucleotide and Small Interference RNA into Lung Cancer Cells, *Molecular Pharmaceutics 3*, 579-588.

68.   Yano, J., Hirabayashi, K., Nakagawa, S.-I., Yamaguchi, T., Naito, H., Kitagawa, H., Ishiyama, K., Ohgi, T., and Irimura, T. (2004) Antitumor Activity of Small Interfering RNA/Cationic Liposome Complex in Mouse Models of Cancer, *Clin. Cancer Res. 10*, 7721-7726.

69.   Pakunlua, R. I., Wang, Y., Tsao, W., Pozharov, V., Cook, T. J., and Minko, T. (2004) Enhancement of the Efficacy of Chemotherapy for Lung Cancer by Simultaneous Suppression of Multidrug Resistance and Antiapoptotic Celluar Defences: Novel Multicomponent Delivery System, *Cancer Reseach 64*, 6214-6224.

70.   Park, C., Crooks, R. E., Siochi, E. J., Harrison, J. S., Evans, N., and Kenik, E. (2003) Adhesion study of polyimide to single-wall carbon nanotube bundles by energy-filtered transmission electron microscopy, *Nanotechnology 14*, L11-L14.

Chapter 4

Non-gatekeeping and Controlled Release of

Doxorubicin from Mesoporous Silica

Nanoparticles for Cancer Therapy

4.1. Introduction

Severe toxicity to normal body tissues remains a critical obstacle in systemic delivery of anticancer drugs for cancer therapy. In an effort to reduce the side effects and improve the therapeutic efficacy of anticancer drugs, many drug delivery systems have been developed, including polymeric conjugates, micelles, liposomes, solid-lipid nanoparticles, and hollow nanoparticles.(*1-13*) Most of these drug delivery systems showed great advantage of protecting anticancer drugs from degradation during delivery. Furthermore, most of the drug delivery systems are in sub-micron size, which can preferentially extravasate into tumors and be retained there, known as enhanced permeability and retention (EPR) effect. Thereby the drug efficacy can be dramatically enhanced. At the same time the side effects of the drugs to normal tissues can be largely reduced. Moreover, due to the versatile structures of these drug delivery systems, they can be further modified with cancer-targeting moieties, enabling targeted delivery of anticancer drugs to cancer cells. Despite the above advantages, there is still much room for further improvement as their application are largely limited by several drawbacks

including low loading capacity, premature leakage of anticancer drugs before reaching the target sites, lack of controlled and complete release in the target sites.

Mesoporous silica nanoparticles with tunable diameters of 50-300 nm and pore size of 2-10 nm have recently emerged as a novel intracellular drug delivery system due to their uniform pore structures, high surface area and pore volumes, high chemical and physical stability as well as its easy functionalization.(*14-18*) MSNs with different functionalization were found to efficiently internalize into different cells without cytotoxic effects and with good biocompatibility.(*17, 19-23*). Due to their tunable uniform pore structures, the ideal zero-release before reaching target sites and controlled stimuli-responsive release in the target sites have been successfully realized by several groups for delivery of various drugs using a gatekeeping approach. Lin's group has developed several gatekeeping stimuli-responsive, MSN-based controlled release delivery systems. (*21, 24-27*) In their approaches, different entities including CdS nanoparticles, Au nanoparticles, Fe_3O_4 nanoparticles or G2.5 and 4.5 PAMAM dendrimers were used to cap the drug-loaded pores via a chemically cleavable disulfide linkage. Their studies demonstrated that while in the absence of a reducing agent, these drug-loaded MSNs showed nearly zero release in H_2O, once a reducing agent (including dithiothreitol (DTT), mercaptoethanol, DHLA or TCEP) was added into the system, the disulfide bonds were reduced and the caps were opened, resulting in efficient release of drug from pores. In addition to chemically stimulated controlled release delivery systems, photo-stimulated(*14*) and electrochemically redox-activated(*15*) controlled MSN-based delivery systems have also been developed by other groups. Despite these attractive features, employing MSNs as a controlled release delivery system to deliver anticancer

drugs to cancer cells have rarely been reported. One recent report by Lu et al.(*16*) has first demonstrated the use of MSNs as an intracellular delivery system for anticancer drugs. They showed the loading of a hydrophobic anticancer drug, camptothecin (CPT), into fluorescent MSNs and efficient delivery into a variety of human cancer cells to induce cell death. The CPT-loaded MSNs were shown to exhibit negligible release in aqueous solution while efficient release after delivery into the hydrophobic regions of the cell compartments. This report represented a non-gatekeeping approach to achieve nearly zero premature release and controlled release in target site using hydrophobic pore surface. However, the loading capacity of CPT in their system is extremely low, only ~0.06 wt%, which makes it highly inapplicable for real applications, where a high dose of anticancer drugs is usually required for effective therapeutic efficacy. In another recent report by Lu et al.,(*17*) fluorescent MSNs was used for loading and delivery of another hydrophobic drug, paclitaxel, into cancer cells; however, detailed information of loading capacity and release mechanism is lacking in this report.

Herein we report the development of MSNs as an intracellular controlled release delivery system to load a representative anticancer drug, doxorubicin, at a very high loading capacity (up to 220 wt%) and then efficiently deliver into human ovarian cancer cells for effective cancer therapy. As illustrated in Figures 1 and 2, we have successfully used a non-gatekeeping approach in achieving nearly zero release of Dox in H_2O, and stimuli-responsive controlled complete release once delivered into the cancer cells. In order to achieve high loading capacity, we have employed a design that allows multiple interactions between Dox and pore surfaces, including hydrophobic interaction, electrostatic interaction, hydrogen bonding as well as possible covalent binding. It was

further demonstrated that the Dox delivered by our system is highly toxic and very effective in killing cancer cells.
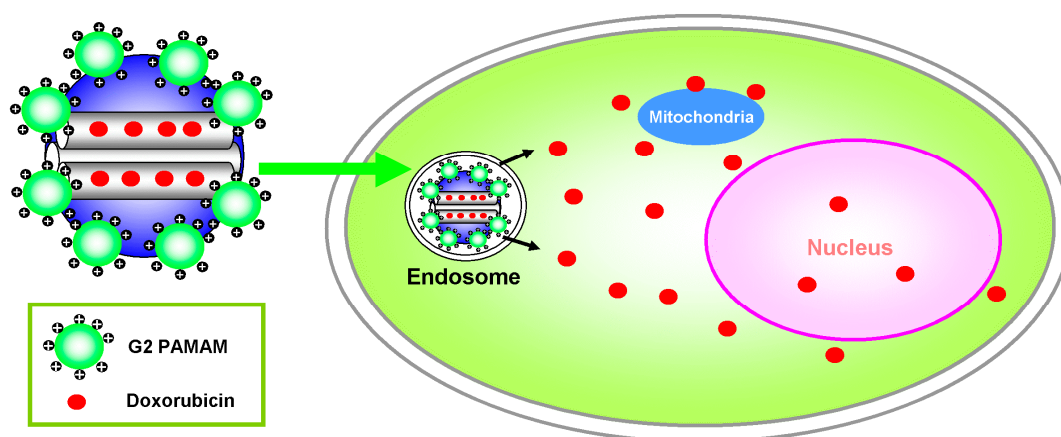
Figure 4.1. Schematic diagram of a MSN-based delivery system for non-gatekeeping and controlled release of Doxorubicin in cancer cells.
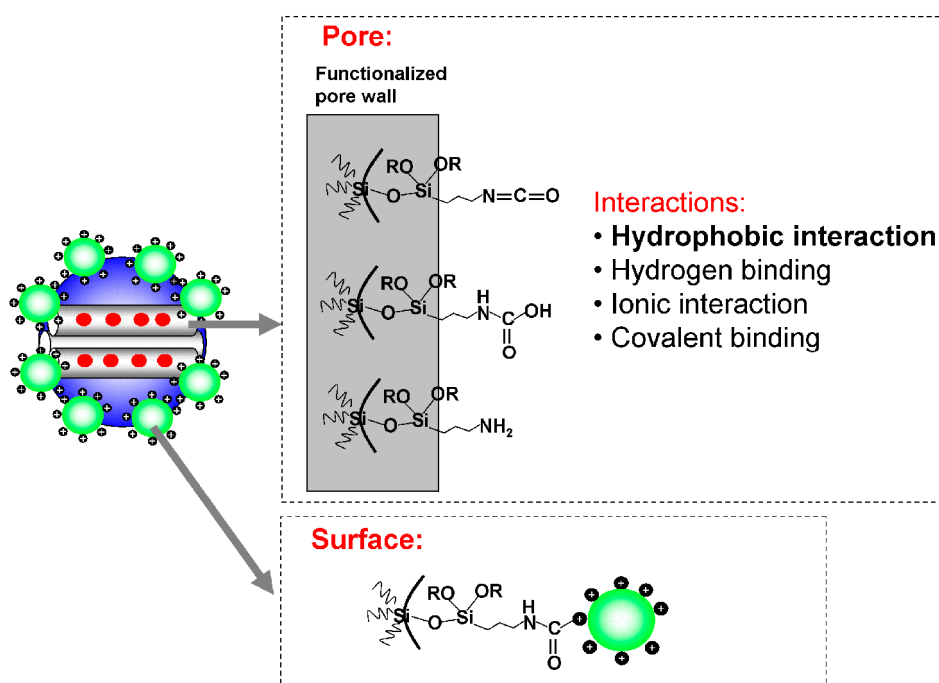
Figure 4.2. A schematic diagram to show the modifications on the pores and surfaces of MSN-Dox-G2. Multiple interactions exist between the pore surfaces and Doxorubicin.

4.2. Results and Discussion

4.2.1. Synthesis and Characterization of ICP-MSN

We synthesized the Mobile Crystalline Material-41 (MCM-41) type of MSNs using a surfactant-templated, base-catalyzed condensation method for our study.(*18*) The MSNs were then reacted with 3-iso-cyanatopropyltriethoxysilane to yield isocyanatopropyl (ICP)-modified surfaces. Then the portion of MSNs with small diameters was isolated by dispersing the MSNs in water first and then collecting the supernatant after settling for 2 h. The supernatant was subsequently lyophilized to obtain MSN powders. Thus obtained ICP-modified MSNs (ICP-MSN) were characterized by transmission electron microscopy (TEM) (Figure 4.3a) which showed a spherical morphology with a hexagonal array of mesoporous channels. Dynamic light scattering (DLS) analysis showed a mean particle size of ~182 nm (Figure 4.3b), which is consistent with the TEM imaging result. Furthermore, the surface areas, pore volumes, and pore size distributions of as-synthesized MSNs and ICP-modified MSNs were respectively analyzed by nitrogen adsorption/desorption techniques using ASAP 2020 (Micromeritics). The adsorption/desorption isotherm is shown in Figure 4.4a and the pore size distributions are shown in Figure 4.4b. The Brunauer–Emmett–Teller (BET) surface area and the pore size and pore volume determined based on BJH model are summarized in Table 4.1. It showed that the ICP-MSNs has a mean pore size of 2.88 nm, surface area of 816 m^2/g, and pore volume of 0.77 cm^3/g. The ICP functionalization of the MSN surfaces was confirmed by solid state ^{13}C CP-MAS NMR, which showed the presence of both isocyanatopropyl groups and propyl carbamate groups due to partial hydrolysis of isocyanatopropyl groups (Figure 4.5).
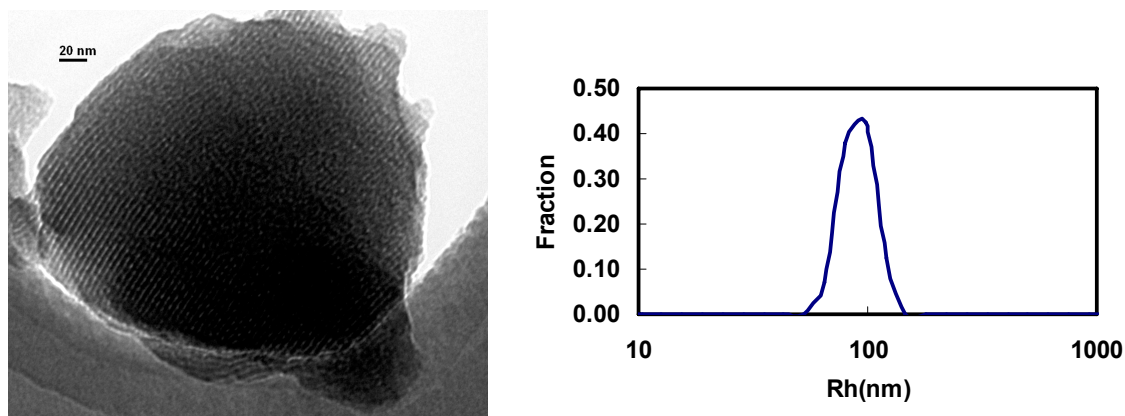
Figure 4.3. (a). TEM image of an ICP-modified mesoporous silica nanoparticles. **(b).** Particle size distribution of MSN-Dox-G2 by DLS. The hydrodynamic radius of MSN-Dox-G2 was determined to be 91±16 nm.
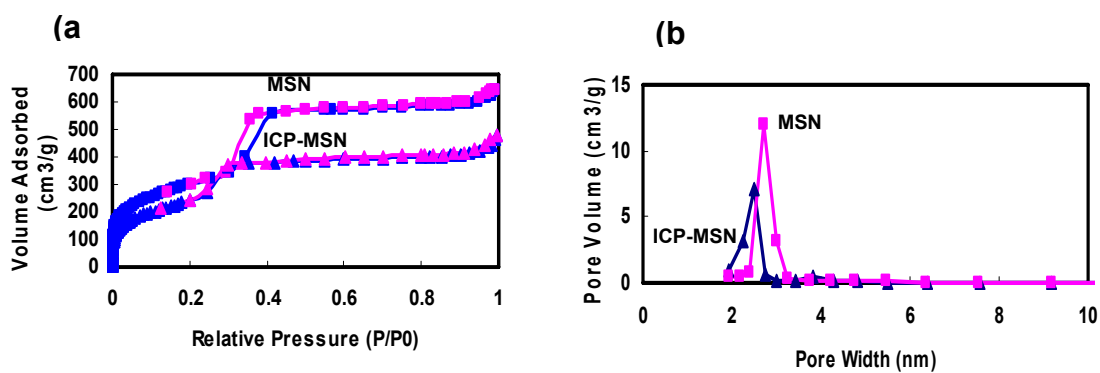
Figure 4.4. (a). BET nitrogen adsorption/desorption isotherms. (b). BJH pore size distributions of MSN and ICP-MSN.

Table 4.1. BET surface area, BJH pore volume and pore size.

Sample	BET surface area (m^2/g)	BJH pore volume (cm^3/g)	BJH pore size (nm)
MSN	1001	1.00	2.99
ICP-MSN	816	0.77	2.88
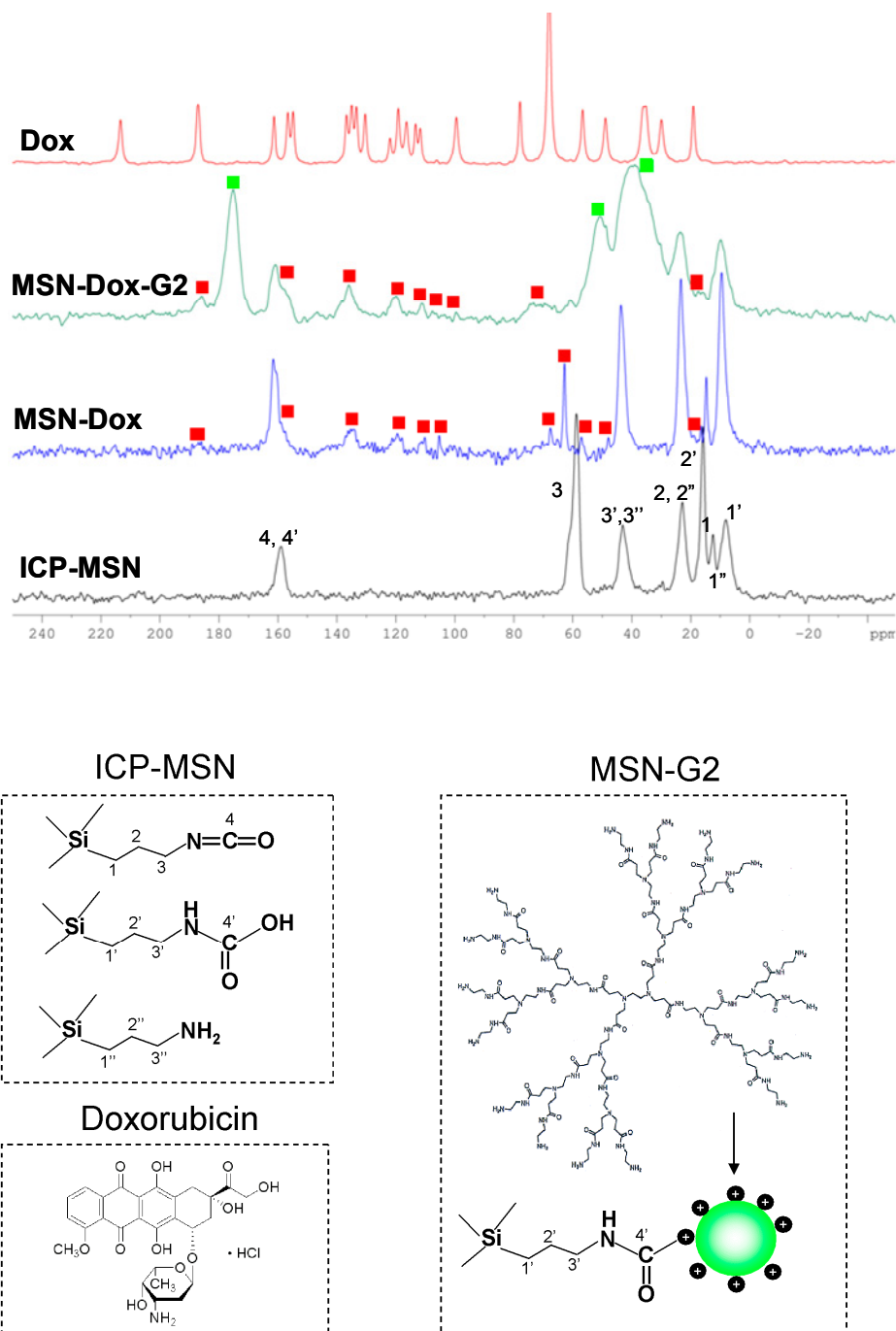
Figure 4.5. ^{13}C Solid State CP-MAS NMR spectra of the isocyanatopropyl-modified MSN (ICP-MSN), Dox-loaded ICP-MSN (MSN-Dox), Dox-loaded ICP-MSN modified by G2 PAMAM (MSN-Dox-G2), and Dox. The red squares indicate the chemical shifts from Dox loaded in MSNs and the green squares indicate the chemical shifts from G2 PAMAM on MSN-Dox-G2.

4.2.2. Loading of Dox into the pores of ICP-MSNs

To encapsulate Dox into the pores of MSNs, ICP-MSNs were suspended in a Dox solution in 3:5 (v:v) MeOH:H_2O co-solvent under continuous stirring for a period of time. After loading, the suspension was centrifuged and the supernatants and pellets were collected respectively. Using UV-Vis spectroscopy, the Dox concentration in the supernatant and in the original loading solvent can be determined respectively and then the difference was used to determine the amount of Dox loaded into the MSNs. To study the effect of feeding ratio (ratio of Dox to MSNs used in the loading experiment) on the encapsulation efficiency (weight ratio of Dox loaded into MSNs to MSNs , w/w%) and the loading efficiency (weight ratio of Dox loaded into MSNs to total amount of Dox fed, w%), the loading was performed by using a constant Dox concentration of 1.21 mg/ml with varying feeding ratios of Dox to MSNs, 1.2, 2.4 and 6.0 respectively. As shown in Figure 4.6, it was found that with all three feeding ratios, the encapsulation and loading efficiency were proportional to the loading time with longer loading time resulting in higher encapsulation and loading efficiency. It also indicated that as the feeding ratio of Dox/MSNs increases, the encapsulation efficiency increases while the loading efficiency decreases. Based on Figure 4.6b, the loading efficiency appeared to reach a constant of 40 wt% after sufficient loading time for all three loading ratios. Use of MeOH:H_2O co-solvent as loading solvent is critical for the high encapsulation efficiency as very low encapsulation efficiency was achieved in our initial experiments when H_2O was used as the loading solvent. Since the pores of ICP-modified MSNs are mainly hydrophobic, we hypothesize that when using H_2O as loading solvent, the H_2O solution was not able to penetrate into the pores, while when using MeOH:H_2O as the loading solvent, the
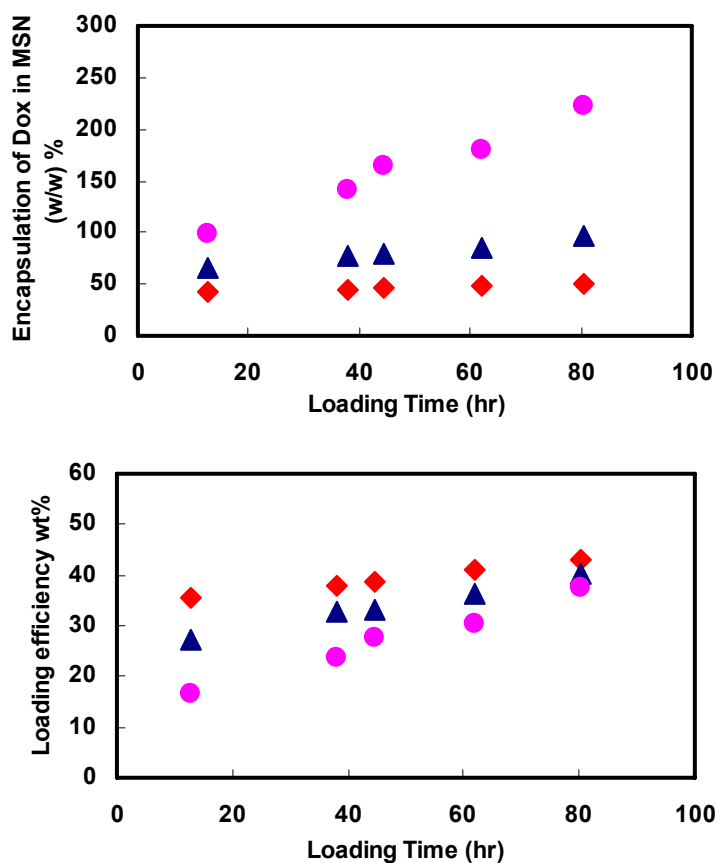
Figure 4.6. (a) Plot of encapsulation of Dox in MSN as a function of loading time. (b). Plot of loading efficiency as a function of loading time. Feeding ratio of Dox to MSNs: ◆ 1.2, ▲ 2.4, ● 6.0.

solution was able to penetrate into the hydrophobic pores, allowing Dox to interact with the MSN pore surfaces. Several types of interactions between Dox and MSN pore surfaces might exist in our system. First, a significant amount of Dox remains deprotonated and are hydrophobic under our loading conditions (pKa of Dox=8.25)(*8, 11*) and therefore exists strong hydrophobic interaction between Dox and hydrophobic pore surfaces; second, as confirmed by solid state ^{13}C NMR, part of the ICP groups were hydrolyzed into propyl carbamate groups, which could then induce electrostatic

interaction with the protonated amine groups of Dox as well as hydrogen bonding with the non-protonated amine groups of Dox. Additionally, a fraction of the amine groups of Dox might react with the labile ICP groups on the pore surfaces, forming chemical urea linkages between Dox and pore surfaces. As shown in Figure 4.6a, the encapsulation efficiency can reach as high as 220 wt% when a feeding ratio of 6 (Dox/MSN) and 80-h loading time were employed. To the best of our knowledge, this encapsulation efficiency is superior to all other reported MSN-based delivery systems, where an encapsulation efficiency of 0.01-40 wt% was typically achieved.(*16, 19*) We speculate that the coexistence of multiple interactions between Dox and pore surfaces is critical for the superior encapsulation efficiency of Dox in our system

4.2.3. Modification of Dox-loaded ICP-MSNs with G2 PAMAM

Previous studies showed that MSNs with different functionalization exhibited different internalization efficiency into cancer cells. Lin *et al.* (*18*) demonstrated the MSNs modified by G2 PAMAM groups were able to complex with plasmid DNA and internalize into various types of cancer cells efficiently. In addition, G2 PAMAM has a rich number of tertiary amines, known to have proton sponge effect(*20*) to facilitate efficient release from endosome into cytoplasm. For these reasons, we chose to modify our Dox-loaded ICP-MSNs with G2 PAMAM to render the MSN surfaces positively charged for efficient internalization into cancer cells and subsequent efficient release to cytoplasm from endosome.

To perform the modification, the Dox-loaded ICP-MSNs were dispersed into H_2O and then reacted with G2 PAMAM to form urea linkages between amines of G2

PAMAM and ICP groups of MSN for 3 h under continuous shaking. Then the suspension was centrifuged to remove the supernatant. The pellet was then washed extensively with H_2O to remove residual free Dox and free G2 PAMAM by redispersing and centrifuging a few times. The successful modification of G2 PAMAM on MSN surfaces were confirmed by ^{13}C solid state NMR (Figure 4.5).

4.2.4. Release of Dox from MSN-Dox-G2

The release of Dox from Dox-loaded ICP-MSNs modified with G2 PAMAM (MSN-Dox-G2) was studied by suspending MSN-Dox-G2 in different media at 37 °C and then monitoring the fluorescence of the suspension at different time points. It was found that the fluorescence of Dox was completely quenched after loaded into MSNs (Figure 4.7). Therefore the fluorescence of Dox in a suspension of MSN-Dox-G2 is solely due to the released Dox and was used to quantify the amount of released Dox based on the fluorescence calibration curve of free Dox in each respective medium.
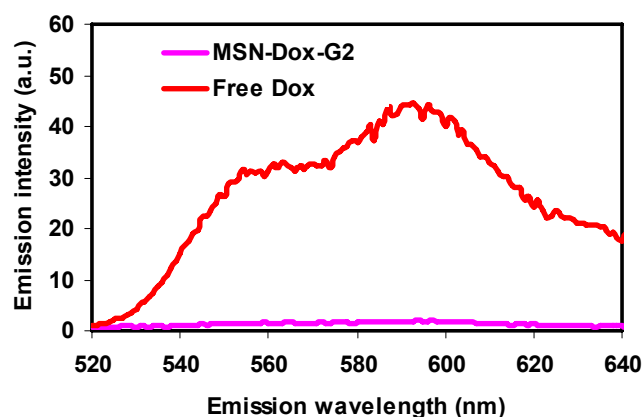
Figure 4.7. Fluorescence of a suspension of MSN-Dox-G2 in H2O vs. free Dox solution. The Dox concentration was same for both samples, 0.147 mg/ml. It showed that the fluorescence of Dox encapsulated inside MSN pores was completely quenched.

The Dox release profiles in H_2O, Dulbecco's phosphate buffered saline (DPBS), cell medium, 10% human serum in H_2O, A2780/AD cell-free extract, dimethyl sulfoxide (DMSO), and 4.9 mM glutathione in H_2O at 37 °C as a function of release time are presented in Figure 4.8. Burst release has been evident in many delivery systems.(*8*) In our experiment, we found that the burst release in H_2O is nearly negligible with only ~2%. The burst release in DPBS, cell medium, 10% human serum in H_2O, cell-free extract and 4.9 mM glutathione in H_2O is higher in an increased order, 4.9, 6.0, 9.2, 15.1 and 16.9%, respectively. In contrast, a very high burst release of ~51% was observed in DMSO. The burst release was reported to be often due to some drugs being physically adsorbed on the surface of delivery systems rather than being encapsulated inside.(*8*) In our case, the dramatic difference of burst release in DMSO than other aqueous mediums suggested some different mechanism. It is known that for MSN-based drug delivery systems with hydrophobic pore surfaces, the release of drug in aqueous medium can be impeded. This is because an aqueous medium does not easily penetrate inside the pores.(*19*) DMSO is
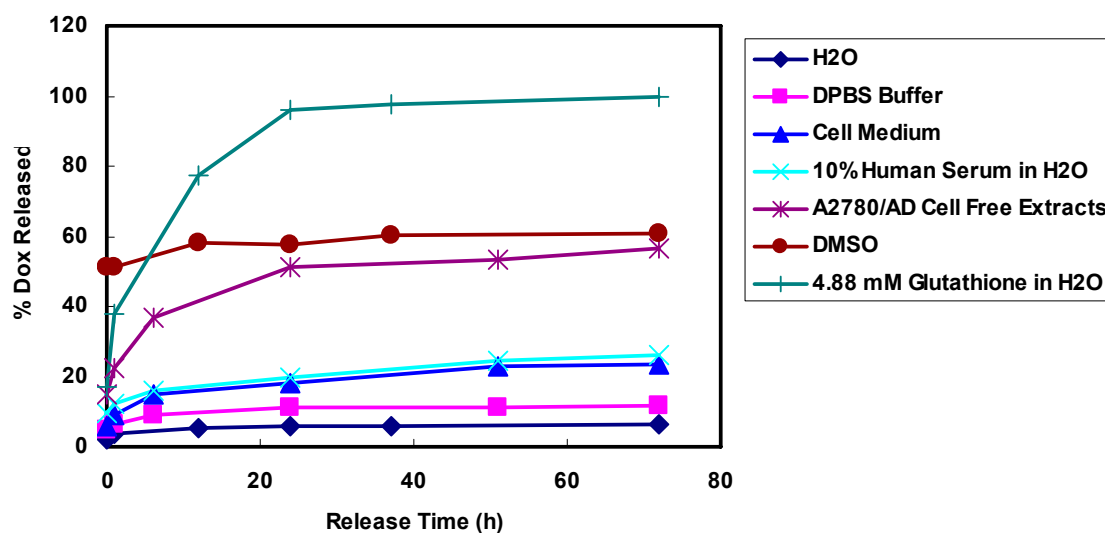
Figure 4.8. Doxorubicin release profiles from MSN-Dox-G2 in different mediums at 37 °C.

known to be both hydrophilic and hydrophobic. Its hydrophobicity is attributed to the two methyl groups, which make DMSO to be able to penetrate into the hydrophobic MSN pores.

Furthermore, DMSO is expected to have strong molecular interactions with Dox, which can be predicted by Hansen solubility parameters (δ)(*21*) (see table 4.2). Once penetrating into MSN pores, its strong interactions with Dox resulted in immediate release of the Dox that were encapsulated through relatively weak interaction with pore surfaces, while those Dox with stronger interaction with pore surfaces remained inside.

The solubility parameter of each molecule can be grouped into three different parameters, δd for dispersion interactions, δp for polar interaction, and δh for hydrogen bonding interaction. As listed in Table 4.2, the values of all three parameters are very high for both DMSO and H_2O. These high values suggest both solvents should have strong interaction with Dox. However, due to the hydrophobicity of MSN pores, H_2O is unable to enter the pores, therefore the release of Dox in water is negligible. However, in the case of DMSO, it can enter the pores due to its partial hydrophobicity. This, combined with its strong molecular interactions with Dox, resulted in the immediate release of the physically adsorbed Dox into DMSO.

Table 4.2. Hansen solubility parameters for solvents at 25 °C(*21*)

Solvent	δt[a]	δd[b]	δp[c]	δh[d]
DMSO	26.7	18.4	16.4	10.2
H2O	47.8	15.6	16	42.3

[a] δt = Total Hildebrand solubility parameter.
[b] δd = Dispersion solubility parameter
[c] δp = Polar solubility parameter
[d] δh = Hydrogen bonding solubility parameter.

The significantly higher burst release in ions or chemicals-containing aqueous media than in H_2O suggested some significant effect of ions and chemicals on the burst release. It is possible that a similar mechanism as that in DMSO might exist in that the presence of ions, serum or glutathione renders the whole solvent more wettable to the pore surface and therefore enables the solvent to penetrate into the pores and release the portion of Dox that is weakly absorbed.

The release profiles in Figure 4.8 further indicated that over a release time of up to 72 h, the Dox remains encapsulated inside MSN pores in H_2O with only ~6.2 % released. The release in DPBS was higher, ~11.9% after 72 h. This suggests a significant effect of ions on the release of Dox. The release in 10% human serum in H_2O after 72 h is ~26.1%, which is significantly higher than in H_2O, suggesting that serum significantly facilitated the release of Dox. Relative to the release in DPBS, the release in cell medium after 72 h is significantly higher, ~23.6%. The cell medium is comprised of RPMI 1640 medium supplemented with 10% fetal bovine serum. Given that the release in 10% human serum in H_2O is significantly higher than that in H_2O, we can therefore infer that the increased release in cell medium relative to DPBS is likely attributed to the presence of 10% fetal bovine serum. These data showed various effects of ions and serum on the release of Dox. In all , the release of Dox in aqueous mediums containing ions or serum showed ~11.9-23.6% release after 72 h at 37 °C while the release in H_2O is nearly negligible, only ~6.2%.

In sharp contrast, when suspended in 4.9 mM glutathione in H_2O, ~96% Dox was released after 24 h and all Dox was released after 72 h. It was reported that an approximately 5 mM of glutathione is present in animal cells. Our finding that Dox can

be completely released from MSN-Dox-G2 in 4.9 mM glutathione is of great importance to the application of our delivery systems for intracellular delivery and release. This suggests that once delivered into the cancer cells, Dox can be efficiently and completely released. Not surprisingly, when performing the release experiment in 10000-time diluted solution of cell-free extract (that contains glutathione) in H_2O at 37 °C, 56.6% Dox release was achieved after 72 h. The actual medium inside the cells is much more concentrated and is expected to dramatically increase the release rate and percentage. While it is not possible with these data to exclude the possible effects of chemicals other than glutathione in cell-free extract on the release of Dox, it is apparent that the presence of 4.9 mM glutathione itself is sufficient to enable complete release of Dox inside the cells. Parallel release profile of Dox in DMSO was also obtained. It showed that following initial burst release of 51.2% Dox, over the release course of 72 h, an additional of 13.4% was released, resulting in a total of 64.6% release. This release profile exhibited a substantial difference from that in 4.9 mM glutathione. In the latter, a burst release of only 16.9% was observed with a complete release after 72 h; while in the former, a significantly higher amount of Dox was burst released, followed by small amount of additional release over the course of 72 h. We speculate that in the case of DMSO, while DMSO penetrates into pores and enables the immediate release of weakly absorbed Dox from the pores, it is not able to release most of the residual Dox that are more strongly interacted through electrostatic attraction, hydrogen-bonding or chemical conjugation with the pore surfaces. In contrast, in the case of 4.9 mM glutathione, due to its much weaker effect on the polarity of solvent as well as the wettability to the pore surfaces, it is only able to burst release 16.9% of Dox and then gradually release the

remaining Dox that is weakly absorbed. At the same time, it is likely that those Dox strongly interacting with the pore surfaces through electrostatic attraction, hydrogen bonding or chemical conjugation are also completely disrupted by the glutathione and can eventually release out of pores governed by diffusion.

The kinetics of the release of drugs from porous carrier materials is frequently described using the Higuchi model. (*8, 21-25*) According to this model, the release of a drug from an insoluble, porous carrier matrix can be described as a square root of a time-dependent process based on Fickian diffusion. The amount of drug released, Q_t, per unit of exposed area at time t can then be described by the simple equation:

$$Q_t = k_H \sqrt{t} \quad (1)$$

Where k_H is the release rate constant. Thus for a purely diffusion controlled process, the amount of drug released exhibits a linear relationship if plotted against the square root of time. To understand whether the release of Dox in 4.9 mM glutathione and in cell-free extract from our delivery system is purely diffusion controlled process, the release data were fitted to Higuchi model. Given that the release after 24 h appeared to gradually reach a plateau, the data points up to 24 h release were used for fitting. Indeed, as shown in Figure 4.9, good fits were obtained for the release data both in 4.9 mM glutathione and in cell-free extracts, with a correlation coefficient of 0.995 and 0.988 respectively. The slopes, which are the release rate constant, were found to be 16.1 and 7.5, for release in 4.9 mM glutathione and cell-free extract, respectively. This result confirmed that the release of Dox in these two mediums from our delivery systems is purely diffusion-controlled after initial burst release. In addition, a semi-empirical power law equation as shown below(*8, 22*) can also be used to describe a diffusion-driven release process.

$$\frac{M_t}{M_\infty} = \frac{M_b}{M_\infty} + kt^n \quad (n=0.43) \quad (2)$$

Where M_t, M_∞ are the amount of drug released at time t and infinite time, M_b the amount of burst released drug, k the release constant and n is the release exponent. The value of n depends on the geometry of the relative device and the mechanism. For spheres and diffusion-driven release, n is 0.43. Again, excellent fits to this equation were obtained for release data both in 4.9 mM glutathione and in cell-free extract as shown in Figure 4.10, with a correlation coefficient of 0.999 and 0.992 respectively. These results further confirmed the purely diffusion-controlled release mechanism from spheres in both mediums after burst release. This result suggests that although complete release of Dox in 4.9 mM glutathione requires the disruption of all interactions of Dox with pore surfaces, this disruption process is much faster than the diffusion process and not rate-determining step, resulting in a purely diffusion-controlled release process after initial burst release.
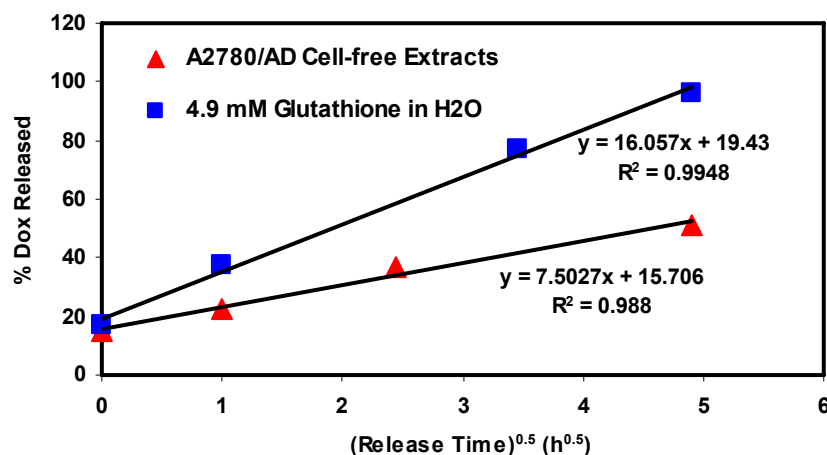
Figure 4.9. Diffusional release of doxorubicin from MSN-Dox-G2 in A2780/AD cell-free extracts and 4.9 mM glutathione in H_2O at 37 °C, a fit to Higuchi model.
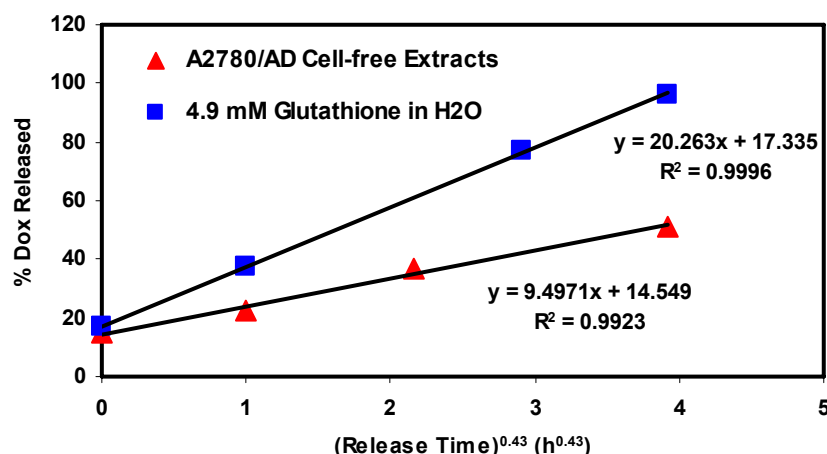
Figure 4.10. Diffusional release of doxorubicin from MSN-Dox-G2 in A2780/AD cell-free extracts and 4.9 mM glutathione in H$_2$O at 37 °C, a fit to semi-empirical power law equation

$$\frac{M_t}{M_\infty} = \frac{M_b}{M_\infty} + kt^n \ (n=0.43).$$

Our results clearly demonstrated the use of hydrophobic pore surface to encapsulate hydrophobic drug inside pores and achieve nearly zero release in H$_2$O. The nearly zero release in H$_2$O is especially important for anti-cancer drug delivery systems as premature drug release can cause severe side effects to normal tissues during delivery. This similar approach has been used previously for delivery of different hydrophobic drugs including anti-cancer drugs.(*16, 19*) In a recent report by Lu et al.,(*16*) hydrophobic anti-cancer drug camptothecin (CPT) was loaded into FITC-modified MSNs and efficiently internalized into a variety of human cancer cells. It was shown that while only negligible amount of CPT was released in aqueous solution, significant amount of Dox could be released once delivered into cancer cells. Their study represents the first report of utilizing MSNs as delivery system for hydrophobic anti-cancer drugs with nearly zero release of drug in H$_2$O and efficient release inside cancer cells. However, the

encapsulation efficiency in their system is very low, only ~0.06 wt% and unfeasible for real applications, where a high drug loading is required. In our delivery system, the MSN pore surfaces were modified by ICP groups. The function of ICP modification is multi-fold. With regard to the pore surface, the ICP modification renders the pore surface hydrophobic, generating hydrophobic interaction with the deprotonated portion of Dox as well as allowing the use of hydrophobic surface to achieve nearly zero release in H_2O. Some of the ICP groups were hydrolyzed to propyl carbamate, which could then interact with Dox through electrostatic interaction as well as hydrogen bonding. Furthermore, part of the ICP group can react with the amine groups of Dox to form urea linkage, allowing additional loading of Dox. The extremely high encapsulation efficiency in our delivery system as compared to the low encapsulation efficiency in Lu et al's report(*16*), where primarily hydrophobic interaction is present, suggested that the existence of multiple interactions is important for the high encapsulation efficiency. With regard to the external surface of MSNs, the ICP provides the function to further conjugate with G2 PAMAM, rendering G2 PAMAM-modified surfaces for efficient internalization into cancer cells and efficient release of MSNs into cytoplasm due to the proton sponge effect of G2 PAMAM.

In addition to the high encapsulation efficiency and the nearly zero release of Dox in H_2O, our system also exhibited complete release of Dox in 4.9 mM glutathione, which mimics the concentration of glutathione in most animal cells. Although the exact mechanism of glutathione effect on the complete release of Dox requires further investigation, our preliminary data clearly suggests that glutathione completely disrupts

the strong interaction of encapsulated Dox with pore surfaces, which can not be completely disrupted in other mediums, including DMSO.

Diffusion-controlled release of Dox allows control over release kinetics of the drug and is advantageous over other delivery systems, where the release is not well controlled or complete release occurs immediately upon stimulation. In 4.9 mM glutathione, our system exhibited 16.9 % burst release and then followed a diffusion-controlled release over a course of 24 h. This suggests that once delivered into the cells, it may also exhibit a similar burst release, followed by diffusion-controlled release over a long period of time. For chemotherapy with anti-cancer drugs, the maintaining of a high concentration of drug inside the cells is important, this diffusion-controlled release might prove advantageous in sustaining a high concentration of Dox over a long period of time as compared to other delivery systems where all drug is immediately released, subsequently subject to diffusion of drug out of cells.

As mentioned previously, Lin's group has previously demonstrated a gate-keeping approach to achieve nearly zero release of drug in aqueous solution by using G2.5 or G4.5 PAMAM dendrimers as caps to cap the pores through a disulfide linker.(*23*) In their report, the system showed nearly zero release in H_2O while addition of two reducing agents, Dithiothreitol (DTT) and tris(2-carboxyethyl)phosphine (TCEP) resulted in significant release of encapsulated adenosine 5-triphosphate (ATP) In their case, the PAMAM capping appeared to be responsible for the nearly zero release in H_2O, while in our delivery system, although a similar G2 PAMAM modification on the MSN surfaces was employed, the nearly zero release of Dox in H_2O was not due to the capping of G2 PAMAM on the pores but due to the hydrophobic feature of pore surfaces. To prove this,

a release experiment of Dox-loaded ICP-MSNs (MSN-Dox) without G2 PAMAM modification was performed in H_2O and it showed similar nearly zero release of Dox in H_2O. Furthermore, in our delivery systems, the G2 PAMAM modification appeared to have minimal effect on protecting Dox from releasing out of MSN pores as significant amount of Dox release was achieved in DMSO and complete release was achieved in 4.9 mM glutathione. In the beginning, we speculated that G2 PAMAM dendrimer, with a diameter of ~2.9 nm, was not able to efficient cap the pores with a diameter of 2.88 nm in our system. This is different from Lin's report,(*23*) in which larger G2.5 or G4.5 PAMAM dendrimer and MSNs with smaller pore diameter of 2.3 nm were used. In another experiment, we used G4 PAMAM dendrimer (with a diameter of ~4.5 nm) to cap the opening of the pores. However, by regular fluorescence study, we found that Dox still can release out of the pores upon delivery of the MSN-Dox-G4 complex with siRNA into cancer cells (Figure 4.11).
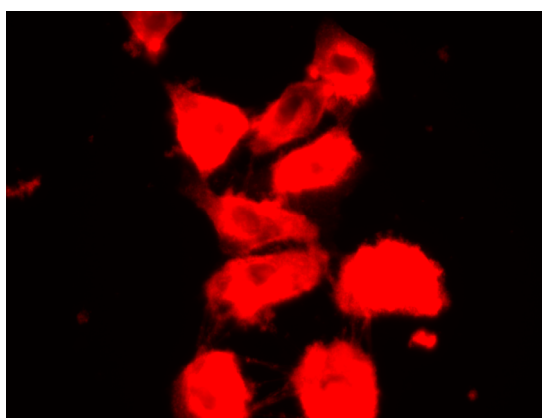
Figure 4.11. A representative red fluorescence image of A549 lung cancer cells incubated with Si-Dox-G4 complex with siRNA. An N/P ratio of 1 and 24 h incubation at 37 °C was used.

4.2.5. Internalization of MSN-Dox-G2 and the Intracellular Release and Localization of Dox vs. Free Dox

To further investigate the internalization efficiency of MSN-Dox-G2 and the intracellular release of Dox, MSN-Dox-G2 was added to A2780/AD human ovarian cancer cells on a 6-well plate (20,000 cells/well in 1.5 ml of cell growth medium) and incubated for 5 h at 37 °C. The cells were then washed with DPBS and added with fresh medium for fluorescence imaging. The red fluorescence imaging was performed to image the released Dox. As previously discussed, the fluorescence of Dox encapsulated inside the MSN pores is completely quenched and therefore the red fluorescence is a hallmark of the Dox released from the MSN pores. As shown in Figure 4.12a, the cells showed strong red fluorescence, indicating efficient release of Dox after MSN-Dox-G2 internalizing into the cells. It was further shown that the released Dox were located in both cytoplasm and nuclei with the amount of released Dox in cytoplasm substantially higher than in nuclei. Additionally, it is worth noting that the released Dox in cytoplasm is mainly located in perinuclear region. This observation that majority of released Dox in cytoplasm are in perinuclear region while almost none is located in the regions close to cell membrane is particularly interesting. Nanoparticles have been reported to be able to overcome or reduce the multidrug resistance induced by membrane-associated P-glycoprotein through endocytosis.(*1, 3, 7, 9, 10, 38-40*) It was reported that conjugating Dox to dextran decreased its removal rate from P-glycoprotein (P-gp) over-expressing, multidrug-resistant KB-V1 cells.(*3*) Similarly, a folate-targeted liposome delivery of Dox has been shown to increase tumor cell-selective cytotoxicity of Dox by bypassing multidrug-resistance efflux pump.(*7*) Another recent report(*10*) showed that using a polymer-lipid

hybrid nanoparticles system to deliver Dox, the membrane-associated P-gp can also be bypassed and the Dox can be better retained within the multi-drug resistant cells. The fluorescence microscopy data (Figure 4.12a) strongly suggested that our delivery system might show similar effects of bypassing the multi-drug resistance efflux pump by delivering and releasing the Dox directly into the perinuclear region. This distribution of released Dox inside cells is very different from the distribution when free Dox was delivered into the cells. Figure 4.12b showed the red fluorescence image of cells which were incubated with free Dox with same concentration as that in MSN-Dox-G2 under same conditions. It showed that in the case of free Dox delivery, Dox was primarily delivered into nuclei with very small amount of Dox located in cytoplasm. The delivery systems were reported to have significant effect on the distribution of released Dox. Gillies et al. (*5*) showed that while pH-responsive copolymer assemblies could efficiently
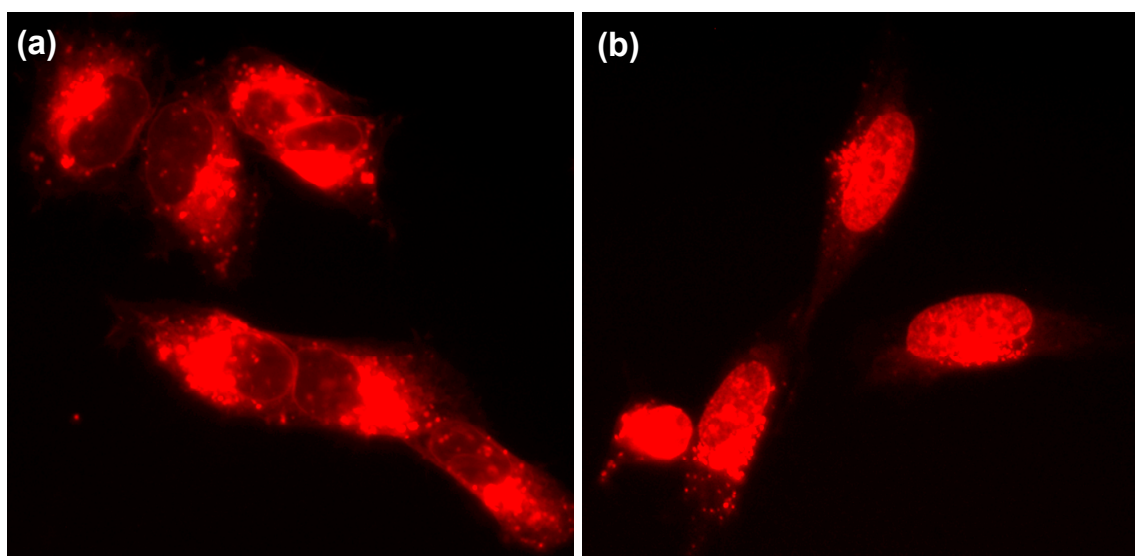
Figure 4.12. Regular fluorescence microscopy images of A2780/AD cells incubated at 37 °C for 5 h with (a) MSN-Dox-G2 and (b) Free Dox.

release Dox, the released Dox is primarily located in the cytoplasm. While the exact mechanism of how the delivery systems affect the distribution of released Dox inside the cells requires more investigation, in our system, based on the release profile in 4.9 mM glutathione, one can speculate that over the course of 24 h, the diffusion of Dox out of MSN pores is a continuous process, which can subsequently result in gradual accumulation of Dox in cytoplasm if the released Dox is not promptly diffused and delivered into the nuclei. Furthermore, some physical interaction of released Dox with MSN surfaces might exist, inhibiting the diffusion of released Dox into nuclei.

4.2.6. *In vitro* Toxicity of MSN-Dox-G2 vs. Free Dox

In vitro toxicity of free Dox and MSN-Dox-G2 was assessed by MTT assay. The A2780/AD cells were separately incubated in 96-well plates with different concentrations of free Dox and MSN-Dox-G2 in the cell growth medium and incubated for 24 h at 37 °C. Based on these measurements, the IC50 dose (the dose that kills 50% of cells) of free Dox was determined to be 2.25 µM and that of MSN-Dox-G2 was determined to be 1.07 µM (Figure 4.13). The MSN-Dox-G2 showed about one-fold increase in cytotoxicity than the free Dox. This increased cytotoxicity was shown not to be due to MSN-G2 as MSN-G2 alone showed minimal toxicity at the concentration used (Figure 4.14). While it is not possible with these data to determine the exact cause of the higher toxicity of MSN-Dox-G2, in combination with previous reports, we speculate the higher toxicity of MSN-Dox-G2 might be related to the different distribution of released Dox inside the cells. While one important mechanism of action of Dox involves the DNA intercalation which requires the nuclear delivery of Dox, other mechanisms have also been proposed, including the inhibition of mitochondrial function, which might be involved in our
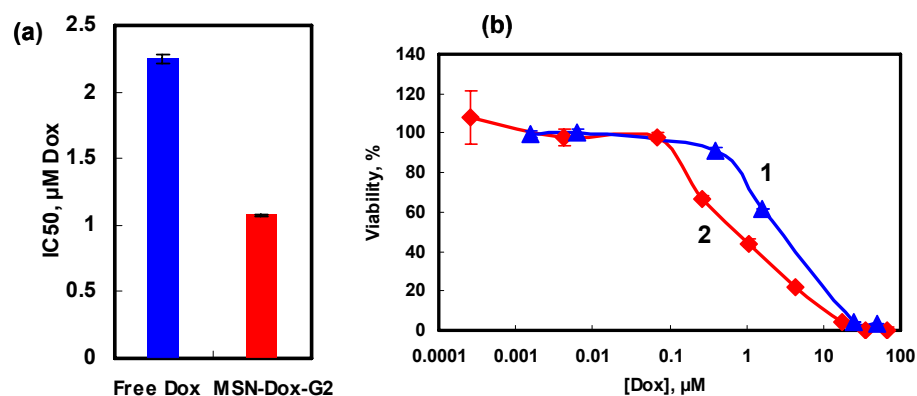
Figure 4.13. Viability of A2780/AD human ovarian cancer cells incubated for 24 h with the indicated formulations. (a). Cytotoxicity of formulations that contain Dox; (b). Actual dose-response curves of formulations that contain Dox. 1—Free Dox, 2—MSN-Dox-G2.
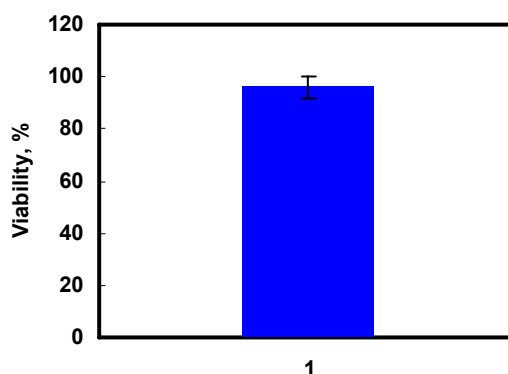
Figure 4.14. Viability of A2780/AD cells after incubated for 24 h at 37 °C with MSN-G2 nanoparticles, at a concentration of 0.0011 mg/ml. 0.0011 mg/ml MSN-G2 corresponds to the concentration of MSN-G2 in IC50 dose of MSN-Dox-G2 (that kills 50% of the cells).

delivery system. Moreover, one can speculate that similar to N-(2-Hydroxypropyl)methacrylamide (HPMA) copolymer-bound Dox,(*2, 24*) the Dox encapsulated inside the MSN pores can be protected from the drug degradation by intracellular enzymes and environment during delivery and therefore preserves its anti-

cancer activity. Last but not least, as discussed previously, the gradual diffusional release of Dox into the cytoplasm might help sustain a high concentration of Dox over a long period of time and may also contribute to the increased toxicity of MSN-Dox-G2. More *in vitro* studies will be necessary in order to further explore the mechanism of action of Dox in our delivery systems.

4.3. Conclusions

In summary, we have loaded anti-cancer drugs Doxorubicin into mesoporous silica nanoparticles with very high encapsulation efficiency and successfully delivered into human ovarian cancer cells. Our results suggested that the extreme high encapsulation efficiency are attributed to the existence of multiple interactions between Dox and the modified pore surfaces, including hydrophobic interaction, electrostatic interaction, hydrogen bonding as well as possible chemical conjugation. Using a non-gatekeeping approach, our delivery systems exhibited nearly zero release of Dox in H_2O while complete release in 4.9 mM glutathione in H_2O, that mimics the concentration of glutathione in common animal cells. Comprehensive release studies showed that the release of Dox is purely diffusion-controlled process in all mediums investigated following initial burst release. In the case of 4.9 mM glutathione in H_2O, the complete release appeared to be attributed to the glutathione being able to disrupt all interactions between Dox and pore surfaces, while in all other mediums investigated, some strong interaction between Dox and pore surfaces remain un-disrupted. Furthermore, regular fluorescence microscopy imaging showed efficient internalization of MSN-Dox-G2 into cancer cells, followed by efficient release of Dox into cytoplasm as well as into nuclei.

However, as compared to free Dox, the released Dox from MSN-Dox-G2 showed different distribution with majority located in cytoplasma, while free Dox is mainly delivered and located into nuclei. Despite the different distribution, the MSN-Dox-G2 exhibited superior toxicity, about 1-fold higher than free Dox. Our result represents the first example of loading large amount of anti-cancer drugs into MSNs with nearly zero release in cell media while complete stimuli-controlled release in cancer cells. We expect the developed approach can be applied to deliver various types of anti-cancer drugs into cancer cells. The versatile structures of MSNs will allow easy PEGylation and modification with cancer-targeting moieties for *in vivo* targeted delivery.

4.4. Experimental Section

4.4.1. Materials

G2 amine-terminated PAMAM dendrimer, doxorubicin hydrochloride and other chemicals used in this study were purchased from Sigma Aldrich (Milwaukee, WI), and used without further purification. siRNA that are sequence specific for human Bcl-2 mRNA was custom synthesized by Ambion (Austin, TX).

4.4.2. Synthesis of MCM-41 MSN and Modification with ICP

0.5 g of N-Cetyltrimethylammonium bromide (CTAB) was dissolved in 240 ml of deionized (DI) water and then added with 1.75 ml of aqueous sodium hydroxide solution (2.00 M) in a 500ml round-bottom flask. The temperature of the mixture was adjusted to 353 K and 2.50 ml of Tetraethoxysilane (TEOS) was added dropwise to the flask under stirring. The reaction was allowed to proceed for 2 h under continuous stirring. The resulting white precipitate was filtered and washed with 40 ml of DI water, and dried at

60 °C under vacuum with N_2 to yield the as-synthesized MSN. To remove the surfactant template (CTAB), the as-synthesized MSN was refluxed for 17 h in a mixture of 9.0 ml of HCl (37.4 wt% in H_2O) and 160.0 mL of methanol. The resulting material was filtered and extensively washed with H_2O and methanol. The surfactant-free MSNs were then dried under high vacuum at 60 °C overnight to remove the remaining solvent.

0.25 ml of 3-isocyanatopropyltriethoxysilane (ICP) was added to 100 ml of anhydrous toluene in a flask. Then 1 g of surfactant-free MSNs (pre-dried under vacuum at 100 °C for 1 h right before reaction) was added. After 20 h refluxing, the heating was stopped and the vessel was let to cool down to ~ 35 °C. The resulting powder suspension was then centrifuged at 20000 rpm for 20 min to remove the free ICP and toluene. Then the precipitate was re-dispersed into pure toluene and centrifuged again. Thus-obtained powder was dried under vacuum at 100 °C overnight to remove any remaining solvent.

4.4.3. Preparation of ICP-modified MSNs with Small Diameters

The MSNs with small diameters were isolated and used in our experiments. The ICP-modified MSNs were dispersed in water by sonicating for 20 min and then the suspension was allowed to settle overnight. The supernatant was then collected, lyophilized. The powder thus-obtained were then dried under vacuum at 60 °C overnight and used in all experiments.

4.4.4. Loading of Dox inside the Pores of ICP-modified MSN and Modification with G2 PAMAM

4.9 mg of ICP-modified MSNs were added into 8.0 ml of Dox solution in 3:5 (v:v) MeOH:H_2O cosolvent (4.5 mg/ml) and sonicated for 5 min to obtain a well-dispersed suspension. This suspension was then stirred at room temperature for 24 h to allow the

Dox to be encapsulated inside the pores of ICP-modified MSN. After that, the suspension was centrifuged at 15000 rpm for 15 minutes and the supernatant was removed. The residual pellet was collected and redispersed into 2.0 ml of H_2O by sonicating for 2 min. The suspension was then added to 0.172 g of 20% G2 PAMAM in MeOH solution, for which MeOH was pre-removed by evaporation. The reaction between amino groups of the G2-PAMAM and ICP functional groups on the MSN surface was allowed to proceed for 3 h. The resultant suspension was then centrifuged at 15000 rpm for 10 minutes and the supernatants removed. The pellet was then collected, redispersed into 1.0 ml of H_2O and centrifuged again at 15000 rpm for 10 min. This centrifuge-redisperse cycle was repeated for a total of 4 times to remove any free dendrimer, free Dox and residual MeOH. The resulting pellet was then redispersed into 1.0 ml of water to form a stock solution of MSN-Dox-G2.

4.4.5. Dynamic Light Scattering

Dynamic light scattering (DLS) studies were performed using the Wyatt Dawn EOS modified with a Wyatt QELS attachment. An aliquot of MSN-Dox-G2 stock solution was diluted ~3000 times in H_2O and then transferred to a quartz cuvette for analysis. Data were collected at an angle of 108° using an avalanche photodiode and an optical fiber and processed with the Wyatt QELS software (regularization analysis).

4.4.6. UV-Vis Absorbance

120 µl of appropriated diluted solutions of sample were transferred to a quartz cuvette for analysis by Cary 300 UV-Vis Spectrophotometer (Varian Inc., CA). The sample was typically scanned from 800 nm to 200 nm.

4.4.7. Transmission Electron Microscopy (TEM)

TEM image of MSN-Dox-G2 was performed using a LEO 922 electron microscope with a CCD camera. A carbon coated 200 mesh copper grid was pre-rinsed with 5 ul of EtOH and then deposited with 5 µl of MSN-Dox-G2 suspension in H_2O. After 3 min, the sample was drained off with a filter paper and further dried with a flow of N_2 gas. Then the sample was viewed on the electron microscope and photographs were taken using a camera attached to the microscope.

4.4.8. Solid-state ^{13}C CP-MAS NMR

Solid-state ^{13}C cross-polarization magic angle spinning (CPMAS) NMR spectra with TPPM decoupling during acquisition of isocyanatopropyl-modified MSN (ICP-MSN), Dox-loaded ICP-MSN (MSN-Dox), Dox-loaded ICP-MSN modified by G2 PAMAM (MSN-Dox-G2), and Dox were recorded on 400 and 500 MHz Bruker Advance spectrometers. In particular, the ^{13}C spectra of Dox and MSN-Dox-G2 were collected on a 500 MHz instrument equipped with a 2.5 mm HFX MAS probe, spinning the sample at 25 kHz, and using a pulse delay of 2 s, a contact time of 5 ms, a decoupling power level of 100 kHz, a spectral width of 100 kHz, 2048 points per FID, and 30 Hz of line broadening during data processing. 150000 and 4500 scans were collected for the MSN-Dox-G2 and DOX samples, respectively. The ^{13}C spectrum of the MSN-Dox sample was collected on a 500 MHz instrument equipped with a 4 mm HXY MAS probe, spinning the sample at 12 kHz, and using a pulse delay of 2 s, a contact time of 5 ms, a decoupling power level of 80 kHz, a spectral width of 100 kHz, 2048 points in the FID, and 30 Hz of line broadening during data processing. Signal averaging for the MSN-Dox sample was performed for 120000 scans. The ^{13}C spectrum of the ICP-MSN sample was collected on

a 400 MHz spectrometer equipped with a 4 mm HX MAS probe, spinning the sample at 10 kHz, using a pulse delay of 15 s, a contact time of 3 ms, a decoupling power level of 80 kHz, a spectral width of 80 kHz, 2048 points in the FID, and 50 Hz of line broadening during data processing. 16000 scans were collected for the ICP-MSN sample. All chemical shifts reported are externally referenced to the chemical shift of the carbonyl carbon in glycine of 176.70 ppm, previously determined relative to liquid Me_4Si (TMS).

4.4.9. Cell Lines

The human multidrug resistant ovarian carcinoma A2780/AD cell line was obtained from Dr. T. C. Hamilton (Fox Chase Cancer Center). The human lung cancer A549 cell line was obtained from the ATTC (Manassas, VA, USA). Cells were cultured in RPMI 1640 medium (Sigma, St. Louis, MO) supplemented with 10% fetal bovine serum (Fisher Chemicals, Fairlawn, NJ). Cells were grown at 37 °C in a humidified atmosphere of 5% CO_2 (v/v) in air. All experiments were performed on cells in the exponential growth phase.

4.4.10. Cytotoxicity

The cellular cytotoxicity of formulations was assessed using a modified MTT (3-(4,5-dimethylthiazol-2-yl)-2,5-diphenyltetrazolium bromide) assay. Cells were seeded into 96-well microtiter plates at the density of 10,000 cells per well. After incubation for 24 h, medium were aspirated and various concentrations of drugs (free Dox, MSN-Dox-G2) in fresh cell growth medium (200 ul/well) were added. Control cells were added with equivalent volume of fresh media. Cells were cultured for 24 h before the cell viability assay was performed. The old medium was removed and 100 ul of fresh medium and 25 ul of a 5 mg/ml MTT (Fluka) solution in DPBS was added to each well. Plates were then

incubated under cell culture conditions for 3 h. Every well was then added with 100 ul of 50% (v/v) dimethylformamide in water containing 20% (w/v) sodium doecyl sulfate (with pH adjusted to 4.7 by acetic acid) and incubated overnight to dissolve the formazan crystals. The absorbance of each sample was measured at 570 nm with a background correction at 630 nm. Based on these measurements, IC_{50} doses of Dox in free and MSN formulations of Dox delivery systems (the concentrations of Dox necessary to inhibit the cell growth by 50%) were calculated.

4.4.11. Cellular Internalization

Cellular internalization of Dox was studied by fluorescence microscope. A2780/AD cells were plated (20, 000 cells/well) in 6-well tissue culture plate and cultured for 24 h. The old medium was then removed and the cells were treated with MSN-Dox-G2 or free Dox (Thermo Fisher Scientific, Lafayette, CO) in 1.5 ml cell growth medium. The cells were cultured for 5 h at 37 °C and then the old medium removed. The cells were washed with Dulbecco's phosphate buffered saline (DPBS) buffer three times and then added with 1.5 ml fresh medium for fluorescence imaging.

4.5. References

1. Wong, H. L., Bendayan, R., Rauth, A. M., Li, Y., and Wu, X. Y. (2007) Chemotherapy with anti-cancer drugs encapsulated in solid lipid nanoparticles, *Advanced Drug Delivery Reviews 59*, 491-504.

2. Minko, T., Kopeckova, P., and Kopecek, J. (2000) Efficacy of the chemotherapeutic action of HPMA copolymer-bound doxorubicin in a solid tumor model of ovarian carcinoma, *Int. J. Cancer. 86*, 108-117.

3.   Lam, W., Leung, C.-H., Chan, H.-L., and Fong, W.-F. (2000) Toxicity and DNA binding of dextran-doxorubicin conjugates in multidrug-resistant KB-V1 cells: optimization of dextran size, *Anticancer Drugs 11*, 377-384.

4.   Dubowchik, G. M., Firestone, R. A., Padilla, L., Willner, D., Hofstead, S. J., Mosure, K., Knipe, J. O., Lasch, S. J., and Trail, P. A. (2002) Cathepsin B-Labile Dipeptide Linkers for Lysosomal Release of Doxorubicin from Internalizing Immunoconjugates: Model Studies of Enzymatic Drug Release and Antigen-Specific In Vitro Anticancer Activity, *Bioconjugate Chemistry 13*, 855-869.

5.   Gillies, E. R., and Frechet, J. M. J. (2005) pH-Responsive Copolymer Assemblies for Controlled Release of Doxorubicin, *Bioconjugate Chemistry 16*, 361-368.

6.   Nystrom, A. M., Xu, Z., Xu, J., Taylor, S., Nittis, T., Stewart, S. A., Leonard, J., and Wooley, K. L. (2008) SCKs as Nanoparticle Carriers of Doxorubicin: Investigation of Core Composition on the Loading, Release and Cytotoxicity Profiles, *Chem. Commun.*, 3579-3581.

7.   Goren, D., Horowitz, A. T., Tzemach, D., Tarshish, M., Zalipsky, S., and Gabizon, A. (2000) Nuclear delivery of doxorubicin via folate-targeted liposomes with bypass of multidrug-resistance efflux pump, *Clinical Cancer Research 6*, 1949-1957.

8.   Missirlis, D., Kawamura, R., Tirelli, N., and Hubbell, J. A. (2006) Doxorubicin Encapsulation and Diffusional Release from Stable, Polymeric, Hydrogel Nanoparticles, *European Journal of Pharmaceutical Sciences 29*, 120-129.

9.   Lee, E. S., Na, K., and Bae, Y. H. (2005) Doxorubicin loaded pH-sensitive polymeric micelles for reversal of resistant MCF-7 tumor, *Journal of controlled release 103*, 405-418.

10.   Wong, H. L., Bendayan, R., Rauth, A. M., Xue, H. Y., Babakhanian, K., and Wu, X. Y. (2006) A mechanistic study of enhanced doxorubicin uptake and retention in multidrug resistant breast cancer cells using a polymer-lipid hybrid nanoparticle system, *J. Pharm. Exper. Ther. 317*, 1372-1381.

11.   Choucair, A., Soo, P. L., and Eisenberg, A. (2005) Active Loading and Tunable Release of Doxorubicin from Block Copolymer Vesicles, *Langmuir 21*, 9308-9313.

12.   Jayant, S., Khandare, J. J., Wang, Y., Singh, A. P., Vorsa, N., and Minko, T. (2007) Targeted Sialic Acid–Doxorubicin Prodrugs for Intracellular Delivery and Cancer Treatment, *Pharmaceutical Research 24*, 2120-2130.

13.   Yang, J., Lee, J., Kang, J., Lee, K., Suh, J.-S., Yoon, H.-G., Huh, Y.-M., and Haam, S. (2008) Hollow Silica Nanocontainers as Drug Delivery Vehicles, *Langmuir 24*, 3417-3421.

14.   Mal, N. K., Fujiwara, M., and Tanaka, Y. (2003) Photocontrolled Reversible Release of Guest Molecules from Coumarin-modified Mesoporous Silica, *Nature 421*, 350-353.

15.   Hernandez, R., Tseng, H.-R., Wong, J. W., Stoddart, J. F., and Zink, J. I. (2004) An Operational Supramolecular Nanovalve, *J. Am. Chem. Soc. 126*, 3370-3371.

16. Lu, J., Liong, M., Zink, J. I., and Tamanoi, F. (2007) Mesoporous silica nanoparticles as a delivery system for hydrophobic anticancer drugs, *Small 3*, 1341-1346.

17. Lu, J., Liong, M., Sherman, S., Xia, T., Kovochich, M., Nel, A. E., Zink, J. I., and Tamanoi, F. (2007) Mesoporous Silica Nanoparticles for Cancer Therapy: Energy-Dependent Cellular Uptake and Deliery of Paclitaxel to Cancer Cells, *Nanobiotechnology*, 3189-3195.

18. Radu, D. R., Lai, C.-Y., Jeftinija, K., Rowe, E. W., Jeftinija, S., and Lin, V. S.-Y. (2004) A polyamidoamine dendrimer-capped mesoporous silica nanosphere-based gene transfection reagent, *J. Am. Chem. Soc. 126*, 13216-13217.

19. Vallet-Regi, M., Balas, F., and Arcos, D. (2007) Mesoporous materials for drug delivery, *Angew. Chem. Int. Ed. 46*, 7548-7558.

20. Cho, Y. W., Kim, J.-D., and Park, K. (2003) Polycation Gene Delivery Systems: Escape from Endosomes to Cytosol, *Journal of Pharmacy and Pharmacology 55*, 721-734.

21. Hansen, C. M. (2007) *Hansen Solubility Parameters: A User's Handbook, 2nd Ed.*, CRC Press.

22. Siepmann, J., and Peppas, N. A. (2001) Modeling of Drug Release from Delivery Systems Based on Hydroxypropyl Methylcellulose (HPMC), *Advanced Drug Delivery Systems 48*, 139-157.

23. Gruenhagen, J. A., Lai, C.-Y., Radu, D. R., Lin, V. S.-Y., and Yeung, E. S. (2005) Real-time Imaging of Tunable Adenosine 5-Triphosphate Release from an MCM-

41-Type Mesoporous Silica Nanosphere-Based Delivery System, *Applied Spectroscopy 59*, 424-431.

24.   Minko, T., Kopeckova, P., and Kopecek, J. (1999) Comparison of the anticancer effect of free and HPMA copolymer-bound adriamycin in human ovarian carcinoma cells, *Pharmaceutical Research 16*, 986-996.

Chapter 5

Co-delivery of Doxorubicin and Bcl-2 siRNA by Mesoporous Silica Nanoparticles Enhances the Efficacy of Chemotherapy in Multidrug Resistant Cancer Cells

5.1. Introduction

Development of multidrug resistance in cancer cells and adverse side effects are the major obstacles for effective cancer chemotherapy.(*1-3*) Therapeutic strategies to overcome drug resistance and specific tumor targeting with minimal premature drug release should have a great impact on the treatment of cancer. The multidrug resistance can be divided into two distinct classes, pump and nonpump resistance.(*3*) The pump resistance is caused by certain proteins that form membrane-bound ATP-dependent active drug efflux pumps, which significantly decrease the intracellular concentration of the drug and thereby the efficacy of the treatment. The main mechanism of nonpump resistance is an activation of cellular antiapoptotic defense, mainly by Bcl-2 protein. Most of the anticancer drugs trigger apoptosis and simultaneously activate cellular defense of multidrug resistance, which prevents cell death. Therefore, to effectively suppress the overall cancer resistance to chemotherapy, it is essential to simultaneously inhibit both

pump and nonpump mechanisms of cellular resistance by targeting all the intracellular molecular targets.(*3, 4*)

There is increasing enthusiasm for developing therapies based on RNA interference (RNAi) with short interference RNAs (siRNAs) (*5, 6*) due to its high specificity and potency of gene silencing.(*7*) Special sequences of siRNAs targeted against mRNA encoding major proteins responsible for pump and nonpump cellular defense have been developed and showed a substantial efficacy in vitro.(*8-11*) However, reports delivering such types of siRNA simultaneously with a traditional anticancer drug to cancer cells for enhanced chemotherapy efficacy have been scant, due to the lack of efficient co-delivery methods.(*3, 8*)

Recent studies have shown that mesoporous silica nanoparticles (MSNs) with various functionalizations can efficiently internalize into mammalian cells via an endocytosis pathway.(*12, 13*) Its large pore volumes and surface areas make it an ideal platform to load a large amount of chemical drugs inside the pores (*14, 15*) and genes on the surface and then simultaneously deliver into cells.(*16*) Lin and co-workers (*16*) (*17*)reported that by encapsulating a fluorescent dye inside the pores and complexing with plasmid DNA on the surface, MSNs can efficiently deliver the plasmid DNA into cancer cells using the fluorescent dye to visualize the interaction of MSNs and cells.(*17*) In another recent report by them,(*18, 19*) it was further demonstrated that MSNs can simultaneously deliver DNA and chemicals into plants. However, this ideal feature of MSNs has not been utilized to codeliver a hydrophobic anticancer drug together with siRNAs for a synergistic cancer therapy effect.

Herein we report the first of such efforts of utilizing MSNs to codeliver doxorubicin (Dox) (as a model hydrophobic apoptosis-inducing anticancer drug), and a siRNA (as a suppressor of cellular antiapoptotic defense) simultaneously into multidrug resistant cancer cells. As illustrated in Figure 5.1, the MSNs were modified to encapsulate Dox inside the pores to achieve minimal premature drug release. Then the Dox-loaded MSNs were modified with generation 2 (G2) amine-terminated polyamidoamine (PAMAM) dendrimers. The dendrimer-modified MSN can efficiently complex with siRNAs targeted against mRNA encoding Bcl-2 protein, which is the main player for non-pump resistance. We found that thus-formed complex can be delivered into multi-drug resistant A2780/AD human ovarian cancer cells to induce cell death. The anticancer efficacy of Dox increased 132 times compared to free Dox, mainly because the simultaneously delivered siRNA significantly suppressed the Bcl-2 mRNA, and efficiently overcome the non-pump resistance. Moreover, our data suggested that the delivered Dox by the MSNs are primarily localized in perinuclear region upon internalization, providing additional advantage in possibly bypassing pump resistance, therefore further enhancing the drug efficacy. This result is much different from some liposome codelivery systems, in which antisense oligonucleotides targeted to pump and nonpump resistances must be simultaneously delivered in order to significantly increase drug efficacy.(*3, 4*) We attributed this difference to the different internalization pathway and drug release mechanism. We envisioned that this codelivery system can be generalized to other anticancer drugs and other cancer cell lines.
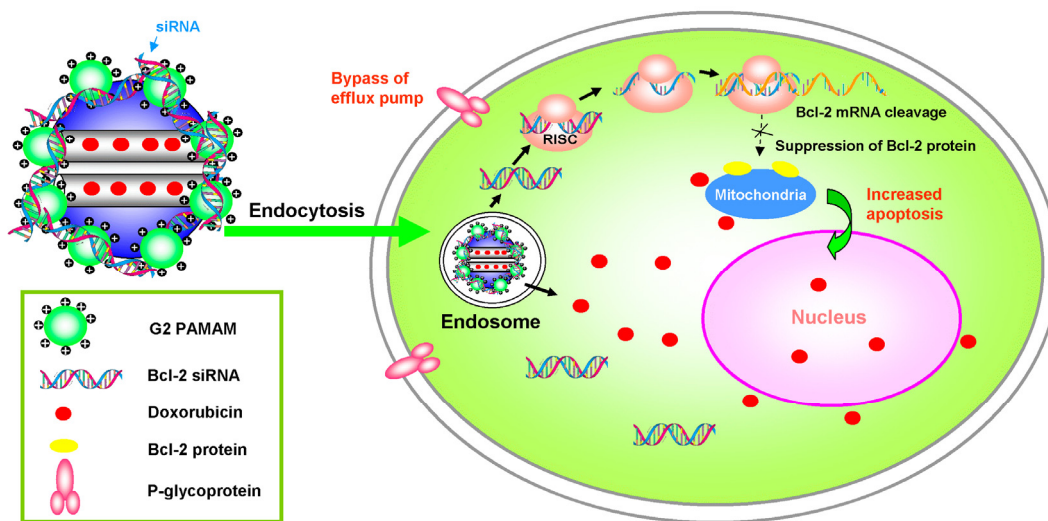
Figure 5.1. Schematic diagram of a codelivery system based on MSNs to deliver Dox and Bcl-2-targeted siRNA simultaneously to A2780/AD human ovarian cancer cells for enhanced chemotherapy efficacy.

5.2. Results and Discussion

The Dox-loaded and G2 PAMAM-modified MSNs (MSN-Dox-G2) were prepared using the same procedure as described in Chapter IV. As mentioned previously, it was found that the fluorescence of Dox was completely quenched after encapsulated into the MSNs. The same phenomenon was observed when Dox was encapsulated in liposomes and micelles, which was attributed to a self-quenching effect of Dox.(*3, 20, 21*) This feature is extremely useful as it enables us to use fluorescence to directly monitor the Dox release from the MSN both outside and inside cells. We evaluated the release of Dox from MSN-Dox-G2 in PBS buffer at room temperature and found that only ~2.6% Dox was released up to 24 h. However, upon internalized into the cells, almost 100% of Dox can be released and the detailed releasing mechanism study was reported in Chapter IV.

It is widely accepted that the main prerequisite for delivery of siRNA into cytoplasm where it can guide sequence specific mRNA degradation is their packaging into nanometer sized complexes by their delivery vehicle, which is the Dox-loaded and G2 PAMAM-modified MSNs in our case. The complex formation is driven mainly by electrostatic interaction between negatively charged siRNA and positively charged dendrimers on the MSNs. Such binding led to the formation of positively charged complexes that can be retarded in gel electrophoresis when compared with free siRNA which can not. Therefore the sufficient amount of MSN-Dox-G2 needed for the complex formation can be determined from an agarose gel electrophoresis experiment. As shown in Figure 5.2, when the N/P (nitrogen/phosphate) ratio, which refers to the ratio of the positively charged primary amine groups of the G2 dendrimer on the MSNs to negatively charged phosphate groups from siRNAs, was around 1, the siRNA was completely retained in the sample wells with no electrophoretic shift corresponding to free siRNA was observed. This indicated that all siRNAs formed stable complex with MSN-Dox-G2 at N/P=1. The morphology of MSN-Dox-G2 complex with siRNA was further visualized by TEM, showing that a ~20-nm thick layer of siRNAs were formed surrounding the surface of MSN-Dox-G2 (Figure 5.3b).

To investigate the cellular internalization and the intracellular release of Dox and siRNA, MSN-Dox-G2 was complexed with siGLO green siRNA transfection indicator (FAM-labeled) and then added to A2780/AD human ovarian cancer cells and incubated for 6 h at 37 °C. The cells were then washed with PBS buffer and then fresh medium was added for fluorescence imaging. Red and green fluorescence imaging was performed to image the released Dox and siRNAs respectively. Since the fluorescence of Dox
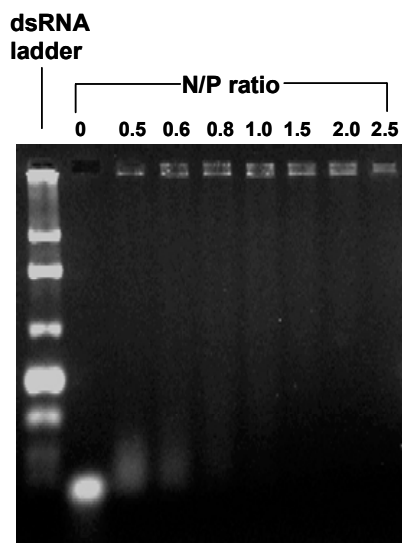
Figure 5.2. Electrophoretic mobility of siRNA complex with MSN-Dox-G2 at different N/P ratio.
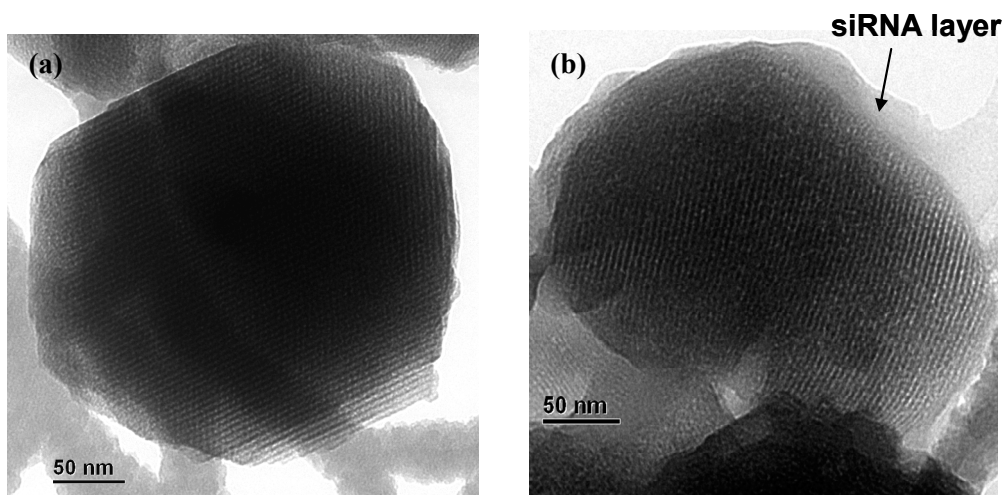
Figure 5.3. TEM image of (a). MSN-Dox-G2 nanoparticle; (b). MSN-Dox-G2 complex with siRNA. Bar indicates 50 nm.

encapsulated inside the MSN pores was completely quenched, the presence of red fluorescence is a hallmark of the Dox released from the MSN pores. As shown in Figure

5.4c, the cells showed strong red fluorescence both in perinuclear regions of cytoplasm and in nucleus, indicating efficient release of Dox after being delivered inside the cells.
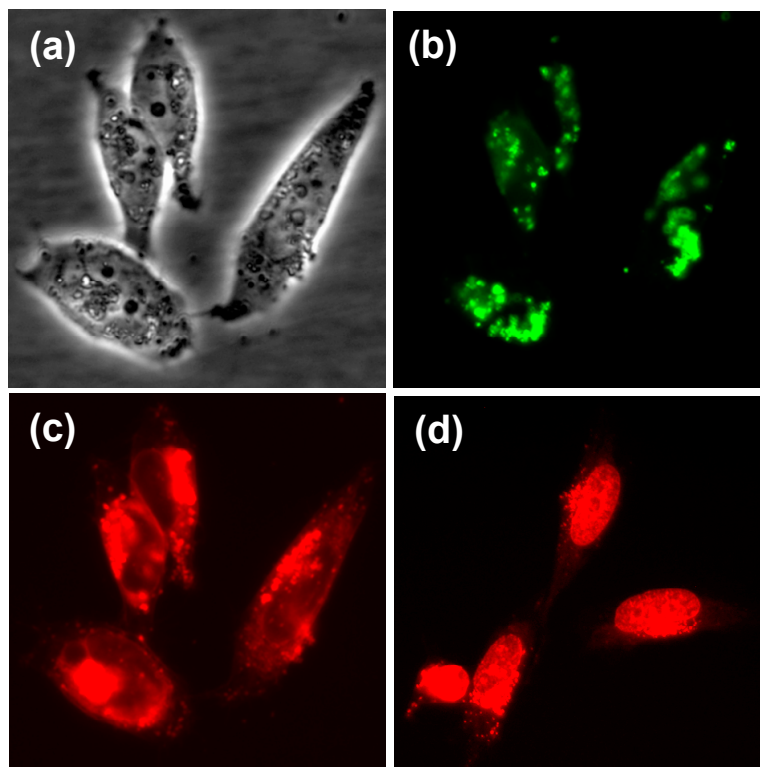
Figure 5.4. Fluorescence microscopy images of A2780/AD human ovarian cancer cells (a) light image. (b) green fluorescence. (c) red fluorescence, after incubated with MSN-Dox-G2 complex with siGLO green siRNA transfection indicator (FAM-labeled) for 6 h at 37 °C or (d) red fluorescence image after incubation with free Dox for 5 h at 37 °C. The red fluorescence indicated the released Dox from MSN pores.

Strong green fluorescence was also shown in similar perinuclear regions of cytoplasm indicating efficient co-delivery of siRNA into cytoplasm. However, no significant green fluorescence signals were detected in nucleus, suggesting the absence of siRNAs inside nucleus. The absence of siRNAs in nucleus is an advantage for RNA interference as

RNAi occurs in cytoplasm and delivery of siRNA into nucleus may lower the siRNA activity.(*22*) Furthermore, for the case of Dox, it was noted that the red fluorescence in perinuclear regions was much stronger than that in nucleus, which was in contrast with that observed when incubating cells with free Dox, where Dox was primarily localized in nucleus as shown in Figure 5.4d, similar as previously reports.(*20, 23*) These observations are important for several reasons. First, the different distribution of Dox in the cells from the free Dox suggested the MSN delivery system was stable in the presence of cells and serum-containing cell medium, achieving minimal premature release of Dox, as the rapid release of Dox in the extracellular environment and subsequent release of Dox outside the cell would be expected to result in an image similar to that observed for free Dox. In addition, the primary localization of both Dox and siRNA in perinuclear regions of cytoplasm with very weak signals in the regions close to cell membrane suggested our delivery system likely internalized through endocytosis and could bypass the efflux pump resistance as reported for several other delivery systems.(*1, 24-26*) This is because P-glycoprotein (Pgp) and multidrug resistance-associated protein (MRP), which are the two main ATP binding transporter proteins responsible to reduce cellular drug accumulation, are mainly located in the plasma membrane. These proteins recognize and efflux drugs out of the cell only when the drug is internalized by passive diffusion, present in or close to the plasma membrane, and not when the drug is delivered directly into perinuclear region of cells, through endocytosis.[1, 2, 24, 27-29]

We next studied the ability of the MSN-Dox-G2/siRNA complexes to silence the targeted mRNA expression with quantitative reverse transcriptase-polymerase chain

reaction (RT-PCR). The Bcl-2-targeted siRNA was used for this study. Gene expression was calculated as the ratio of mean band density of analyzed RT-PCR product to that of the internal standard (β_2-m) and then the ratio of each sample was normalized to that of sample without treatment. As shown in Figure 5.5, after the cells incubated with MSN-Dox-G2/siRNA complexes at 37 °C for 24 h, the Bcl-2 mRNA level was effectively suppressed to ~20%, while cells incubated with MSN-Dox-G2 without Bcl-2 siRNA showed similar Bcl-2 mRNA level as the control cells without treatment. This data indicated that our codelivery system can not only efficiently deliver the siRNA simultaneously with Dox into cytoplasm, thus-delivered siRNA can also be efficiently released and effectively silence the targeted mRNAs.

To further examine whether the efficient knockdown of Bcl-2 mRNA can effectively translate into a synergistic effect to increase the chemotherapy efficacy of Dox, the cellular cytotoxicity of free Dox and MSN-Dox-G2 with or without Bcl-2 siRNA was assessed by MTT (3-(4,5-dimethylthiazol-2-yl)-2,5-diphenyltetrazolium bromide) assay. The A2780/AD cells in the cell growth medium were separately incubated in 96-well plates with different concentrations of free Dox, MSN-Dox-G2, and MSN-Dox-G2/Bcl-2 siRNA, respectively, for 24 h at 37 °C. Based on these measurements, the IC_{50} dose (the dose that kills 50% of cells) of free Dox was determined to be 2.25 μM and that of MSN-Dox-G2 was determined to be 1.07 μM (Figure 5.6). The MSN-Dox-G2 showed significantly higher cytotoxicity than the free Dox. This increased cytotoxicity was not due to MSN-G2 as the MSN-G2 alone showed minimal toxicity at the concentration used (Figure 5.7). Combined with the fluorescence microscopy data, the higher cytotoxicity of MSN-Dox-G2 than free Dox can be explained by the possible higher accumulation of
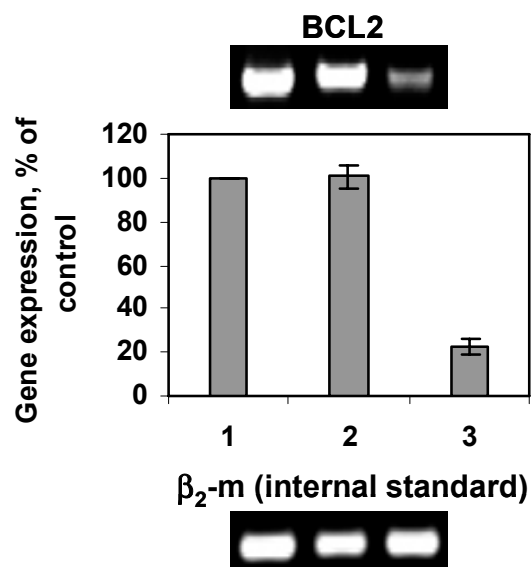
Figure 5.5. Effect of MSN-Dox-G2 complex with siRNA on the silencing of Bcl-2 mRNA in A2780/AD human ovarian cancer cells. (1). No treatment. (2). MSN-Dox-G2. (3). MSN-Dox-G2 with Bcl-2 siRNA. Gene expression was calculated as a ratio of band intensity of Bcl-2 gene to that of internal standard, β_2-m and then the ratio of each sample was normalized to that of sample without treatment.

Dox inside the cell by bypassing the pump resistance.(*1, 24, 28*) Moreover, one can speculate that the Dox encapsulated inside the MSN pores can be protected from the drug degradation by intracellular enzymes and environment during delivery and therefore preserves its anticancer activity.(*30*) While one important mechanism of action of Dox involves DNA intercalation,(*31*) other mechanisms have also been proposed, including the inhibition of mitochondrial function.(*32*) Therefore, last but not least, the coexistence of Dox both in the nucleus and cytoplasm of cells may exert synergistic cytotoxicity effects to the cells, thus contributing to the higher toxicity of Dox by this delivery system. More detailed investigation is underway in order to further explore the mechanism of cell

uptake and intracellular trafficking, and cytotoxic mechanism of Dox delivered by this system.

The major goal of this present investigation is to confirm whether the simultaneous delivery of Bcl-2 siRNA and Dox can enhance the cytotoxicity of Dox and thus its chemotherapy efficacy. As shown in Figure 5.6, indeed the MSN-Dox-G2/Bcl-2 siRNA complex significantly enhanced the cytotoxicity of Dox by decreasing the IC_{50}
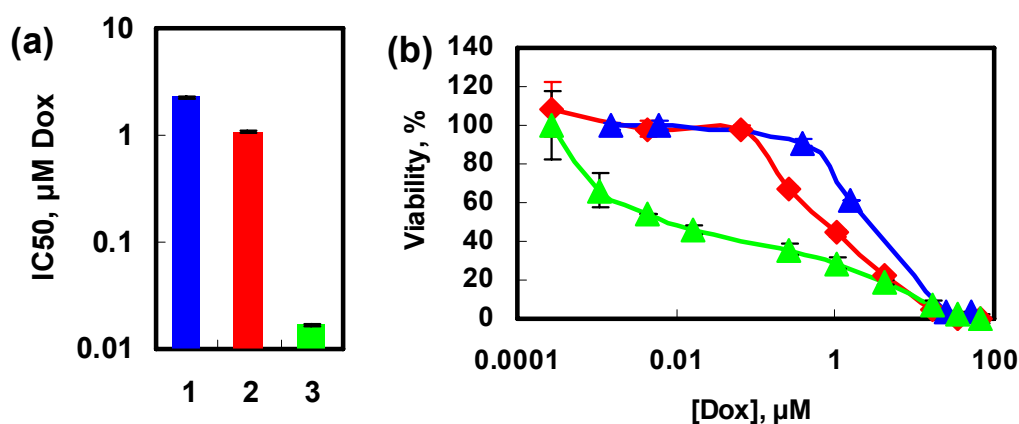
Figure 5.6. Viability of A2780/AD human ovarian cancer cells incubated for 24 h with the indicated formulations. (a). Cytotoxicity of formulations that contain Dox; (b). Actual dose-response curves of formulations that contain Dox. 1. Free Dox; 2. MSN-Dox-G2; 3. MSN-Dox-G2 and Bcl-2 siRNA.

64-fold to 0.017 µM from 1.07 µM for MSN- Dox-G2 alone. This represents a ~132-fold increase of cytotoxicity of Dox when compared to free Dox. This data confirmed that by codelivering Dox and Bcl-2 siRNA using MSNs, the cytotoxicity of Dox can be significantly enhanced by efficiently knocking down the Bcl-2 mRNA and possibly bypassing the efflux pump resistance due to the different cell uptake pathway than free Dox.
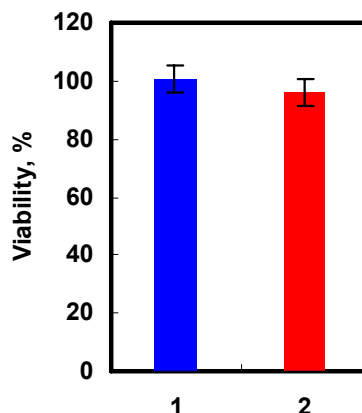
Figure 5.7. Viability of A2780/AD cells after incubated for 24 h at 37 °C with (1). Bcl-2 siRNA, at a concentration of 0.0078 μM. (2). MSN-G2 nanoparticles, at a concentration of 0.0011 mg/ml. 0.0011 mg/ml MSN-G2 corresponds to the concentration of MSN-G2 in IC50 dose of MSN-Dox-G2 (that kills 50% of the cells). 0.078 μM of Bcl-2 siRNA corresponds to the concentration of siRNA used to complex with IC_{50} dose of MSN-Dox-G2.

To further confirm that the enhanced cytotoxicity was indeed due to increased apoptosis not due to necrosis,(*33*) the cell apoptosis was analyzed based on the detection of single- and double-stranded DNA breaks (nicks) by an in situ cell death detection kit using terminal deoxynucleotidyl transferase mediated dUTP-fluorescein nick end labeling (TUNEL) method.(*34*) Briefly, after incubation with MSN-Dox-G2/Bcl-2 siRNA for 24 h, the cells were fixed, permeabilized and incubated with the TUNEL reaction mixture. The label incorporated at the damaged sites of the DNA was visualized by a fluorescence microscope. As shown in Figure 5.8, control cells without treatment showed almost no green fluorescence, indicating the absence of apoptosis. The cells incubated with MSN-Dox-G2 (0.13 μM Dox) showed some weak fluorescence, indicating the activity of

apoptosis in some cells. In contrast, when incubated with MSN-Dox-G2 of the same concentration with an addition of only 0.95 nM of Bcl-2 siRNA, very strong fluorescence were shown in almost every cells, indicating significantly enhanced apoptosis.

| Control | MSN-Dox-G2 | MSN-Dox-G2 with Bcl-2 siRNA |
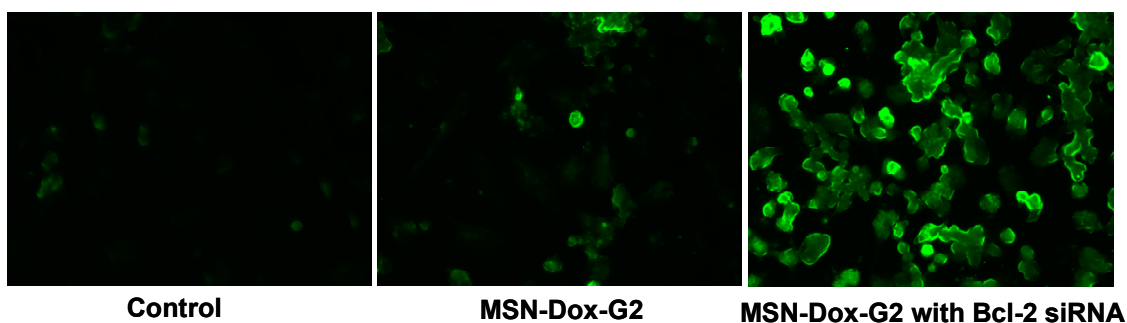
Figure 5.8. Typical fluorescence microscope images of TUNEL-labeled A2780/AD human ovarian cancer cells. Cells were incubated without treatment (control), with MSN-Dox-G2 and with MSN-Dox-G2 and Bcl-2 siRNA respectively for 24 h.

5.3. Conclusions

In summary, we have reported the first effort of utilizing MSNs as a codelivery system to simultaneously deliver Dox and Bcl-2-targeted siRNA into A2780/AD human ovarian cancer cells for enhanced chemotherapy efficacy. Our results showed that by delivering Dox and Bcl-2 siRNA simultaneously into cancer cells, the Bcl-2 siRNA can effectively silence the Bcl-2 mRNA and significantly suppress the non-pump resistance and substantially enhance the anticancer action of Dox. Our data also suggested that the Dox delivered by MSNs has minimal premature release in the extracellular environment, which can greatly eliminate side effects of Dox. Furthermore, the Dox was primarily localized in the perinuclear region after internalization, possibly bypassing the efflux pump resistance and further enhancing the cytotoxicity. This delivery system may be more appealing when it is conjugated with tumor cell targeting moieties and coupled with

in vivo pharmacological advantages of long-circulating nanometer sized MSN complex, such as selective tumor accumulation, stable drug retention, by the enhanced permeation and retention effect and tumor cell targeting effect.

5.4. Experimental Section

5.4.1. Materials

G2 amine-terminated PAMAM dendrimer, doxorubicin hydrochloride and other chemicals used in this study were purchased from Sigma Aldrich (Milwaukee, WI), and used without further purification. siRNA that are sequence specific for human Bcl-2 mRNA was custom synthesized by Ambion (Austin, TX). The sequence of the siRNA used as follows: sense strand, 5'-GUGAAGUCAACAUGCCUGC-dTdT-3'; antisense strand, 5'-GCAGGCAUGUUGACUUCAC-dTdT-3'.

5.4.2. Preparation of MSN-Dox-G2

Same procedure as that described in Chapter IV was used.

5.4.3. Determination of G2 PAMAM Dendrimer Concentration in the MSN-Dox-G2 Nanoparticles

To determine the G2 PAMAM dendrimer concentration in the MSN-Dox-G2 nanoparticles, an improved 2, 4, 6-Trinitrobenzenesulfonic acid (TNBS) method was used. Briefly, 3.0 µl of aqueous TNBS solution (0.0288 M) was added to 150.0 µl of sodium tetraborate buffer (0.042 M) containing different amount of samples. Thus-

obtained solution was shaken in a shaking block for 2 h and then 120 µl of the resultant solution was transferred to a quartz cuvette for UV-Vis analysis. The absorbance at 420 nm from a series of G2 PAMAM solution of known concentration was used to plot the calibration curve and to determine the amine concentration in the MSN-Dox-G2 stock solution.

5.4.4. Dynamic Light Scattering, UV-Vis Absorbance, Transmission Electron Microscopy (TEM)

Same procedures as those described in Chapter IV were used.

5.4.5. Cell Lines

The human multidrug resistant ovarian carcinoma A2780/AD cell line was obtained from Dr. T. C. Hamilton (Fox Chase Cancer Center). Cells were cultured in RPMI 1640 medium (Sigma, St. Louis, MO) supplemented with 10% fetal bovine serum (Fisher Chemicals, Fairlawn, NJ). Cells were grown at 37 °C in a humidified atmosphere of 5% CO_2 (v/v) in air. All experiments were performed on cells in the exponential growth phase.

5.4.6. Cytotoxicity

The cellular cytotoxicity of formulations was assessed using a modified MTT (3-(4,5-dimethylthiazol-2-yl)-2,5-diphenyltetrazolium bromide) assay. Cells were seeded into 96-well microtiter plates at the density of 10,000 cells per well. After incubation for 24 h, medium were aspirated and various concentrations of drugs (free Dox, MSN-Dox-G2 and

MSN-Dox-G2 complex with Bcl-2 siRNA) in fresh cell growth medium (200 µl/well) were added. Control cells were added with equivalent volume of fresh media. Cells were cultured for 24 h before the cell viability assay was performed. The old medium was removed and 100 µl of fresh medium and 25 µl of a 5 mg/ml MTT (Fluka) solution in Dulbecco's phosphate buffered saline (DPBS) was added to each well. Plates were then incubated under cell culture conditions for 3 h. Every well was then added with 100 µl of 50% (v/v) dimethylformamide in water containing 20% (w/v) sodium doecyl sulfate (with pH adjusted to 4.7 by acetic acid) and incubated overnight to dissolve the formazan crystals. The absorbance of each sample was measured at 570 nm with a background correction at 630 nm. Based on these measurements, IC_{50} doses of Dox in free and MSN formulations of Dox delivery systems (the concentrations of Dox necessary to inhibit the cell growth by 50%) were calculated.

5.4.7. Cellular Internalization

Cellular internalization of Dox and siRNA was studied by fluorescence microscope (Olympus America Inc., Melville, NY). A2780/AD cells were plated (20, 000 cells/well) in 6-well tissue culture plate and cultured for 24 h. The old medium was then removed and treated with MSN-Dox-G2 complex with siGLO green siRNA transfection indicator (Thermo Fisher Scientific, Lafayette, CO) in 1.5 ml cell growth medium. The cells were cultured for 6 h at 37 °C and then the old medium removed. The cells were washed with DPBS three times and then added with 1.5 ml fresh medium for fluorescenc imaging. An N/P ratio of 1 was used in the complexation and the final concentration of siGLO green transfection indicator was 0.20 µM. In the case of cellular internalization of free Dox,

similar procedure was applied and the final concentration of free Dox is 1.51 μM and the incubation time was 5 h.

5.4.8. Gene Knockdown

The ability of the MSN-Dox-G2 complex with Bcl-2 siRNAs to knock down the target mRNA expression were studied with quantitative reverse transcriptase-polymerase chain reaction (RT-PCR). A2780/AD cells were incubated without treatment, with MSN-Dox-G2 or MSN-Dox-G2/siRNA complex respectively for 24 h at 37 °C. Then RNA was isolated using an RNeasy kit (Qiagen, Valencia, CA). First strand cDNA was synthesized by Ready-To-GO You-Prime First-Strand Beads (Amersham Biosciences, Piscataway, NJ) with 4mg of total cellular RNA and 100 ng of random hexadeoxynucleotide primer (Amersham Bioscience). After synthesis, the reaction mixture was immediately subjected to polymerase chain reaction, which was carried out using GenAmp PCR System 2400. The following pairs of Bcl-2 and β_2-m primers were used to amplify each type of cDNA: *BCL2*—GGA TTG TGG CCT TCT TTG AG (sense), CCA AAC TGA GCA GAG TCT TC (antisense); *β_2-microglobulin* (*β_2-m*, internal standard)—ACC CCC ACT GAA AAA GAT GA (sense), ATC TTC AAA CCT CCA TGA TG (antisense). PCR products were seperated in 4% NuSieve 3:1 Reliant agarose gels in **1**×TBE buffer (0.089 M Tris/Borate, 0.002 M EDTA, pH 8.3; Research Organic Inc., Cleveland OH) by submarine electrophoresis. The gels were stained with ethidium bromide, digitally photographed and scanned using Gel Documentation System 920 (NucleoTech, San Mateo, CA). Gene expression was calculated as the ratio of mean band density of analyzed RT-PCR product to that of the internal standard (β2-m) and then the ratio of each sample was normalized

to that of sample without treatment. An N/P ratio of 1 was used in the complexation of MSN-Dox-G2 with siRNA and the final concentration of siRNA and Dox in the cell growth medium was 0.0625 µM and 6.23 µM respectively. For treatment with MSN-Dox-G2, the final concentration of Dox in cell growth medium was 6.23 µM.

5.4.9. Apoptosis by TUNEL method

The analysis of apoptosis was based on the detection of single- and double-stranded DNA breaks (nicks) by an *in situ* cell death detection kit (Roche, Nutley, NJ) using terminal deoxynucleotidyl transferase mediated dUTP-fluorescein nick end labeling (TUNEL) method. Cells were seeded into 4-well glass slides (Lab-Tek™ II chamber slide system, Nalge Nunc International Corp.) at a density of 200,000 cells/well. The cells were cultured for 24 h and then the old medium aspirated. MSN-Dox-G2 and MSN-Dox-G2 with Bcl-2 siRNA in 1.0 ml of fresh medium were added to two wells respectively. Control cells were added with equivalent volume of fresh medium. Cells were cultured for 24 h and then old medium was removed. Each well was added with 200 µl of acetone precooled at -20 °C and then incubated at -20 °C for 10 minutes for cell fixation and permeabilization. Acetone was removed and the cells were washed with Dulbecco's phosphate buffered saline (DPBS) twice. Then each well was added with 120 µl of TUNEL reaction mixture (50 µl of enzyme solution mixed with 450 µl of label solution) and incubated under cell culture conditions for 1 h. The well was then washed with DPBS three times and imaged under fluorescence microscope. The label incorporated at the damaged sites of the DNA was visualized by a fluorescence microscope.

5.5. References

1. Dubikovskaya, E. A., Thorne, S. H., Pillow, T. H., Contag, C. H., and Wender, P. A. (2008) Overcoming Multidrug Resistance of Small-Molecule Therapeutics through Conjugation with Releasble Octaarginine Transporters, *Proc. Natl. Acad. Sci, USA 105*, 12128-12133.

2. Gottesman, M. M., Fojo, T., and Bates, S. E. (2002) Multidrug Resistance in Cancer: Role of ATP-Dependent Transporters, *Nature Rev. Cancer 2*, 48-58.

3. Pakunlu, R. I., Wang, Y., Tsao, W., Pozharov, V., Cook, T. J., and Minko, T. (2004) Enhancement of the Efficacy of Chemotherapy for Lung Cancer by Simultaneous Suppression of Multidrug Resistance and Antiapoptotic Celluar Defences: Novel Multicomponent Delivery System, *Cancer Res. 64*, 6214-6224.

4. Pakunlu, R. I., Cook, T. J., and Minko, T. (2003) Simultaneous Modulation of Multidrug Resistance and Antiapoptotic Cellular Defense by MDR1 and BCL-2 Targeted Antisense Oligonucleotides Enhances the Anticancer Efficacy of Doxorubicin, *Pharm. Res. 20*, 351-359.

5. Menendez, J. A., Vellon, L., Colomer, R., and Lupu, R. (2005) Pharmacological and small interference RNA-mediated inhibition of breast cancer-associated fatty acid synthase (oncogenic antigen-519) synergistically enhances Taxol (paclitaxel)-induced cytotoxicity, *Int. J. Cancer. 115*, 19-35.

6. Hannon, G. J., and Rossi, J. J. (2004) Unlocking the potential of the human genome with RNA interference, *Nature 431*, 371-378.

7. Menendez, J. A., Vellon, L., Colomer, R., and Lupu, R. (2005) Pharmacological and Small Interference RNA-mediated Inhibition of Breast Cancer Associated

Fatty Acid Synthase (Ongogenic Antigen-519) Synergistically Enhances Taxol (Paclitaxel)-Induced Cytotoxicity, *Int. J. Cancer 115*, 19-35.

8.   Wang, Y., Gao, S., Ye, W. H., Yoon, H. S., and Yang, Y. Y. (2006) Co-delivery of Drugs and DNA from Cationic Core-Shell Nanoparticles Self-Assembled from a Biodegradable Copolymer, *Nat. Mater. 5*, 791-796.

9.   Yano, J., Hirabayashi, K., Nakagawa, S.-I., Yamaguchi, T., Naito, H., Kitagawa, H., Ishiyama, K., Ohgi, T., and Irimura, T. (2004) Antitumor Activity of Small Interfering RNA/Cationic Liposome Complex in Mouse Models of Cancer, *Clin. Cancer Res. 10*, 7721-7726.

10.   Yano, J., Hirabayashi, K., Nakagawa, S.-i., Yamaguchi, T., Nogawa, M., Kashimori, I., Naito, H., Kitagawa, H., Ishiyama, K., Ohgi, T., and Irimura, T. (2004) Antitumor Activity of Small Interfering RNA/Cationic Liposome Complex in Mouse Models of Cancer, *Cancer Research 10*, 7721-7726.

11.   Wang, Y., Gao, S., Ye, W.-H., Yoon, H. S., and Yang, Y.-Y. (2006) Co-delivery of drugs and DNA from cationic core-shell nanoparticles self-assembeled from a biodegradable copolymer, *Nature Materials 5*, 791-796.

12.   Slowing, I., Trewyn, B. G., and Lin, C. S.-Y. (2006) Effect of Surface Functionalization of MCM-41 Type Mesoporous Silica Nanoparticles on the Endocytosis by Human Cancer Cells, *J. Am. Chem. Soc. 128*, 14792-14793.

13.   Slowing, I., Vivero-Escoto, J. L., Wu, C.-W., and Lin, V. S.-Y. (2008) Mesoporous Silica Nanoparparticles as Controlled Release Drug Delivery and Gene Transfection Carriers, *Adv. Drug Deliv. Rev. 60*, 1278-1288.

14. Vallet-Regi, M., Balas, F., and Aros, D. (2007) Mesoporous Materials for Drug Delivery, *Angew. Chem. Int. Ed. 46*, 7548-7558.

15. Lu, J., Liong, M., Zink, J. I., and Tamanoi, F. (2007) Mesoporous Silica Nanoparticles as a Delivery System for Hydrophobic Anticancer Drugs, *Small 3*, 1341-1346.

16. Radu, D. R., Lai, C.-Y., Jeftinija, K., Rowe, E. W., Jeftinija, S., and Lin, C. S.-Y. (2004) A Polyamidoamine Dendrimer-Capped Mesoporous Silica Nanosphere-Based Gene Transfection Reagent, *J. Am. Chem. Soc. 126*, 13216-13217.

17. Radu, D. R., Lai, C.-Y., Jeftinija, K., Rowe, E. W., Jeftinija, S., and Lin, V. S.-Y. (2004) A polyamidoamine dendrimer-capped mesoporous silica nanosphere-based gene transfection reagent, *J. Am. Chem. Soc. 126*, 13216-13217.

18. Torney, F., Trewyn, B. G., Lin, V. S. Y., and Wang, K. (2007) Mesoporous Silica Nanoparticles Deliver DNA and Chemicals into Plants, *Nature Nanotech. 2*, 295-300.

19. Torney, F., Trewyn, B. G., Lin, V. S.-Y., and Wang, K. (2007) Mesoporous silica nanoparticles deliver DNA and chemicals into plants, *Nature Nanotechnology 2*, 295-300.

20. Gillies, E. R., and Frechet, M. J. (2005) pH-Responsive Copolymer Assemblies for Controlled Release of Doxorubicin, *Bioconjugate Chem. 16*, 361-368.

21. Pakunlu, R. I., Wang, Y., Tsao, W., Pozharov, V., Cook, T. J., and Minko, T. (2004) Enhancement of the efficacy of chemotherapy for lung cancer by simultaneous suppression of multidrug resistance and antiapoptotic cellular defense: novel multicomponent delivery system, *Cancer Research 64*, 6214-6224.

22. Chiu, Y.-L., Ali, A., Chu, C. Y., Cao, H., and Rana, T. M. (2004) Visualizing a Correction between siRNA Localization, Cellular Uptake, and RNAi in Living Cells, *Chem. & Biol. 11*, 1165-1175.

23. Coley, H. M., Amoa, W. B., Twentyman, P. R., and Workman, P. (1993) Examination by Laser Scanning Confocal Fluorescence Imaging Microscopy of the Subcellular Localization of ANthracyclines in Parent and Multidrug Resistant Cells Lines, *Br. J. Cancer 67*, 1316-1323.

24. Wong, H. L., Bendayan, R., Rauth, A. M., Xue, H. Y., Babakhanian, K., and Wu, X. Y. (2006) A Mechanistic Study of Enhanced Doxotubicin Uptake and Pretention in Multidrug Resistant Breast Cancer Cells Using a Polymer-Lipid Hybrid Nanoparticle System, *J. Pharm. Exper. Ther. 317*, 1372-1381.

25. Goren, D., Horowitz, A. T., Tzemach, D., Tarshish, M., Zalipsky, S., and Gabizon, A. (2000) Nuclear delivery of doxorubicin via folate-targeted liposomes with bypass of multidrug-resistance efflux pump, *Clinical Cancer Research 6*, 1949-1957.

26. Wong, H. L., Bendayan, R., Rauth, A. M., Xue, H. Y., Babakhanian, K., and Wu, X. Y. (2006) A mechanistic study of enhanced doxorubicin uptake and retention in multidrug resistant breast cancer cells using a polymer-lipid hybrid nanoparticle system, *J. Pharm. Exper. Ther. 317*, 1372-1381.

27. Goren, D., Horowitz, A. T., Tzemach, D., Tarshish, M., Zalipsky, S., and A., G. (2000) Nuclear Delivery of Doxorubicin via Folate-targeted Liposomes with Bypass of Multidrug-resistance Efflux Pump, *Clin. Cancer Res. 6*, 1949-1957.

28. Larsen, A. K., Escargueil, A. E., and Skladanowski, A. (2000) Resistance Mechanism Associated with Altered Intracellular Distribution of Anticancer Agents, *Pharmacol. Ther. 88*, 217-229.

29. Bennis, S., Chapey, C., Couvreur, P., and Robert, J. (1994) Enhanced Cytotoxicity of Doxorubicin Encapsulated in Polyhexylcyanoacrylate Nanospheres against Multi-drug Resistant Tumor Cells in Culture, *Eur. J. Cancer A 30*, 89-93.

30. Minko, T., Kopeckova, P., and Kopecek, J. (1999) Comparison of the Anticancer effect of Free and HPMA Copolymer-bound Adriamycin in Human Ovarian Carcinoma Cells, *Pharm. Res. 16*, 986-996.

31. Gabbay, E. J., Grier, D., Fingerie, R. E., Reimer, R., Levy, R., Pearce, S. W., and Wilson, W. D. (1976) Interaction Specificity of the Anthracyclines with DNA, *Biochemistry 15*, 2062-2070.

32. Huigsloot, M., Tijdens, I. B., Mulder, G. J., and van de Water, B. (2002) Differential Regulation of Doxorubicin-induced Mitochondrial Dysfunction and Apopotisis by Bcl-2 in Mammary Adenocarcinoma (MTLn3) Cells, *J. Biol. Chem. 277*, 35869-35879.

33. Hovorka, O., M.St'astny, Etrych, T., Subr, V., Strohalm, J., Ulbrich, K., and Rıhova, B. (2002) Differences in the intracellular fate of free and polymer-bound doxorubicin, *Journal of controlled release 80*, 101-117.

34. Minko, T., Kopeckova, P., and Kopecek, J. (2000) Efficacy of the chemotherapeutic action of HPMA copolymer-bound doxorubicin in a solid tumor model of ovarian carcinoma, *Int. J. Cancer. 86*, 108-117.

Chapter 6

Effects of Different Components of a Mesoporous Silica Nanoparticle-based Codelivery System on Cell Uptake Efficiency of siRNA into A549 Human Lung Cancer Cells

6.1. Introduction

There has been growing interest for developing therapies based on RNA interference (RNAi) with short interference RNAs (siRNAs) (*1-9*) due to its high specificity and potency of gene silencing since its discovery by Fire et al. in 1998 (*10*). Many delivery systems, including liposomes, cationic polymers and nanoparticles, have been widely investigated as delivery systems.(*3-9*) Despite significant advances in recent years, ideal non-toxic delivery systems that are capable of efficiently delivering siRNA into cells and then effectively releasing into cytoplasm for RNAi are still lacking. Mesoporous silica nanoparticles (MSNs), with large pore volume and surface area, recently emerged as a promising delivery system for chemical drugs and plasmid DNA or codelivery of both due to its efficient internalization into mammalian cells with good biocompatibility. (*11-15*) We envisioned that it would also become a promising delivery system for siRNA due to the similar structures of siRNA as the plasmid DNA.

As the first attempt to demonstrate the capability of MSNs in delivering siRNA into cells, we took one step further by encapsulating an anticancer drug, doxorubicin (Dox), into the MSN pores while complexing with BCL-2-targeted siRNA on the surface. Our data showed that the BCL-2-targeted siRNA thus co-delivered with Dox can be efficiently delivered into A2780/AD cancer cells, effectively released into cytoplasm for RNAi and significantly silenced the BCL-2 mRNA. As a result, the antiapoptotic cellular defense of BCL-2 protein was substantially suppressed and the anticancer action of Dox was dramatically enhanced. The design of this delivery system consists of three main components, isocyanate-modified MSNs, Dox and generation 2 polyamidoamine (G2 PAMAM) dendrimer. The intended role of each component is different in this delivery system. Isocyanate groups provide multiple interactions to the anticancer drug, Dox, so a high loading of Dox as well as a nearly zero premature release in H_2O can be achieved. The isocyanate groups on the MSN surface were used to conjugate with G2 PAMAM. The amine-terminated G2 PAMAM is to efficiently complex with siRNA as well as to provide proton sponge effect through its tertiary amines to enable efficient release of the delivery systems from endosome into cytoplasm.

It was previously reported that by incorporating a chemically cleavable disulfide linkage between MSN and G2.5 or G4.5 PAMAM dendrimers, the PAMAM dendrimers can be efficiently released from MSN pores inside cells upon the reduction of disulfide. (*16-20*) In these reports, the cleavage of PAMAM dendrimer is necessary for efficient release of the drugs encapsulated inside pores. This is because the PAMAM dendrimer also serves as caps of the pores to ensure nearly zero premature release of the loaded drugs into H_2O besides its roles of complexing with plasmid DNA and exerting proton

sponge effects. However, the roles of G2 PAMAM dendrimer are different in our delivery system of Dox-loaded isocyanate-modified MSNs modified with G2 PAMAM dendrimer (MSN-Dox-G2). As shown previously, on one hand, G2 PAMAM dendrimer was not able to cap the pores probably due to smaller size of our dendrimer and larger diameter of the pores; on the other hand, it was also not necessary to cap the pores for nearly zero premature release of drugs in H_2O, which was ensured by the hydrophobic surfaces of pores. For these reasons, disulfide groups were not incorporated in our delivery systems in most of our drug release and codelivery studies for its simplicity. Indeed, as demonstrated in our previous results, both Dox and siRNA can be efficiently released into cytoplasm for their respective therapy effects. However, it is still fundamentally interesting to investigate how the incorporation of disulfide might affect the cell uptake and release of our delivery system as one can reason that the incorporation of disulfide group will result in efficient cleavage of G2 PAMAM dendrimer from the MSN surface inside cells, which can ultimately affect the de-complexation of siRNA from G2 PAMAM and its subsequent RNAi.

In the field of drug delivery, including plasmid DNA and siRNA delivery, contradictory or conflicting data were often reported for the same types of delivery systems. These discrepancies were often attributed to different cells under investigation or different techniques being employed. Taking a closer look into these discrepancies, however, one would find that these discrepancies were constantly due to some real difference in the design of the delivery systems rather than the above-mentioned factors. For example, in studying the cell uptake of a drug delivery system, fluorescein isothiocyanate (FITC) with green fluorescence was often conjugated to a delivery system

as imaging moiety to track the internalization and intracellular trafficking of delivery system without appropriately addressing the possible effects of FITC on the delivery. Furthermore, for those delivery systems consisting of several components, the results were constantly interpreted according to the intended roles of each component, without systematically studying the possible non-intended but significant roles of each component in the delivery.

The specific aims of this investigation were (1) to develop a new delivery system of MSN-Dox-AEDP-G2 by incorporating a disulfide linkage between MSN surfaces and G2 PAMAM and to study the cell uptake, intracellular release and localization of the complex of siRNA with the new delivery system (MSN-Dox-AEDP-G2-siRNA) in A549 human lung cancer cells; (2) to assess the effect of disulfide linkage on the intracellular release and localization of siRNA and Dox by comparing confocal fluorescence of cells incubated by MSN-Dox-AEDP-G2-siRNA to that of cells incubated by the complex of siRNA with MSN-Dox-G2 (MSN-Dox-G2-siRNA) ; (3) to understand the role of each component in delivery system of MSN-Dox-G2 on the cell uptake and intracellular distribution of siRNA by systematically studying the effect of each component as its own or in a binary component system (MSN-G2, MSN-Dox) and tertiary component system (MSN-Dox-G2); (4) to investigate the effect of Dox on the gene knockdown efficacy of siRNA by comparing the gene knockdown efficacy of Bcl-2-targeted siRNA delivered by MSN-Dox-G2 to that delivered by MSN-G2.

By confocal fluorescence imaging of live cells, we demonstrated that MSN-Dox-AEDP-G2-siRNA started internalizing into cancer cells after 5 min incubation at 37 °C and efficiently released Dox into the cytoplasm immediately after internalization. Our

data suggested minimal effects of disulfide linkage on the intracellular release and localization of Dox and siRNA, confirming that disulfide linkages are not needed for efficient release in the delivery system of MSN-Dox-G2. Furthermore, we found that while G2 PAMAM is the most critical component in MSN-Dox-G2 delivery system for ensuring efficient cell uptake and effective endosomal release into cytoplasm, the presence of Dox provided additional enhancement on the cell uptake. More importantly, it appeared to be the key element in ensuring homogeneous distribution of siRNA in cytoplasm and subsequently achieving effective silencing of targeted mRNA.

6.2. Results and Discussion

6.2.1. Kinetics of Cell Internalization and Intracellular Release of MSN-Dox-AEDP-G2-siRNA

To understand the kinetics of cell internalization and the intracellular release of Dox and siRNA at 37 °C, MSN-Dox-AEDP-G2 was complexed with a siRNA green transfection indicator and then added to the A549 human lung cancer cells pre-cultured in a single well for 24 h. The imaging was then performed on a single live cell under 37 °C at different time points. The fluorescence of Dox encapsulated inside the MSN pores is completely quenched and therefore the presence of red fluorescence is a hallmark of the Dox released from the MSN pores. Figure 6.1 shows the light, red fluorescent and green fluorescent images taken at 0, 5, 30, 130, 150, 180 and 210 minutes respectively. No substantial red fluorescence was detected at 0 min (before adding drugs) inside and outside cells. However, after 5-min incubation, red fluorescence appeared inside the cells. As incubation time increased up to 130 min, the red fluorescence signals inside the cells

gradually increased, indicating more Dox was gradually delivered and released into the cells. At the same time, it was noted that the red fluorescence remained absent in the cell medium outside the cells during the course of imaging, further confirming our previous
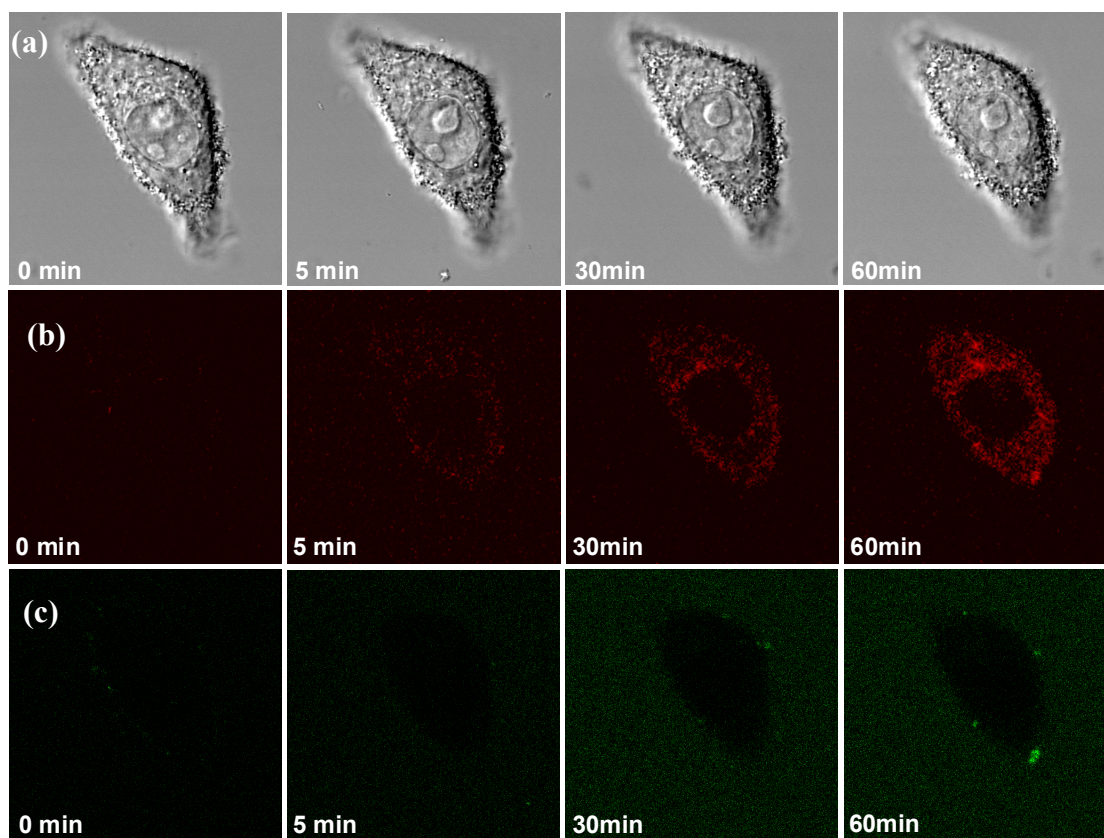
Figure 6.1. Confocal fluorescence microscopy images of A549 human lung cancer cells before (0 min) and after (5-60 min) incubation with MSN-Dox-AEDP-G2-siRNA. (a). Light images. (b). Red fluorescence, indicating released doxorubicin. (c). Green fluorescence, indicating the siRNA green transfection indicator.

finding that fluorescence of Dox inside MSN pores is completely quenched and the release of Dox from MSN pores is minimal in cell medium at 37 °C. This suggested that the Dox inside cells is primarily released from MSN-Dox-AEDP-G2-siRNA after internalization rather than from internalization of free Dox that is released before

internalization. Our finding is different from the delivery and release of Dox from a liposome formulation investigated by Pakunlu et al. (*21*), who showed that in the beginning of incubation, part of liposomes first fused with the plasma membrane and then released Dox from liposome near the membrane as indicated by strong red fluorescence on the cell membrane. From the green fluorescence images taken at the same time points up to 130 min, we found that strong green signals remained present outside the cells during the course of imaging, which was expected as the green fluorescence is not quenched in the cell medium outside the cells. The green fluorescence signals in the cell medium around the single cell also appeared to increase as incubation time increased, likely due to diffusion of more drugs to nearby the single cell under imaging. This was because only slight shaking was applied after addition of drugs into the cell growth media, and it takes time for the drugs to diffuse to the cell medium nearby the cells. It was realized that due to the relatively strong green fluorescence signals in cell medium outside the cells, the green fluorescence signals inside the cells appeared to be very weak during the course of live imaging. To further confirm the cell uptake of siRNA, after the live imaging, the cell mediums were removed and the cells were then washed with DPBS and added with fresh medium for imaging. As shown in Figure 6.2, indeed, after replacing with fresh medium without drugs, significant green fluorescence was observed inside the cells. This data will be discussed later in next section.

6.2.2. Intracellular Release and Localization of Dox and siRNA from MSN-Dox-AEDP-G2-siRNA
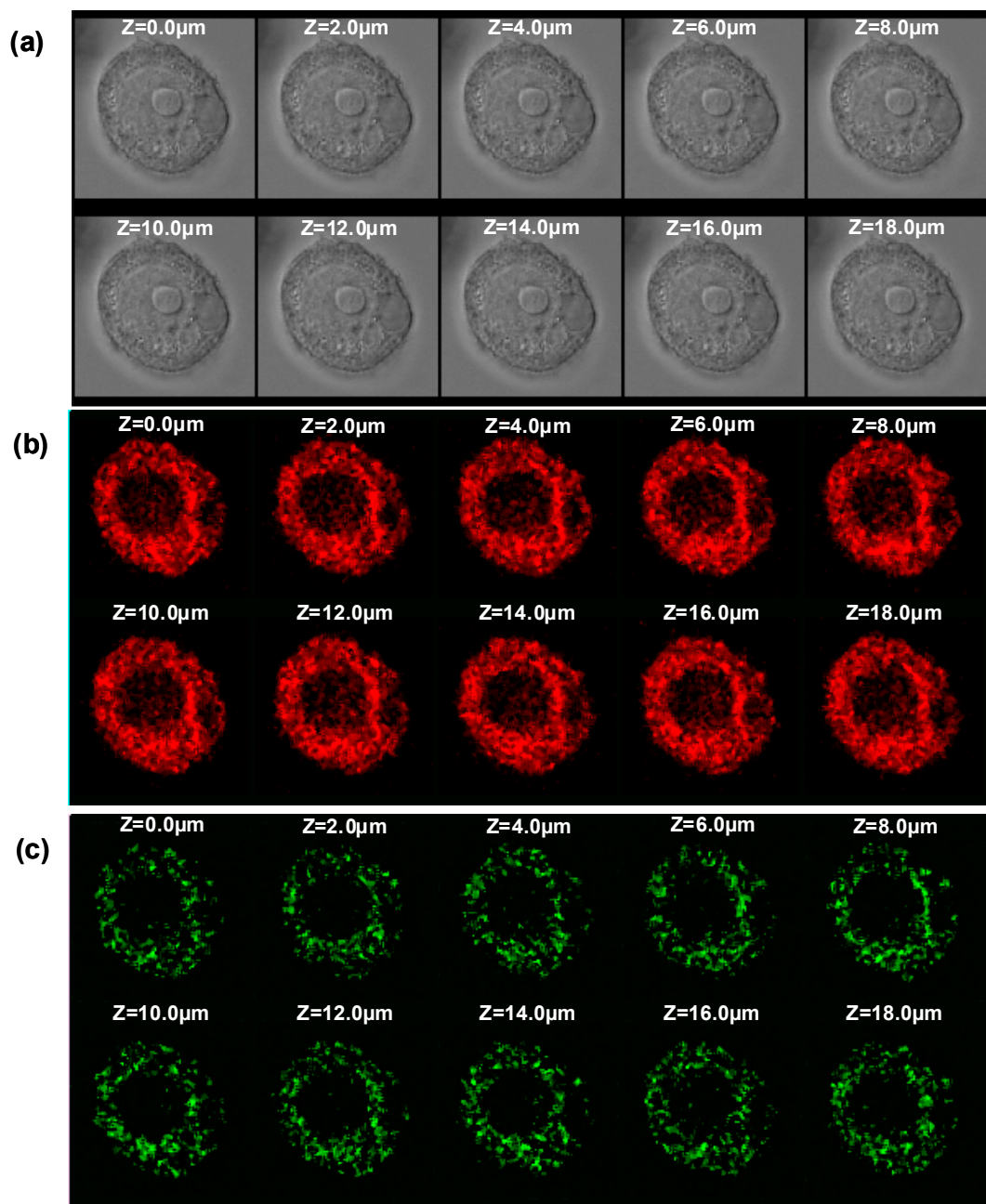
Figure 6.2. Confocal fluorescence microscopy images of A549 human lung cancer cells incubated for 4 h at 37 °C with MSN-Dox-AEDP-G2-siRNA (z-series, from the bottom of the cell to the top). (a). Light images. (b). Red fluorescence images, indicating released doxorubicin. (c). Green fluorescence images, indicating the siRNA green transfection indicator.

After 4-hr live imaging at 37 °C, the old medium was removed and the cells were washed with DPBS buffer and then added with fresh cell medium for imaging. Theoretically, MSN-Dox-AEDP-G2-siRNA could adhere to the surface of cancer cells and erroneously be visualized on microscopic images as internalized within cells. To exclude such type of errors, we analyzed the distribution of Dox and labeled siRNA in different cellular layers from the lower to upper of a single live cell using confocal fluorescent microscopy (z-sections, Figure 6.2).

In contrast to live imaging, significant green fluorescence signals were clearly observed inside the cells, indicating efficient uptake of siRNA into the cells. It showed that the green fluorescence was located in cytoplasm but not in nuclei. Similar to the green fluorescence, red fluorescence is also primarily localized in cytoplasm, with only very weak signals localized in nuclei. Comparing the green fluorescence and red fluorescence data, we found that the green and red fluorescence signal are mainly colocalized except in the nuclei where very weak red fluorescence is observed while no green fluorescence is detected. The co-localization of siRNA and Dox in cytoplasm might be an advantage in that it may enhance their synergistic effects due to the relative similar ratio of two drugs in different part of cells. Furthermore, it showed that the distribution of Dox or siRNA was very similar in different cell layers. It is also worth noting that the distribution of red and green fluorescence appeared to be very homogenous, suggesting the efficient release of Dox and siRNA into cytoplasm, rather than being trapped in endosomes and showing discrete small aggregates as reported in some other delivery systems.

6.2.3. Cell Uptake of MSN-Dox-AEDP-G2-siRNA at 22 °C

Many MSN-based delivery systems were found to internalize into cells through endocytosis, a temperature and energy-dependent process.(*22*) To assess the temperature effect on the cell uptake of our delivery system, A549 lung cancer cells were incubated with the complex of MSN-Dox-AEDP-G2 with labelled siRNA for 2.5 h at 22 °C. The cells were then imaged by confocal fluorescence microscopy. As shown in Figure 6.3, it showed that after 2.5-h incubation at 22 °C, the cell uptake of our delivery system is very efficient as indicated by strong green and red fluorescence inside cells. Furthermore, the distribution of Dox and siRNA were also similar to those incubated at 37 °C. These preliminary data suggested that the cell uptake of our delivery system was not inhibited by lower temperature. More detailed quantitative investigation on the temperature effect on cell uptake and on the internalization mechanism of our delivery system using flow cytometry is underway.

Figure 6.3. Confocal fluorescence microscopy images of A549 human lung cancer cells incubated for 2.5 h at 22 °C with MSN-Dox-AEDP-G2-siRNA (a). Light images. (b). Red fluorescence images, indicating released doxorubicin. (c). Green fluorescence images, indicating the siRNA green transfection indicator.

6.2.4. Cell Uptake of MSN-Dox-AEDP-G2-siRNA vs. MSN-Dox-G2-siRNA

To assess the effect of disulfide linkage on the cell uptake and intracellular release and localization of Dox and siRNA, A549 cells were incubated with complex of MSN-Dox-G2 with siRNA at 37 °C for 24 h and then imaged by confocal fluorescence microscopy. As shown in Figure 6.4, the distribution of Dox and siRNA appeared to be similar as those observed when cells were incubated with complex of MSN-Dox-AEDP-G2 with siRNA at 37 °C for 4 h. It showed that the green fluorescence and red fluorescence are both primarily localized in cytoplasm with some weak red fluorescence also observed in nuclei. Our previous extracellular release study of MSN-Dox-G2 showed that Dox can be sufficiently and completely released in the presence of 4.9 mM glutathione, which is similar to the glutathione concentration in many animal cells. In addition, our previous cell uptake study of MSN-Dox-G2 complex with siRNA by regular fluorescence also showed similar distribution of Dox and siRNA in A2780/AD human ovarian cancer
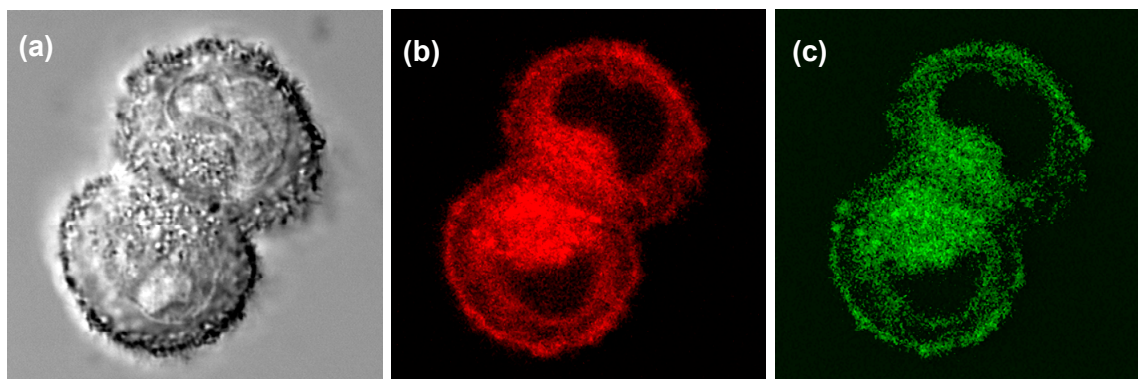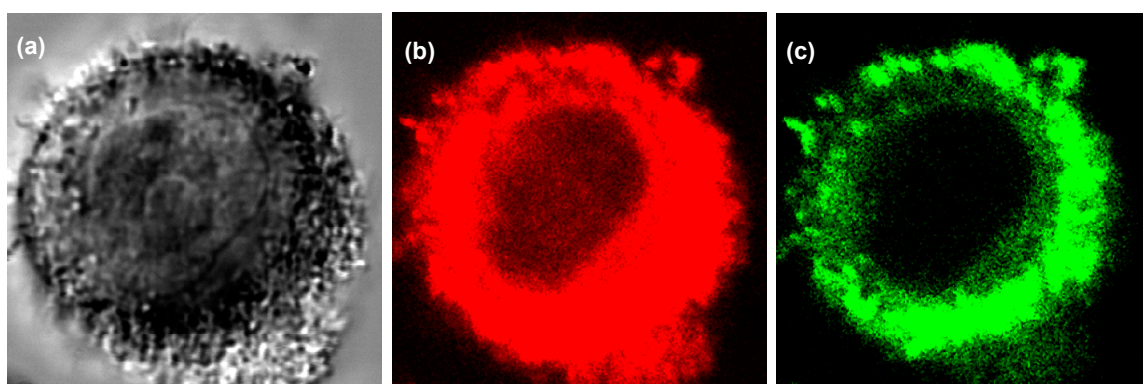

Figure 6.4. Confocal fluorescence microscopy images of A549 human lung cancer cells incubated for 7 h at 37 °C with complex of MSN-Dox-G2 with labelled siRNA (a). Light images. (b). Red fluorescence images, indicating released doxorubicin. (c). Green fluorescence images, indicating the siRNA green transfection indicator. An N/P ratio of 2 was used.

cells. On one hand, this data clearly confirmed that the disulfide linkage is not necessary for efficient release of Dox from the pores as the G2 PAMAM dendrimers do not effectively cap the pores in our delivery system and the presence of disulfide linkage does not appear to affect the Dox and siRNA release and distribution inside the cells; on the other hand, it further confirmed that despite efficient release of Dox from delivery systems (both with disulfide or without disulfide linkage) into cytoplasm, the released Dox appeared to preferentially remain in cytoplasm rather than entering the nuclei, which is the preferred localization region for free Dox. The exact reason for the released Dox to primarily remain in cytoplasm is still unknown although it was previously reported for several other delivery systems, including polymer-based delivery systems.(*23*) We speculate that some physical interaction of released Dox and MSNs, G2 PAMAM, or siRNA may exist after release of Dox from the pores, thus inhibiting the diffusion of Dox into nuclei. Furthermore, it is possible that the presence of MSNs in the cytoplasm may become a physical barrier to partially block the diffusion of Dox into nuclei. More detailed investigation on this phenomenon is still underway. Nevertheless, the Dox remaining in cytoplasm appeared to retain its toxic effects to cancer cells and even be more toxic when compared to free Dox, as we previously found in A2780/AD cells. While one important mechanism of action of Dox involves the DNA intercalation which requires the nuclear delivery of Dox, other mechanisms have also been proposed, including the inhibition of mitochondrial function. This might be involved in our delivery system and explain the effective anticancer toxicity of Dox primarily localized in cytoplasm.

Theoretically, it is possible that the cleavage of G2 PAMAM from MSNs may affect the de-complexion of siRNA as the interaction of free G2 PAMAM with siRNA is much weaker compared to the coherent interaction provided by the multiple PAMAMs on each of the MSNs. The confocal fluorescence data suggested no significant difference in the distribution of siRNAs delivered by MSN-Dox-AEDP-G2 vs. MSN-Dox-G2. Furthermore, as to be demonstrated in our gene knockdown data later, the siRNAs delivered by MSN-Dox-G2 (without disulfide linkage) are very effective in silencing the targeted mRNA.

6.2.5. Cell Uptake of siRNA by G2 PAMAM, MSN, MSN-G2, Dox and MSN-Dox

As demonstrated above and previously, the Dox-loaded MSN-G2 delivery system (MSN-Dox-G2) can be efficiently complexed with siRNA and then delivered into both A549 lung cancer cells and A2780/AD ovarian cancer cells. To gain more insight of this efficient co-delivery system, we set out to investigate the effects of different components in this delivery system on the cell uptake efficiency of siRNA.

G2 PAMAM, MSN, G2 PAMAM -modified MSN (MSN-G2), free Dox, Dox-loaded MSN (MSN-Dox) were respectively complexed with siRNA and then added to A549 cells for incubation at 37 °C for a certain period of time. As shown in Figure 6.5(a-c), G2 PAMAM was not able to deliver siRNA into cancer cells, indicated by the absence of any green fluorescence signals inside the cells. It was further noted that no green fluorescence was detected on the outside of cell membrane either, suggesting that G2 PAMAM was not able to help the adsorption of siRNA onto the cell membrane or the adsorption of siRNA/ complex of G2 PAMAM and siRNA on the cell membrane was

relatively weak so it was completely washed away during PBS buffer wash before imaging. This data was not surprising as low generation PAMAM dendrimer was
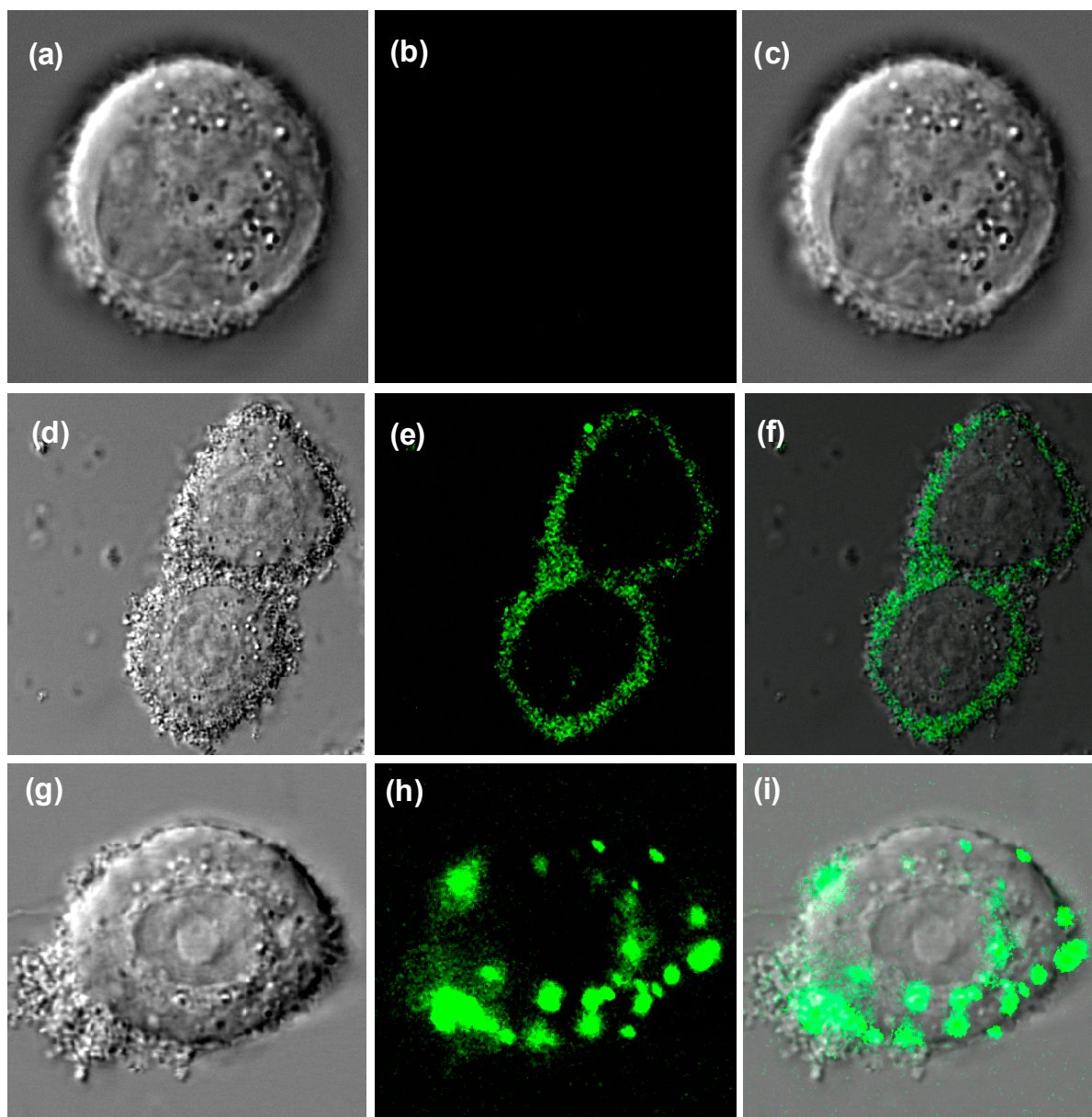
Figure 6.5. Confocal fluorescence microscopy images of A549 human lung cancer cells incubated with (a-c). G2 PAMAM-siRNA for 24 h at 37 °C; (d-f). MSN-siRNA for 24 hr at 37 °C; (g-i). MSN-G2-siRNA for 7 h at 37 °C. (a, d, g) are light images; (b, e, h) are green fluorescence images, indicating the siRNA green transfection indicator; (c, f, i) are superpositions of light and green fluorescence images.

previously reported to be inefficient in forming strong complex with DNA or siRNA to internalize into cells.(*24*) When designing our co-delivery system, this was already in our mind, however, by modifying MSNs with G2 PAMAM, we expected that the MSN-G2 would behave like higher generation dendrimers, becoming efficient in complexing with siRNA and delivering it into cells, while retaining the low toxicity of G2 PAMAM dendrimer as compared to higher generation dendrimers.

In contrast, as shown in Figure 6.5(d-f), after incubated with complex of MSNs and siRNA, although no green fluorescence was observed inside cells, strong green fluorescence signals were shown on the outside of cell membrane, indicating the adsorption of siRNA on the cell membrane. While it was not known based on our data whether the MSNs alone were able to efficiently internalize into cells, the fluorescence data clearly indicated that MSNs helped the adsorption of siRNA onto the cell membrane. One can reason that the isocyanatopropyl-modified MSNs are highly hydrophobic and therefore have strong interaction with hydrophobic surface of cell membrane. After MSNs get adsorbed on the cell membrane, siRNA might get strongly adsorbed on the cell membrane through interaction with MSNs and therefore were not washed away during DPBS buffer wash before imaging. It is also possible that the MSNs interact with siRNAs first and then the complex of MSNs and siRNAs became strongly adsorbed on the cell membrane. Part of the isocyanate groups on the MSN surfaces probably hydrolyze and convert to amine groups, which can then interact with siRNA through electrostatic interaction. Furthermore, due to the small particle size and large surface area of MSNs, strong hydrophobic interactions might also exist between siRNAs and MSNs, while the

hydrophobic interaction is relatively weak between siRNAs and cell membrane, due to the smaller surface area and less flexible surface of cell membrane.

Next, we studied the delivery of siRNA by MSN-G2 and found that the MSN-G2 was able to efficiently deliver siRNA into cells as shown in Figure 6.5(g-h). However, the distribution of siRNA inside cells appeared to be inhomogeneous as indicated by the discrete large aggregates of green fluorescence signals. This, when compared to the complex of PAMAM-G2 and siRNA, indeed confirmed our initial hypothesis that after modification of G2 PAMAM on MSN surfaces, MSN-G2 will behave like higher generation dendrimers and be able to efficiently complex with and deliver siRNA into cells. In comparing with the inefficient delivery of siRNA by MSNs alone, we can therefore conclude that the G2 PAMAM dendrimer on MSN surface are critical for efficient delivery of siRNA into cells in the MSN-G2 delivery system.

After studying the effects of G2 PAMAM, MSN, MSN-G2 on the cell uptake of siRNA, we then evaluated the effect of Dox on the cell uptake of siRNA. First, we studied the effect of free Dox on the cell uptake of siRNA by incubating cells with a mixture of free Dox and siRNA for 2 h at 37 °C. As shown in Figure 6.6(a-d), free Dox can efficiently internalize into cells and are primarily localized in the nuclei, similar to our previous finding on cell uptake of free Dox into A2780/AD cells. This suggested minimal effect of siRNA on the cell uptake and distribution of free Dox. Furthermore, no significant green fluorescence was detected either in nuclei or in cytoplasm, indicating no uptake of siRNA into cells. Similar to the delivery of siRNA by MSNs, however, some green fluorescence signals were observed on the outside of cell membrane, indicating some adsorption of siRNA on the cell membrane. It was further noted that some strong

red fluorescence signals were also observed on the outside of cell membrane. This coexistence of Dox and siRNA on the cell membrane strongly indicated that Dox likely
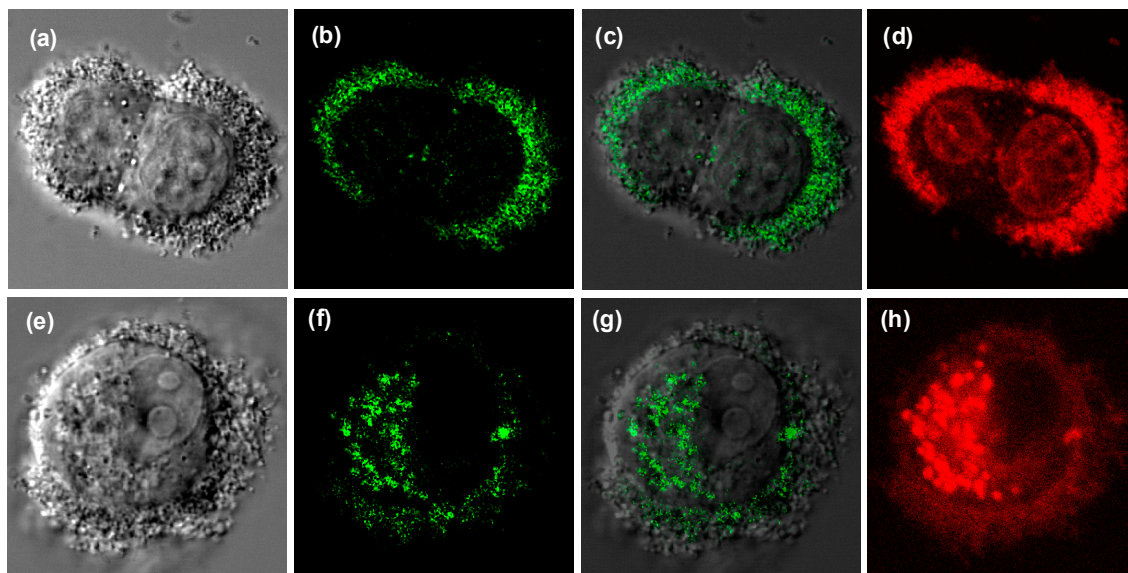
Figure 6.6. Confocal fluorescence microscopy images of A549 human lung cancer cells incubated with (a-d). Dox-siRNA for 2 h at 37 °C; (e-h). MSN-Dox-siRNA for 24 hr at 37 °C. (a, e) are light images; (b, f) are green fluorescence images, corresponding to siRNA green transfection indicator; (c, g) are superpositions of light and green fluorescence images; (d, h) are red fluorescence images, indicating released Dox.

interacts with siRNA (through electrostatic interaction, hydrophobic or intercalation) and help its adsorption on the cell membrane. On one hand, a significant amount of Dox remains deprotonated and are hydrophobic in the cell growth medium (pH=7.4) (pKa of Dox=8.25)(*25, 26*) and therefore can have strong hydrophobic interaction with hydrophobic cell membrane; on the other hand, the protonated Dox have positive charges and will interact with negatively charged cell membrane through electrostatic interaction. Both interactions can explain the strong adhesion of Dox onto the cell membrane. Despite

the strong interaction of Dox with cell membrane and its efficient internalization into cancer cells, our data suggested that it was not able to help the internalization of siRNA. It was known that Dox enter the cells through a passive mechanism due to its relative small size and amphipatic property,(*27*) however siRNA with relatively larger size and highly hydrophilic and negatively charged, was generally not able to enter the cells through passive mechanism. It is likely the formed complex of Dox and siRNA are neither able to enter the cells through endocytosis possibly due to insufficient compactability nor able to enter the cell through passive mechanism due to its relatively large size. As a result, part of the Dox decomplexed from siRNA and internalized by its own.

Following this, we then studied the cell uptake efficiency of siRNA by MSN-Dox. As shown in Figure 6.6(e-h), it was found that MSN-Dox was able to internalize into cells and effectively release Dox. The released Dox is mainly localized in cytoplasm with very weak signals in nuclei, similar as our finding in MSN-Dox-G2 delivery system. However, the red fluorescence appeared to be inhomogeneous as indicated by the discrete small aggregates. We speculate this might be due to the released Dox trapped inside endosomes due to lack of proton sponge effects from G2 PAMAM to break the endosomes and release Dox into cytoplasm. At the same time, some weak green fluorescence was also observed inside cells. As compared to siRNA delivered by MSN-Dox-G2 (Figure 6.4), the green fluorescence delivered by MSN-Dox appeared to less homogeneous, probably due to same lack of proton sponge effect accounting for inhomogeneous distribution of Dox inside cells. Given that both free Dox and MSNs are able to help adsorption of siRNA onto cell membranes but neither of them can deliver

siRNA into cells, the fact that MSN-Dox is able to deliver siRNA into cells suggests that the presence of Dox in MSNs is able to help MSNs interact with siRNA stronger and deliver siRNA into cells possibly through endocytosis similar as some other MSN-based delivery systems.(*22*) On one hand, some small amount of Dox might be strongly adsorbed on the MSN surface or some Dox encapsulated inside pores might have some functions exposed out of pores, making the Dox interaction with siRNA possible; On the other hand, the encapsulation of hydrophobic Dox inside pores might render the MSN more hydrophobic as a whole, thus having stronger hydrophobic interaction with siRNA as well as with cell membrane, enabling the delivery of siRNA into cells. Despite this, it was clearly noted that the green fluorescence signal inside cells is much weaker as compared to the cells incubated with MSN-Dox-G2 complex with siRNA. For MSN-Dox-G2, it utilizes strong electrostatic interaction between phosphate groups of siRNA and primary amines of G2 PAMAM for efficient complexation, whereas for MSN-Dox, the main interaction involved is hydrophobic interaction, insufficient to complex with a large amount of siRNA, resulting in a relatively weak uptake efficiency of siRNA. This data clearly indicated modification of MSN-Dox with G2 PAMAM is necessary and critical not only for proton sponge effects to ensure effective release from endosome into cytoplasm but also for efficient complexation with and cell uptake of siRNA.

Taking all data together, we can now have a clear idea of how each component in our codelivery system of MSN-Dox-G2 affects the siRNA complexation and its cell uptake and intracellular release and localization. While G2 PAMAM alone can not form efficient complex with siRNA and deliver it into cells, once modified on MSN-Dox as in the codelivery system, it is the key component in forming efficient complex with siRNA

through electrostatic interaction, delivering it into cells and ensuring its effective release into cytoplasm through the proton sponge effects. Either MSN or Dox alone appeared to form additional interaction with siRNA, possibly enhancing the overall interaction of codelivery system with siRNA. Furthermore, it showed MSN-Dox could also help cell uptake of siRNA, despite being much less efficient than MSN-Dox-G2. It is particularly worth noting that while the role of each component as its own (such as MSN, Dox, or G2) or as in a binary component system (such as MSN-Dox or MSN-G2) can provide important implication for its role in a tertiary component system (MSN-Dox-G2), the role of each component in a single component, binary component or tertiary component system can be very different due to the mutual influence of each component. Besides the different effects of G2 as its own than as in MSN-G2 or in the codelivery system of MSN-Dox-G2 as mentioned above, the role of Dox also seemed to be significantly different in the single component system (free Dox), binary component system (MSN-Dox) and tertiary component system (MSN-Dox-G2). As free Dox alone, it can interact with siRNA and help its adsorption onto cell membrane, but was not able to deliver it into cells, due to incapability to initiate endocytosis or non-endocytoic internalization mechanism. When in MSN-Dox system, Dox appeared to help deliver siRNA into cells through its interaction with siRNA or its effect on the hydrophobicity of MSN-Dox as a whole, although neither of MSN and Dox alone was able to do so. When using MSN-Dox-G2 delivery system, efficient cell uptake of siRNA and homogeneous intracellular release was achieved. On first glimpse, this was mainly attributed to the G2 PAMAM as the cell uptake efficiency is much more efficient than that delivered by MSN-Dox. However, in closer look, it was found that siRNA delivered by MSN-G2 without Dox is

distributed in cells in discrete large aggregates while the siRNA delivered by MSN-Dox-G2 is evenly distributed in cells, indicating significant effect of Dox on the siRNA distribution inside cells. Furthermore, it also seemed that the green fluorescence signals in cells incubated with MSN-Dox-G2/siRNA complex is stronger than those in cells incubated with MSN-G2 complex with siRNA, further suggesting the effect of Dox on cell uptake of siRNA in MSN-Dox-G2 delivery system. Therefore, the effect of Dox on cell uptake of siRNA and its intracellular release in the tertiary component delivery system of MSN-Dox-G2 is much more significant than that inferred from the effect of Dox in the binary component delivery system of MSN-Dox. While the effect of Dox on enhanced cell uptake of siRNA can be attributed to similar factors that accounted for the effect of Dox on siRNA uptake in MSN-Dox delivery system, the exact mechanism of its effect on intracellular distribution of siRNA is unknown. We speculate that, once released into cytoplasm, Dox might be easier to diffuse and localize homogeneously in cytoplasm due to its smaller size and subsequently, the siRNA can diffuse and distribute homogeneously in cytoplasm due to its possible interaction with Dox (electrostatic, hydrophobic or intercalation). While more investigation is required to confirm this hypothesis, it is of additional interest to further investigate how the difference in intracellular distribution of siRNA might affect its efficacy in silencing the targeted mRNA. For this purpose, we further studied the gene knockdown efficiency of siRNA delivered by MSN-G2 vs. MSN-Dox-G2.

6.2.6. Gene Knockdown Efficacy of BCL-2-targeted siRNA Delivered by MSN-G2 vs. MSN-Dox-G2

We chose to deliver siRNA that is targeted to BCL-2 protein responsible for non-pump resistance in cancer therapy and then studied the effect of siRNA on the expression of Bcl-2 mRNA by reverse transcription polymerase chain reaction (RT-PCR). As shown in Figure 6.7, the cells incubated with MSN-Dox-G2 in the absence of BCL-2 siRNA showed slightly lower BCL-2 mRNA level than the control cells without treatment; however, when co-delivered with BCL-2 siRNA at N/P ratio (ratio of primary amines in MSN-Dox-G2 to phosphate groups of siRNA) of 1, the BCL-2 mRNA level was effectively suppressed to ~29%. When a higher N/P ratio of 2 was used, the BCL-2 mRNA level was almost completely suppressed, to ~1.8%. This data indicated that the siRNA delivered by MSN-Dox-G2 can not only be homogeneously distributed into cytoplasm, the siRNA can also effectively silence the targeted mRNAs. In contrast, the cells incubated with MSN-G2 complex with siRNA at N/P ratio of 2 showed no suppression of BCL-2 mRNA. While it is unknown whether using a higher N/P ratio will enhance the gene knockdown efficiency of siRNA delivered by MSN-G2, it is evident from the above data, when using an N/P ratio of 1 and 2, siRNA delivered by MSN-Dox-G2 can effectively silence the targeted mRNA while the siRNA delivered by MSN-G2 can not suppress the targeted mRNA at all when an N/P ratio of 2 was used. This data strongly suggests that the distribution of siRNA inside cells plays an important role in its gene knockdown efficacy. In the case of siRNA delivered by MSN-G2, the siRNA appeared to be localized only in part of cytoplasm in discrete large aggregates with some part of cytoplasm not reached, indicated by the absence of green fluorescence. This inhomogeneous distribution and formation of siRNA aggregates possibly affected the formation of RISC and subsequently resulted in ineffective RNAi; whereas in the case of

siRNA delivered by MSN-Dox-G2, the siRNA is homogeneously distributed in all parts of cytoplasm and siRNA can effectively form RISC and initiated effective RNAi. It was reported by Wang et al. (*5*) that significantly enhanced expression of
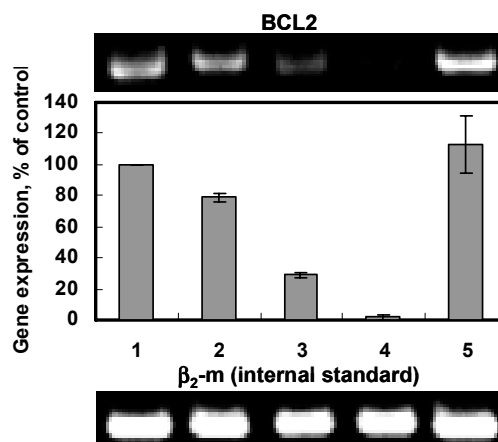
Figure 6.7. Effect of different formulation on the expression of the gene encoding BCL2 protein in A549 human lung cancer cells. (1). No treatment; (2). MSN-Dox-G2 PAMAM; (3). MSN-Dox-G2 PAMAM with BCL2 siRNA (N/P=1); (4). MSN-Dox-G2 PAMAM with BCL2 siRNA (N/P=2); (5). MSN-G2 with BCL2 siRNA (N/P=2). Gene expression was calculated as a ratio of band intensity of BCL2 gene to that of internal standard, $\beta 2$-m and then the ratio of each sample was normalized to that of sample without treatment.

luciferase and GFP reporter genes in cancer cells was achieved both in vitro and in vivo when the genes were delivered by paclitaxel-loaded nanoparticles as compared to that delivered by nanoparticles alone. This enhancement was thought to be likely due to the anti-mitotic function of paclitaxel in their report similar as some other reports.(*28, 29*) While similar anti-mitotic effect can not be the case here, since Dox is not an anti-mitotic anticancer drug, it is evident that the codelivery of Dox also directly helped the

homogeneous distribution of siRNA, which is critical for the effective RNAi and gene knockdown efficiency as illustrated in our experiment. The detailed mechanism needs further investigation.

6.3. Conclusions

In summary, we systematically investigated the effect of each component in a novel MSN-based codelivery system on the siRNA uptake efficiency and its intracellular release and localization. Our result suggested it is highly likely that the same component may play different roles when used in different multi-component delivery system and this needs to be seriously taken into account in designing multi-component delivery system. Furthermore, our data suggested that the Dox in our codelivery system of MSN-Dox-G2-siRNA is very critical for homogeneous distribution of siRNA inside cells and in ensuring the effective gene knockdown of siRNA. Without Dox, although the delivery system of MSN-G2 was still able to efficiently deliver siRNA into cells, the delivered siRNA was distributed in discrete large aggregates inside cells and was not able to silence the targeted mRNA.

6.4. Experimental Section

6.4.1. Materials

G2 amine-terminated PAMAM dendrimer, doxorubicin hydrochloride and other chemicals used in this study were purchased from Sigma Aldrich (Milwaukee, WI), and used without further purification. siRNA that are sequence specific for human BCL-2

mRNA was custom synthesized by Ambion (Austin, TX). The sequence of the siRNA used as follows: sense strand, 5'-GUGAAGUCAACAUGCCUGC-dTdT-3'; antisense strand, 5'-GCAGGCAUGUUGACUUCAC-dTdT-3'.

6.4.2. Preparation of MSN-Dox-G2

Same procedure as that described in Chapter IV was used.

6.4.3. Synthesis of MSN-G2

~58 ml of aqueous suspension of ICP-modified MSNs (0.9 mg/ml) was mixed with 0.8110 g of 20 wt% G2 PAMAM in MeOH in a beaker and then stirred for 3.5 h at RT. After that, the suspension was centrifuged and washed several times to obtain the MSN-G2 sample.

6.4.4. Cell Lines

The human lung cancer A549 cell line was obtained from the ATTC (Manassas, VA, USA). Cells were cultured in RPMI 1640 medium (Sigma, St. Louis, MO) supplemented with 10% fetal bovine serum (Fisher Chemicals, Fairlawn, NJ). Cells were grown at 37 °C in a humidified atmosphere of 5% CO_2 (v/v) in air. All experiments were performed on cells in the exponential growth phase.

6.4.5. Cellular Internalization

Cellular internalization was studied by confocal fluorescence microscopy (Leica Microsystems Inc., Bannockburn, IL). A549 cells were plated (20, 000 cells/well) in a

single well and pre-cultured for 24 h. The old medium was then removed and the cells were treated with different formulations (complexes of siRNA green transfection indicator with MSN-Dox-G2, G2 PAMAM, MSN, MSN-G2, Dox or MSN-Dox) in 1.5 ml cell growth medium. The cells were cultured at 37 °C for different periods of time with different formulations and the incubation time are respectively: G2-siRNA (24h), MSN-siRNA (24h), MSN-Dox-siRNA (24 h), MSN-Dox-G2-siRNA (7 h), MSN-G2-siRNA (7 h) and Dox-siRNA (2 h). After incubation, then the old medium was removed, the cells were washed with Dulbecco's phosphate buffered saline (DPBS) buffer three times and then added with 1.5 ml fresh medium for fluorescence imaging. For complex of siRNA green transfection indicator with MSN-Dox-AEDP-G2, its internalization at 37 °C was monitored by confocal fluorescence microscopy for 4 h. After 4-hr imaging of live cells, the old medium were removed and the cells were washed with DPBS buffer three times and then added with fresh medium for imaging again. The N/P ratio (ratio of primary amine groups to phosphate groups) used in the complex of siRNA green transfection indicator with different formulations were respectively: G2 (N/P=2), MSN-Dox-G2 (N/P=2), MSN-G2 (N/P=2), MSN-Dox-AEDP-G2 (N/P=1). For Dox complex with siRNA, the final concentration of Dox in cell growth medium was 2.65 μM. For MSN-Dox complex with siRNA, the final concentration of MSN and Dox in cell growth medium was 8.2 μg/ml and 12.1 μM respectively. For MSN complex with siRNA, the final concentration of MSN in cell growth medium was 1.0 μg/ml. For all samples, the final concentration of siRNA in cell growth medium was 0.2 μM.

6.4.6. Gene Knockdown

The ability of MSN-Dox-G2 or MSN-G2 complex with Bcl-2 siRNAs to knock down the target mRNA expression were studied with quantitative reverse transcriptase-polymerase chain reaction (RT-PCR). RNA was isolated 24 hrs after treatment of A2780/AD cells using an RNeasy kit (Qiagen, Valencia, CA). First strand cDNA was synthesized by Ready-To-GO You-Prime First-Strand Beads (Amersham Biosciences, Piscataway, NJ) with 4mg of total cellular RNA and 100 ng of random hexadeoxynucleotide primer (Amersham Bioscience). After synthesis, the reaction mixture was immediately subjected to polymerase chain reaction, which was carried out using GenAmp PCR System 2400. The following pairs of Bcl-2 and β_2-m primers were used to amplify each type of cDNA: *BCL2*—GGA TTG TGG CCT TCT TTG AG (sense), CCA AAC TGA GCA GAG TCT TC (antisense); β_2-*microglobulin* (β_2-*m*, internal standard)—ACC CCC ACT GAA AAA GAT GA (sense), ATC TTC AAA CCT CCA TGA TG (antisense). PCR products were separated in 4% NuSieve 3:1 Reliant agarose gels in **1**×TBE buffer (0.089 M Tris/Borate, 0.002 M EDTA, pH 8.3; Research Organic Inc., Cleveland OH) by submarine electrophoresis. The gels were stained with ethidium bromide, digitally photographed and scanned using Gel Documentation System 920 (NucleoTech, San Mateo, CA). Gene expression was calculated as the ratio of mean band density of analyzed RT-PCR product to that of the internal standard (β2-m) and then the ratio of each sample was normalized to that of sample without treatment**.**

6.5. References

1.   Menendez, J. A., Vellon, L., Colomer, R., and Lupu, R. (2005) Pharmacological and small interference RNA-mediated inhibition of breast cancer-associated fatty acid synthase (oncogenic antigen-519) synergistically enhances Taxol (paclitaxel)-induced cytotoxicity, *Int. J. Cancer. 115*, 19-35.

2.   Hannon, G. J., and Rossi, J. J. (2004) Unlocking the potential of the human genome with RNA interference, *Nature 431*, 371-378.

3.   Gary, D. J., Puri, N., and Won, Y.-Y. (2007) Polymer-based siRNA Delivery: Perspectives on the Fundamental and Phenomenological Distinctions from Polymer-based DNA Delivery, *Journal of controlled release 121*, 64-73.

4.   Kim, W. J., Chang, C.-W., Lee, M., and Kim, S. W. (2007) Efficient siRNA delivery using water soluble lipopolymer for anti-angiogenic gene therapy, *Journal of controlled release 118*, 357-363.

5.   Wang, Y., Gao, S., Ye, W.-H., Yoon, H. S., and Yang, Y.-Y. (2006) Co-delivery of drugs and DNA from cationic core-shell nanoparticles self-assembeled from a biodegradable copolymer, *Nature Materials 5*, 791-796.

6.   Zhang, S., Zhao, B., Jiang, H., Wang, B., and Ma, B. (2007) Cationic lipids and polymers mediated vectors for delivery of siRNA, *Journal of controlled release 123*, 1-10.

7.   Zhang, C., Tang, N., Liu, X., Liang, W., Xu, W., and P., T. V. (2006) Sirna-containing liposomes modified with polyarginine effectively silence the targeted gene``, *Journal of controlled release 112*, 229-239.

8.   Zimmermann, T. S., Lee, A. C. H., Akinc, A., Bramlage, B., Bumcrot, D., Fedoruk, M. N., Harborth, J., Heyes, J. A., Jeffs, L. B., John, M., Judge, A. D.,

Lam, K., McClintock, K., Nechev, L. V., Palmer, L. R., Racie, T., Rohl, I., Seiffert, S., Shanmugam, S., Sood, V., Soutschek, J., Toudjarska, I., Wheat, A. J., Yaworski, E., Zedalis, W., Koteliansky, V., Manoharan, M., Vornlocher, H.-P., and MacLachlan, I. (2006) RNAi-mediated gene silencing in non-human primates, *Nature 441*, 111-114.

9. Akhtar, S., and Benter, I. F. (2007) Nonviral delivery of synthetic siRNAs in vivo, *Journal of Clinical Investigation 117*, 3623-3632.

10. Fire, A., Xu, S., Montgomery, M. K., Kostas, S. A., Driver, S. E., and Mello, C. C. (1998) Potent and specific genetic interference by double-stranded RNA in Caenorhabditis elegans, *Nature 391*, 806-811.

11. Han, Y., and Ying, J. Y. (2005) Generalized Fluorocarbon-surfactant-mediated Synthesis of Nanoparticles with Various Mesoporous Structures, *Angew. Chem. Int. Ed. 44*, 288-292.

12. Huh, S., Wiench, J. W., Yoo, J.-C., Pruski, M., and Lin, V. S. Y. (2003) Organic Functionalization and Morphology Control of Mesoporous Silicas via A Co-condensation Synthesis Method, *Chem. Mater. 15*, 4247-4256.

13. Moeller, K., Kobler, J., and Bein, T. (2007) Colloidal Suspensions of Nanometer-sized Mesoporous Silica, *Adv. Funct. Mater. 17*, 605-612.

14. Slowing, I. I., Trewyn, B. G., and Lin, V. S.-Y. (2007) Mesoporous silica nanoparticles for intracellular delivery of membrane-impermeable proteins, *J. Am. Chem. Soc. 129*, 8845-8849.

15. Gu, J., Fan, W., Shimojima, A., and Okubo, T. (2007) Organic-inorganic mesoporous nanocarriers integrated with biogenic ligands, *Small 3*, 1740-1744.

16. Slowing, I. I., Vivero-Escoto, J. L., Wu, C.-W., and Lin, V. S.-Y. (2008) Mesoporous Silica Nanoparticles as Controlled Release Drug Delivery and Gene Transfection Carriers, *Advanced Drug Delivery Reviews 60*, 1278-1288.

17. Giri, S., Trewyn, B. r. G., Stellmaker, M. P., and Lin, V. S.-Y. (2005) Stimuli-responsive controlled-release delivery system based on mesoporous silica nanorods capped with magnetic nanoparticles, *Angew. Chem. Int. Ed. 44*, 5038-5044.

18. Gruenhagen, J. A., Lai, C.-Y., Radu, D. R., Lin, V. S.-Y., and Yeung, E. S. (2005) Real-time Imaging of Tunable Adenosine 5-Triphosphate Release from an MCM-41-Type Mesoporous Silica Nanosphere-Based Delivery System, *Applied Spectroscopy 59*, 424-431.

19. Lai, C.-Y., Trewyn, B. G., Jeftinija, D. M., Jeftinija, K., Xu, S., Jeftinija, S., and Lin, V. S.-Y. (2003) A mesoporous silica nanosphere-based carrier system with chemically removable CdS nanoparticle caps for stimuli-responsive controlled release of neurotransmitters and drug molecules, *J. Am. Chem. Soc. 125*, 4451-4459.

20. Torney, F., Trewyn, B. G., Lin, V. S.-Y., and Wang, K. (2007) Mesoporous silica nanoparticles deliver DNA and chemicals into plants, *Nature Nanotechnology 2*, 295-300.

21. Pakunlu, R. I., Wang, Y., Saad, M., Khandare, J. J., Starovoytov, V., and Minko, T. (2006) In vitro and in vivo intracellular liposomal delivery of antisense oligonucleotides and anticancer drug, *J. Controlled Release 114*, 153-162.

22. Slowing, I., Trewyn, B. G., and Lin, V. S.-Y. (2006) Effect of surface functionalization of MCM-41-type mesoporous silica nanoparticles on the endocytosis by human cancer cells, *J. Am. Chem. Soc. 128*, 14792-14793.

23. Gillies, E. R., and Frechet, J. M. J. (2005) pH-Responsive Copolymer Assemblies for Controlled Release of Doxorubicin, *Bioconjugate Chemistry 16*, 361-368.

24. Patil, M., Zhang, M., Betigeri, S., Taratula, O., He, H., and Minko, T. (2008) Surface-modified and Internally Cationic Polyamindoamine Dendrimers for Efficient siRNA Delivery, *Bioconjugate Chemistry 19*, 1396-1403.

25. Choucair, A., Soo, P. L., and Eisenberg, A. (2005) Active Loading and Tunable Release of Doxorubicin from Block Copolymer Vesicles, *Langmuir 21*, 9308-9313.

26. Missirlis, D., Kawamura, R., Tirelli, N., and Hubbell, J. A. (2006) Doxorubicin Encapsulation and Diffusional Release from Stable, Polymeric, Hydrogel Nanoparticles, *European Journal of Pharmaceutical Sciences 29*, 120-129.

27. Eytan, G. D. (2005) Mechanism of Multidrug Resistance in Relation to Passive Membrane Permeation, *Biomedicine and Pharmacotherapy 59*, 90-97.

28. Nair, R. R., Rodgers, J. R., and Schwarz, L. A. (2002) Enhancement of Transgene Expression by Combining Glucocorticoids and Anti-mitotic Agents during Transient Transfection Using DNA-Cationic Liposomes, *Molecular Therapy 5*, 455-462.

29. Son, K., and Huang, L. (1994) Exposure of Human Ovarian Carcinoma to Cisplatin Transiently Sensitizes the Tumor Cells for Liposome-mediated Gene Transfer, *PNAS 91*, 12669-12672.

Chapter 7

Probing the Internalization Mechanism of a Mesoporous Silica Nanoparticle-based Drug Delivery System: a Possible Non-endocytic Internalization Process

7.1. Introduction

Nanoparticles (NPs) are attractive as drug delivery systems due to their unique physicochemical properties. Most NPs have been reported to internalize into cells through an energy-dependent process known as endocytosis. Endocytosis can be primarily subdivided into three types: clathrin-mediated endocytosis, lipid raft/caveolae-mediated endocytosis and macropinocytosis. The type of endocytosis through which the NPs internalize into cells is dependent on many factors, including their surface functionalization and surface charge, their size as well as their shape.(*1*) A classical example of size effect on internalization mechanism was reported by Rejman et al.(*2*) They showed that polystyrene nanoparticles with a diameter of < 200 nm were internalized through clathrin-mediated endocytosis, while with increasing size, the internalization mechanism shifted to caveolae-mediated endocytosis, which became predominant internalization pathway when size reached 500 nm. Furthermore, it was found that the endocytosis can also be cell-dependent, with different endocytosis mechanisms employed by the same NPs for internalization into different types of cells.(*1*)

In addition to endocytosis, non-endocytic internalization mechanisms were reported to exist for some NPs despite being much less common. One remarkable example is carbon nanotubes functionalized with small molecular weight molecules, which were found to cross membranes of many different types of cells following a spontaneous translocation mechanism termed a nanoneedle mechanism.(*3-6*). The mechanism was further supported by a recent molecular dynamics simulation study, which suggested that hydrophobic nanotubes with hydrophilic functional groups can spontaneously insert into a lipid bilayer. The semi-rigid and elongated form of the carbon nanotubes was believed to rule out an endocytic process. Another example of NPs internalizing into cells through a non-endocytic mechanism is TAT peptides or TAT peptide conjugated cargos. In an early report of cell uptake of TAT peptide,(*7*) it was found that the uptake of TAT peptide was not inhibited at 4 °C. In addition, conjugation of the peptide to other peptides or oligodeoxynucleotides (ODNs) also helped their internalization. Following this report, many other reports have shown a receptor-independent(*8*) and energy-independent[10-14] non-endocytic internalization mechanism for TAT-peptides or TAT peptide conjugated cargos. However, this was recently questioned by some reports which showed that an endocytic mechanism was also involved in TAT peptides or TAT peptide conjugated cargos such as TAT-modified lipoplexes.(*9, 10*) Although the entry mechanism of TAT peptides or TAT peptide conjugated cargos remains controversial until now, there exists clear evidence that some TAT peptides and TAP peptide conjugated cargos, together with other nanosized entities such as antennapedia homeodomain peptide(11) and core histones(12), can enter cells through a non-endocytic membrane translocation mechanism.

Mesoporous silica nanoparticles (MSNs) have recently emerged as an attractive type of NP delivery system for chemical and gene therapy drugs due to their unique pore structures with high pore volume and high surface area as well as good biocompatibility. Our own studies have demonstrated that MSNs can be used as an ideal delivery system to load a large quantity of hydrophobic anticancer drugs to achieve stimuli-responsive controlled release inside cells while minimal premature release before entering the cancer cells. Furthermore, our data showed that MSNs can also act as a codelivery system to load anticancer chemotherapy drugs inside pores and gene therapeutic drugs on the surface and then deliver them simultaneously into cancer cells to achieve synergistic anticancer efficacy, as described in Chapter V. It was believed, similar to most NPs, that MSNs enter cells through an endocytosis mechanism. In one report by Lin's group(13), effect of different functionalization on endocytosis of MSNs into HeLa human cervical cancer cells was investigated. They concluded that fluorescein isothiocyanate-modified MSNs (FITC-MSNs) and 3-(N-folateamino)propyl-modified FITC-MSNs (FAP-MSNs) were endocytosed via a clathrin-pitted mechanism as the uptakes were inhibited by 450 mM sucrose. They further concluded that internalized FAP-MSNs were also mediated by folic acid receptors as uptake of FAP-MSNs were partially inhibited in the presence of 1 mM folic acid. In contrast, they found that the endocytosis of 3-aminopropyl-modified FITC-MSNs (AP-MSNs) and 3-Guanidiniopropyl-modified FITC-MSN (GP-MSNs) were affected by a caveolar inhibitor, genistein, suggesting these materials were endocytosed via a caveolae-mediated mechanism. However, 3-[N-(2-guanidinioethyl)guanidinio]propyl-modified FITC-MSNs (GEGP-MSN) internalized through an unknown mechanism as the uptake was not dramatically affected by any of

the inhibitors under their investigation. It is worth noting that although inhibition of uptake by sucrose is considered a strong evidence for clathrin-mediated endocytosis, sucrose can also interfere with non-clathrin-mediated internalization pathways as found in many reports that it can interfere with all three major endocytic internalization pathways(14). Therefore, it is necessary to point out that it is possibly premature to conclude based on the sucrose inhibition data that both FITC-MSNs and FAP-MSNs internalized through a clathrin-mediated endocytosis, although it is sufficient to conclude both internalized through an endocytosis mechanism. Nevertheless, the major point taken from this report is that the functionalization of MSNs has dramatic effect on its internalization mechanism. Furthermore, it is interesting to note that uptake of GEGP-MSNs was not inhibited by any of the inhibitors, suggesting a possibility that GEGP-MSNs internalize through a non-endocytic mechanism. Separately, by using several inhibitors including phenylarsine oxide (PAO) (clathrin inhibitor), sodium azide and 6-deoxyglucose (metabolic inhibitor), filipin (caveolae inhibitor), Huang et al.(15) explored the mechanisms of FITC-MSNs uptake in 3T3-L1 cells and human mesenchymal stem cells (hMSCs). They found that FITC-MSNs internalized into both cells through a clathrin-mediated endocytosis as well as phagocytosis, but was not internalized through caveolae-mediated endocytosis. In another recent report by the same group(1), they further investigated the effect of surface charge on the uptake of red emitting rhodamine-B-isothiocyanate-modified MSNs (RITC-MSNs) in 3T3-L1 and hMSCs cells using different inhibitors. They found that, all RITC-MSNs internalized into 3T3-L1 cells through a clathrin-meidated endocytosis. However, the internalization of RITC-MSNs into hMSCs was highly dependent on the surface charge. Unmodified, weakly positively-

charged or moderately positively-charged RITC-MSNs internalized through a clathrin- and an actin-dependent endocytosis. However, the strongly positively-charged RITC-MSN was not as its uptake was not inhibited by any of the inhibitors. This data not only suggested that the uptake of MSNs by hMSCs can be regulated by a threshold of positive surface charge but also implied that the modulation of surface charge on the MSN uptake is specific to cell type. Furthermore, it is interesting to note that the strongly positively-charged RITC-MSN appeared not to internalize through any of the three main endocytosis internalization pathways, similar to the finding for GEGP-MSN in the report by Lin's group.(13) Unfortunately, no further detailed investigation was performed to further confirm whether the strongly positive-charged RITC-MSN or GEGP-MSN internalizes into cells through a non-endocytic mechanism, similar to that for CNTs, TAT peptides or TAT peptide conjugated cargos as discussed above.

Doxorubicin is a potent anticancer drug that has been used for cancer therapy for more than 30 years. It enters the cells through a passive transport mechanism which can be described in terms of the following steps(*16, 17*): (1) massive immediate binding of the drugs to the outer leaflet of the plasma membrane resulting in a practical equilibrium between extremely high drug concentration at the cell surface compared to the drug concentration in the medium. (2) Due to the amphipathic nature, Dox is practically excluded from the lipid core of the membrane by a distinct flip-flop event that occurs after an average period of 0.7 min at 37 °C. (3) The drug reaching the inner leaflet of the plasma membrane is in a practical equilibrium with the drug present in the cytoplasm. (4) Almost all the amounts of anticancer drugs present in the cells are bound by molecular sinks, such as DNA or cytoskeleton elements. In this mechanism, the transbilayer

movement of Dox is described in terms of distinct events of flip-flop across the membrane and not as diffusion down a continuous gradient located in the membrane core. It was found that the transbilayer movement rate of Dox is significantly decreased as temperature decreases, as a result of less fluidization of membrane at lower temperatures as well as a direct temperature effect. Therefore, it was generally found that the cell uptake of Dox is significantly reduced at lower temperatures. As reported by Lane et al.(*18*), the uptake of Dox into L1210 cells was reduced to about 40% when the incubation temperature was reduced from 37 °C to 0 °C.

However, the effect of temperature on cell uptake of Dox into multidrug resistant (MDR) cells has rarely been reported. In MDR cells, at least two proteins, P-glycoprotein (Pgp) and multidrug resistance-associated protein (MRP), can confer pump resistance that decrease the intracellular drug concentration by active efflux pump. The Pgp are evolutionarily well-conserved ATP-binding, membrane-spanning proteins. Based on the above model, the slow flip-flop transbilayer movement of Dox will allow the active Pgp removal of Dox after it is transported across cell membrane and thus result in lower intracellular drug concentration. At lower temperature, the transbilayer movement rate of Dox is significantly reduced, which will directly result in lower uptake of Dox, like the case in non-MDR cells. However, at the same time, since the efflux pump by Pgp is also an energy dependent process, at lower temperature, less drug will also be removed. As a result, the effect of temperature on cell uptake of Dox into MDR cells might be very different than non-MDR cells. If the reduction of Dox transport into cell due to temperature decrease is more significant than the decrease of Pgp removal of drug, then the effect of temperature on the intracellular Dox concentration may be less significant in

MDR-cells than in MDR cells. On the contrary, if the reduction of Dox transport into cell due to temperature decrease is less significant than the decrease of Pgp removal of drug, then the intracellular Dox concentration at low temperature may be reduced less significantly when compared to non-MDR cells. Therefore, the effect of temperature on DOX uptake into MDR cells is worth a detailed investigation, which is one of our efforts of this chapter.

On the other hand, due to its severe side effects to normal body tissues, direct delivery of Dox in its free form was non-ideal. Therefore, Dox was commonly loaded into delivery systems or conjugated with polymers with an aim to minimize the side effects and improve the anticancer efficacy. As a result, the circulation time of Dox in blood stream as well as many other pharmacological properties can be significantly affected by the delivery systems. Among all, the effect on cell uptake mechanism especially attracted our attention. The Dox cell uptake mechanism will be changed from the passive transport mechanism to the mechanism that is employed by the delivery system, which, in our case, is the Dox-loaded MSNs modified with G2 PAMAM. Such dramatic change of cell uptake mechanism is expected to have significant effects on the uptake kinetics, intracellular release, intracellular distribution, intracellular concentration as well as the cytotoxicity of Dox. A direct comparison of cell uptake kinetics, intracellular concentration and the temperatures effects on free Dox vs. Dox delivered by a delivery system therefore will provide useful information for better designing an optimal anticancer drug delivery system.

The present investigation is aimed at answering several important and interesting questions discussed above. We have specifically studied (1) the kinetics and efficiency of

uptake of free Dox vs. Dox that is delivered as MSN-Dox-G2 into MDR A2780/AD human ovarian cancer cells; (2) the effect of temperature on the uptake of free Dox vs. MSN-Dox-G2; (3) the influence of metabolic and endocytic inhibitors on cell uptake of MSN-Dox-G2; (4) the localization of Dox in relative to early endosomes by tracking the early endosomes using a green fluorescence probe-conjugated secondary antibody.

7.2. Results and Discussion

7.2.1. Kinetics and Efficiency of Uptake of Free Dox vs. MSN-Dox-G2

In order to compare the kinetics and efficiency of uptake of free Dox vs. MSN-Dox-G2, A2780/AD cells in 6-well plates were incubated with free Dox or MSN-Dox-G2 at the same concentration of 2.42 μM Dox at 37 °C for different periods of time. Then the cells
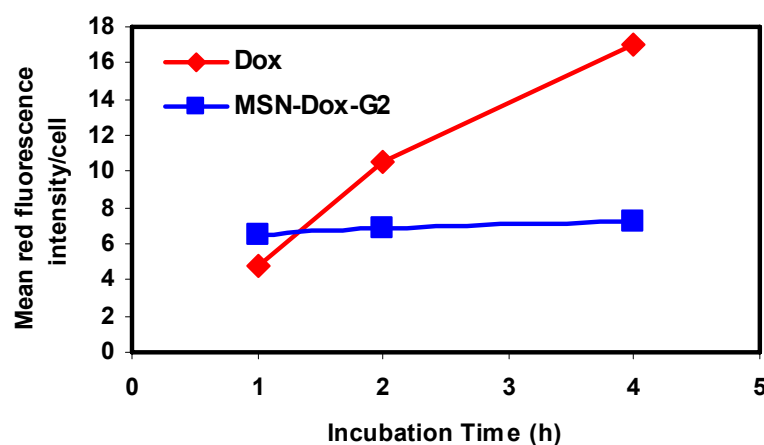
Figure 7.1. Kinetics of cell uptake of free Dox vs. MSN-Dox-G2 by flow cytometry. A2780/AD cells were incubated by free Dox (2.42 μM) and MSN-Dox-G2 (2.42 μM Dox) respectively at 37 °C for different periods of time. This data showed that MSN-Dox-G2 appeared to internalize into cells and reach a steady state much faster than free Dox, however, the intracellular Dox concentration at steady state in the case of MSN-Dox-G2 is significantly lower than that in the case of free Dox.

were washed with PBS buffer and trypsinized for flow cytometry analysis. The mean fluorescence intensities of 10000 cells of each sample were then plotted against the incubation times and shown in Figure 7.1.

The data indicated that after 1 h incubation, the intracellular Dox concentration is higher in cells incubated with MSN-Dox-G2 than those incubated with free Dox. However, after 2 and 4 h incubation, the order is reversed in that the intracellular Dox concentration became significantly higher in cells incubated with free Dox than those incubated with MSN-Dox-G2. On the other hand, for MSN-Dox-G2, its uptake appeared to reach a steady state after 1 h, with longer incubation (2 h or 4 h) resulting in only slightly increased uptake; while for free Dox, its uptake continuously increased as the incubation time increased. The mean fluorescence intensity for cells with 2 h and 4 h incubation has respectively increased to ~2.2 times and ~3.5 times that of cells incubated with 1 h.

In our previous study, we found that MSN-Dox-G2 is about twice as toxic as free Dox and the toxicity of MSN-Dox-G2 is not due to MSN-G2. We speculated that several factors might contribute to the increased toxicity of MSN-Dox-G2. Those factors included the possible higher accumulation of Dox inside cells by bypassing the pump resistance of Pgp, the protection of Dox from the degradation by intracellular enzymes and environment during delivery as well as the synergistic cytotoxicity effects due to the coexistence of Dox in both nuclei and cytoplasm. It should be noted that a different experimental setting was employed in cytotoxicity studies than that employed in current flow cytometry study. In cytotoxicity studies, the incubation time was 24 h and the density of cells in each well was significantly less. Despite these differences, based on the

kinetic profile of uptake of free Dox vs. MSN-Dox-G2 as shown in Figure 7.1, it is reasonable to expect that the intracellular concentration of Dox in cells incubated with free Dox will be higher than those incubated with MSN-Dox-G2 during most time of the 24 h incubation. Therefore, this data strongly suggested that the increased toxicity of MSN-Dox-G2 is not likely due to the increased intracellular concentration of Dox. Given the 2-fold increase of the toxicity as well as the significantly different distribution of Dox in cells incubated with MSN-Dox-G2 than those incubated with free Dox, we can now speculate that the increased cytotoxicity of MSN-Dox-G2 is more likely due to the synergistic anticancer action of Dox due to its coexistence in both nuclei and cytoplasm.

As previously discussed, the free Dox enters the cells through a passive flip-flop transbilayer transport process, which is relatively slow with each flip-flop event taking an average of 0.7 min. This may explain why the kinetics of free Dox uptake process is slower than that of MSN-Dox-G2, which internalizes through a different pathway. As a result, the intracellular Dox concentration in cells incubated with MSN-Dox-G2 is higher than that in cells incubated with free Dox after 1 h incubation. However, the intracellular concentration at steady state appeared to be much higher in the case of free Dox than that in the case of MSN-Dox-G2. In our study, the free Dox appeared not to reach a steady state after 4 h incubation, therefore the intracellular concentration at its steady state is expected to be even higher than that with 4 h incubation, which is already much higher than the intracellular concentration of Dox in cells incubated with MSN-Dox-G2 for same period of time. The cell uptake kinetics and intracellular concentration of Dox at steady state delivered as free Dox vs. solid lipid nanoparticles (SLNs) containing Dox was previously studied by Wong et al. (*19*). Their studies showed that the kinetics of cell

uptake of free Dox vs. SLN-Dox is similar while the intracellular concentration at steady state is higher in the case of SLN-Dox. This data indicated that our delivery system MSN-Dox-G2 may internalize through different mechanisms and has very different intracellular concentration at steady state. Furthermore, it is worth noting that in their study the free Dox appeared to reach a steady state within 2 h while in our case, the steady state was not reached even after 4 h incubation. This may be due to different experimental setting as well as different cell lines under investigation.

7.2.2. Effect of Temperate on Cell Uptake of Free Dox vs. MSN-Dox-G2

Effect of temperature on cell uptake of free Dox into MDR cancer cells has been rarely studied. A previous study using non-MDR cell showed that the Dox uptake was reduced to ~40% when the incubation temperature was reduced from 37 °C to 0 °C. The decreased cell uptake was theoretically expected as the transbilayer process is slowed as temperature decreases. We hypothesized that for MDR cells, a less or more significant decrease of cell uptake of free Dox at low temperature may be expected depending on the relative effect of temperature on two competing process, transport of free Dox across cell membrane and removal of Dox by Pgp. To investigate this, we have studied the cell uptake of free Dox at three different temperatures, 37 °C, 21 °C and 4 °C in MDR A2780/AD cells. Cells were incubated with same concentration of 2.42 μM free Dox for 2 h before being washed and trypsinized for flow cytometry analysis. The mean fluorescence intensity at three temperatures was plotted in Figure 7.2. The result indeed showed that for free Dox, its passive transport process was temperature dependent and the cell uptake was significantly inhibited at low temperature. At 21 °C, the cell uptake of

free Dox was reduced to ~ half of that at 37 °C and at 4 °C, the cell uptake was almost completely inhibited. This, compared to the data in non-MDR cells as previously reported by Lane et al.(*18*), showed much more significant effect of low temperature on cell uptake of free Dox. On one hand, the nearly complete inhibition of free Dox uptake into
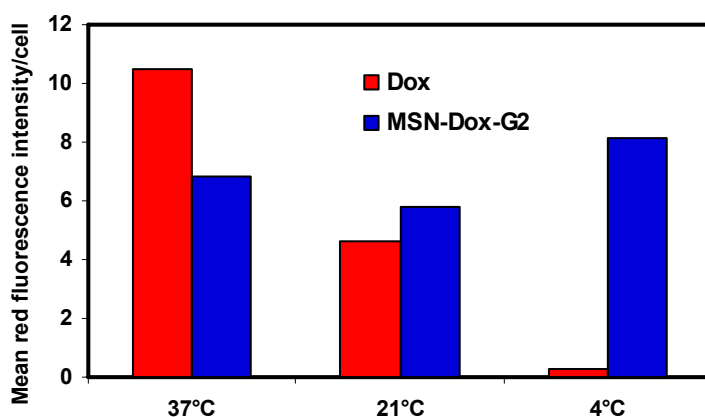
Figure 7.2. Relative mean red fluorescence intensity by flow cytometry of A2780/AD cells incubated by free Dox (2.42 µM) or MSN-Dox-G2 (2.42 µM Dox) for 2 h at 37 °C, 21 °C and 4 °C respectively.

MDR A2780/AD cells at 4 °C appeared to prove our hypothesis proposed above, in addition, this may result from a combination of temperature effect on all processes involved in the uptake of Dox, including the immediate binding of Dox to outer membrane leaflet, the transport from outer membrane leaflet to inner membrane leaflet, the transport from inner membrane leaflet to cytoplasm and the efflux pump exerted by Pgp. More detailed investigation is required to fully understand this.

At the same time, we have studied the temperature effect on uptake of Dox when delivered as MSN-Dox-G2. Exact same experimental conditions as that for free Dox were employed. Much to our surprise, it was found that when delivered as MSN-Dox-G2,

while the cell uptake of Dox was slightly inhibited at 22 °C when compared to that at 37 °C, its cell uptake at 4 °C was even slightly higher than at 37 °C. Endocytosis is known to be temperature and energy dependent and thus a significantly inhibition of uptake at low temperature is expected for nanoparticles that internalize through endocytosis. This data strongly suggested that MSN-Dox-G2 internalize through a non-endocytic process. To further investigate how the incubation time affect the uptake difference between 37 °C and 4 °C incubation for free Dox and MSN-Dox-G2 respectively, experiments were also performed with 4 h incubation at 37 °C and 4 °C respectively and the mean fluorescence intensities by flow cytometry were plotted in Figure 7.3. This data indicated that after 4 h incubation, the cell uptake of MSN-Dox-G2 at 4 °C became more significantly higher than that at 37 °C. In contrast, the cell uptake of free Dox was still almost completely inhibited at 4 °C after 4 h incubation.

Theoretically, one may question that the strong fluorescence intensity observed for cells incubated with MSN-Dox-G2 at 4 °C may be due to strong adsorption of MSN-
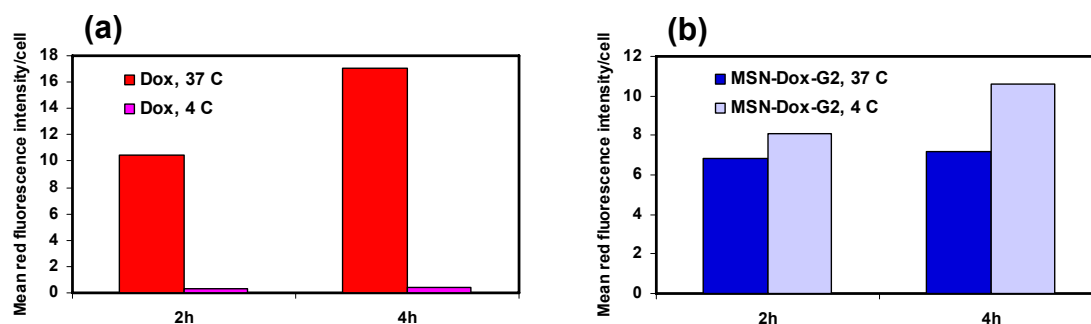

Figure 7.3. Relative mean red fluorescence intensity by flow cytometry of A2780/AD cells incubated by free Dox (2.42 µM) or MSN-Dox-G2 (2.42 µM Dox) for 2 h or 4 h at 37 °C and 4 °C respectively.

Dox- G2 to the surface of cell membrane rather than real internalization of Dox into cells. From our previous studies, we know that the fluorescence of Dox is completely quenched when encapsulated in MSN pores and that release of Dox from MSN pores outside cells is minimal, therefore, no significant red fluorescence will be expected if the MSN-Dox-G2 doesn't internalize into cells and subsequently release Dox. Regardless, to exclude the above possibility, an aliquot of suspension of trypsinized cells in PBS buffer that were incubated with MSN-Dox-G2 at 4 °C for 2 h was transferred to a glass slide and then analyzed by regular fluorescence microscopy. As shown in Figure 7.4(a-b), it can be clearly seen that the red fluorescence is indeed from the inside of cells rather than from the surface of cell membrane. As we found previously, when Dox was adsorbed only on the surface of cell membrane, the red fluorescence surrounded the cell membrane like a ring, which was not observed in this case. In comparison, the regular fluorescence of trypsinized and suspended cells that were incubated with same concentration of free Dox at 4 °C for 2 h was also analyzed by regular fluorescence and shown in Figure 7.4(c-d). Consistent with the finding from flow cytometry data, no red fluorescence was detected, indicating nearly complete inhibition of free Dox uptake at 4 °C.

Another artifact that could result in efficient cellular uptake of MSN-Dox-G2 at 4 °C is that the MSN-Dox-G2 may damage the cell membrane and make it permeable to MSN-Dox-G2 regardless of the temperature. To rule out this possibility, cells were incubated with free Dox alone or free Dox together with MSN-G2 for 4 h at 37 °C with same concentration of 1.51 μM Dox and then the cell uptake was analyzed and compared with flow cytometry. As shown in Figure 7.5, the data indicated minimal effect of MSN-G2 on the cell uptake of free Dox, suggesting that the presence of MSN-G2 does not

affect the integrity and the permeability of cell membrane. Consequently, we can conclude that the efficient cell uptake of MSN-Dox-G2 at 4 °C is real, neither due to adsorption on cell membrane nor due to damaged cell membrane.

Figure 7.4. Regular fluorescence of A2780/AD cells after incubated with MSN-Dox-G2 (a-b) or free Dox (c-d) for 2 h at 4 C (2.42 µM Dox) and then trypsinized and suspended in PBS buffer (a, c) light image; (b, d) red fluorescence image.
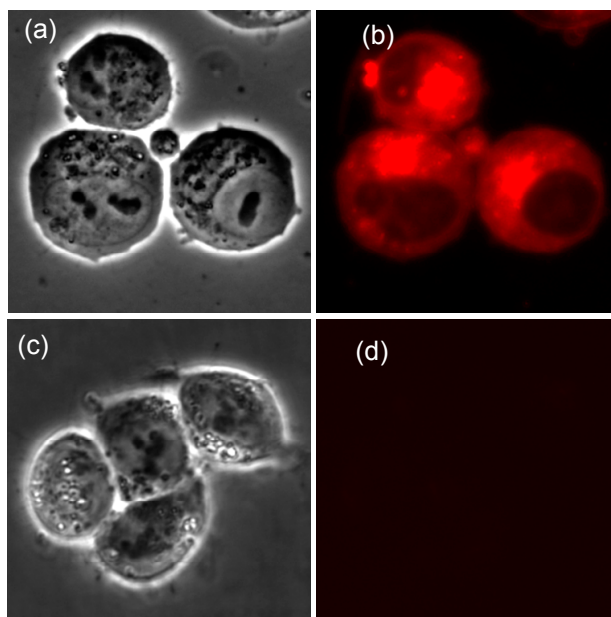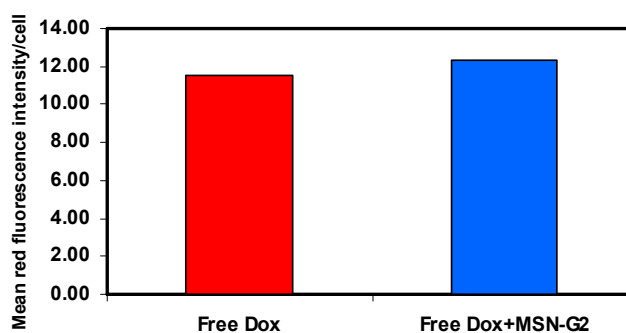

Figure 7.5. Relative mean red fluorescence intensity by flow cytometry of A2780/AD cells incubated by free Dox (1.51 µM) or a mixture of MSN-G2 and free Dox (1.51 µM) for 4 h at 37 °C.

A cell uptake study of MSN-Dox-G2 by flow cytometry in our case is more complex than other systems where the fluorescence intensity of the cell is directly related to the drugs internalized. In our study, we have used red fluorescence of Dox as indication for uptake of MSN-Dox-G2. However, one must be aware that only the Dox that is released from MSN-Dox-G2 shows the red fluorescence while fluorescence of those unreleased is completely quenched. Therefore, the red fluorescence intensity essentially is only an indication of the amount of DOX that that is internalized into cells in the form of MSN-Dox-G2 and subsequently released from MSN-G2. If there existed a percentage of MSN-Dox-G2 that was internalized but remained unreleased, then the actual cell uptake would be higher than what we determined in our study. In our previous extra-cellular study, we found that MSN-Dox-G2 can release completely in 4.9 mM glutathione within 24 h at 37 °C and it can release ~57% Dox in a 10000-time diluted extract of A2780/AD cells. Based on this data, we expect that an efficient and complete release will occur once delivered into the animal cells where a concentration of ~4.9 mM glutathione is present. However, it is possible that within the short incubation time employed in our study (up to 4 h), some portion of Dox may remain encapsulated and therefore the actual cell uptake of MSN-Dox-G2 is higher than what was determined. To some extent, this may jeopardize our conclusion regarding the uptake kinetics and the intracellular concentration at steady state for MSN-Dox-G2 system. However, based on the fact that the red fluorescence intensity of cells with 4 h incubation of MSN-Dox-G2 at 37 °C is only slightly higher than those cells with 1 h incubation of MSN-Dox-G2, we think most probably, the majority of Dox rapidly released after MSN-Dox-G2 being

internalized into cells at 37 °C and the portion of unreleased Dox in MSN-Dox-G2 is probably minimal.

Nevertheless, the incubation time appeared to affect the red fluorescence intensity of cells incubated with MSN-Dox-G2 at 4 °C more significantly than that at 37 °C. When incubated with MSN-Dox-G2 at 4 °C, the red fluorescence intensity of cells with 4 h incubation increased ~ 30% when compared to those with 2 h incubation; in contrast, in the case of incubation at 37 °C, the red fluorescence intensity with 4 h incubation is only ~ 5% higher than that with 2 h incubation. On one hand, this difference could indicate that MSN-Dox-G2 did not reach a steady state yet as the red fluorescence intensity was still on rise after 4 h incubation at 4 °C, which suggested that actual intracellular concentration at steady state could be even higher than the current observed value, making the uptake of MSN-Dox-G2 at 4 °C even more significantly higher than that at 37 °C; on the other hand, the more significant increase of mean red fluorescence intensity could be simply due to a slower release kinetics of MSN-Dox-G2 at 4 °C, in other words, although similar as the case of 37 °C, the MSN-Dox-G2 uptake might quickly reach a steady state after 1 or 2 h incubation, its release with 2 h incubation was not complete and as incubation increased to 4 h, more Dox was released, resulting in an increase of red fluorescence intensity. If the latter one was the case, then we would expect that an incubation at 4 °C followed by an incubation at 37 °C may result in a maximal released Dox concentration as a result of combination of optimal cell uptake at 4 °C and optimal Dox release inside cells at 37 °C.

To confirm whether this ideal scenario can be achieved, we performed an uptake experiment by incubating A2780/AD cells with MSN-Dox-G2 or Dox respectively

([Dox]=2.42 μM) at 4 °C for 2 h and then incubating at 37 °C for an additional 2 h. The red fluorescence intensities of cells were then analyzed by flow cytometry after being washed, trypsinized and then suspended in PBS buffer. The mean fluorescence intensities with different incubations are shown in Figure 7.6. The data clearly showed that for free Dox, the combination of 2 h incubation at 4 °C and 2 h incubation at 37 °C resulted in significantly lower red fluorescence than that of cells incubated at 37 °C for 4 h. This is expected as at 4 °C, the uptake of free Dox was completely inhibited and the combination of 2 h at 4 °C and 2 h at 37 °C should result in uptake no higher than 2 h at 37 °C alone and much less than 4 h at 37 °C. In contrast, for MSN-Dox-G2, the combination of 2 h incubation at 4 °C and 2 h incubation at 37 °C resulted in significantly higher uptake than 2 h incubation at 4 °C, 2 h incubation at 37 °C or 4 hr incubation at 37 °C. This data indeed confirmed that release of Dox from MSN-Dox-G2 inside cells at 4 °C is slower than at 37 °C and by a combination of initial low temperature incubation and later high temperature incubation, a maximal intracellular released Dox concentration can be achieved, which could ultimately maximize the cytotoxicity of Dox.
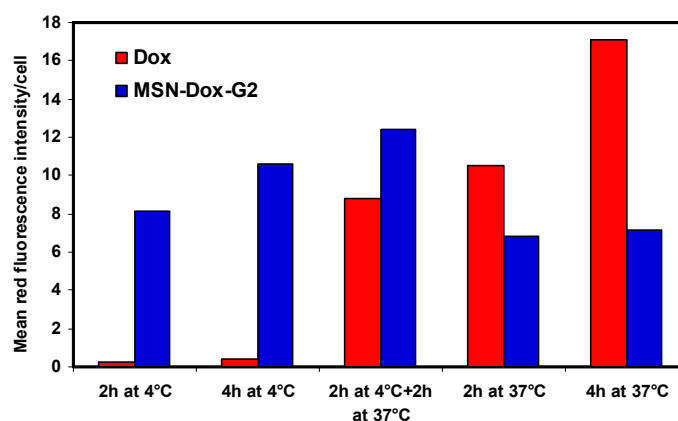
Figure 7.6. Effect of temperature and incubation time on internalization of MSN-Dox-G2 vs. Dox. The data showed that for MSN-Dox-G2, acombination of 4 °C and 37 °C incubation

resulted in maximum concentration of Dox inside cell, as a result of combined optimal cell uptake and optimal Dox release.

7.2.3. Influence of Metabolic and Endocytic Inhibitors on Cell Uptake of MSN-Dox-G2

The efficient cell uptake of MSN-Dox-G2 at 4 °C strongly suggested that the internalization of MSN-Dox-G2 go through a non-endocytic process. To further confirm this, we performed cell uptake studies by pre-incubating cells with metabolic inhibitor or different endocytosis inhibitors for 30 min and then incubating with MSN-Dox-G2 in the presence of inhibitors for 1 h. Different types of inhibitors have been chosen in our study and the function of each inhibitor is listed in Table 7.1.

Table 7.1. List of inhibitors used for each sample and their respective function

ID	Inhibitor	Function
1	None	None
2	0.1 w/v% sodium azide	Metabolic inhibitor to Inhibit cellular respiration and decrease intracellular ATP concentration
3	10ug/ml chlorpromazine	Clathrin-mediated endocytosis inhibitor
4	450 mM sucrose	Mainly clathrin-mediated endocytosis inhibitor, also fluid-phase endocytosis and lipid-raft mediated endocytosis inhibitor
5	200 ug/ml genistein	Caveolae-mediated endocytosis inhibitor
6	1ug/ml filipin	Caveolae/lipid raft-mediated endocytosis inhibitor
7	33 μM nocodazole	Clathrin-mediated and Caveolin-mediated endocytosis inhibitor by inhibiting microtubules, which are involved in vesicular movements
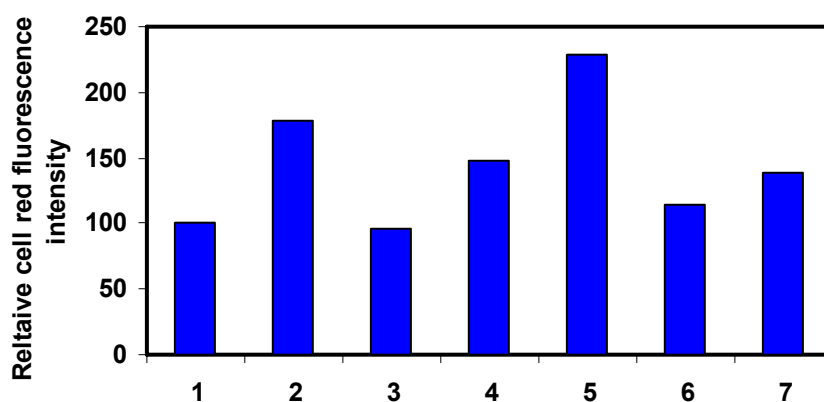
Figure 7.7. Relative mean red fluorescence intensity by flow cytometry of A2780/AD cells incubated at 37 °C by MSN-Dox-G2, 1 - without inhibitor or with inhibitor, 2 - 0.1 w/v% sodium azide, 3 – 10 µg/ml chlorpromazine, 4 - 450 mM sucrose, 5 - 200 µg/ml genistein, 6 - 1ug/ml filipin, 7 - 33 µM nocodazole.

Sodium azide, known to inhibit cellular respiration and decrease intracellular ATP concentration, was chosen as a metabolic inhibitor to inhibit all types of endocytosis, which are energy-dependent. Chlorpromazine is a cationic amphipathic drug that was known to inhibit clathrin mediated uptake. Exposure of cells to hypertonic sucrose is known to inhibit clathrin-mediated endocytosis, fluid-phase endocytosis as well as lipid-raft-mediated endocytosis in some cases. Genistein was known to perturb caveolae-mediated endocytosis. Filipin binds cholesterol and is known to inhibit caveloae/lipid raft mediated endocytosis. Nocodazole inhibits microtubules, which are involved in vesicular movements in the cell. The microtubule cytoskeleton and actin filaments are necessary for organelle movement within the cell. Nocodazole disrupts the migration of vesicles in cells including movement of cavicles to caveosomes or vesicular movement from early endosomes to late endosomes, or from late endosomes to lysosomes. In addition, it also

affects the movement of vesicles from Golgi complex to plasma membrane. This in turn results in entrapment of endocytosed material in organelles such as early endosomes and prevents the recycling of the vesicles to the cell surface. Thus nocodazole treatment has been shown to inhibit both caveolae-mediated and clathrin-mediated endocytosis.

Uptake of MSN-Dox-G2 was found not to be inhibited by any of the inhibitors and the data are shown in Figure 7.7. The presence of chlorpromazine (clathrin inhibitor) and filipin (caveolae inhibitor) appeared to have minimal effect on the cell uptake of MSN-Dox-G2. Furthermore, the sodium azide, sucrose, genistein and nocodazole appeared to even significantly increase cell uptake of MSN-Dox-G2. It is important to point out that some caution should be taken when interpreting these data and using them to deduce the internalization mechanism. As previously mentioned, we used fluorescence of Dox to quantify the cell uptake of MSN-Dox-G2 and this is only correct when the Dox is completely released inside cells. It is possible that some small portion of Dox remains unreleased within 1 h incubation. Therefore, the apparently increased red fluorescence intensity of cells when preincubated for 30-min and then co-incubated for 1 h with some of the inhibitors could partially be a result of increased release of Dox from MSN-Dox-G2 in addition to being possibly a result of real upper regulation of cell uptake of MSN-Dox-G2. Furthermore, it is possible that the presence of some inhibitors inside cells may generate a local environment with increased dielectric constant (reduced hydrophobicity) for released Dox and subsequently affect the fluorescence emission quantum yield of Dox and increase the red fluorescence intensity. In all, it is important to note that none of the inhibitors appeared to reduce the cell uptake of MSN-Dox-G2 and can serve as complementary evidence to our previous finding on temperature influence on the cell

uptake, suggesting that MSN-Dox-G2 likely internalize into A2780/AD cells through a non-endocytic process.

Internalization mechanisms of MSNs with different functionalizations have previously been studied by many groups and most MSNs were found to enter cells through an endocytic process. However, the internalization of at least two types of MSNs was reported not to be inhibited by any endocytosis inhibitors studied in each respective report. One example is the uptake of GEGP-MSNs into HeLa cells reported by Lin's group (13) and the other is the uptake of strongly positively-charged RITC-MSNs into hMSC cells reported by Chung et al. (1). The fact that none of the endocytosis inhibitors inhibited the cell uptake of these two types of MSNs in their respective cell lines suggested that both MSNs may internalize through a non-endocytic process. Our system may represent another MSN-based delivery system that possibly internalize into cells through a non-endocytic internalization mechanism. Our finding further confirmed the dramatic influence of functionalization on the internalization mechanism of MSNs.

Non-endocytic internalization mechanism have previously been reported for other nanoparticles, including carbon nanotubes, TAP peptides and TAP peptide conjugated cargos. As for carbon nanotubes, a nanoneedle mechanism, supported by both experimental data and molecular simulation, was proposed to explain the non-endocytic transmembrane process. Based on our data, the Dox or PAMAM G2 likely plays a critical role in the non-endocytic internalization process and a further investigation is required to fully reveal its mechanism.

7.2.4. Localization of Dox Delivered as MSN-Dox-G2 in Relative to Early Endosomes

As an additional effort to investigation the internalization mechanism of MSN-Dox-G2, we stained the early endosomes which are antigen-1-positive (EEA1-positive) with green fluorescence and examined the localization of the red fluorescence of Dox inside cells relative to the early endosomes. In this method, the cells after incubation with MSN-Dox-G2 were first washed with PBS buffer, fixed and permeabilized. After that, the cells were incubated with mouse anti-EEA1 antibody (primary antibody). Primary antibody specifically targets the EEA-1 localized in early endosomes and therefore will be specifically localized into early endosomes during this incubation. After that, cells were further incubated with green-fluorescent Alexa Fluor 488 goat anti-mouse IgG (H+L) (secondary antibody). The secondary antibody specifically bound to the primary antibody and consequently stained the endosomes with green fluorescence. As shown in Figure 7.8 (a-e), the red fluorescence appeared to be partially co-localized with green fluorescence, as indicated by the yellow color in the superposition image (Figure 7.8e). However, the majority of red fluorescence appeared to be localized in different spots than green fluorescence, as indicated by the separate red color and green color in Figure 7.8e. While it is impossible from this data alone to rule out the endocytosis mechanism, because the MSN-Dox-G2 can escape from the early endosomes and result in different localization of Dox from early endosomes., it is important to note that this data is consistent with what might be expected from a non-endocytic process.

As a control, early endosomes of cells incubated with 2.9 µM free Dox were also stained and then analyzed by fluorescence microscopy. The representative fluorescence

image shown in Figure 7.9(a-e) clearly showed a nearly non-detectable red fluorescence in cytoplasm, indicating the primary location of Dox in nuclei. This data is consistent with our previous finding which showed that free Dox is primarily localized in nuclei, while Dox delivered by MSN-Dox-G2 is localized in both nuclei and perinuclear region of cytoplasm. As a result, only green fluorescence is shown in the superposition image (Figure 7.9e), indicating the localization of endosomes. Theoretically, it is possible that the secondary antibody may also nonspecifically bind to some other places inside cells. To exclude this possibility, as an additional control, we also incubated the cells with
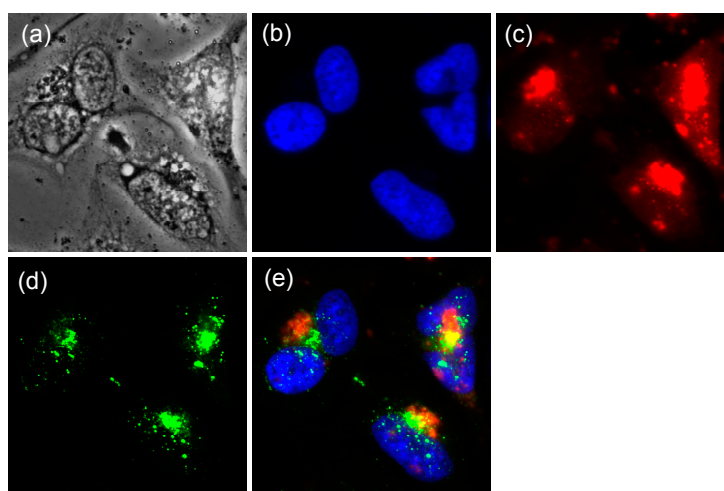
Figure 7.8. Regular fluorescence images of A2780/AD cells stained with Alexa Fluor 488 goat anti-mouse IgG (H+L) after incubated with MSN-Dox-G2 ([Dox]=2.9 μM) for 10 h at 37 °C. (a). light image; (b). blue fluorescence indicating the stained nuclei; (c). red fluorescence indicating the released Dox. (d). green fluorescence indicating the stained endosomes; (e). superposition of blue, red and green fluorescence images. It showed that the red fluorescence appeared to be partially co-localized with green fluorescence, as indicated by the yellow color in the superposition image. However, the majority of red fluorescence appeared to be localized in different spots than green fluorescence, as indicated by the separate red color and green color in panel e.

secondary antibody alone without pre-incubating with primary antibody, our data in Figure 7.10(a-e) showed that no green fluorescence could be detected inside cells, indicating that secondary antibody has minimal non-specific binding inside cells. This data further confirmed that the green fluorescence is truly indicative of the early endosomes, where primary antibody was specifically localized. Fixation and permeabilization was found in some studies(*10*) to generate artifacts of drug uptake and distribution inside cells. In our case, we found that the Dox distribution after fixation and permeabilization is similar as the distribution observed on live cells for both cases of MSN-Dox-G2 and free Dox.
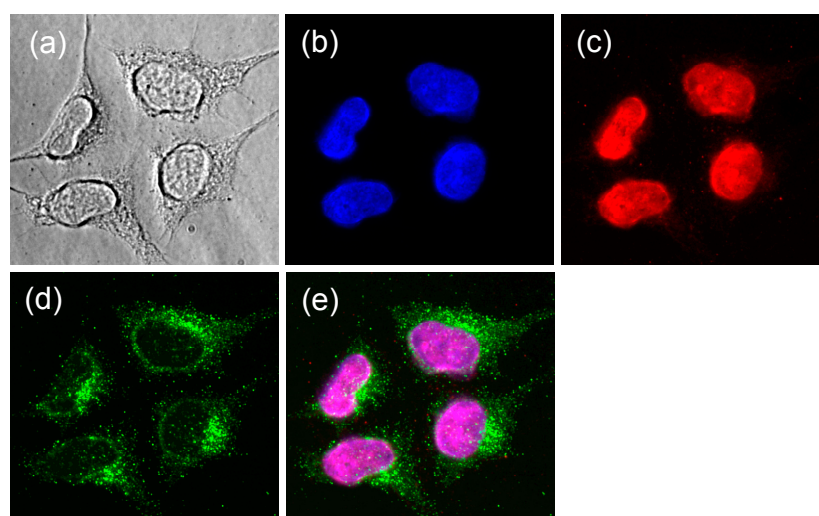
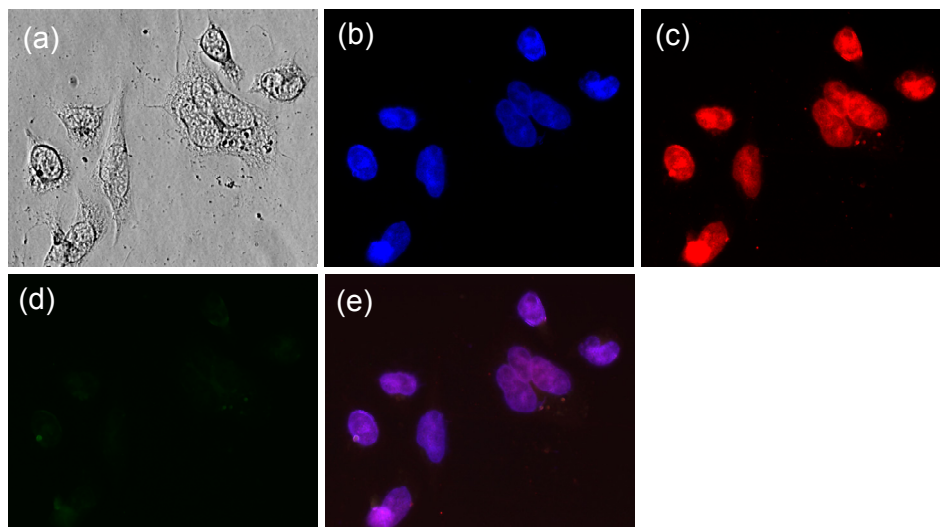

Figure 7.9. Regular fluorescence images of A2780/AD cells stained with Alexa Fluor 488 goat anti-mouse IgG (H+L) after incubated with 2.9 µM free Dox for 10 h at 37 °C. (a). light image; (b). blue fluorescence indicating the stained nuclei; (c). red fluorescence indicating the released Dox. (d). green fluorescence indicating the stained endosomes; (e). superposition of blue, red and green fluorescence images. It showed a nearly non-detectable red fluorescence in cytoplasm, indicating the primary location of Dox in nuclei. As a result, only green fluorescence is shown in the superposition image, indicating the localization of endosomes.

Figure 7.10. Regular fluorescence images of A2780/AD cells incubated with Alexa Fluor 488 goat anti-mouse IgG (H+L) alone without incubating with mouse anti-EEA1 antibody first after incubated with 2.9 µM free Dox for 10 h at 37 °C. (a). light image; (b). blue fluorescence indicating the stained nuclei; (c). red fluorescence indicating the released Dox. (d). green fluorescence indicating the stained endosomes; (e). superposition of blue, red and green fluorescence images. As a control, the cells were incubated with secondary antibody alone without pre-incubating with primary antibody. It showed that no green fluorescence could be detected inside cells, indicating that secondary antibody has minimal non-specific binding inside cells.

7.3. Conclusions

In summary, we studied the kinetics and efficiency of uptake of free Dox vs. Dox that is delivered as MSN-Dox-G2 into MDR A2780/AD human ovarian cancer cells by flow cytometry. We found that the MSN-Dox-G2 internalized into cells faster than free Dox. As a result, after 1 h incubation, the cell uptake of MSN-Dox-G2 was higher than free Dox. Furthermore, MSN-Dox-G2 appeared to reach a steady state after 1 h incubation while free Dox didn't reach the steady state even after 4 h incubation. The intracellular

Dox concentration at steady state was significantly higher in the case of free Dox than that delivered by MSN-G2. This data confirmed that the higher toxicity of MSN-Dox-G2 than free Dox that we previously reported was likely due to the synergistic anticancer action of Dox due to the coexistence of Dox in both nuclei and cytoplasm when delivered as MSN-Dox-G2 rather than due to the higher intracellular Dox concentration as previously speculated.

We further systematically studied the effect of temperature on the cell uptake of free Dox vs. MSN-Dox-G2 into the MDR A2780/AD cancer cells. Our data showed that the uptake of free Dox into MDR cell was decreased as temperature decreased and was completely inhibited when temperature decreased to 4 °C. This data was very different from a previous report on uptake of Dox into a non-MDR cell line, where the uptake of free Dox at 0 °C was only inhibited to 40% of that at 37 °C. We speculated this difference may be due to the efflux pump of Pgp on MDR cells in our study. At low temperature, the flip-flop transbilayer process of free Dox from outer membrane leaflet to inner membrane leaflet was significantly slowed, as a result, the Pgp might be able to pump out all Dox that was internalized before it was transported from inner membrane leaflet to cytoplasm. In contrast, while the cell uptake of MSN-Dox-G2 was also slightly decreased at 21 °C when compared to that at 37 °C, the cell uptake of MSN-Dox-G2 was not inhibited at 4 °C. On the contrary, it was even slightly higher than that at 37 °C. This data strongly suggested that the MSN-Dox-G2 internalize into cells through a non-endocytic process. We further demonstrated that in the case of MSN-Dox-G2, by combining the optimal low-temperature cell uptake of MSN-Dox-G2 and optimal high-

temperature intracellular Dox release from MSN pores, a maximal intracellular Dox concentration was achieved, which could ultimately maximize the cytotoxicity of Dox.

Third, we investigated the influence of metabolic inhibitor and different endocytosis inhibitors on the cell uptake of MSN-Dox-G2 and found none of the inhibitors appeared to inhibit the cell uptake of MSN-Dox-G2. This provided additional evidence suggesting a non-endocytic uptake process in addition to the data showing efficient cell uptake of MSN-Dox-G2 at low temperature.

Last, by staining the EEA1-positive early endosomes with green fluorescence, we found that the majority of Dox delivered by MSN-Dox-G2 into cells are not localized in the early endosomes, which was consistent with what might be expected from a non-endocytic process.

Our report represented the first detailed investigation on a possible non-endocytic internalization process of a MSN-based delivery system. Although more investigation is required to further reveal the non-endocytic mechanism of our delivery system, our data confirmed the critical role of functionalization in determining the cell uptake mechanism and stressed the necessity of studying the internalization mechanism of a delivery system with different functionalization before assuming it internalize through an endocytic process.

7.4. Experimental Section

7.4.1. Materials

Mouse anti-EEA1 antibody was from BD Biosciences. Alexa Fluor 488 goat anti-mouse IgG (H+L) was from Molecular Probes (Eugene, OR).

7.4.2. Early Endosomes Tracking

A2780/AD cells were seeded into 4-well glass slides (Lab-Tek™ II chamber slide system, Nalge Nunc International Corp.) at a density of 50,000 cells/well. The cells were grown for 24 h and then the old medium aspirated. Cells were then incubated with MSN-Dox-G2 or Dox ([Dox]=2.9 µM) in 1 ml cell growth medium at 37 °C for 10 h. After removing the old medium and washing the cells with DPBS buffer three times, the cells were then fixed and permeabilized by 200 µl of acetone (pre-cooled to -20 °C) for 10 min at -20 °C. Afterwards, the cells were washed with DPBS buffer twice and then incubated with 200 µl of 5% goat serum in DPBS buffer for 1 h at room temperature. Then the old medium were removed and the cells were incubated with mouse anti-EEA1 antibody (1:250) at 4 °C for 24 h. Following the removal of old medium and washing with DPBS buffer 4 times, the cells were further incubated with Alexa Fluor 488 goat anti-mouse IgG (H+L) (1:500) at room temperature for 2 h. After washing, the cells were finally incubated with 200 µl of 7.6 µM Hoechst in DPBS buffer at room temperature for 20 min. In the end, the slides were washed and then analyzed by regular fluorescence microscopy. For free Dox, a control experiment was performed parallel with same condition as above except that the step of incubation with mouse anti-EEA1 antibody was removed.

7.5. References

1. Chung, T.-H., Wu, S.-H., Yao, M., Lu, C.-W., Lin, Y.-S., Hung, Y., Mou, C.-Y., Chen, Y.-C., and Huang, D.-M. (2007) The effect of surface charge on the uptake and biological function of mesoporous silica nanoparticles in 3T3-L1 cells and human mesenchymal stem cells, *Biomaterials 28*, 2959-2966.

2.   Rejman, J., Oberle, V., Zuhorn, I. S., and Hoekstra, D. (2004) Size-dependent internalization of particles via the pathways of clathrin and caveolae-mediated endocytosis, *Biochemical Journal 377*, 159-169.

3.   Prato, M., Kostarelos, K., and Bianco, A. (2008) Functionalized Carbon Nanotubes in Drug Design and Discovery, *Accounts of Chemical Research 41*, 60-68.

4.   Shi, X., Kong, Y., and Gao, H. (2008) Coarse grained molecular dynamics and theoretical studies of carbon nanotubes entering cell membrane, *Acta Mechanica Sinica 24*, 161-169.

5.   Pantarotto, D., Singh, R., McCarthy, D., Erhardt, M., Briand, J.-P., Prato, M., Kostarelos, K., and Bianco, A. (2004) Functionalized Carbon Nanotubes for Plasmid DNA Gene Delivery, *Angewandte Chemie International Edition 43*, 5242-5246.

6.   Kostarelos, K., Lacerda, L., Pastorin, G., Wu, W., Wieckowski, S., Luangsivilay, J., Godefroy, S., Pantarotto, D., Briand, J.-P., Muller, S., Prato, M., and Bianco, A. (2006) Cellular uptake of functionalized carbon nanotubes is independent of functional group and cell type, *Nature Nanotechnology 2*, 108-113.

7.   Vives, E., Brodin, P., and Lebleu, B. (1997) A truncated HIV-1 tat protein basic domain rapidly translocates through the plasma membrane and accumulates in the cell nucleus, *The Journal of Biological Chemistry 272*, 16010-16017.

8.   Suzuki, T., Futaki, S., Niwa, M., Tanaka, S., Ueda, K., and Sugiura, Y. (2002) Possible Existence of Common Internalization Mechanisms among Arginine-rich Peptides, *The Journal of Biological Chemistry 277*, 2437-2443.

9.   Vandenbroucke, R. E., Smedt, S. C. D., Demeester, J., and Sanders, N. N. (2007) Cellular Entry Pathway and Gene Transfer Capacity of TAT-modified Lipoplexes, *Biochimica et Biophysica Acta 1768*, 571-579.

10.   Futaki, S. (2006) Oligoarginine vectors for intracellular delivery: design and cellular-uptake mechanisms, *Biopolymers 84*, 241-249.

11.   Derossi, D., Joliot, A., Chassaing, G., and Prochiantz, A. (1994) The third helix of the antennapedia homeodomain translocates through biological membranes, *Journal of the biological chemistry 269*, 10444-10450.

12.   Rosenbluha, J., Singhb, S. K., Gafnib, Y., Graessmannc, A., and Loyter, A. (2004) Non-endocytic penetration of core histones into petunia protoplasts and cultured cells: a novel mechanism for the introduction of macromolecules into plant cells, *Biochimica et Biophysica Acta (BBA) - Biomembranes 1664*, 230-240.

13.   Slowing, I., Trewyn, B. G., and Lin, V. S.-Y. (2006) Effect of surface functionalization of MCM-41-type mesoporous silica nanoparticles on the endocytosis by human cancer cells, *J. Am. Chem. Soc. 128*, 14792-14793.

14.   Ivanov, A. I., (Ed.) (2008) *Pharmacological inhibition of endocytic pathways: is it specific enough to be useful?*, Vol. 440, Springer.

15.   Huang, D.-M., Hung, Y., Ko, B.-S., Hsu, S.-C., Chen, W.-H., Chien, C.-L., Tsai, C.-P., Kuo, C.-T., Kang, J.-C., Yang, C.-S., Mou, C.-Y., and Chen, Y.-C. (2005) Highly efficient cellular labeling of mesoporous nanoparticles in human mesenchymal stem cells: implication for stem cell tracking, *FASEB J 19*, 2014-2016.

16.   Eytan, G. D. (2005) Mechanism of Multidrug Resistance in Relation to Passive Membrane Permeation, *Biomedicine and Pharmacotherapy 59*, 90-97.

17.   Regev, R., and Eytan, G. D. (1997) Flip-flop of doxorubicin across erythrocyte and lipid membranes, *Biochemical Pharmacology 54*, 1151-1158.

18.   Lane, P., Vichi, P., Bain, D. L., and Tritton, T. R. (1987) Temperature dependence studies of adriamycin uptake and cytotoxicity, *Cancer Research 47*, 4038-4042.

19.   Wong, H. L., Bendayan, R., Rauth, A. M., Xue, H. Y., Babakhanian, K., and Wu, X. Y. (2006) A mechanistic study of enhanced doxorubicin uptake and retention in multidrug resistant breast cancer cells using a polymer-lipid hybrid nanoparticle system, *J. Pharm. Exper. Ther. 317*, 1372-1381.

Chapter 8

Toward In-vivo Targeting Codelivery of Doxorubicin and siRNA for Effective Cancer Therapy

8.1. Introduction

The combination of chemotherapy and gene therapy has been recognized as an attractive approach for achieving enhanced anticancer efficacy. However, the lack of efficient delivery system for codelivery of chemotherapy and gene therapy drugs into cancer cells remains one of the major obstacles(*1, 2*). In some cases, although delivery systems were able to deliver both chemotherapy and gene therapy drugs simultaneously into cancer cells, the drugs failed to work synergistically to achieve an enhanced anticancer efficacy (*1*). In Chapter 5, we demonstrated that mesoporous silica nanoparticles (MSNs) can be used as a codelivery system to successfully deliver anticancer chemical drug, Doxorubicin (Dox), and gene therapeutic drug, siRNA, together into multidrug resistant cancer cells *in vitro* for an enhanced anticancer efficacy. In our approach, siRNA targeted against mRNA encoding Bcl-2 protein, which is the main player for non-pump resistance, significantly suppressed the Bcl-2 mRNA and efficiently overcame the non-pump resistance of Bcl-2 protein. As a result, the anticancer efficacy of Dox was increased 132 times compared to free Dox.
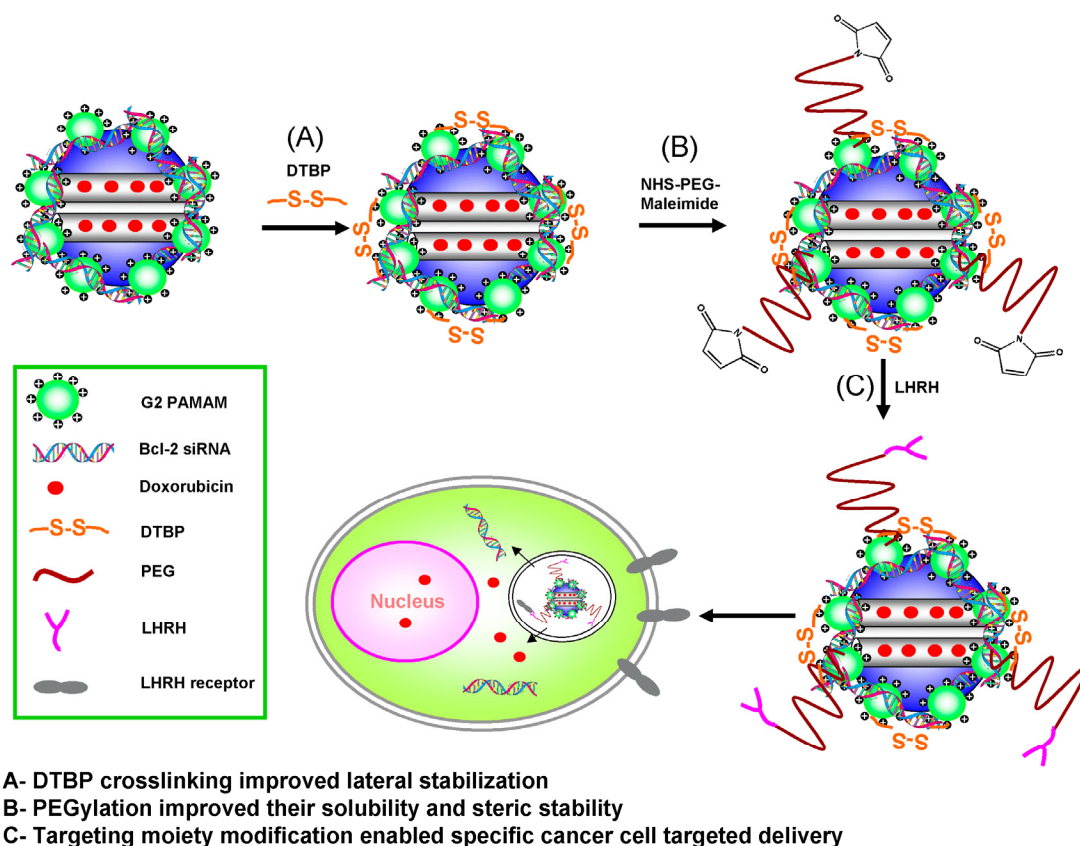
Based on the promising data from our *in vitro* experiment, we envisioned that this delivery system would be more appealing when it can be proved to be successful for *in vivo* systemic delivery. The challenges for *in vivo* systemic delivery of drugs are very different from those for *in vitro* delivery (*3, 4*). The first challenge for systemic delivery of drugs by nanoparticles is to increase the circulation time of the delivery system in the blood. It has been reported that by modifying nanoparticles with hydrophilic PEG polymer on the surface, longer blood circulation time and retention in the body can be achieved and the removal of nanoparticles due to the immune response can be overcome.(*5*) The second major challenge of systemic delivery of drugs, especially for the toxic chemotherapy drugs for cancer therapy, is their absorption to normal body tissues. This challenge can be partially overcome by using nanoparticles as delivery systems.(*6-18*) The sub-micron size featured by the nanoparticles enabled them to preferentially extravasate into the leaky tumor sites and be retained there due to an enhanced permeability and retention (EPR) effect. This phenomenon is constantly called passive targeting. However, this passive targeting is not clinically satisfactory. The treatment of cancers by chemotherapy drugs delivered by nanoparticles has still been largely hampered by their toxic side effects to normal body tissues. Furthermore, for most chemotherapy drugs such as Dox, the toxicity to normal body tissues can also be accumulated and thus limit the total dose that may be administered to each patient.(*4*) Therefore, it is of urgent need to develop delivery systems that can deliver chemotherapy drugs to tumor tissues with greater target specificity (i.e. active targeting).(*19*) Thanks to the versatile structures and relatively large surface area of nanoparticles, one common

approach has been to tag the nanoparticle surfaces with cancer-targeting ligands, which can specifically interact with receptors that are only rich in cancer cells.(*19*)

In addition to the above two challenges, for systemic delivery of gene therapy drugs, including siRNA delivery, there exists another major obstacle, which is the stability in the extracellular environment before reaching the target sites.(*20*) It was reported that siRNA can be rapidly degraded by the nucleolytic enzymes present in the extracellular environment and therefore necessary protection should be made before subjecting siRNA to systemic delivery.(*21*) It was found that by complexing the siRNA with cationic polymers, or loading into liposomes and other nanoparticles, the extracellular stability of siRNA can be greatly improved; however, further protection by PEGylation is often needed to ensure satisfactory protection from the aggressive extracellular environment and to achieve a sufficient stability for systemic delivery.

It is apparent from the above discussion that, in order to make our codelivery system most applicable *in vivo*, each abovementioned challenge has to be overcome. Towards this ultimate goal, we have therefore conducted further investigation on the MSN-based codelivery system and here is the report on our preliminary finding. As illustrated in Figure 8.1, in this study, we have PEGylated the MSN-Dox-G2/siRNA complex and then tagged it with a specific cancer-targeting group, Luteinizing hormone-releasing hormone (LHRH) peptide, which can be targeted for tumor cells in which LHRH receptors are over-expressed, including breast, lung, ovarian and prostate cancer cells. Our data demonstrated that the complex thus packaged showed enhanced stability in serum for up to 48 h. After conjugation of a tumor cell targeting moiety onto the distal end of the PEG, the complex can be efficiently internalized into LHRH-receptor positive

cancer cells such as A549 lung cancer cells and A2780/AD cancer cells, with minimal internalization into LHRH-receptor negative cancer cells such as SKOV-3 cancer cells. This preliminary finding indicated a great promise for successful application of our MSN-based codelivery systems *in vivo* and is expected to overcome all three challenges facing the systemic codelivery of chemotherapy drugs and gene therapy drugs to a significant extent.

A- DTBP crosslinking improved lateral stabilization
B- PEGylation improved their solubility and steric stability
C- Targeting moiety modification enabled specific cancer cell targeted delivery

Figure 8.1. Schematic diagram of a specific cancer cell-targeted MSN-based codelivery system that can deliver Dox and siRNA simultaneously to LHRH-positive cancer cells.

8.2. Results and Discussion

8.2.1. Stabilization of MSN-Dox-G2/siRNA Complex by Caging with Dithiol Containing Cross-linkers and PEGylation

Taratula *et al.*(*22*) in our group have demonstrated that caging siRNA nanoparticles formulated with generation-5 (G5) polypropylemine (PPI) dendrimers with an intracellular cleavable dithiol-containing cross linker, dimethyl-3-3'-Dithiobispropionimidate-HCl (DTBP) and then PEGylated by PEG_{5000}, both optimal lateral stability (by DTBP) and optimal steric stability (by PEG) can be achieved. In contrast, PEGylation of siRNA nanoparticles without packaging with DTBP first resulted in incomplete protection of siRNA nanoparticles. Therefore we have chosen the same protection approach to package the MSN-Dox-G2/siRNA complex with DTBP first and then with PEG_{5000} to ensure both lateral stability and steric stability. To confirm the successful packaging, we have used the same ethidium bromide (EtBr) replacement assay as developed by Taratula *et al.*(*22*) In this assay, 153 µl of MSN-Dox-G2/siRNA complex without packaging with DTBP (MSN-Dox-G2/siRNA), with DTBP packaging only (MSN-Dox-G2/siRNA-DTBP) or with both DTBP and PEG packaging (MSN-Dox-G2/siRNA-DTBP-PEG_{5000}) in pH=8.0 HEPES buffer ([siRNA]=0.261µM) were respectively mixed with 2 µl of 0.082 mg/ml EtBr. At this state, in all three samples, siRNA was strongly complexed with MSN-Dox-G2 and therefore was not available for intercalation with EtBr. As a result, the EtBr only displayed very weak fluorescence as shown in Figure 8.2. Then, polymethacrylic acid (PMAA), a strong polyanion known to disrupt polycation/siRNA complex, was gradually added to each solution and the fluorescence of EtBr was monitored as an increase of PMAA concentration. Upon addition of PMAA, depending on the strength of the complex as well as how well

protected the complex is by the packaging, the MSN-Dox-G2/siRNA complex will be disrupted to different extents. Consequently, different amount of siRNA will be de-complexed and becomes available to intercalate with EtBr. As a result, the fluorescence of EtBr will be increased. The increase of fluorescence can be directly related to the amount of siRNA decomplexed and subsequently related to the stability of MSN-Dox-G2/siRNA complex. As shown in Figure 8.2, the data clearly showed that the MSN-Dox-G2 complex with siRNA packaged by DTBP and PEG was stable and almost no complex was disrupted upon addition of PMAA. While in the case of MSN-Dox-G2/siRNA without packaging, upon addition of PMAA, the fluorescence significantly increased as a result of disruption of the complex and more siRNA becoming available for intercalation with EtBr. Additionally, as a control, we found that by packaging MSN-Dox-G2/siRNA with DTBP alone, the stability of MSN-Dox-G2/siRNA was also substantially increased, as reflected in much slower increase of EtBr fluorescence upon addition of PMAA than
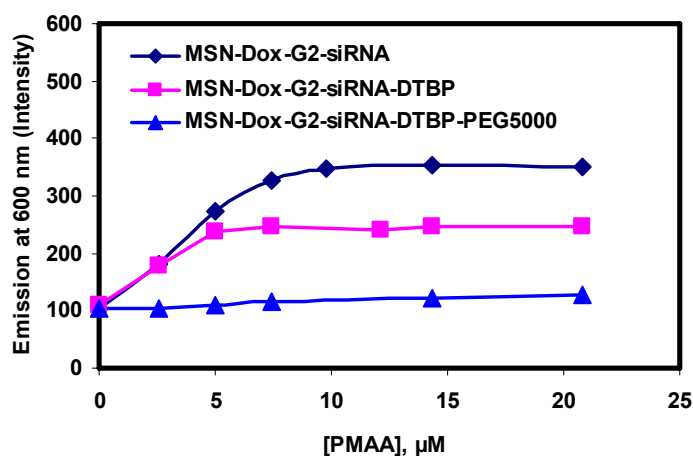

Figure 8.2. Ethidium bromide (EtBr) replacement assay to study the stability of MSN-Dox-G2 complex with siRNA without or with DTBP crosslinking or with both DTBP crosslinking and PEGylation. Before addition of PMAA, the concentration of siRNA and EtBr in the mixture was 0.258 μM and 0.001 mg/ml respectively.

that observed in the case of MSN-Dox-G2/siRNA without packaging. However, a significant amount of siRNA was still disrupted, indicating an incomplete protection of MSN-Dox-G2-siRNA. This further confirmed the PEGylation was necessary to ensure complete protection of siRNA and sufficient stability.

8.2.2. siRNA Serum Stability

The EtBr replacement assay discussed above confirmed a successful protection of the Dox/siRNA-loaded codelivery systems and suggested a great stability of the packaged nanoparticles. To test the stability of the system against nuclease degradation, the serum stability of siRNA in the packaged codelivery systems (MSN-Dox-G2/siRNA-DTBP-PEG) was investigated by incubating the packaged nanoparticles in 50% human serum at 37 °C for different amounts of time and then determining the degradation of siRNA at each time point by gel electrophoresis.
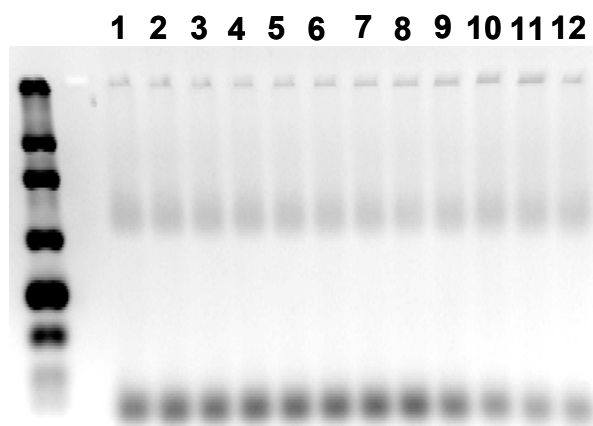

Figure 8.3. Stability of MSN-Dox-G2/siRNA-DTBP-PEG$_{5000}$-LHRH nanoparticles in human serum at 37 °C. Lane 1- 0min; 2 - 15min; 3 - 30min; 4- 45min; 5-1h; 6- 2h; 7- 3h; 8- 4h; 9- 8h; 10- 12h; 11- 24h; 12- 48h, respectively.

The gel electrophoresis data are shown in Figure 8.3. It indicated that the packaged nanoparticles are stable with no significant degradation at 37 °C for at least 8 h. Even after 48 h incubation at 37 °C, significant portion of siRNA remained stable. Stability of free siRNA was previously studied by Taratula et al. In their report, it was shown that at 37 °C, free siRNA started degrading after 5-min incubation and completely degraded after 2 h incubation. Our data therefore clearly confirmed that stability of siRNA was significantly enhanced by complexing with MSN-Dox-G2 and subsequently packaged by DTBP and PEG$_{5000}$ in serum. The siRNA in packaged nanoparticles are stable with no degradation in serum at 37 °C for at least 8 h.

8.2.3. Targeted Delivery of MSN-Dox-G2-siRNA-DTBP-PEG-LHRH into LHRH-Receptor Positive Cancer Cells

LHRH was chosen as a targeting moiety in our study. It has been demonstrated as a good cancer targeting moiety for targeting to cancer cells or tumors over-expressing LHRH receptors(*23, 24*). In our design, a heterofunctional PEG$_{5000}$, specifically α-maleimide-ω-N-hydroxysuccinimide ester poly(ethylene glycol) (NHS-PEG$_{5000}$-Maleimide), was employed. While the amine-reactive NHS ester was used to covalently react with the residual amine groups of PAMAM G2 on MSN-Dox-G2/siRNA-DTBP and subsequently made the nanoparticles PEGylated, upon packaging, the maleimide was then used to react with the thiol group on the cysteine of LHRH. The nanoparticles after modification were subsequently dialyzed to remove the residual chemicals from the reaction and then the amount of LHRH was determined by a standard bicinchoninic acid (BCA) protein assay. A series of LHRH solutions of known concentration were respectively subject to the

assay and then their purple reaction products were analyzed by UV-Vis spectroscopy (Figure 8.4a). Based on the absorbance spectra, the calibration curve was then obtained by plotting the concentration of LHRH against the absorbance at 556 nm of the final reaction products and shown in Figure 8.4b.
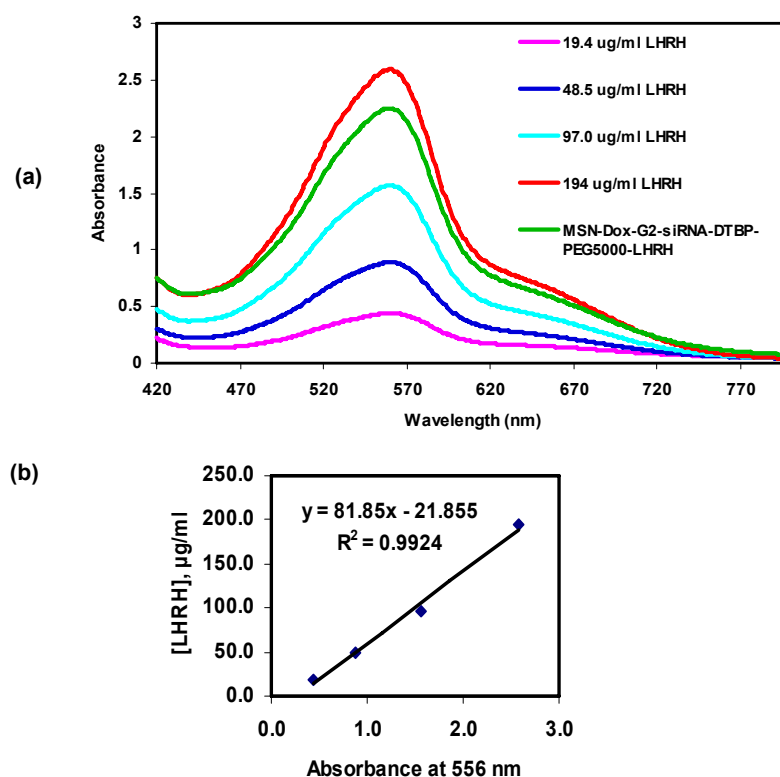
Figure 8.4. (a). UV-Vis spectra of final reaction products of various LHRH solutions of known concentration and an appropriately diluted solution of MSN-Dox-G2-DTBP-PEG-LHRH with BCA assay reagents. (b). A calibration plot of concentration of known LHRH solutions against the absorbance at 556 nm of their final reaction products with BCA assay reagents.

To further investigate whether the caged nanoparticles tagged with LHRH groups can be specifically delivered into LHRH-receptor positive cancer cells, the caged nanoparticles with LHRH groups were added to two LHRH-receptor positive cancer cells, A549 lung cancer cell and A2780/AD ovarian cancer cell respectively, and one LHRH-

receptor negative cancer cell. After incubated at 37 °C for 24 h, the cells were then washed with PBS buffer and then fresh medium was added for fluorescence imaging. In this experiment, siGLO green siRNA transfection indicator (FAM-labeled)(*25*) was used to complex with MSN-Dox-G2 and subsequently subject to packaging and modification in order to monitor the delivery of siRNA by fluorescence microscopy. Red and green fluorescence imaging was both performed to image the released Dox and siRNAs respectively. As previously discussed,(*26*) the fluorescence of Dox inside MSN pores is completely quenched and therefore the presence of red fluorescence is a hallmark of the Dox released from the MSN pores. As shown in Figure 8.5, both red fluorescence and green fluorescence are very strong in LHRH-receptor positive A549 cells and A2780/AD cells, while those in LHRH-receptor negative cells are significantly weaker. While more quantitative cell uptake study by flow cytometry will give us a better comparison and offer us a more definite conclusion regarding the specificity of our targeted-delivery systems, these preliminary data clearly indicated that cell uptake into LHRH-receptor negative SKOV-3 cells was significantly lower than that into LHRH-receptor positive A549 and A2780/AD cells and suggested a good targeted delivery of packaged and LHRH-modified nanoparticles into LHRH-receptor positive cancer cells. Furthermore, it was noted that the distribution of Dox and siRNA inside A549 or A2780/AD cells were similar as those previously observed for the same cells incubated with nanoparticles without packaging and modification. The strong red fluorescence signals inside A549 or A2780/AD cells indicated that the Dox was efficiently released once delivered into the cells. This indicated that upon delivery of the packaged and modified nanoparticles into cells, the packaging of PEG molecule on the nanoparticles possibly became weaker or

dissociated so that the dithiol group of cross-linked DTBP molecules can be efficiently cleaved by the glutathione inside cells(*27*) and the efficient release of Dox is not inhibited.
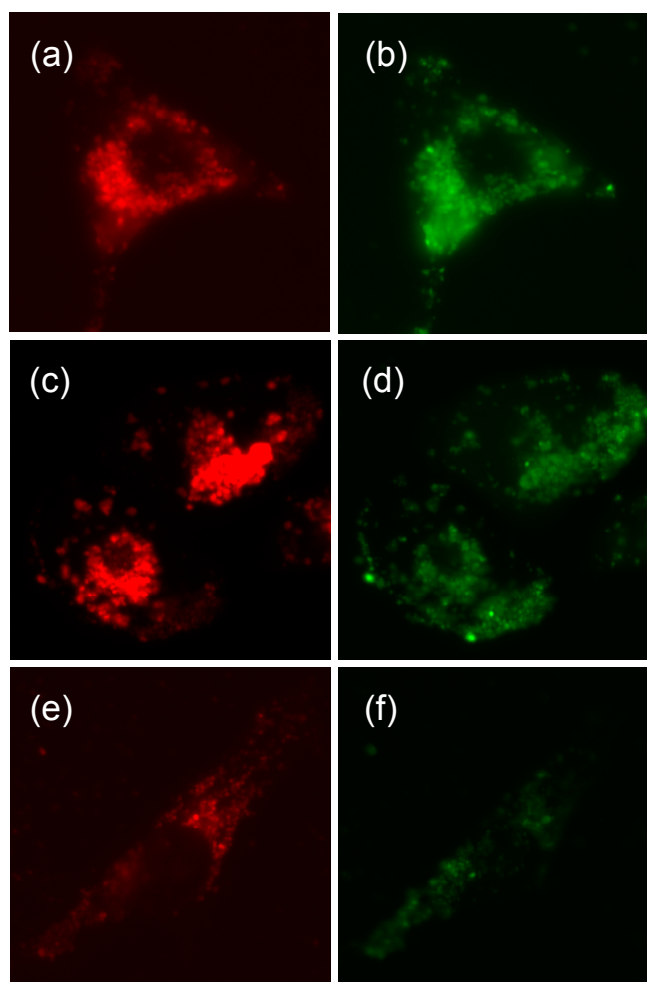
Figure 8.5. Representative fluorescence microscopic images of cellular uptake of the MSN-Dox-G2/siRNA-DTBP-PEG$_{5000}$-LHRH nanoparticles by LHRH-receptor positive, (A) A549 cells, (B) A2780/AD cells, and LHRH-receptor negative (C) SKOV-3 cancer cells. The incubation was 24 h at 37 °C.

8.3. Conclusions

In summary, we have conducted a preliminary investigation on the PEGylation of the MSN-based codelivery system and subsequent modification with cancer-targeting moiety for targeted delivery. Our results suggested a great potential for success of applying this MSN-based codelivery system for systemic *in vivo* targeted codelivery of chemotherapy drugs and gene therapy drugs. Our data indicated that upon packaging with DTBP and PEG_{5000}, the stability of siRNA in human serum was significantly enhanced and the siRNA was stable without any degradation in 50% human serum at 37 °C for at least 8 h. Furthermore, once tagged with LHRH groups, the caged nanoparticles showed specific delivery to LHRH-receptor positive cancer cells while the non-specific delivery to LHRH-receptor negative cancer cells was minimal. It was also found that the Dox thus delivered can be efficiently released after internalization of the nanoparticles into cancer cells and the distribution of siRNA and release Dox is similar as those observed for cells incubated with nanoparticles without packaging and modification.

8.4. Experimental Section

8.4.1. Materials

LHRH peptide was synthesized according to our design by American Peptide Company, Inc (Sunnyvale, CA).(*28*) The sequence of native LHRH peptide, which is similar in human, mouse, and rat, was modified to provide a reactive amino group only on the side chain of a lysine residue, which replaced Gly at position 6 to yield the superactive, degradation-resistant-Lys-6-des-Gly-10-Pro-9-ethylamide LHRH analog. The modified sequence of the peptide is: Gln-His-Trp-Ser-Tyr-DLys(DCys)-Leu-Arg-Pro-NHEt.

siGLO green transfection indicator was purchased from Thermo Fisher Scientific, Lafayette, CO. BCA protein assay reagent was from Pierce (Rockford, IL). α-maleimide-ω-N-hydroxysuccinimide ester poly(ethylene glycol) (MAL-PEG$_{5000}$-NHS) was purchased from NOF Corporation. 4% NuSieve 3:1 Reliant agarose gels was obtained from BMA, Rockland, ME.

8.4.2. Preparation of MSN-Dox-G2/siRNA-DTBP-PEG-LHRH for Cell Internalization Study

20 µl of 100 µM siGLO green siRNA transfection indicator (Fam-labeled) in H$_2$O was mixed with 80 µl of aqueous suspension of MSN-Dox-G2 (C(Dox)=1.05 mg/ml). Then the mixture was diluted with 178 µl of 3.93 mM HEPES buffer (pH~8.0). After incubation at RT for ~20 min, 1.86 µl of freshly prepared DTBP solution (100 mg/ml) was added. The mixture in small vial was then put onto a vortex machine for vibration for 1.3 h. After that, 11.46 mg of the heterofunctional PEG$_{5000}$ (NHS-PEG$_{5000}$-Maleimide), was added and the mixture was further vibrated for 2 h at RT. Finally, 2.1 mg of LHRH peptide was added. After 1.5 h reaction at RT with continuous vibration, the final solution was dialyzed using a dialysis tube (10k-Da cutoff) by centrifuge to remove the unreacted DTBP, PEG, LHRH. Finally, the samples left on the upper part of the dialysis tube was collected and added with water to make a total stock solution of 0.68 ml. Thus-obtained MSN-Dox-G2/siRNA complex protected by DTBP and PEG and modified with LHRH was used for cell internalization study by fluorescence microscopy. In this reaction, the molar ratio of DTBP to total primary amines of G2 PAMAM was 3 and the molar ratio of PEG$_{5000}$ to total primary amine was 6.6. The final concentration of siRNA and Dox in the reaction mixture was 7.2 µM and 0.30 mg/ml respectively. The final

concentration of HEPES buffer was 2.52 µM. An N/P ratio of 2 was used during complexation of MSN-Dox-G2 with siRNA.

8.4.3. Cellular Internalization

Cellular internalization of MSN-Dox-G2/siRNA-DTBP-PEG$_{5000}$-LHRH was studied by fluorescence microscope (Olympus America Inc., Melville, NY). A549, A2780/AD and SKOV-3 cancer cells were respectively plated (20, 000 cells/well) in 6-well tissue culture plate and cultured for 24 h. The old medium was then removed and cells were treated with MSN-Dox-G2/siRNA-DTBP-PEG$_{5000}$-LHRH nanoparticles prepared using FAM-labeled green fluorescent siRNA in 1.5 ml cell growth medium. After incubation for 16 h at 37 °C, the old medium was removed and the cells were added with fresh cell medium for imaging by fluorescence microscopy. An N/P ratio of 2 was used in the complexation and the final concentration of Fam-labeled siRNA in the cell growth medium was 0.20 µM.

8.4.4. Preparation of MSN-Dox-G2/siRNA, MSN-Dox-G2/siRNA-DTBP, MSN-Dox-G2/siRNA-DTBP-PEG$_{5000}$ for EtBr Replacement Assay

To prepare MSN-Dox-G2/siRNA, 9.6 µl of 6.25 µM 21-bp siRNA in H$_2$O was mixed with 24 µl of aqueous suspension of MSN-Dox-G2 (C(Dox)=0.36 mg/ml). Then the mixture was diluted with 189 µl of 20 mM HEPES buffer (pH~8.0). Three identical mixtures were prepared parallel. One mixture was collected and was used for EtBr replacement assay as MSN-Dox-G2/siRNA. The other two mixtures were further crosslinked with DTBP by adding 6.23 µl of freshly prepared DTBP solution (3 mg/ml) to each mixture and then reacting for 1 h with continuous vibration on a vortex machine.

After that, one mixture was again collected and was used for EtBr replacement assay as MSN-Dox-G2/siRNA-DTBP. The remaining mixture was subject to further PEGylation. To do so, 1.5 mg of the heterofunctional PEG$_{5000}$ (NHS-PEG$_{5000}$-Maleimide) was added to the mixture and the mixture was allowed to react for 2 h at RT with continuous vibration. An N/P ratio of 2 was used in the complexation. In the reaction, the molar ratio of DTBP to total primary amines of G2 PAMAM was 7.2 and the molar ratio of PEG$_{5000}$ to total primary amine was approximately 34.3. The final concentration of siRNA and Dox in the reaction mixture was 0.26 μM and 0.038 mg/ml respectively. The final concentration of HEPES buffer was 16.5 μM. An N/P ratio of 3.35 was used during complexation of MSN-Dox-G2 with siRNA.

8.4.5. Stability of MSN-Dox-G2/siRNA, MSN-Dox-G2/siRNA-DTBP, MSN-Dox-G2/siRNA-DTBP-PEG against Polyanion Disruption with PMAA

153 μl of three complex solutions prepared above with different extent of protection were respectively mixed with 2 μl of 0.082 mg/ml EtBr and then analyzed by fluorescence spectroscopy (Varian Cary-Eclipse spectrometer). The fluorescence emission intensity at 600 nm was measured with an excitation wavelength of 260 nm. To study the stability of each complex against the polyanion disruption, 200 μM of polymethacrylic acid (PMAA) was gradually added to each solution to result in a final concentration of PMAA in the range of 2.5-20.8 μM. After using pipette to mix the solution several times after each addition of PMAA, the fluorescence emission intensity was immediately measured. It was found that the fluorescence emission intensity immediately reached equilibrium upon addition of PMAA and mixing, therefore, no additional equilibration time was needed.

8.4.6. Quantification of LHRH on MSN-Dox-G2/siRNA-DTBP-PEG-LHRH by BCA

Peptide Assay

BCA protein assay reagent was used to determine the amount of LHRH on the final complex of MSN-Dox-G2/siRNA-DTBP-PEG-LHRH. 120 µl of BCA protein reagent A was mixed with 2.4 µl of BCA protein reagent B and then mixed with 30 µl of complex solution (C(Dox)=0.10 mg/ml, C(siRNA)=5.3 µM). The thus-mixed solution was then incubated at 48 ˚C for 45 min and then analyzed by Varian Cary 5000 UV-vis-NIR spectrophotometer in the range of 300-700 nm. The absorbance at 556 nm was used to determine the concentration of LHRH based on the calibration curve that was obtained on LHRH solution of different known concentration using similar procedure.

8.4.7. Serum Stability

To investigate the stability of MSN-Dox-G2/siRNA-DTBP-PEG$_{5000}$-LHRH in human serum, 120 µl of complex solution (C(Dox)=0.10 mg/ml, C(siRNA)=5.3 µM) was mixed with 120 µl of human serum. Then 18 µl of the mixed solution was transferred to 11 small vials respectively and incubated at 37 ºC. At each predetermined time interval (0, 15, 30 min, 1, 2, 3, 4, 8, 12, 24 and 48 h), one sample was removed and stored at -20 ºC until gel electrophoresis was performed. In order to release siRNA from the complexes for gel electrophoresis, before gel electrophoresis, each sample was mixed with 1 µl of 50 mM of reduced glutathione and 4 µl of 200 µM of PMAA. Then 3.5 µl of glycerol blue was added to each mixture. Finally, 20 µl of each resultant mixture was loaded onto 4% NuSieve 3:1 Reliant agarose gels in 1×TBE buffer by submarine electrophoresis. The gels were stained with ethidium bromide, digitally photographed and scanned using Gel Documentation System 920 (NucleoTech, San Mateo, CA).

8.5. References

1.   Wang, Y., Gao, S., Ye, W.-H., Yoon, H. S., and Yang, Y.-Y. (2006) Co-delivery of drugs and DNA from cationic core-shell nanoparticles self-assembled from a biodegradable copolymer, *Nature Materials 5*, 791-796.

2.   Pakunlu, R. I., Wang, Y., Tsao, W., Pozharov, V., Cook, T. J., and Minko, T. (2004) Enhancement of the efficacy of chemotherapy for lung cancer by simultaneous suppression of multidrug resistance and antiapoptotic cellular defense: novel multicomponent delivery system, *Cancer Research 64*, 6214-6224.

3.   Liu, F., and Huang, L. (2002) Development of non-viral vectors for systemic gene delivery, *Journal of controlled release 78*, 259-266.

4.   Ranson, M. R., Cheeseman, S., White, S., and Margison, J. (2001) Caelyx (stealth liposomal doxorubicin) in the treatment of advanced breast cancer, *Critical Reviews in Oncology:Hematology 37*, 115-120.

5.   Zahr, A. S., Davis, C. A., and Pishko, M. V. (2006) Macrophage Uptake of Core-Shell Nanoparticles Surface Modified with Poly(ethylene glycol), *Langmuir 22*, 8178-8185.

6.   Wong, H. L., Bendayan, R., Rauth, A. M., Li, Y., and Wu, X. Y. (2007) Chemotherapy with anticancer drugs encapsulated in solid lipid nanoparticles, *Advanced Drug Delivery Reviews 59*, 491-504.

7.   Minko, T., Kopeckova, P., and Kopecek, J. (2000) Efficacy of the chemotherapeutic action of HPMA copolymer-bound doxorubicin in a solid tumor model of ovarian carcinoma, *Int. J. Cancer. 86*, 108-117.

8. Lam, W., Leung, C.-H., Chan, H.-L., and Fong, W.-F. (2000) Toxicity and DNA binding of dextran-doxorubicin conjugates in multidrug-resistant KB-V1 cells: optimization of dextran size, *Anticancer Drugs 11*, 377-384.

9. Dubowchik, G. M., Firestone, R. A., Padilla, L., Willner, D., Hofstead, S. J., Mosure, K., Knipe, J. O., Lasch, S. J., and Trail, P. A. (2002) Cathepsin B-Labile Dipeptide Linkers for Lysosomal Release of Doxorubicin from Internalizing Immunoconjugates: Model Studies of Enzymatic Drug Release and Antigen-Specific In Vitro Anticancer Activity, *Bioconjugate Chemistry 13*, 855-869.

10. Gillies, E. R., and Frechet, J. M. J. (2005) pH-Responsive Copolymer Assemblies for Controlled Release of Doxorubicin, *Bioconjugate Chemistry 16*, 361-368.

11. Nystrom, A. M., Xu, Z., Xu, J., Taylor, S., Nittis, T., Stewart, S. A., Leonard, J., and Wooley, K. L. (2008) SCKs as Nanoparticle Carriers of Doxorubicin: Investigation of Core Composition on the Loading, Release and Cytotoxicity Profiles, *Chem. Commun.*, 3579-3581.

12. Goren, D., Horowitz, A. T., Tzemach, D., Tarshish, M., Zalipsky, S., and Gabizon, A. (2000) Nuclear delivery of doxorubicin via folate-targeted liposomes with bypass of multidrug-resistance efflux pump, *Clinical Cancer Research 6*, 1949-1957.

13. Missirlis, D., Kawamura, R., Tirelli, N., and Hubbell, J. A. (2006) Doxorubicin Encapsulation and Diffusional Release from Stable, Polymeric, Hydrogel Nanoparticles, *European Journal of Pharmaceutical Sciences 29*, 120-129.

14.   Lee, E. S., Na, K., and Bae, Y. H. (2005) Doxorubicin loaded pH-sensitive polymeric micelles for reversal of resistant MCF-7 tumor, *Journal of controlled release 103*, 405-418.

15.   Wong, H. L., Bendayan, R., Rauth, A. M., Xue, H. Y., Babakhanian, K., and Wu, X. Y. (2006) A mechanistic study of enhanced doxorubicin uptake and retention in multidrug resistant breast cancer cells using a polymer-lipid hybrid nanoparticle system, *J. Pharm. Exper. Ther. 317*, 1372-1381.

16.   Choucair, A., Soo, P. L., and Eisenberg, A. (2005) Active Loading and Tunable Release of Doxorubicin from Block Copolymer Vesicles, *Langmuir 21*, 9308-9313.

17.   Jayant, S., Khandare, J. J., Wang, Y., Singh, A. P., Vorsa, N., and Minko, T. (2007) Targeted Sialic Acid–Doxorubicin Prodrugs for Intracellular Delivery and Cancer Treatment, *Pharmaceutical Research 24*, 2120-2130.

18.   Yang, J., Lee, J., Kang, J., Lee, K., Suh, J.-S., Yoon, H.-G., Huh, Y.-M., and Haam, S. (2008) Hollow Silica Nanocontainers as Drug Delivery Vehicles, *Langmuir 24*, 3417-3421.

19.   Petrak, K. (2005) Essential properties of drug-targeting delivery systems, *Drug Discover Today 10*, 1667-1673.

20.   Nielsen, P. E. (2005) Systemic delivery: The last hurdle?, *Gene Therapy 12*, 956-957.

21.   Bartlett, D. W., and Davis, M. E. (2006) Effect of siRNA nuclease stability on the in vitro and in vivo kinetics of siRNA-mediated gene silencing, *Biotechnology and Bioengineering 97*, 909-921.

22. Taratula, O., Kirkpatrick, P., R.Salva, Pandya, I., Minko, T., and He, H. (2008) Toward in vivo Targeting Delivery of siRNA for Efficient Cancer Therapy.

23. Khandare, J., Chandna, P., Wang, Y., Pozharov, V., and Minko, T. (2006) Novel polymeric prodrug with multivalent components for cancer therapy, *The Journal of Pharmacology and Experimental Therapeutics 317*, 929-937.

24. Dharap, S., Qiu, B., Williams, G., Sinko, P., Stein, S., and Minko, T. (2003) Molecular targeting of drug delivery systems to ovarian cancer by BH3 and LHRH peptides, *Journal of controlled release 91*, 61-73.

25. Patil, M., Zhang, M., Betigeri, S., Taratula, O., He, H., and Minko, T. (2008) Surface-modified and Internally Cationic Polyamindoamine Dendrimers for Efficient siRNA Delivery, *Bioconjugate Chemistry 19*, 1396-1403.

26. Chen, A. M., Zhang, M., Wei, D., Taratula, O., Minko, T., and He, H. (2008) Co-delivery of Doxorubicin and siRNAs into Multidrug Resistant Cancer Cells by Mesoporous Silica Nanoparticles for Enhanced Chemotherapy Efficacy.

27. Oupicky, D., Carlisle, R., and Seymour, L. (2001) Triggered intracellular activation of disulfide crosslinked polyelectrolyte gene delivery complexes with extended systemic circulation in vivo, *Gene Therapy 8*, 713-724.

28. Dharap, S. S., Wang, Y., Chandna, P., Khandare, J. J., Qiu, B., Gunaseelan, S., Sinko, P. J., Stein, S., Farmanfarmaian, A., and Minko, T. (2005) Tumor-specific targeting of an anticancer drug delivery system by LHRH peptide, *PNAS 102*, 12962-12967.

CURRICULUM VITAE

Minhua Chen

Date of Birth   Oct 19th, 1978

Birth Place   Shang'ge, Pan'an, Zhejiang, China

Education:

2003 – 2009   Ph.D., Chemistry

                   Rutgers, The State University of New Jersey, Newark, USA

                   Advisors: Dr. Huixin He and Dr. Tamara Minko

2000-2002   M.S., Chemistry, University of North Texas, Denton, USA

1996-2000   B.S., Chemistry, Peking University, Beijing, China

Publications:

1. Y. Ma, P. L. Chiu, A. Serrano, S. R Ali, A. M Chen, H. He, *JACS*, **2008**, 130(25), 7921-7928
2. A. M. Chen, Y. Wang, R. Wenslow, *Org Process Res Dev*, **2008**, 12(2), 271-281
3. Y. Wang, A. M. Chen, *Org Process Res Dev,* **2008**, 12(2), 282-290
4. A.M. Chen, O. Taratula, D. Wei, T. Minko, H. He, *Technical Proceedings of the 2008 Nanotechnology Conference and Trade Show*, **2008**, 2, 324-325
5. O. Taratula, A. M. Chen, J. Zhang, J. Chaudry, L. Nagahara, I. Banerjee and H. He, *The Journal of Physical Chemistry C*, **2007**, *111*(21), 7666–7670
6. A.M. Chen, M. Ellison, A. Peresypkin, R.M. Wenslow, N. Variankaval, C.G. Savarin, T.K. Natishan, D.J. Mathre, P.G. Dormer, D.H. Euler, R.G. Ball, Z. Ye, Y. Wang, I. Santos, *Chemical Communications*, **2007**, 4, 419-421
7. A.M. Chen, L.M. Santhakumaran, S.K. Nair, P.S. Amenta, T. Thomas, H. He and T.J. Thomas, *Nanotechnology*, **2006**, 17, 5449-5460
8. A.M. Chen, S.K. Nair, T.T. Thomas, T.J. Thomas and H. He., *Technical Proceedings of the 2006 Nanotechnology Conference and Trade Show*, **2006**, 2, 29-32
9. S K Nair, T J Thomas, N J Greenfield, A Chen, H He and T Thomas, *Journal of Molecular Endocrinology*, **2005**, 35, 211-223
10. L. M. Santhakumaran, A. Chen, C.K.S. Pillai, T. Thomas, H. He, and T.J. Thomas, Book chapter: "Nanotechnology in Nonviral Gene Delivery", in *Nanofabrication for Biomedical Applications: Techniques, Tools, Applications, and Impact*, Eds: J. Hormes, C. Kumar, and C. Leuschner, Wiley-VCH, **2004**, 253-280
11. A. M. Chen, C. Pingsuthiwong, and T. D. Golden, *J. Mater. Res.*, **2003**, 18(7), 1561-1565